Novel therapeutic approaches for open-angle glaucoma

Trinity College Dublin

The University of Dublin

A thesis submitted to the University of Dublin for the degree of Doctor of Philosophy

Ruth Kelly

April 2021

Declaration

I declare that this thesis has not been submitted as an exercise for a degree at this or any other university and it is entirely my own work, except where otherwise stated.

I agree to deposit this thesis in the University's open access institutional repository or allow the Library to do so on my behalf, subject to Irish Copyright Legislation and Trinity College Library conditions of use and acknowledgement.

I consent to the examiner retaining a copy of the thesis beyond the examining period, should they so wish (EU GDPR May 2018).

Signed

Ruth Kelly

April 2021

Summary

Glaucoma is the leading cause of blindness worldwide after cataract and it is estimated that the global prevalence of glaucoma will increase to 111.8 million by 2040 (1, 2). Primary open-angle glaucoma (POAG) is characterized by elevated intraocular pressure (IOP) owing to a build-up of aqueous humor (AH) outflow, which occurs predominantly in the conventional outflow pathway, the latter mainly comprised of the trabecular meshwork (TM) and Schlemm's canal (SC) (3). Elevations in IOP cause damage to the retina, ganglion cell loss as well as damage to the optic nerve being characteristic features of disease pathology (4). Damage to ganglion cells results in irreversible vision loss and IOP-lowering drugs remain the main focus of therapy (5). Most topically applied therapeutics either reduce AH production by the ciliary body or enhance its clearance through the uveoscleral (unconventional) route and there is a current unmet clinical need for therapies directly targeting the conventional outflow pathway.

Chapter 1 provides an overall introduction to AH outflow dynamics, and the pathologies associated with the various forms of glaucoma. Treatments currently available and those in development are also considered. In Chapter 2, results from an *in vitro* study exploring changes occurring to glaucomatous human Schlemm's canal endothelial cells (SCEC) are presented. Glaucomatous SCEC displayed increased expression of fibrotic alpha smooth muscle actin (α-SMA) and adhesion vascular endothelial cadherin (VE-cadherin) markers, associated with an increase in cell size, cell migration and proliferation, as well as evidence of mitochondrial dysfunction compared to healthy SCEC. All of these changes have the potential to negatively influence AH outflow facility and thus IOP.

In Chapter 3, a novel approach to enhancement of aqueous outflow facility by siRNA-mediated downregulation of SC endothelial tight junction (TJ) proteins, ZO-1 and tricellulin, resulting in an increase in paracellular permeability of SCEC, was tested in a clinically relevant setting. Systemic or localized use of glucocorticoids can result in

dangerously high ocular hypertension (OHT), and there is currently a need for an effective means of rapid intervention. Data are presented in which siRNA-mediated suppression of SC endothelial TJs was used in a dexamethasone-induced murine model of steroid-induced OHT and resulted in significantly increased AH outflow facility and reduced IOP in these animals. In Chapter 4, use of the siRNA-mediated technique was also explored in a $MYOC^{Y437H}$ transgenic mouse model of OHT, *MYOC* (myocilin) mutations having been encountered in rare hereditary forms of glaucoma and also in a proportion of adult-onset cases. In this study a significant reduction in IOP was observed.

In the final chapter of this work (Chapter 5), an AAV-based therapeutic approach was assessed in the $MYOC^{Y437H}$ mouse model. Chadderton and colleagues (6) have shown that AAV-mediated expression of *NDI1*, a yeast nuclear gene substituting for a number of mutations in the mitochondrial respiratory NADH-ubiquinone oxidoreductase complex (Complex 1) protects ganglion cells following intravitreal inoculation of the virus in a murine model of Leber hereditary optic neuropathy (LHON). Given evidence which has accumulated for mitochondrial dysfunction in glaucoma, an assessment was made of the possible therapeutic effects of *NDI1* in $MYOC^{Y437H}$ mice. *NDI1* expression was obtained in both retina and in tissues of the anterior chamber (most obviously in corneal endothelia) in $MYOC^{Y437H}$ mice following intravitreal and intracameral inoculation of virus. Data obtained from intracameral injections suggested a potentially beneficial effect in reducing IOP over a six-month period. However, further investigations are required in order to determine the mechanistic basis for such reduction.

In summary, the initial focus of this work lay in explorations of the physical, morphological and molecular differences between glaucomatous and healthy SCEC, which may bear relevance to future approaches to disease prevention. An siRNA-mediated strategy targeting steroid-induced glaucoma has been successfully validated in rodents, potentially representing a focused approach to clinical application in a sight-threatening acute scenario,

the same approach having been assessed in a murine glaucoma model expressing a myocilin mutation. An AAV-based gene therapy approach has also been explored, providing encouraging initial results. Given that a significant number of POAG patients do not respond, or become resistant to current pressure-reducing medications, research in which new avenues of therapy are explored may hopefully eventually provide meaningful benefit to such patients.

Acknowledgements

Firstly, I would like to thank my supervisor Professor Pete Humphries for giving me the opportunity to undertake this PhD project in his lab. I would like to thank him for his support and guidance throughout. I would also like to thank Professor Matt Campbell, Professor Jane Farrar, Dr. Sophie Kiang, Dr. Darragh Crosbie, Dr. Natalie Hudson, Dr. Daniel Maloney, Dr. Adrian Dockery, Dr. Ciara Shortall and Dr. Marian Humphries for their assistance with various techniques and experimental design throughout my time in the lab. I am also grateful to our collaborators Charles Murray, Professor Colm O' Brien, Professor Dan Stamer, Kristin Perkumas, Professor Darryl Overby and Dr. Joseph Sherwood, without whom various techniques would not have been possible. *MYOC*^{Y437H} mice were kindly provided by Professor Val Sheffield. Special thanks are reserved for Dr. Jeffrey O' Callaghan and Dr. Paul Cassidy, who were of paramount significance in the progression of various projects and providing support throughout my time in the lab. Their help and guidance throughout were significant and I am so grateful to them both. I am thankful for all those in the lab, the extended department and close friends for their support, guidance and understanding throughout. I am especially appreciative of my family for their continued support and wisdom and of my boyfriend Ronan for his unwavering encouragement throughout.

Publications

Arising from this work:

Cassidy, P. S., and Kelly, R. A., et al. (2021). “siRNA targeting Schlemm’s canal endothelial tight junctions enhances outflow facility and reduces IOP in a steroid-induced OHT rodent model.” Molecular Therapy-Methods & Clinical Development **20**: 86-94.

- Cassidy and Kelly joint co-first authors.

Funding

Glaucoma research at the Ocular Genetics Unit at the University of Dublin, Trinity College Dublin was supported by Science Foundation Ireland [16/1A/4452] and the European Research Council [ERC-2012-AdG].

Table of Contents

Glossary of Abbreviations

AAV	Adeno-associated virus
AAV-EGFP	AAV constitutively expressing GFP
AAV-*NDI1*	AAV constitutively expressing Ndi1
AAV-OptEGFP	AAV-EGFP with tyrosine capsid mutation
AAV-Opt*NDI1*	AAV-*NDI1* with tyrosine capsid mutation
AD	Alzheimer's disease
ADP	Adenosine diphosphate
AH	Aqueous humor
AMD	Age related macular degeneration
AQP	Aquaporins
ATP	Adenosine triphosphate
AV	Adenovirus
BCA	Bicinchoninic acid
BSA	Bovine serum albumin
C	Outflow facility
CAV	Caveolin
CD31	Cluster of differentiation 31
CH3L1	Chitinase-3-like protein 1
CI	Confidence interval
CLAN	Cross-linked actin network
CTGF	Connective growth factor
CNV	Copy number variant
CP	Ciliary process
Cx43	Connexin 43
DEX	Dexamethasone

DNA	Deoxyribonucleic acid
ECM	Extracellular matrix
EGFP	Enhanced green fluorescence protein
EM	Electron microscopy
EMT	Epithelial to mesenchymal transition
EndMT	Endothelial to mesenchymal transition
ER	Endoplasmic reticulum
F	Phenylalanine
FA	Focal adhesion
F-actin	Filamentous actin
FBS	Fetal bovine serum
FITC	Fluorescein isothiocyanate
GC	Glucocorticoid
GFP	Green fluorescent protein
GOF	Gain-of-function
GWAS	Genome-wide association studies
HPRA	The Health Products Regulatory Authority
ICC	Immunocytochemistry
IHC	Immunohistochemistry
IOP	Intraocular pressure
IW	Inner wall
JCT	Juxtacanalicular tissue
LC	Lamina cribrosa
LCA	Leber congenital amaurosis
LCM	Laser capture microdissection
LHON	Leber hereditary optic neuropathy

MEMRI	Magnetic resonance imaging
mmHg	Millimetres of mercury
MMPs	Matrix metalloproteinase
mRNA	Messenger ribonucleic acid
MYOC	Myocilin
$MYOC^{WT}$	Negative for the myocilin transgene
$MYOC^{Y437H}$	Positive for the myocilin transgene
NADH	Nicotinamide adenine dinucleotide
NDI1	NADH- quinone oxidoreductase
NO	Nitric oxide
NT	Non-targeting
NTG	Normal tension glaucoma
OCR	Oxygen consumption rate
OHT	Ocular hypertension
ON	Optic nerve
ONH	Optic nerve head
OPTN	Optineurin
OXPHOS	Oxygen phosphorylation
P	Pressure
PACG	Primary angle-closure glaucoma
PAI-1	Plasminogen activator inhibitor-1
Papp	Apparent permeability
PBA	Phenylbutyric acid
PBS	Phosphate-buffered saline
PCR	Polymerase chain reaction
PDG	Pigment dispersion glaucoma

POAG	Primary open angled glaucoma
PXG	Pseudoexfoliative glaucoma
p53	Tumour protein
qPCR	Quantitative PCR
RNA	Ribonucleic acid
ROCK	Rho-kinase
ROCKi	Rho-kinase inhibitor
ROS	Reactive oxygen species
RT-PCR	Real time PCR
Q	Flow
rER	Rough endoplasmic reticulum
RFU	Relative fluorescent unit
RGC	Retinal ganglion cell
RNA	Ribonucleic acid
RNAi	RNA interference
ROCK	Rho-associated protein kinase
ROS	Reactive oxygen species
SC	Schlemm's canal
scAAV	Self-complimentary AAV
SCEC	Schlemm's canal endothelial cells
SEM	Scanning electron microscopy
SCg	Glaucomatous SCEC
shRNA	Short hairpin RNA
siRNA	Short interfering RNA
SMA	Smooth muscle actin
αSMA	Alpha smooth muscle actin

SPARC	Secreted protein acidic and cysteine-rich
T	Targeting
TBS	Tris-buffered saline
TBST	Tris-buffered saline with 0.1% Tween®
TEER	Trans-endothelial electrical resistance
TEM	Transmission electron microscopy
TGF-β	Transforming growth factor beta
TGF-β2	Transforming growth factor beta-2
TIGR	TM-inducible glucocorticoid response
TJ	Tight junction
TM	Trabecular meshwork
TNF	Tumour necrosis factor
TYR437HIS	Mutation of tyrosine to histidine at point 437
U	Uveoscleral pathway
VE-cadherin	Vascular endothelial cadherin
VEGF	Vascular endothelial growth factor
vWF	Von Willebrand factor
WT	Wild type
Y	Tyrosine
Y437H	Mutation of tyrosine to histidine at point 437
ZO-1	Zonula occludens-1

Chapter 1

Aqueous humor outflow dynamics and glaucoma pathology

Abstract

Open-angle glaucoma, an optic neuropathy involving progressive degeneration of the optic nerve head and loss of visual fields, is one of the most prevalent global causes of visual handicap. Following a brief introduction to the anatomy of the human eye and to visual processing by the retina, this chapter will be devoted to a discussion of the dynamics of aqueous humor outflow and how disturbance of such can lead to reduced outflow facility and elevated intraocular pressure, the major pathological hallmark of most forms of glaucoma. Clinical features of the disease, contributing factors, epidemiology, genetic factors, as well as a summary of current treatments available and the need for improved therapies will also be discussed.

Introduction

Anatomy of the human eye

The eye contains a number of components including the iris, cornea, pupil and lens, located towards the front of the eye in the anterior chamber (Figure 1.1). The lens focuses light onto the retina and is held in place by suspensory ligaments. The iridocorneal angle describes the area where the iris and cornea meet. The anterior chamber contains aqueous humor (AH) which nourishes the surrounding tissues and has a high turnover rate. The constant flow of AH around the front of the eye provides mechanical support and maintains a constant pressure inside the eye termed intraocular pressure (IOP).

The vitreous chamber, towards the back of the eye, contains vitreous humor, a clear jelly-like substance that has a low turnover rate. At the very back of the eye is the retina, containing the photoreceptor cells. The macula, which is located near the centre of the retina, is comprised mainly of cones and is associated with high-acuity central vision perception. The fovea, in the centre of the macula, contains cone cells exclusively.

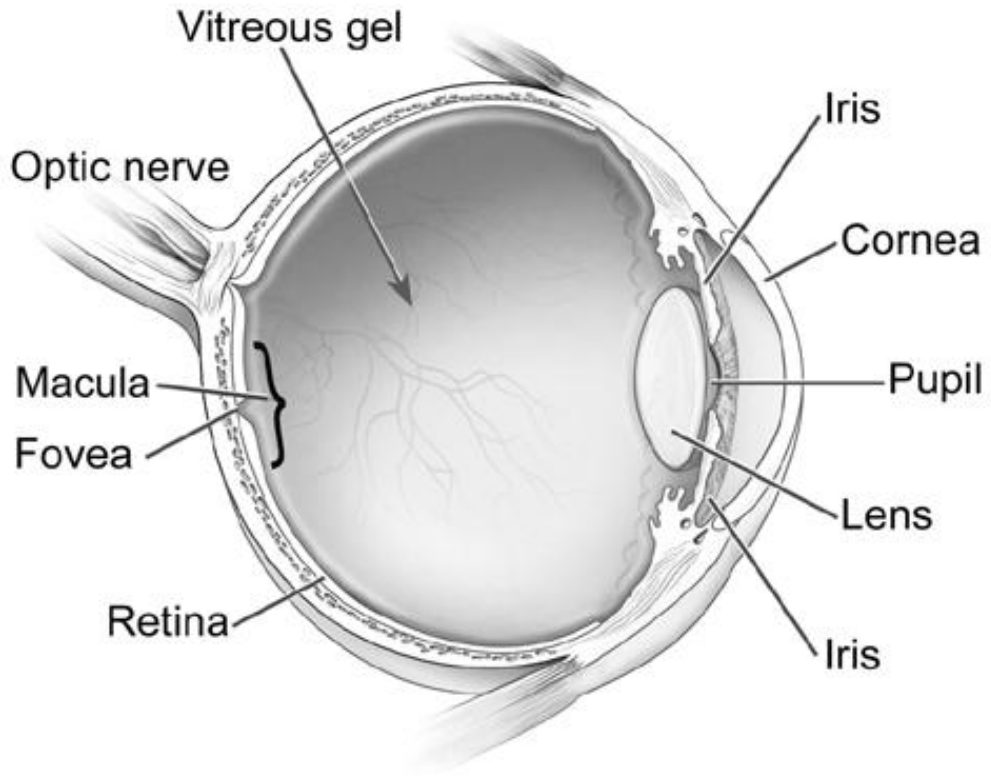

Figure 1.1: The human eye and associated tissues.

The main tissues of the human eye are labelled above. The iris, cornea, pupil, lens and iris are located towards the front of the eye. While the retina, fovea, macula and optic nerve are located towards the back of the eye. Image taken from the National Eye Institute image bank.

The human retina has up to six classes of neurons. There are approximately 120 million light sensitive rods and 6 million cones responsible for night and colour vision, respectively. Light absorption hyperpolarises the photoreceptors, resulting in cessation of secretion of the neurotransmitter glutamate. Visual information is then processed by a series of second-order retinal neurons – the bipolar, horizontal, inter-plexiform and amacrine cells. Horizontal cells, along with amacrine cells, enable lateral signalling across their respective layers, which allows the system to maintain contrast sensitivity across a range of light intensities (Figure 1.2) (7). Visual information is finally transmitted to the output neurons of the retina, the

ganglion cells, of which in humans there are 3-5 million, the axons of which converge at the optic nerve head for transmission to the higher visual centres in the neocortex. The very substantial reduction in numbers of photoreceptors in comparison to ganglion cells exemplifies the retina as a truly neuronal processing machine – "an approachable part of the brain" to quote the famous saying by John Dowling. Hence, substantial visual processing has been undertaken by the retina even before visual information is transmitted to the brain.

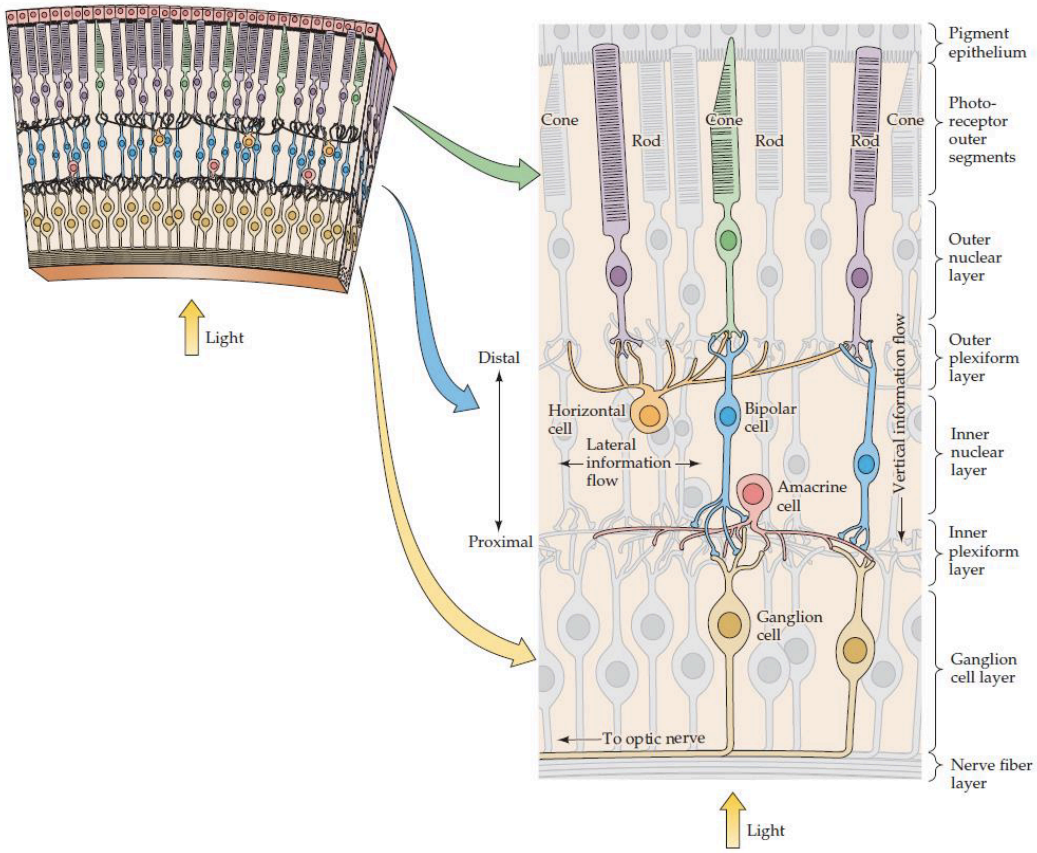

Figure 1.2: Structure and layers of the retina.

Overall structure of the retina, with the bottom of the diagram representing the anterior direction through which light enters the eye. The neuronal layers of the retina, through which visual signalling is processed from the photoreceptors (rods and cones), to the bipolar cells and finally to the ganglion cells, where information can be carried to the brain by the optic nerve. Taken from Purves et al. (2001) (7).

The movement of aqueous humor

AH is a clear fluid that fills the anterior chamber allowing the passage of light through the lens and cornea. AH has an important role in providing nutrients to the surrounding tissues of the anterior chamber (3). AH also removes excretory products from surrounding ocular tissues and most importantly regulates homeostasis of tissues in the eye (3).

AH is produced by the ciliary body and travels around the lens, through the iris, separating the two distinct chambers, and continues towards the iridocorneal angle (Figure 1.3). Here it is secreted by two main routes, the conventional and unconventional pathways. The conventional pathway involves the movement of AH through the trabecular meshwork (TM) and across the inner wall of Schlemm's canal (SC), where it is drained into collector channels and eventually into the episcleral veins (8, 9). The unconventional pathway is comprised of the uveal meshwork and ciliary body. AH enters the connective tissue, through the suprachoroidal space and exits through the sclera (Figure 1.3) (10).

An equilibrium exists between the production and drainage of AH that is important in maintaining the homeostatic environment inside the eye. Disruption of AH drainage through the conventional pathway can lead to an increase in IOP, which is one of the major risk factors of glaucoma (11).

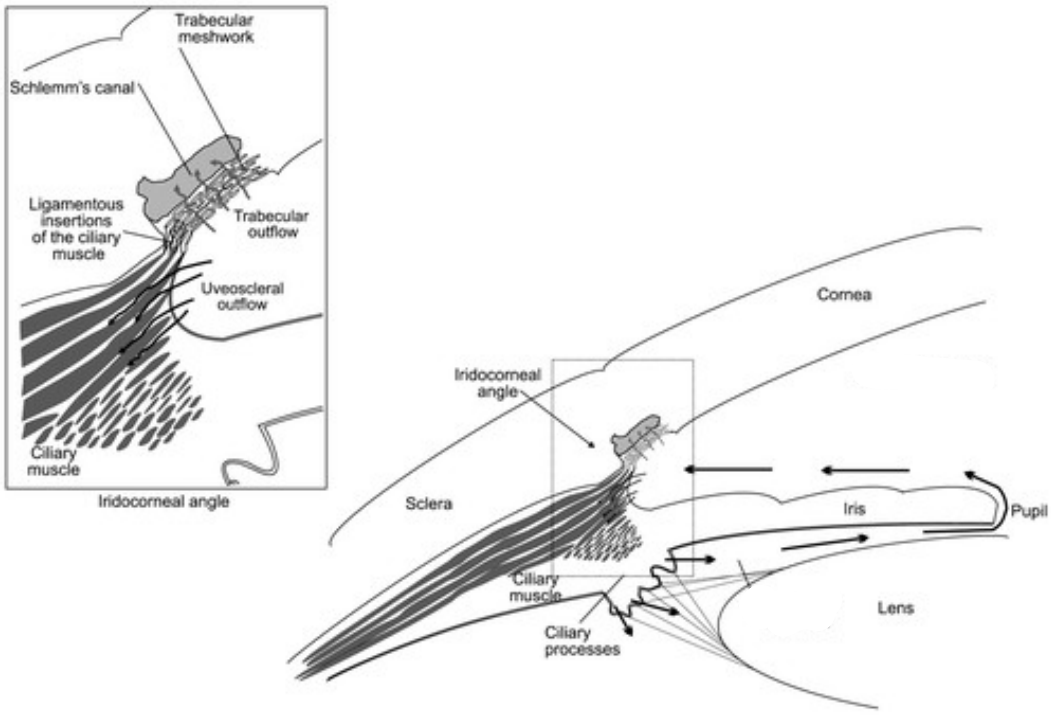

Figure 1.3: Schematic of the conventional outflow pathway.

The majority of aqueous humor (AH) drained from the eye does so through the conventional outflow pathway. Here AH travels through the three layers of the TM, across the inner wall of SC and is finally drained into collector channels. Taken from Llobet et al. (2003) (12).

The trabecular meshwork

The majority of AH drained from the eye is through the TM or conventional outflow pathway. The TM contains three distinct layers. The layer closest to the anterior chamber is known as the uveal meshwork layer. This layer does not have a major part to play in outflow resistance, as the intercellular spaces are quite large (12). The next layer is called the corneoscleral meshwork layer, which is comprised of a thin basal membrane covered in endothelial-like cells. This layer contains glycoproteins, collagen, hyaluronic acid and elastin fibres. The organisation of this layer, along with its narrow intercellular spaces is responsible for the increase in outflow resistance (12). The final layer of the TM is in direct contact with SC inner wall and is known as the juxtacanalicular tissue (JCT) or cribriform meshwork layer (Figure 1.4). This layer consists of dense extracellular matrix (ECM) and

the majority of resistance to AH outflow is thought to occur in this layer owing to its narrow intercellular spaces. The inner wall endothelium of SC is the last barrier to filtration before AH exists the eye. Owing to the high density of pores found along this surface layer, this region could account for ~10% of all AH resistance in the conventional pathway (13).

AH enters SC through two routes: a transcellular route through pores that develop in the endothelial cells lining the inner wall (14) and a paracellular route, through the junctions formed between these same endothelial cells (15).

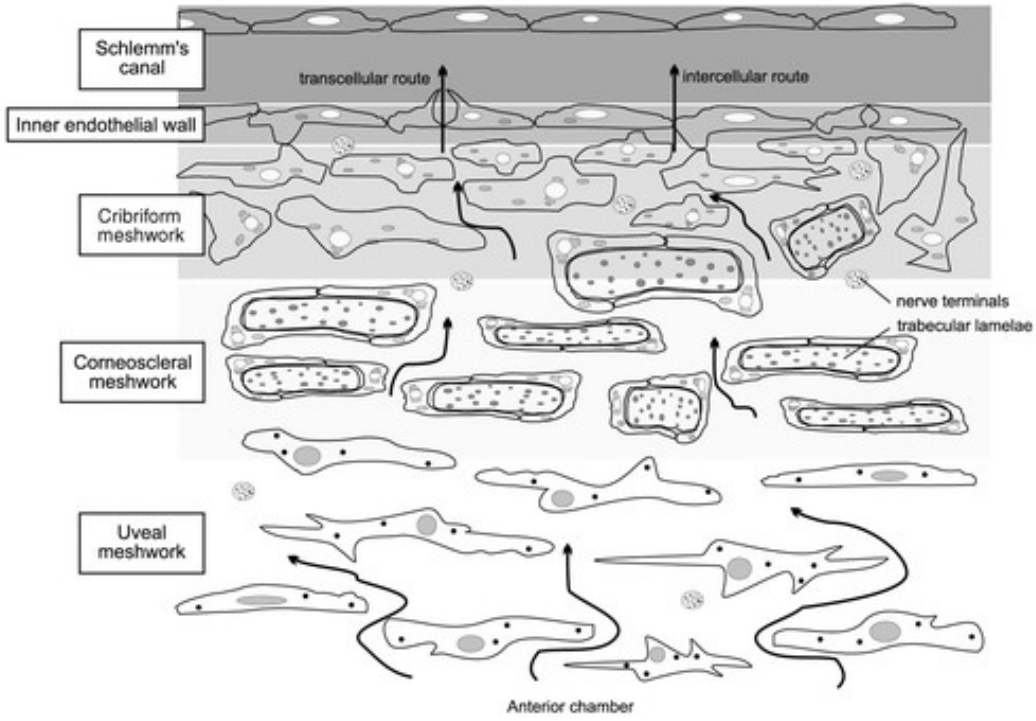

Figure 1.4: Layers of the trabecular meshwork.

The trabecular meshwork (TM) is comprised of three layers: the uveal meshwork, the corneoscleral meshwork and the cribriform meshwork layers. Aqueous humor (AH) flows from the anterior chamber through the layers of the TM and finally reaches the last barrier of AH filtration, the inner wall of SC. Taken from Llobet et al. (2003) (12).

SC cells express cluster of differentiation 31 (CD31) and vascular endothelial cadherin (VE-cadherin), typical of vascular endothelial cell types (16). In contrast, not all TM cells express chitinase 3-like 1 (CH3L1) (17), which suggests heterogeneity in this cell type. It is

important that we gain a greater understanding of these cell types, in order to progress more sophisticated therapies that could better target such tissues of the outflow pathway. In this regard, an *in vitro* exploration into the changes occurring in Schlemm's canal endothelial cells (SCEC) in glaucoma is reported in Chapter 2 of this thesis.

Trabecular meshwork permeability

Movement of the ciliary muscle has an important role in modulating the permeability of the TM to AH outflow (18). When the ciliary muscle contracts, the intercellular spaces in the TM widen and AH can flow more freely throughout the meshwork, increasing AH outflow. In contrast, when the ciliary muscle relaxes, the intercellular spaces become narrower and AH outflow is therefore reduced. Correspondingly, uveoscleral outflow is increased (12). Levels of AH outflow therefore vary between the trabecular and uveoscleral pathways, depending on movement of the ciliary muscle (19).

It has been shown in bovine eyes that the TM tissue itself is a contractile tissue. It displays smooth muscle actin (SMA) properties and contracts/relaxes when exposed to muscle agonists/relaxers respectively. Contraction of TM cells reduces TM permeability owing to reduction in intercellular space. When TM cells are relaxed, the opposite occurs, and increased permeability of the TM results (19).

Aqueous humor production

AH production by the ciliary body involves three main process: diffusion, ultrafiltration and active secretion (20). Both diffusion and ultrafiltration are passive processes. Diffusion is a process by which solutes, especially lipids, travel through lipid membranes in tissues, concentration gradients playing an important role (21). Ultrafiltration describes a process in which water-soluble substances travel through capillary endothelia as a result of an osmotic gradient (21). Diffusion and ultrafiltration result in the production of plasma ultrafiltrate

from the stroma of the ciliary body, from which AH originates (22, 23). It has been hypothesized that active secretion is responsible for the majority of all AH production (24). Epithelial cells are the primary location for active transport, especially across the blood-brain-barrier. Aquaporins (AQP1 and AQP4) are molecular water channels which are present in epithelial cells of the ciliary body and are involved in active AH secretion, a process involving conversion of adenosine triphosphate (ATP) bound to AQP1 and AQP4 to adenosine diphosphate (ADP) (25, 26). In humans, AH turnover rates have been estimated to be 1-1.5% of the total volume of the anterior chamber per minute (3). The major difference between AH and plasma is the concentration of protein and ascorbate present in both. AH has 200 times less protein than plasma and 20-50 times more ascorbate (27). Molecules associated with ECM deposition, for example collagen, have also been found in AH, which may increase resistance to outflow and IOP (28).

The unconventional outflow pathway

The unconventional or uveoscleral pathway has been more difficult to study than its conventional counterpart and less is understood about it. The uveoscleral outflow pathway was first described in an experiment in which fluorescent tracers were used to map the pathway in monkey eyes (29). The pathway was further characterised through animal experiments (30, 31) and through the development of a mathematical formula, the Goldmann equation:

$$F = (P_i - P_e) \text{ X } C+U$$

where F represents the rate of AH production, P_i is IOP, P_e is episcleral venous pressure, C is facility outflow and U is uveoscleral outflow (29). This model describes AH outflow as a passive movement of fluid across a pressure gradient (32, 33). The main challenges in calculating AH outflow using this equation were calculating episcleral venous pressure and establishing that uveoscleral flow and IOP were independent. The equation is also over

simplified, as it implies that pressure in pressure-dependent measurements resulted from a single episcleral vessel (34). Uveoscleral outflow can be influenced by a number of factors, including everyday ocular functions such as ciliary muscle contraction (35). It can also be influenced by ocular therapeutics. For example, Prostanglandin F2α can increase AH outflow through the uveoscleral pathway by decreasing AH resistance in interstitial spaces of the ciliary muscle (36, 37).

In the uveoscleral pathway, AH enters the ciliary muscle and exists through the supraciliary space and across the sclera into choroidal vessels (38). The overall proportion of AH entering through this pathway is of contentious debate. It is now known however, that the uveoscleral pathway can account for nearly 60% of all AH drainage in nonhuman primates (30). The amount can vary in different animals. It accounts for 3 to 8% in rabbits (38) and up to 80% in mice (39). In humans, it has been reported to range between 4 and 60% of all AH drainage (40, 41). Age tends to decrease uveoscleral outflow in humans and hence the conventional outflow pathway must compensate for this in preventing increases in IOP over time (42). There has been little recent advancement in methods for measurement of uveoscleral outflow and hence the Goldmann equation is still used. There is clearly an unmet need for more precise methods of measurement of uveoscleral outflow. The field has recently been the subject of a detailed review by Johnson et al. (2017) (43).

The conventional outflow pathway

IOP is predominantly controlled by AH outflow in the conventional pathway. The precise locations of AH outflow resistance have not yet been fully determined, but as mention above, it is known that a large proportion of resistance is generated in the JCT region and inner wall of SC. The large pores in the uveal and corneoscleral meshwork layers do not generate appreciable resistance, as it has been shown that a single pore in this region can allow for the transport of the entirety of AH outflow (44). SC lumen and the episcleral veins, located

downstream of the JCT region and Schlemm's canal, can also be excluded as having a major role in AH outflow resistance as their large diameters have been shown to have no significant contribution to outflow resistance (44). It has been shown in primates that pressure in SC lumen is the same level as episcleral venous pressure (8 mmHg below IOP), indicating that pressure drop occurs before this point, directly focused on SC inner wall and/or the JCT region (45).

Endothelial cells of SC inner wall have several unique characteristics. Firstly, they can form "giant vacuoles" which appear to be intracellular structures, but are actually outpouchings of the endothelial cells into SC, caused by pressure gradients across the membrane itself (46). 20 to 30% of these vacuoles also have distal openings or pores, and can therefore function as transcellular channels (44). The inner wall endothelium of SC has an unusually high hydraulic conductivity rate, higher than any other endothelial cell layer in the body (44). Ultrastructural visualisation of this area revealed an explanation for this. A very large number of pores or giant vacuoles are located on the inner wall of SC, up to 1000 pores/mm^2 (47). In spite of the very large number of endothelial pores, SC inner wall only accounts for up to 10% of all AH outflow resistance in the anterior chamber (48). It has been reported that it is less porous at the inner wall of SC and areas of paracellular pore density have been shown to co-localise with areas of high flow rate in the anterior chamber (49).

The JCT region would therefore be expected to account for the remaining outflow resistance in the conventional pathway. It has been found that excess ECM material is present in the JCT region in individuals with glaucoma, "clogging" the intercellular space and increasing outflow resistance (44, 50). Additionally, it has been shown that matrix metalloproteases (MMPs), which degrade ECM, reduces outflow resistance when perfused into enucleated eyes and when secreted directly into AH (51, 52). This highlights the role of ECM on outflow resistance in the JCT region in glaucoma. It is still unclear however, as to the exact amount of outflow resistance that is generated in the JCT region.

Since the precise location of the greatest amount of resistance in the conventional outflow pathway has yet to be determined, a synergistic model of outflow resistance has been proposed. Both the JCT and SC regions are pivotal to the role of AH outflow resistance and so the "funnelling model" below shows the movement of AH from the JCT region towards SC inner wall pores (Figure 1.5). As AH funnels from the wider JCT region towards the narrow pores of the inner wall of SC, AH outflow resistance increases at this particular area. This is predicted to be a 15-fold increase, when both pore density and giant vacuoles are considered (53, 54). "Washout" effect studies support this "funnelling model", where outflow resistance decreases over time during perfusion studies. This can then be reversed by lowering IOP to 0 mmHg and normal resistance is then seen after this pressure reduction. This effect is thought to be caused by the separation of the JCT from the inner wall of SC and so removing any funnelling effect that was previously seen, reducing outflow resistance (Figure 1.5). Lowering IOP allows the tissue to reattach and outflow resistance returns to normal (53, 55).

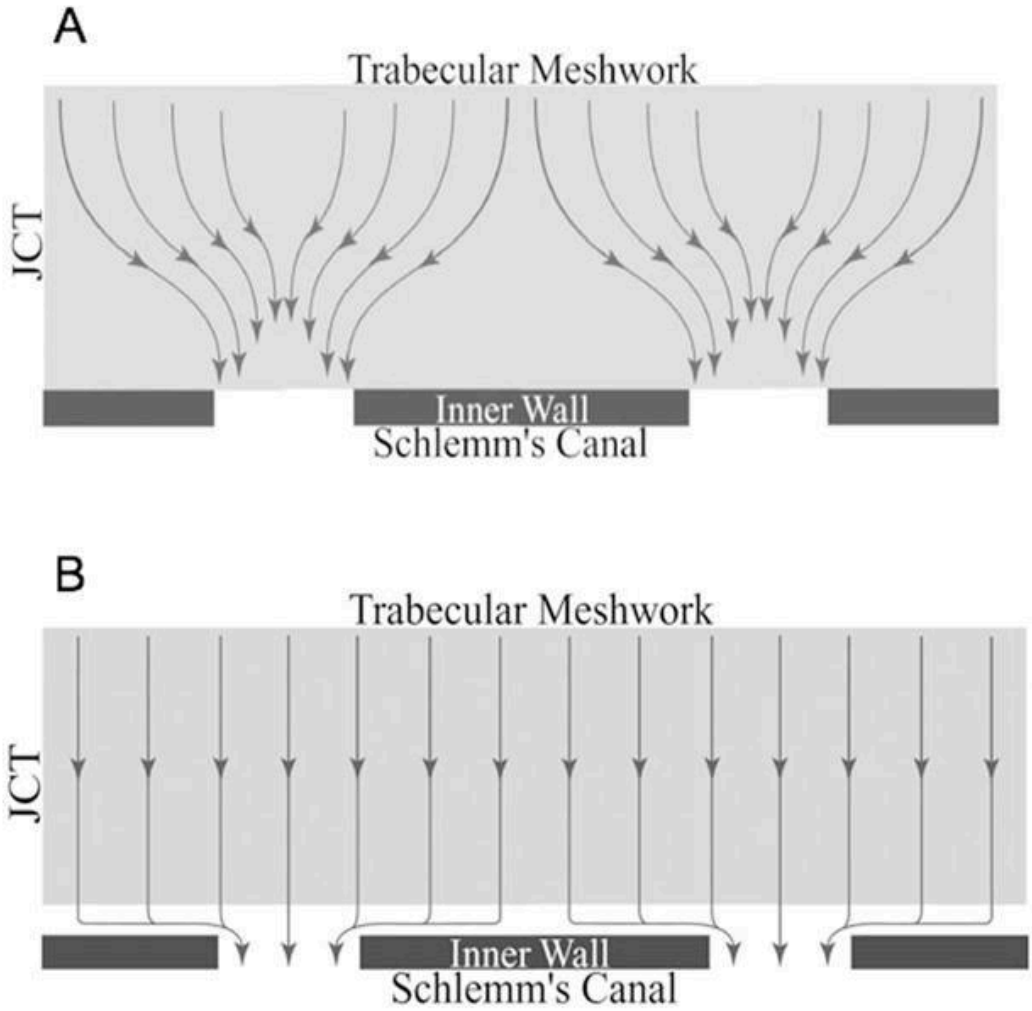

Figure 1.5: The funnelling model of AH outflow.

(A) AH funnelling from the wider JCT region towards the narrow pores of SC inner wall, creating resistance at this region. (B) Once the JCT and SC inner wall are separated however, uniform AH flow occurs. Taken from Overby et al. 2009 (53).

Ongoing studies of the conventional pathway have sometimes resulted in paradigm-shifts in our understanding of fundamental concepts on outflow resistance. In one such experiment, anterior segments were perfused at physiological flow rates until IOP stabilized, flow rates were then doubled and IOP was also observed to almost double, indicating no initial change to outflow resistance. However, perfusing these segments at this constant high flow rate over the course of several days revealed that IOP gradually decreased, until it reached the initial level of the original flow rate. This showed a clear adaptation of outflow resistance in

response to increased pressure. Doubling of initial perfusion pressure also showed an immediate influx of perfusate, which increased over time, to account for elevated IOP (56).

It is of interest also to note that following a trabeculotomy procedure, 25% of all AH outflow resistance remains, which indicates that the collector channels contribute to outflow resistance. This would indicate that the site of increased outflow facility is located near the collector channels of the outflow pathway (57-59).

Other factors, apart from the anatomy of the outflow pathway itself, have been shown to play a role in the development of increased outflow resistance. Heart rate can have a direct impact on the outflow pathway. Increased venous pressure can hinder AH outflow and cause blood reflux in SC (60). It has been shown that reducing episcleral venous pressure has advantageous effects on reducing outflow facility, along with IOP lowering drugs (61). It is clear that outflow resistance directly impacts IOP and is therefore of direct relevance to our understanding of the molecular pathology of glaucoma and in the development of IOP-lowering therapeutics.

Glaucoma and ocular hypertension

Glaucoma is an optic neuropathy characterised by the progressive loss of retinal ganglion cells (RGCs) and their axons, leading to damage of the optic nerve, causing visual loss and eventual blindness, if left untreated. Ocular hypertension (OHT) is the result of decreased AH outflow facility and results in a build-up of pressure in the eye, causing elevated IOP. Normal IOP for a healthy individual ranges from 10 to 20 mmHg, while OHT is regarded as an IOP greater than this (62, 63).

The build-up of pressure in the anterior chamber results in damage to the retina and optic nerve head (ONH). The axons of RGCs converge and exit the retina at the ONH, supported by a connective tissue termed the lamina cribrosa (LC). No photoreceptor cells are present at the ONH, which is referred to in non-technical terms as the blind spot. The

ONH and LC are referred to as the optic cup (4). OHT causes damage to the ONH, elevated pressure forcing a deepening or "cupping" of the optic disk, which leads to nerve atrophy and loss of RGCs, inevitably causing vision loss (5, 64, 65).

Different types of glaucoma

Glaucoma can be characterised based on whether an open or closed iridocorneal angle is present in the eye. Primary open-angle glaucoma (POAG) has an open iridocorneal angle and primary angle-closure glaucoma (PACG) has a closed iridocorneal angle. There are several other less common types of glaucoma, including normal tension (NTG), pigment dispersion (PDG), pseudo-exfoliative glaucoma (PXG) and secondary glaucoma. The two forms of glaucoma that are most important to this thesis are POAG and secondary glaucoma and are discussed below.

Primary open-angle glaucoma (POAG)

POAG is a complex disorder that presents in large numbers across the aging population. POAG is the most common form of the disease, representing over 74% of all cases (66). As the name suggests, the iridocorneal angle is open in this form of glaucoma, which is a defining feature of POAG, as well as increased outflow resistance in the conventional outflow pathway, leading to elevated IOP (67) (Figure 1.6). Reduced pore density, increase in ECM, increased IOP, stiffening of both TM and SC cells, dysregulation of segmental flow and/or oxidative stress have all been associated with damage to the conventional outflow pathway observed in POAG (68, 69).

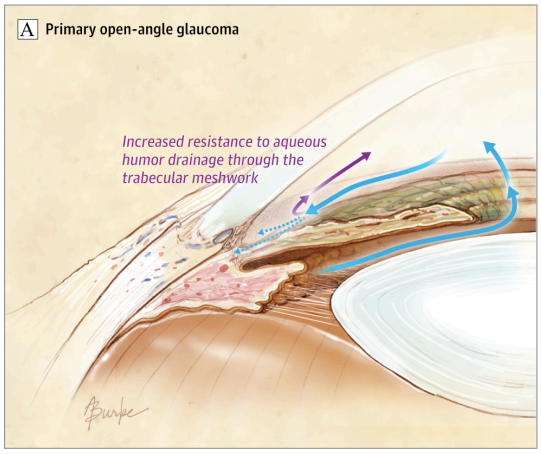

Figure 1.5: Primary open-angle glaucoma.

The iridocorneal angle remains open in POAG and the main contributor to reduced AH outflow facility is the outflow pathway itself. Adapted from Weinreb et al. (2014) (70).

Several molecules (TGF-β2, VEGF, endothelin, PAI and soluble CD44) have been shown to be elevated in AH samples from POAG patients compared to healthy samples (71-75). Increased expression of such molecules may have an impact on the surrounding tissues of the outflow pathway and influence trabecular cells to alter their normal phenotype. For example, TM cells can respond to elevated levels of TGF-β2 by secreting extra ECM material (76). Although this cellular response could be categorised as normal, the result could be an excessive accumulation of ECM material in the TM.

Secondary glaucoma

Secondary glaucoma occurs when glaucoma is the result of a different disease state or treatment. Examples of secondary glaucoma include traumatic glaucoma, due to damage in the eye, uveitis, due to infection or inflammation, and steroid-induced glaucoma, the result of long-term steroid use (77).

Risk factors for glaucoma

Glaucoma is the leading cause of blindness worldwide, after cataract. It is estimated that 13% of all blindness in Europe and 3% of the global population over 40 is caused by

glaucoma, affecting over 6.7 million people (2). It is estimated that the global prevalence of glaucoma will increase to 111.8 million by 2040, disproportionally affecting Asian and African populations, due to large population sizes (1). With better health care and lifestyle choices, an increase in aged populations is one of the major risk factors for glaucoma (1). Many other risk factors are associated with the disease, including ethnicity and genetics. POAG is more prevalent in African populations, while PACG is more prevalent in Asian populations. Gender is also a risk factor for glaucoma. Males are 36% more likely to have POAG than females (1). Other factors, such as the structural differences in the eye itself can impact the risk of disease. For example, a large optic cup-to-disk ratio, high IOP and thin central corneas are all associated risk factors (78).

Genetic factors associated with POAG

POAG is described as a complex, multifactorial disease and not primarily genetic. Most cases of glaucoma are late onset and so are not inherited according to Mendelian segregation patterns. There are, however, rare forms of the disease that are inherited and a number of genes associated with the disease have been identified.

Myocilin (*MYOC*) was the first gene to be associated with POAG (79). The *MYOC* gene encodes for a TM glucocorticoid response protein (TIGR), or myocilin protein. Many ocular tissues produce this protein, but it is only secreted by some, including the TM (80, 81). Myocilin interacts with other ECM components including laminin, fibronectin and decorin (82, 83). Mutations within the *MYOC* gene have not only been found in rare early-onset dominantly inherited forms of the disease, but also in 2 to 4% of adult-onset POAG cases (84, 85). This mutation was associated with juvenile POAG and showed increases in IOP beyond 40 mmHg. Older patients presenting with POAG and this *MYOC* mutation showed IOP ranges between 25 and 40 mmHg (68). The normal function of the *MYOC* gene remains unknown. It is known however, that the wild type (WT) form is secreted, while the

mutated form cannot be secreted properly and so accumulates in the TM (86). This leads to endoplasmic reticulum (ER) stress and TM dysfunction. TM cells that express the dominant human *MYOC* mutation (Tyr437His) show a build-up of ECM materials and a decrease in MMPs expression (87). A mouse model with this dominant mutation has been developed (*MYOC*^{Y437H}), showing reduced AH outflow facility, elevated IOP, among other characteristics of POAG (87, 88) and is described in Chapter 4.

Another gene associated with POAG is optineurin (*OPTN*). It can be passed on through autosomal dominant inheritance and is expressed in the TM, ciliary processes, retina and brain (89). *OPTN* in primarily associated with NTG. A number of *OPTN* mutations have been encountered in open-angle glaucoma including: *E50K*, *M98K*, *H486R*. The *E50K* variant has shown to induce RGC death *in vitro* (90). Transgenic mice expressing *OPTN E50K* variant show death of RGCs (91). Defects in vesicle trafficking, autophagy and mitophagy, processes in which optineurin is known to be involved, are likely to disturb homeostasis leading to death of RGCs (92, 93). Optineurin has been expressed in TM cell cultures in response to high IOPs, exposure to steroids and tumour necrosis factor-alpha (TNFα). It is hypothesised that the expression of the *OPTN* gene is expressed as part of a stress response (94). This gene is usually associated with NTG, but mutations have been associated with POAG as well (95). When combined, both the *OPTN* and *MYOC* mutations have been observed in nearly 5% of all late-onset cases of POAG (84).

POAG associated genes account for only about 5% of all POAG cases (96) and there is still much to be discovered and understood about the genetics of the disease. Genome-wide association studies (GWAS) appear to have uncovered several genes believed to be associated with an increased risk of POAG. These include the caveolins, *CAV1* and *CAV2*, expressed in the retina, TM and SC, and known to be associated with TGF-β signalling (84). Examples of other genes include *FOXC1*, *AFAP1*, *TMCO1*, ABCA1 and *SIX1* which have been shown by GWAS studies to be associated with POAG (97, 98). While a growing

number of genes are being implicated in POAG, the condition is truly multifactorial, with an ethology involving a combination of genetic and environmental components.

Current medical treatments for POAG

Current treatments available to POAG patients include medication, incisional surgery and laser surgery. These are the same for all variations of POAG and aim to relieve the build-up of pressure in the eye, by either reducing AH production or increasing the rate of excess AH outflow. IOP-lowering medications are divided into five main categories: prostanglandin analogues, beta blockers, diuretics, cholinergic agonists and alpha agonists (99). The various methods of action, side effects and efficiencies of each of these medications are summarised below in Table 1.

Table 1 Current treatment drugs for POAG[19–26]

Drug class	Drug and daily frequency	Route	Mechanism of action	Side effects in class
Prostaglandin analogs	Latanoprost 1x Travoprost 1x Unoprostone 2x Bimatoprost 1x	Topical	Increased trabecular drainage	Eye lash thickening, eye lid darkening, eye staining
Beta blockers	Betaxolol 2x (selective) Carteolol 2x Timolol 1–2x Levobunolol 1–2x	Topical	Decreased aqueous fluid production	Eye irritation, hyperemia, blurred vision, impaired lung function
Diuretics (carbonic anhydrase inhibitors)	Brinzolamide 3x Dorzolamide 3x Acetazolamide 2–4x Methazolamide 2–3x	Topical Oral	Decreased aqueous fluid production via HCO_3^- unavailability	Blurred vision, bitter taste, acidosis, hepatic necrosis
Cholinomimetics	Carbachol 3x Pilocarpine 3–4x Physostigmine 1–4x	Topical DOG Plastic film	Open the TM by contraction of ciliary muscle forces	Night blindness, blurred vision, burning eye sensation
Alpha agonists (selective)	Epinephrine 1–2x Dipivefrin 2x	Topical	Increased trabecular flow	Tremor Palpitation
Alpha agonists (non-selective)	Brimonidine[a] 3x Apraclonidine[b] 3x	Topical	Reduced aqueous production and increased uveoscleral flow	Hyperemia, allergic conjunctivitis, itching, lacrimation

Notes: [a]Brimonidine has a dual mechanism of action; [b]apraclonidine only reduces aqueous production.
Abbreviations: POAG, primary open-angle glaucoma; DOG, drops, ointment, gel.

Table 1: List of current medications available for the treatment of POAG.

Each of the drug classes available for POAG treatment are listed above, along with daily frequency of use, route of administration, mechanism of action and possible side effects. Taken from Beideo et al. (2012) (99).

Topical eye drops of the current medications listed above target various sites and have different mechanisms of action. Prostaglandins, like latanoprost, target the uveoscleral outflow pathway and aim to increase uveoscleral outflow by altering permeability or pressure gradients. Beta blockers and carbonic anhydrase inhibitors both target the ciliary body and aim to reduce AH production at the ciliary body. Pilocarpine is the most widely used cholinergic drug for the treatment of glaucoma. This drug aims to widen the angle of the anterior chamber, resulting in increased AH outflow through TM tissue, by stimulating the muscarinic receptors of the ciliary muscle. Finally, alpha agonist brimonidine acts by decreasing AH secretion and increasing uveoscleral outflow (100).

Monotherapy

Monotherapy is the first course of treatment, as patients tend to be more compliant and it decreases the potential of systemic and adverse side effects (101). It will become clear from IOP readings if the drug is working or not and if necessary, medication can then be changed. A monotherapy, like latanoprost, can show a reduction in IOP of over 30% from baseline in patients with IOP ranging from 20 to 24 mmHg. IOP reductions are even greater in patients with IOP greater than 24 mmHg (102). However, reductions in IOP are not seen across all patient cohorts using latanoprost or other prostaglandin drugs. In one study, latanoprost reduced IOP by 30% in only 10% of patients (103). There are therefore varying degrees of efficacy when using this type of medication. Both prostaglandins and beta blockers are, nevertheless, potent drugs and suitable as first-line monotherapies for many cases of POAG (101, 104).

Brimonidine, an alpha agonist, was found to be very successful at reducing IOP, even more so than timolol, a beta blocker also commonly used as a first-line monotherapy. Brimonidine is used as a monotherapy for patients with OHT who are on constant doses of beta blockers, as beta blockers have more severe side effects (105). Both betaxolol and

timolol impact normal lung function and betaxolol raises IOP (106). A study carried out using carteolol, betaxolol and timolol as a monotherapy revealed that these medications did not adequately lower IOP in over 50% of patients in the study over a 7 year period and additional medications were needed (107).

Cholinergic drugs are the most efficient when indirectly targeting the TM. These drugs increase AH outflow by removing the blockage present and so are extremely beneficial for PACG treatment. These drugs cause the ciliary muscle to contract and in doing so, allows for increased AH outflow (99). Their mechanism of action increases the risk of myopia however, which is a risk factor for POAG (108, 109) and so this monotherapy is unsuitable for POAG patients.

Combination therapies

Monotherapy IOP lowering drugs may not be sufficient when treating every patient and so a combination of two is the next step. To improve patient compliance, many drugs are available on the market that already have combined monotherapies included in the one treatment. For example, DuoTrav® is a combination of travoprost and timolol and Xalacom® is a combination of latanoprost and timolol. In a randomised double-blind study, the combination of latanoprost and timolol lowered IOP by more than 30% in 73.5% of patients, when compared to treatment with latanoprost alone (32.8% of patients) (110, 111). Not all combination therapies show increased reduction in IOP compared to monotherapy drugs, however. There was no significant reduction in IOP shown with the combined treatment of timolol and latanoprost compared to travoprost monotherapy in a randomised double-blind study (112). In NTG or POAG cases where IOP has already been sufficiently reduced, combination therapies fail to significantly lower IOP even more (103, 113). Combination therapies can therefore be very effective when attempting to lower high IOP in POAG, but they are not without their own drawbacks. Another approach is combining

drug administration with surgical intervention. There is clearly an unmet clinical need for improved medications directly targeting the outflow pathway itself, where AH outflow resistance is generated.

Current surgical treatments for POAG

There is always a cohort of non-responders - individuals who do not respond to medication, and so surgical intervention is therefore the only treatment option left available. Surgical treatment for POAG can be either incisional or laser based.

The most common surgical intervention for the treatment of POAG is trabeculectomy, where a portion of the TM outflow pathway is removed, creating a new pathway for AH outflow, with the hope of increasing outflow and reducing outflow resistance (67). This procedure carries potential risk, as do all surgical procedures. There is a risk of infection, and scars could form at the TM surgical site, causing blockage of the newly formed outflow pathway (70). A less invasive form of surgery, that does not penetrate the outflow pathway itself, can be carried out instead of a trabeculectomy. Examples of such surgeries include deep sclerectomy, where a portion of the sclera is removed, viscocanalostomy, where viscous gel is injected directly into SC lumen to open up the canal and create a channel from SC to the scleral reservoir and canaloplasty, where the SC lumen is threaded with a catheter and injected with viscoelastic gel, while a suture holds SC open. These less invasive forms of surgery do not have the same IOP lowering effects as a trabeculectomy, but have less severe side effects (114). Surgical devices can also be inserted directly into the outflow pathway to increase AH outflow drainage across the sclera and stents can be inserted to bypass the area of greatest AH outflow resistance. This functions by connecting the outer TM to SC lumen (67).

Laser trabeculectomy exposes the TM to an argon laser, eradicating the need for surgical incision. The exact mechanism by which laser trabeculectomy lowers IOP is not

fully understood, but there are several hypotheses. One theory posed is that the heat energy produced from the laser causes TM tissue damage, which leads to contraction of collagen fibres. This would cause surrounding tissues to stretch, in turn widening the TM and increasing AH outflow. Another theory is that ECM remodelling occurs in the TM, following a laser induced cytokine response (115). In one pilot study, laser trabeculectomy reduced IOP by at least 5 mmHg in 89% of treated eyes (116).

Novel treatments for POAG

As mentioned above, more effective drugs directly targeting the conventional outflow pathway are needed. Drugs targeting the JCT region or the cytoskeleton of cells present in the outflow pathway are under review. One example of such drugs are the rho kinase (ROCK) inhibitors, which have already been approved for use in Japan (Fasudil and Ripasudil) and China (Fasudil). ROCK inhibitors have the potential to reduce IOP and increase AH outflow facility. The mechanism by which this occurs is through expansion of the TM, SC, JCT and episcleral veins (117). ROCK inhibitor Y-27632 has been shown to produce a significant reduction of actin stress fibres in the cytoskeleton of both TM and SC cell cultures (118). ROCK inhibitors may have neuroprotective properties (119, 120) and have been shown to increase AH outflow facility (121, 122). A recent study by Li et al. (2021) reported a significant reduction in IOP in patients with OHT and in a cohort of glucocorticoid (GC)-induced mouse model of OHT, following administration with Netarsudil ROCK inhibitor eye drops 2-3 times per week for 4 weeks (123). Treatment with Netarsudil also decreased expression of fibrotic markers α-smooth muscle actin (α-SMA) and fibronectin, showing anti-fibrotic properties capable of restoring outflow facility function and reducing IOP in these mice (123). To have a drug on the market that not only lowers IOP but potentially prevents RGC death and optic nerve atrophy, is very exciting. A

number of ROCK inhibitors are currently undergoing clinical trials and the potential for these drugs in POAG therapy is clearly evident.

Investigation into the effects of prostaglandins has uncovered further insights into the prostanglandin pathway. This has resulted in the development of drugs that include nitric oxide-donating prostaglandin F2-analogues. These drugs induce increased AH outflow drainage through both the conventional and unconventional pathways. The TM appears to relax following nitric oxide (NO) treatment and reduced actin stress fibres together with vinculin at local adhesion points in one study (124). Interest in the development of EP_2 and EP_4 receptor agonists as a treatment for POAG has grown rapidly. In this regard, an EP_2 agonist has been shown to reduce IOP and to increase outflow facility in both pathways, by relaxing SC cells and decreasing contractility and collagen deposition in TM tissue (124-126). An EP_4 agonist has also been shown to be effective for the treatment of POAG, with increased outflow facility observed, facilitated by the TM and SC (127). It is notable that EP_4 receptors are known to influence MMP expression and hence could be very effective in reducing ECM deposition in POAG (128).

There are also a number of siRNA therapies currently undergoing clinical trial for the treatment of POAG. The mechanism by which these siRNA treatments work is similar to that of beta blockers, mentioned above. They inhibit beta2-adrenergic receptors at the ciliary body, reducing AH production. Studies showed that siRNA, administered through ocular injection, was only present in ocular tissues and so systemic effects might be minimized (129, 130). In a study carried out at this laboratory reported that a once-off intracameral inoculation of siRNA, targeting tight junction (TJ) proteins Zonula occludens-1 (ZO-1) and tricellulin in SC endothelia, resulted in increased outflow facility and reduced IOP in normotensive mice (131). This siRNA-based approach to treatment has also been shown to significantly increase AH outflow and decrease IOP in a steroid induced rodent

model of OHT, a study which is reported in Chapter 3 of this thesis (and was accepted for publication, Appendix 2) (132).

Patient compliance with drug administration is one of the biggest problems encountered by physicians. Long-lasting medication would therefore be of greater benefit to patients. Examples of novel longer-lasting drug treatments currently under investigation are drugs encapsulated by nanospheres, slow release implants, plugs or rings to deliver topical medications to the punctum or conjunctiva respectively (133, 134).

Viral gene delivery has also been used to target the outflow pathway. Adeno-associated viruses (AAVs) are currently the most widely used gene therapy vector system. In its natural state AAV is an innate human virus integrated into the human genome at chromosome 19 and will only replicate when adenoviral (AV) helper functions are present. It is minimally immunogenic, even at high doses (135, 136). AAVs have been used extensively for human trials of gene therapies for retinopathies, especially Leber congenital amaurosis (LCA) and retinitis pigmentosa (RP). AAVs usually have a single stranded DNA genome that generates a second strand of DNA from using host functions. When a second, self-complimentary strand of DNA was inserted into these vectors (scAAV), the virus showed increased transduction efficiency. There is a disadvantage however, with a reduction in size of their DNA handling capabilities (137). Standard AAVs successfully transfect the outflow pathway, but don't appear to be actually expressed in cells of the outflow pathway. High efficacy expression has been shown however, following the use of scAAV. Widespread safe and long-term transfection has been shown in the TM following a once-off intracameral inoculation with GFP-expressing scAAV2 in both rats and non-human primates (138). A successful viral delivery system, following a once-off inoculation, would be the most beneficial form of treatment to combat patient incompliance.

Summary

The aim of this introductory chapter has been to describe the process of AH dynamics along the outflow pathway and how this can be affected in glaucoma pathology. Various mechanical and biological changes can occur to tissues of the outflow pathway in this disease and have the potential to disrupt the natural flow and production of AH. This can result in reduced AH outflow, elevated IOP and long-term damage to the retina and ONH. Different types of glaucoma have been discussed along with epidemiology and various risk factors. Focusing on POAG in particular, current medical and surgical treatments were discussed, along with potential novel treatments currently in the pipeline.

It has been emphasised that there is a current unmet clinical need for direct targeting of tissues of the outflow pathway themselves. There is also a fundamental need to fully characterise and compare both glaucomatous and healthy tissues of the outflow pathway, in order to fully understand what is occurring to these cells once they become glaucomatous in phenotype. This would prove to be beneficial when exploring potential therapeutic intervention for such tissues. A study exploring the *in vitro* changes occurring in glaucomatous human SCEC will be presented in the next chapter.

Chapter 2

In vitro exploration of glaucomatous changes in Schlemm's Canal Endothelial Cells

Abstract

Previous studies have shown that glaucomatous SCEC are stiffer and less porous in phenotype compared to healthy SCEC. They have also been shown to express increased ECM material and show altered ECM gene expression compared to healthy cells. The AH of glaucoma patients contains an abundance of TGF-β2, a known driver of fibrosis. In this study the possibility of fibrotic-like changes occurring at the inner wall of Schlemm's canal in glaucoma was explored. Glaucomatous SCEC showed altered expression of normal endothelial cell characteristics and expressed a more fibrotic phenotype. In addition, glaucomatous SCEC displayed increased expression of fibrotic α-SMA and adhesion VE-cadherin markers, associated with an increase in cell size, cell migration and proliferation and evidence of mitochondrial dysfunction compared to healthy SCEC. All of these changes have the potential to negatively affect IOP and AH outflow facility. Treatment of healthy SCEC with TGF-β2 resulted in many similarities to those found in glaucomatous SCEC.

Introduction

As outlined in the introduction, tissues of the outflow pathway show various differences when cells comprising such tissues become glaucomatous in phenotype. Greater amounts of ECM are present in TM and SC cells, resulting in increased cell stiffness, reduced pore density and an increase in cytokines, summarised by Johnstone et al. (2020) (139). In order to further understand changes that occur to tissues of the outflow pathway in glaucoma, it is important to investigate such at a cellular level. In this chapter, a comparative investigation of cellular and morphological properties of normal and glaucomatous human SCEC will be presented.

Working on the hypothesis that glaucomatous human SCEC have a reduced tendency to express healthy endothelial cell markers, instead expressing more fibrotic characteristics, such cells would then no longer be classifiable as healthy endothelial cells, but more mesenchymal/fibrotic in nature, and undergoing endothelial to mesenchymal-like transition. Should such characteristics be observed in glaucomatous SCEC, then exploration of treatments focusing on an anti-fibrotic element would be warranted. Hence, the focus of this chapter has been to explore the physical, morphological and molecular differences between glaucomatous and healthy SCEC.

Pore formation at the inner wall of Schlemm's canal

AH filtration through micrometre-sized pores located in the inner wall endothelia of SC has an important role in AH outflow dynamics. The size of vacuoles and number of pores in this region can have a significant impact on AH flow rates (140). Pore formation is a typical feature of healthy SCEC (141) and reduced ability to form pores can have a significant impact on IOP and outflow facility (142). In glaucoma, SCEC have been shown to be less porous, which may lead to an increase in IOP and outflow resistance (143, 144).

Glaucomatous SCEC are stiffer than cells from a healthy individual (145, 146). Overexpression of connective tissue growth factor (CTGF) has been shown to increase IOP and cause ON damage observed in glaucomatous tissue, which may be related to fibrosis, potentially resulting in increased outflow resistance and elevated IOP (147). Genes differently expressed in several pathways have been identified in SCEC, including those related to cell adhesion, heparin binding, glycosaminoglycan binding and ECM, all of which may contribute to fibrosis and decreased pore formation in glaucomatous SCEC (148).

Transforming growth factor-beta 2 (TGF-β2)

Elevated expression of TGF-β2 has been reported in the AH of glaucoma patients (74, 149-151). TGF-β is a major driving force of fibrosis (152) and can therefore have a severe impact on tissues of the outflow pathway in such patients (150, 153). Fibrosis is the term given to disruption of the normal structural components that form tissue (154). It involves the accumulation of ECM proteins, which results in the formation of non-functional scar tissue (155). It has been hypothesised that progressive fibrosis along the outflow pathway, specifically the TM, could account for the severe damage in outflow tissues observed in glaucoma pathology (156). Characteristic features of fibrosis found in glaucomatous TM regions include increased ECM and increased expression of TGF-β and of mesenchymal markers, including α-SMA (157, 158). Several *in vitro* studies have shown that TM cells treated with TGF-β2 show elevated expression of collagens, fibronectin, actin stress fibres, thrombospondin-1, lysyl oxidase, transglutaminase and plasminogen activator inhibitor-1 (PAI-1) (159-163). These results indicate that changes in ECM material as well as alterations to cytoskeletal proteins occur in these cells following treatment with TGF-β2 (164). It has also been shown that treating anterior segments *ex vivo* with TGF-β2, for just over a week, reduced outflow facility by 27% and affected the ECM structure of the TM (76). Many of

these studies link the activity of TGF-β2 to the upregulation of ECM deposition and in turn increased IOP and reduced outflow facility (76, 159).

TGF-β2 also induces the formation of cross-linked actin networks (CLANs), which are a morphological characteristic of glaucoma in both TM and LC cells (165, 166). α-SMA is a key component of these CLANs (167). The formation of these CLANs, along with changes in cytoskeletal protein expression, could be a major contributor to the increase in cell stiffness observed in glaucomatous TM tissue (168). The expression of α-SMA in TM cells has been reported to have an influence on the differentiation of these cells towards a myofibroblast-like cell type (158). Tissue injury is the main driving force behind the transformation of dormant tissue-resident cells into a mesenchymal-like cell phenotype, called myofibroblasts. This process involves the formation of these α-SMA stress fibres (169). Myofibroblasts produce large amounts of ECM proteins, such as collagen-I, fibronectin and MMPs, which contribute towards the scarring of the wound (170). Considering age as a major risk factor for glaucoma, as well as increased ECM components and cell stiffness with age, fibrosis may play a more prevalent role in the development of glaucoma than previously thought. Both fibroblast and myofibroblast-like expression patterns have recently been observed in healthy TM cells using single-cell RNA sequencing technique (171). SC endothelia also display a unique combination of lymphatic/blood vascular gene expression profiles (171). This study provided a more comprehensive understanding of both the molecular and cellular classifications of these tissues of the conventional outflow pathway (171).

Endothelial-mesenchymal transition (EndMT)

It has been established that epithelial-mesenchymal transition (EMT) can occur in TM cells (157). This study showed that TM cells exposed to collagen-I, fibronectin and laminin *in vitro* resulted in the dissociation of cell-cell contact and elongation of actin stress fibres.

Following the same stimulation with ECM proteins, the expression of mesenchymal markers such as fibronectin and α-SMA was observed in TM cells. This study raised the concept that EMT may occur in TM cells of glaucomatous patients. However, since TM cells are not epithelial in nature, the myofibroblast trans-differentiation cannot be classified as EMT in the strictest sense, but has been described to display EMT-like features, owing to the loss of cell-cell contact, mesenchymal-like phenotype, increase in cell motility, upregulation of ECM materials and phosphorylation of TGF-β signalling molecules (157).

Endothelial-mesenchymal transition (EndMT) is a variant of EMT but involves endothelial cells instead (172). Exposing such cells to TGF-β can result in the progression of EndMT, resulting in increased expression of α-SMA and abnormal ECM secretion (173). The transition of healthy endothelial cells to a mesenchymal-like state results in the loss of healthy endothelial properties such as pore formation and in turn, a gain of fibrotic-like characteristics, including expression of fibrotic markers, increased cell stiffness and increased ECM stiffness (174, 175).

Increased levels of TGF-β2 have been found in the AH of glaucoma patients (149, 176). Tissues of the outflow pathway, including SC inner wall, are exposed to such AH. It is therefore plausible that TGF-β2-induced EndMT can occur in the endothelial cells along the inner wall of SC particularly, since comparable changes are known to occur in the TM (158, 177, 178).

Endothelial, fibrotic and tight junction markers

To begin this study, relative transcript and protein expressions of various endothelial and fibrotic markers were investigated. The endothelial markers chosen were von Willebrand factor (vWF), VE-cadherin and vinculin. Endothelial cells line both blood and lymphatic vessels and so can be classified as vascular or lymphatic cell markers. vWF, VE-cadherin and vinculin are all vascular endothelial cell markers. vWF mediates platelet aggregation

and adhesion. High levels of vWF have been shown to reflect endothelial dysfunction in vascular disorders (179). VE-cadherin mediates endothelial adhesion and is important for blood vessel development and permeability (180). Vinculin is a cytoskeletal protein associated with cell-cell and cell-matrix adhesion (181).

The fibrotic markers chosen were α-SMA, TGF-β2 and collagen I-α1. As mentioned above, an increase in α-SMA stress fibres have been observed in TM tissue of the outflow pathway in glaucoma (147). Elevated levels of TGF-β2 have also been shown in AH samples of glaucoma patients and so should show elevated expression in tissues of the outflow pathway (182). While TGF-β2 is not a fibrotic marker in the strictest sense but more a profibrotic marker and driver of fibrosis. SCEC treated with TGF-β2 is a positive control sample in this case. Collagen I-α1 is a known ECM pro-fibrotic marker associated with heart failure and so was of interest when investigating whether these cells were undergoing fibrotic changes (183).

Glaucomatous TM cells have previously shown increased expression of TJ protein ZO-1 (184). Steroid-induced glaucoma patients also show increased expression of TJ proteins ZO-1 in TM cells (185). TJ proteins are located in the intercellular spaces between endothelial cells and increased expression of these TJ proteins in glaucomatous cells potentially promotes increased AH outflow resistance, observed in POAG (131). Targeting these TJ proteins, using siRNA therapeutics, showed a significant increase in AH outflow facility and decrease in IOP in both normotensive and hypertensive dexamethasone (DEX)-treated mice (131, 132). Protein and transcript expression of TJ proteins ZO-1 and tricellulin were also investigated in this study.

The aim of this chapter was to investigate and compare the changes observed in both healthy and glaucomatous SCEC *in vitro*. The hypothesis was that glaucomatous SCEC undergo fibrotic/mesenchymal changes and so various endothelial and fibrotic markers were assessed. Various cellular and morphological changes were also investigated, using a

number of assays, as well as mitochondrial activity. Healthy SCEC treated with TGF-β2 was used as a positive control, as glaucomatous SCEC from patient donors have been treated with a variety of IOP lowering drugs.

Results

Three groups of cells were investigated in this project: healthy untreated SCEC (SC), SCEC treated with 10 ng/mL of TGF-β2 for 48 hr (SC+TGF-β2) and glaucomatous SCEC (SCg). More information on TGF-β2 treatment and patient information can be found in the Materials and Methods section (Chapter 6). Healthy SC cells were acquired from 5 patient donors (n=5). TGF-β2 treatment was carried out on healthy SC cells from 3 patient donors (n=3) and glaucomatous SC cells were acquired from 3 patient donors (n=3).

A. Characterisation of endothelial cell markers

Relative mRNA transcript expression (left) and relative protein expression (right) of endothelial cell markers vWF, VE-cadherin and vinculin are shown below (Figure 2.1). An increase in vWF transcript expression of 0.1 [-1.3, 1.4] and 0.2 [-1.1, 1.5] fold change, (mean [confidence interval (CI)], $p > 0.05$, 1-way ANOVA with Tukey's multiple comparisons post-test, n=5 for SC, n=3 for SC+TGF-β2 and n=3 for SCg) was observed in both SC+TGF-β2 and SCg respectively, compared to SC. An increase in vWF protein expression of 0.4 [-0.5, 1.2] and 0.0 [-0.8, 0.9] fold change, ($p > 0.05$, 1-way ANOVA with Tukey's multiple comparisons post-test, n=5 for SC, n=3 for SC+TGF-β2 and n=3 for SCg) was observed in SC+TGF-β2 and SCg respectively, compared to SC. Neither were statistically significant.

An increase in VE-cadherin transcript expression of 0.2 [-1.7, 2.0] and 0.8 [-1.1, 2.7] fold change ($p > 0.05$, 1-way ANOVA with Tukey's multiple comparisons post-test, n=5 for SC, n=3 for SC+TGF-β2 and n=3 for SCg) was observed in SC+TGF-β2 and SCg respectively, compared to SC. A significant increase in VE-cadherin protein expression of 3.7 [-0.8, 6.7] and 3.6 [-1.0, 6.2] fold change ($p < 0.05$, 1-way ANOVA with Tukey's multiple comparisons post-test, n=5 for SC, n=3 for SC+TGF-β2 and n=3 for SCg) was observed in SCg compared to SC+TGF-β2 and SC, respectively.

A decrease in vinculin transcript expression of 0.2 [-0.8, 1.2] and 0.4 [-0.7, 1.4] fold change ($p > 0.05$, 1-way ANOVA with Tukey's multiple comparisons post-test, n=5 for SC,

n=3 for SC+TGF-β2 and n=3 for SCg) was observed in SC+TGF-β2 and SCg respectively, compared to SC. An increase in vinculin protein expression of 0.3 [-0.4, 1.1] and 0.4 [-0.4, 1.1] fold change ($p > 0.05$, 1-way ANOVA with Tukey's multiple comparisons post-test, n=5 for SC, n=3 for SC+TGF-β2 and n=3 for SCg) was observed in SC+TGF-β2 and SCg respectively, compared to SC. All samples were normalised to GAPDH housekeeping gene. GAPDH expression for each cell group was explored and there was no difference observed between them.

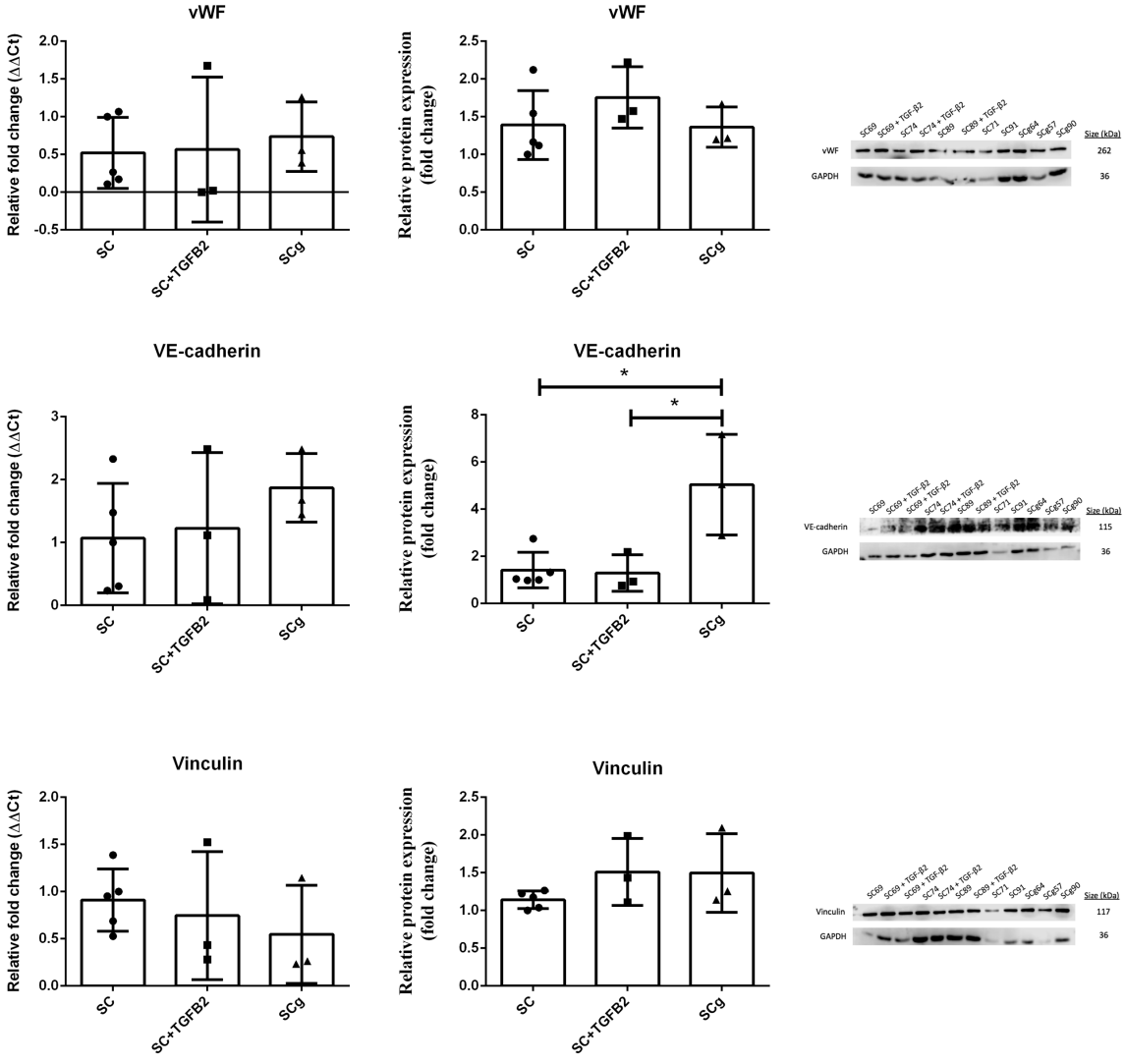

Figure 2.1: Relative mRNA transcript (left) and protein (right) expression of endothelial cell markers.

The change in both transcript (left) and protein (right) expression of endothelial cell markers vWF, VE-cadherin and vinculin between SC, SC+TGF-β2 and SCg is displayed above. A

significant increase in VE-cadherin protein expression was observed in SCg cells compared to both healthy SC and SC+TGF-β2 treated cells ($p < 0.05$ for both, 1-way ANOVA with Tukey's multiple comparisons post-test, n=5 for SC, n=3 for SC+TGF-β2 and n=3 for SCg). No significant change in vWF or vinculin transcript and protein expression was observed between the groups ($p > 0.05$ for both, 1-way ANOVA with Tukey's multiple comparisons post-test, n=5 for SC, n=3 for SC+TGF-β2 and n=3 for SCg). Mean +/- SD is shown above. Each individual data point represents a different biological sample in each group.

B. <u>Characterisation of fibrotic markers</u>

Relative mRNA transcript (left) and protein (right) expression of fibrotic markers α-SMA, TGF-β2 and collagen I-α1 are shown below (Figure 2.2). Biological n=5, 3 and 3 was used for SC, SC+TGF-β2 and SCg samples respectively, and statistical analysis was carried out using one-way ANOVA with Tukey's multiple comparisons post-test.

An increase in α-SMA transcript expression of 2.7 [-0.7, 6.2] and 2.6 [-0.8, 6.0] fold change ($p > 0.05$, 1-way ANOVA with Tukey's multiple comparisons post-test, n=5 for SC, n=3 for SC+TGF-β2 and n=3 for SCg) was observed in SC+ TGF-β2 and SCg respectively, compared to SC. An increase in α-SMA protein expression of 5.1 [-5.1, 15.2] and 9.0 [-1.2, 19.2] fold change ($p > 0.05$, 1-way ANOVA with Tukey's multiple comparisons post-test, n=5 for SC, n=3 for SC+TGF-β2 and n=3 for SCg) was also observed in SC+ TGF-β2 and SCg respectively, compared to SC.

An increase in TGF-β2 transcript expression of 1.0 [-1.2, 3.1] and 1.0 [-1.1, 3.1] fold change ($p > 0.05$, 1-way ANOVA with Tukey's multiple comparisons post-test, n=5 for SC, n=3 for SC+TGF-β2 and n=3 for SCg) was observed in SC+ TGF-β2 and SCg respectively, compared to SC. An increase in TGF-β2 protein expression of 3.0 [-6.0, 12.1] and 4.4 [-4.7, 13.4] fold change ($p > 0.05$, 1-way ANOVA with Tukey's multiple comparisons post-test,

n=5 for SC, n=3 for SC+TGF-β2 and n=3 for SCg) was also observed in SC+ TGF-β2 and SCg respectively, compared to SC.

An increase in collagen I-α1 transcript expression of 1.5 [-1.0, 3.9] and 0.4 [-2.1, 2.9] fold change ($p > 0.05$, 1-way ANOVA with Tukey's multiple comparisons post-test, n=5 for SC, n=3 for SC+TGF-β2 and n=3 for SCg) observed in SC+ TGF-β2 and SCg respectively, compared to SC. A decrease in collagen I-α1 protein expression of 0.0 [-1.1, 1.1] and 0.6 [-0.5, 1.6] fold change ($p > 0.05$, 1-way ANOVA with Tukey's multiple comparisons post-test, n=5 for SC, n=3 for SC+TGF-β2 and n=3 for SCg) observed in SC+ TGF-β2 and SCg respectively, compared to SC.

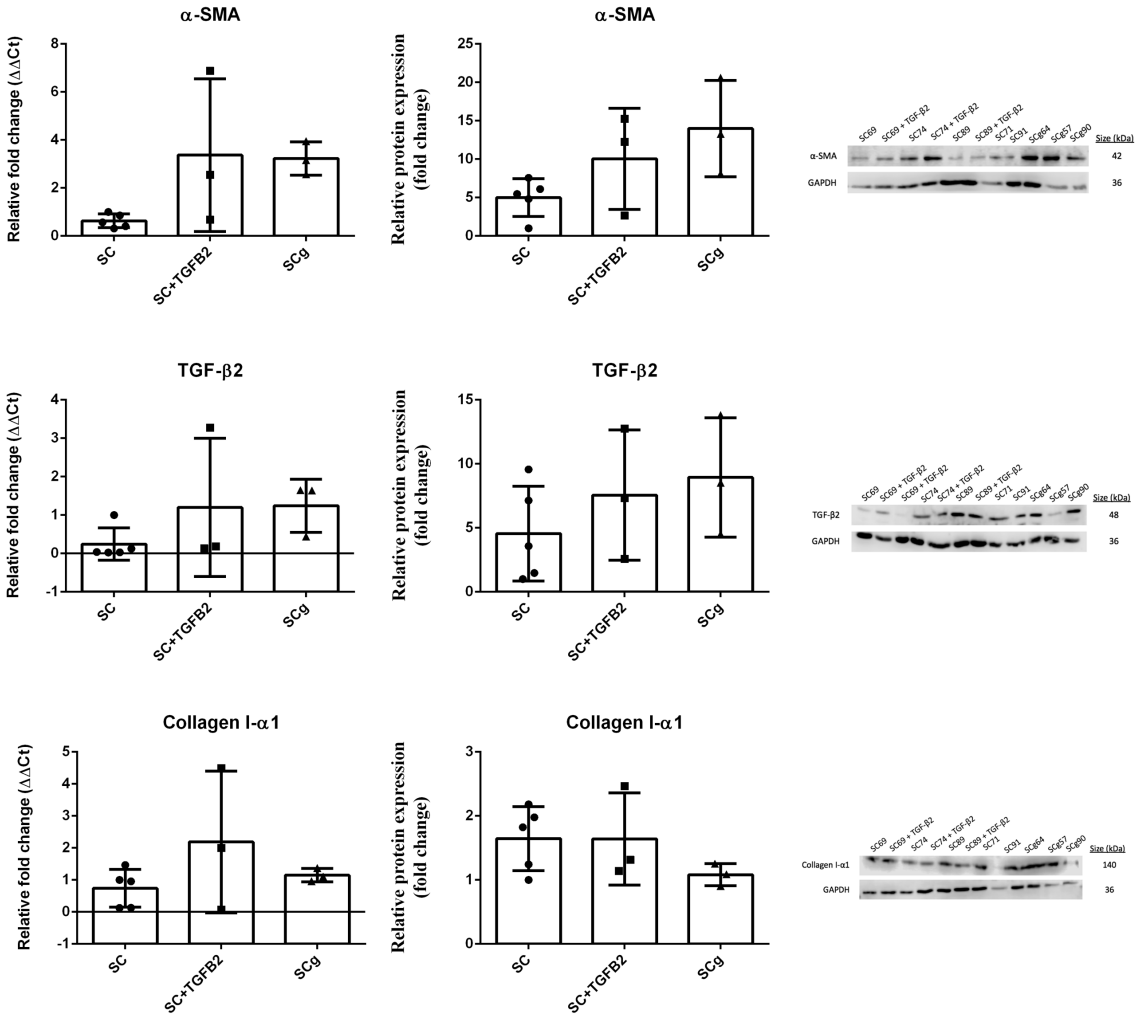

Figure 2.2: Relative mRNA transcript (left) and protein (right) expression of fibrotic markers.

The change in both transcript (left) and protein (right) expression of fibrotic cell markers α-SMA, TGF-β2 and collagen I-α1 between SC, SC+TGF-β2 and SCg is displayed above. While statistical significance was not reached, an increase in both α-SMA and TGF-β2 transcript and protein expression was observed in both SC+TGF-β2 and SCg compared to healthy SC cells ($p > 0.05$, 1-way ANOVA with Tukey's multiple comparisons post-test, n=5 for SC, n=3 for SC+TGF-β2 and n=3 for SCg). No significant change in collagen I-α1 transcript or protein expression was observed between the groups ($p > 0.05$, 1-way ANOVA with Tukey's multiple comparisons post-test, n=5 for SC, n=3 for SC+TGF-β2 and n=3 for SCg). Mean +/- SD is shown above. Each individual data point represents a different biological sample in each group.

C. Characterisation of tight junction proteins ZO-1 and Tricellulin

Relative mRNA transcript (left) and protein (right) expression of tight junction proteins ZO-1 and tricellulin are shown below (Figure 2.3). Biological n=5, 3 and 3 was used for SC, SC+TGF-β2 and SCg samples respectively, and statistical analysis was carried out using one-way ANOVA with Tukey's multiple comparisons post-test.

A significant increase in ZO-1 transcript expression of 1.7 [0.8, 2.6] and 1.6 [0.6, 2.5] fold change ($p < 0.05$, 1-way ANOVA with Tukey's multiple comparisons post-test, n=5 for SC, n=3 for SC+TGF-β2 and n=3 for SCg) was observed in SCg compared to SC and SC+TGF-β2, respectively. A significant increase in ZO-1 protein expression of 5.8 [-0.7, 10.9] fold change ($p < 0.05$, 1-way ANOVA with Tukey's multiple comparisons post-test, n=5 for SC, n=3 for SC+TGF-β2 and n=3 for SCg) was also observed in SCg compared to SC+TGF-β2. However, a decrease in protein expression of 3.6 [-0.9, 8.2] fold change ($p > 0.05$, 1-way ANOVA with Tukey's multiple comparisons post-test, n=5 for SC, n=3 for SC+TGF-β2 and n=3 for SCg) was observed in SC compared to SCg.

An increase in tricellulin transcript expression of 0.7 [-0.5, 1.8] fold change (p > 0.05, 1-way ANOVA with Tukey's multiple comparisons post-test, n=5 for SC, n=3 for SC+TGF-β2 and n=3 for SCg) was observed in SCg compared to SC. However, a decrease in tricellulin protein expression of 2.2 [-7.5, 3.2] fold change (p > 0.05, 1-way ANOVA with Tukey's multiple comparisons post-test, n=5 for SC, n=3 for SC+TGF-β2 and n=3 for SCg) was observed in SCg compared to SC. No real change in tricellulin transcript or protein expression of 0.3 [-0.9, 1.4] and 0.2 [-5.1, 5.6] fold change (p > 0.05, 1-way ANOVA with Tukey's multiple comparisons post-test, n=5 for SC, n=3 for SC+TGF-β2 and n=3 for SCg) was observed between SC and SC+TGF-β2, respectively

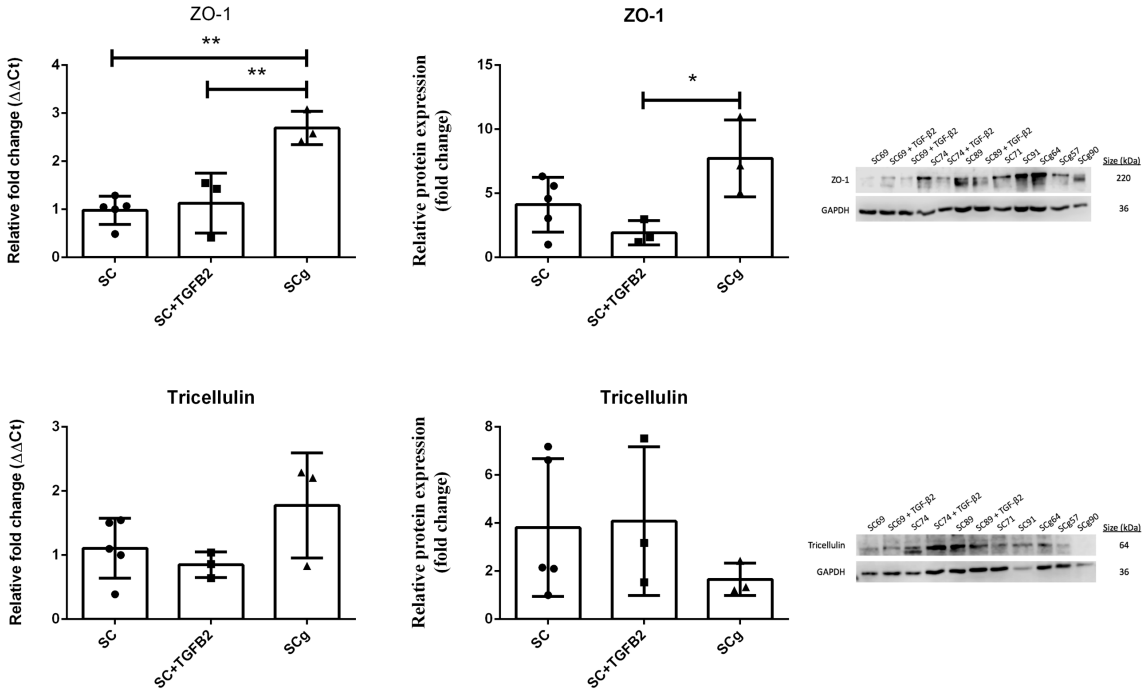

Figure 2.3: Relative mRNA transcript (left) and protein (protein) expression of TJ proteins ZO-1 and tricellulin.

The change in both transcript (left) and protein (right) expression of tight junction proteins ZO-1 and tricellulin between SC, SC+TGF-β2 and SCg is displayed above. A significant increase in ZO-1 transcript and protein expression was observed in SCg cells compared to SC+TGF-β2 cells ($p < 0.01$ and $p < 0.05$ respectively, 1-way ANOVA with Tukey's multiple comparisons post-test, n=5 for SC, n=3 for SC+TGF-β2 and n=3 for SCg). A significant

increase in ZO-1 transcript expression was observed in SCg compared to healthy SC cells ($p < 0.01$, 1-way ANOVA with Tukey's multiple comparisons post-test, n=5 for SC, n=3 for SC+TGF-β2 and n=3 for SCg). No significant change in tricellulin transcript or protein expression was observed between the groups ($p > 0.05$, 1-way ANOVA with Tukey's multiple comparisons post-test, n=5 for SC, n=3 for SC+TGF-β2 and n=3 for SCg). Mean +/- SD is shown above. Each individual data point represents a different biological sample in each group.

D. Immunocytochemistry showing protein expression of α-SMA and F-actin

Immunocytochemistry (ICC) is another technique that can be used to visualise protein expression. Unlike the western blot technique, it is more difficult to quantify protein expression this way, but it is a visual representation of protein expression in cells to go alongside quantified western blot data. Both α-SMA and filamentous actin (F-actin) protein expression can be seen below (Figure 2.4). F-actin is a cytoskeletal protein and Phalloidin is used to counter stain this, alongside α-SMA protein expression. α-SMA and F-actin expression of healthy SCEC are shown in panels A and D respectively. SCEC treated with 10 ng/mL TGF-β2 for 48 hr are shown in panels B and E and glaucomatous SCEC are shown in panels C and F. An increase in α-SMA protein expression is seen in both TGF-β2 treated cells (B) and glaucoma SCEC (C), compared to healthy SCEC (A). This further strengthens the protein quantification data in Figure 2.2, where an increase in both protein and mRNA expression of α-SMA is observed in both SCEC treated with TGF-β2 and glaucomatous SCEC compared to healthy SCEC. F-actin cytoskeletal protein expression appears to be increased in glaucomatous SCEC (F) compared to healthy SCEC (D). F-actin expression does not appear to be significantly increased in SCEC treated with TGF-β2 (E) however, compared to healthy SCEC (D).

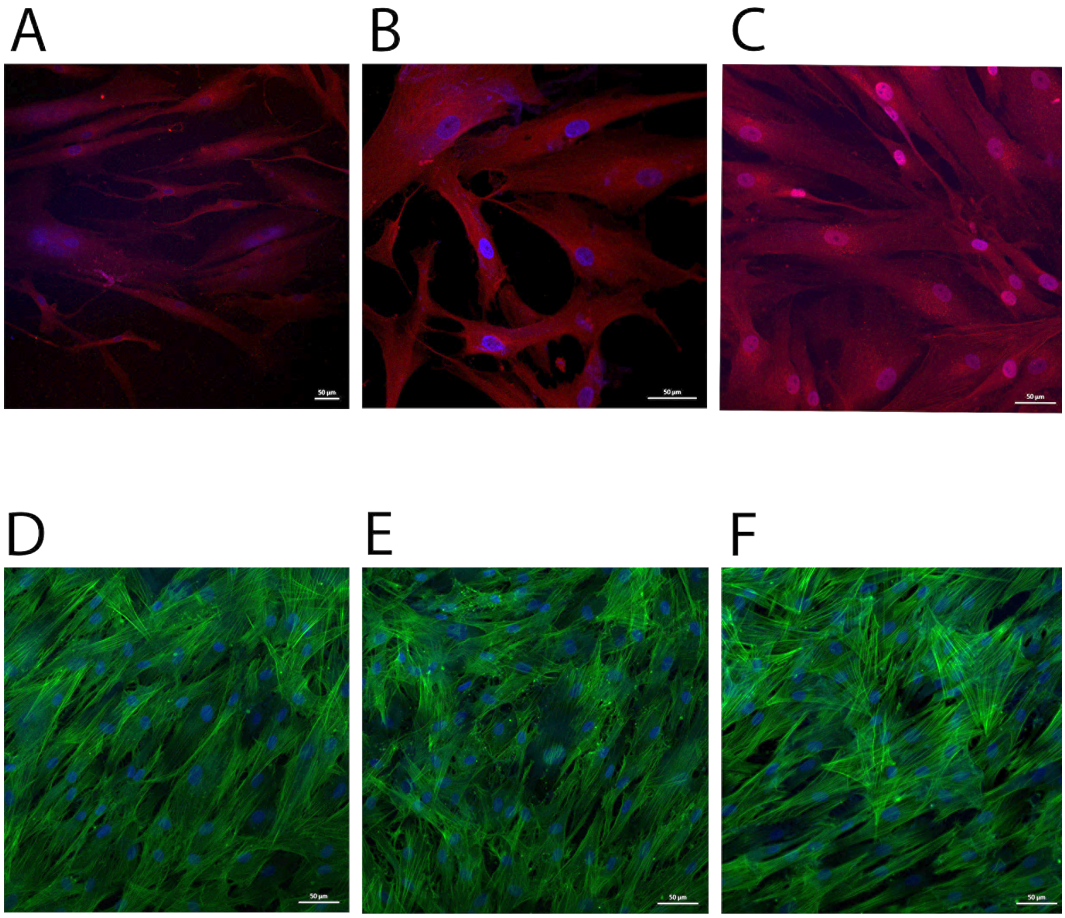

Figure 2.4: Immunocytochemistry showing α-SMA (top) and F-actin (bottom) protein expression.

α-SMA protein expression of healthy SCEC (A), SCEC treated with 10 ng/mL of TGF-β2 for 48 hr (B) and glaucomatous SCEC (C) is shown in the top panel. F-actin protein expression of healthy SCEC (D), SCEC treated with 10 ng/mL of TGF-β2 for 48 hr (E) and glaucomatous SCEC (F) is shown in the bottom panel. An increase in both α-SMA and F-actin protein expression is apparent in both SC+TGF-β2 and SCg compared to healthy SC cells. Cell size and density appear larger in SCg compared to SC cells. Scale bar represents 50 μm.

E. Ionic and paracellular permeability of SC monolayer using TEER and flux assays

Cell permeability of a monolayer of cells in culture is determined by transendothelial electrical resistance (TEER) values and flux assays. These assays determine any changes in

ionic and paracellular macromolecular permeability respectively. TEER values were taken at both 24 and 48 hr post treatment. 1-way ANOVA with Tukey's multiple comparisons post-test was carried out to compare the mean values of each group. In these experiments, treatment with TGF-β2 showed no significant increase in TEER values between SC and SC+TGF-β2 at both 24 hr (0.3 [-3.2, 3.7] ohms.cm^2 ($p > 0.05$, 1-way ANOVA with Tukey's multiple comparisons post-test, n=6) and 48 hr post treatment (0.1 [-3.1, 3.4] ohms.cm^2 ($p > 0.05$, 1-way ANOVA with Tukey's multiple comparisons post-test, n=6) (Figure 2.5). SCg showed reduced TEER values at 24 hr post treatment compared to SC and SC+TGF-β2 of 1.4 [-2.0, 4.8] and 1.7 [-1.6, 4.9] ohms.cm^2 respectively, ($p > 0.05$, 1-way ANOVA with Tukey's multiple comparisons post-test, n=6). SCg also showed reduced TEER values at 48 hr post treatment compared to SC and SC+TGF-β2 of 1.5 [-1.9, 4.9] and 1.4 [-2.1, 4.8] ohms.cm^2 but neither was statistically significant ($p > 0.05$, 1-way ANOVA with Tukey's multiple comparisons post-test, n=6).

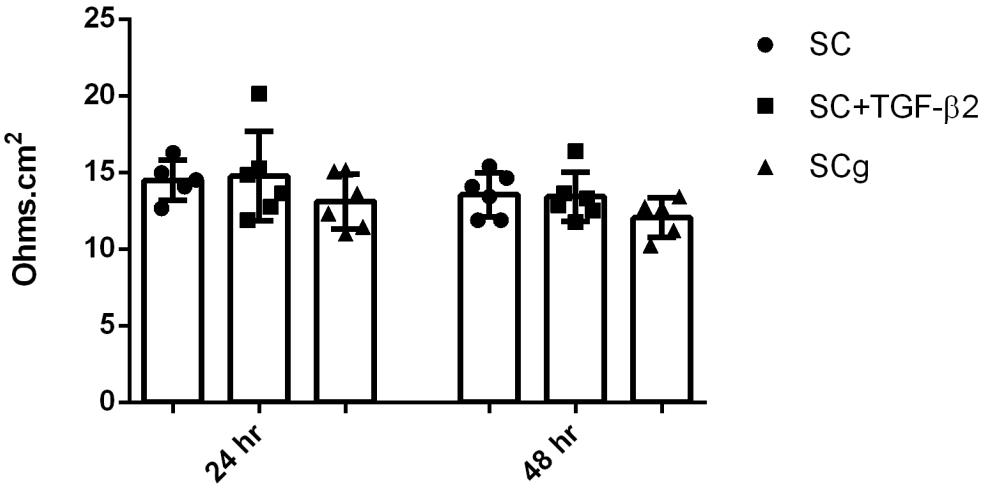

Figure 2.5: Transendothelial electrical resistance (TEER) in SC, SC+TGF-β2 and SCg cells.

Cells were grown to form a confluent monolayer and TEER values of SC, SC+TGF-β2 and SCg cells were then measured at 24 hr and 48 hr post treatment (with TGF-β2). SC treated with TGF-β2 showed no change in TEER values over time compared to untreated, healthy SC cells (p > 0.05, 1-way ANOVA with Tukey's multiple comparisons post-test, n=6). SCg

cells showed reduced TEER values compared to both untreated, healthy SC and SC+TGF-β2 at both time points, but neither was statistically significant (p > 0.05, 1-way ANOVA with Tukey's multiple comparisons post-test, n=6). Mean +/- SD is shown above.

FITC-Dextran flux assay was also undertaken and there was no significant difference in paracellular permeability between untreated SC and SC cells treated with TGF-β2 for 48 hr (p > 0.05, 1-way ANOVA with Tukey's multiple comparisons post-test, n=9 for both SC and SC+ TGF-β2) (Figure 2.6). However, there was a significant increase of 1.1 [0.3, 1.9] and 1.3 [0.4, 2.1] Papp in SCg compared to SC and SC+TGF-β2 respectively, ($p < 0.05$ and $p < 0.01$ respectively, 1-way ANOVA with Tukey's multiple comparisons post-test, n=9 for all) (Figure 2.6).

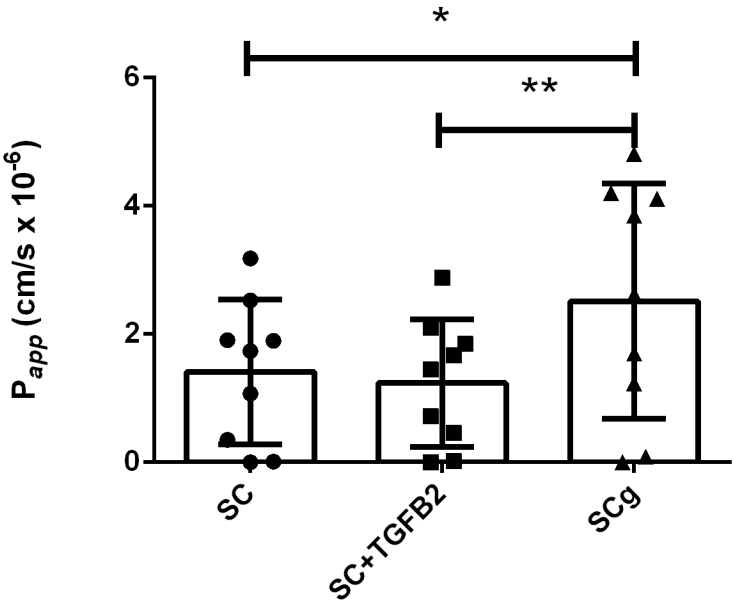

Figure 2.6: FITC-dextran flux assay in SC, SC+TGF-β2 and SCg cells.

FITC-dextran flux assay, using a 70kDa dextran, was carried following 48 hr TEER values to measure paracellular permeability in SC, SC+TGF-β2 and SCg cells. SC cells treated with TGF-β2 for 48 hr showed no significant change in paracellular permeability compared to untreated SC cells (p > 0.05, 1-way ANOVA with Tukey's multiple comparisons post-test, n=9 for both). However, SCg cells showed a significant increase in paracellular

permeability compared to both healthy ($p < 0.05$, 1-way ANOVA with Tukey's multiple comparisons post-test, n=9 for all) and TGF-β2 treated SC cells ($p < 0.01$, 1-way ANOVA with Tukey's multiple comparisons post-test, n=9 for all). Mean +/- SD is shown above with each individual data point (n=9) for each group.

F. SCEC proliferation assessed by MTS assays

MTS assays are used to assess cell proliferation, cell viability and cytotoxicity. The MTS assay is colorimetric assay based on the reduction of the MTS tetrazolium compound by viable mammalian cells to generate a coloured formazan dye that is soluble in cell culture media. This change in dye colour reflects the number of viable cells present. This MTS cell proliferation assay was carried out directly after the FITC-dextran flux assay above. MTS cell proliferation assay carried out on the three different cell groups showed increased relative cell proliferation rates in both SC+TGF-β2 cells of 1.4 [0.4, 2.5] ($p < 0.01$, 1-way ANOVA with Tukey's multiple comparisons post-test, n=10 for all groups) and SCg cells of 1.2 [0.1, 2.3] ($p < 0.05$, 1-way ANOVA with Tukey's multiple comparisons post-test, n=10 for all groups) compared to untreated healthy SC cells. It must be noted that these cells were all seeded at the same density and at the same time.

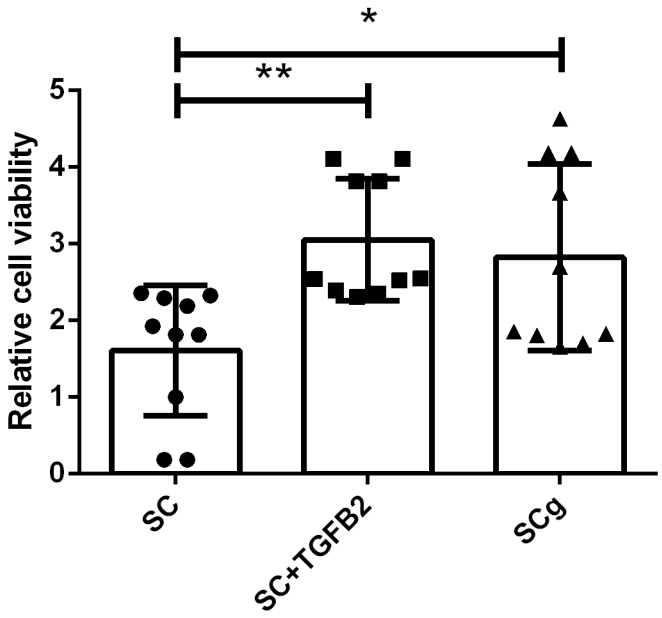

Figure 2.7: Relative cell proliferation of SC, SC+TGF-β2 and SCg cells.

MTS cell proliferation assay was carried out following FITC-dextran flux assay. A significant increase in cell proliferation was observed 48hr post treatment (with TGF-β2) in both SC+TGF-β2 ($p < 0.01$, 1-way ANOVA with Tukey's multiple comparisons post-test, n=10 for all groups) and SCg ($p < 0.05$, 1-way ANOVA with Tukey's multiple comparisons post-test, n=10 for all groups) compared to untreated heathy SC cells. These two groups were proliferating at a higher rate than untreated SC cells. Mean +/- SD is shown above with n=10 individual data points for each group.

G. Mitochondrial function in SCEC

Mitochondrial function was measured using the Agilent Seahorse XF Cell mitochondrial stress test (186). This test measures mitochondrial function in cells seeded onto the Seahorse plate by measuring the oxygen consumption rate (OCR) of these cells. The assay has injection ports that allow for the direct injection of respiration modulators while the assay is running. Basal level of respiration is first read before anything is added. The first modulator added is oligomycin, which inhibits ATP synthesis and in turn, reduces mitochondrial respiration (Figure 2.8). The second modulator added is FCCP, which is an uncoupling agent

that disrupts the mitochondrial membrane potential and results in a sharp increase in OCR. FCCP allows the mitochondria to reach its maximum OCR potential, under these conditions. Lastly, rotenone and antimycin A are both added, and these put a stop to mitochondrial respiration altogether in these cells. The difference between maximal and basal levels of respiration is known as the spare respiratory capacity (Figure 2.8).

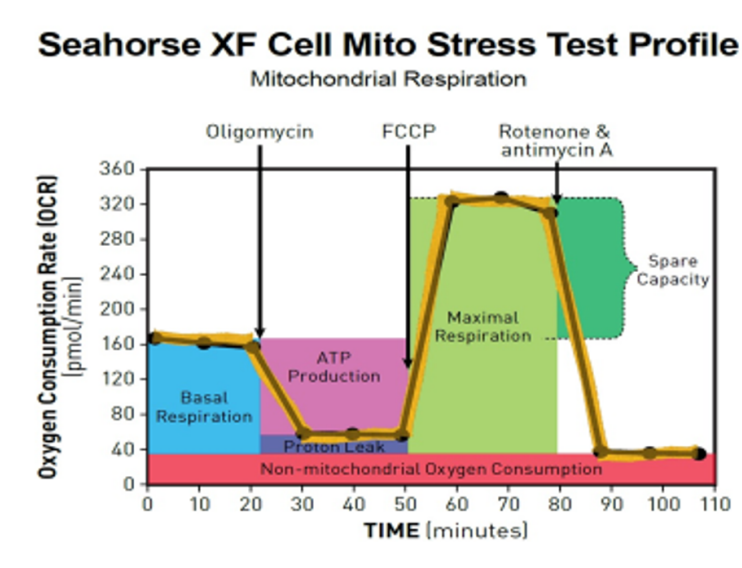

Figure 2.8: Overview of Seahorse mitochondrial stress test assay.

Various modulators of respiration are added directly to the cells throughout the course of the assay. This provides basal and maximal respiration readings, along with ATP production levels of the cells under investigation. The difference between the basal and maximal respiration levels is referred to as the spare respiratory capacity.

A mitochondrial stress test was carried out on SC, SC+TGF-β2 and SCg cells. The spare respiratory capacity and ATP production rates were calculated for each group and displayed as pmol/min below (Figure 2.9A). There was a significant decrease in spare respiratory capacity of 81.4 [50.5, 112.4] pmol/min in SC+TGF-β2 compared to SC cells ($p < 0.0001$, 1-way ANOVA with Tukey's multiple comparison post-test, n=6 and n=8 respectively) (Figure 2.9A). There was also a significant decrease in spare respiratory capacity of 68.2 [38.6, 97.9] pmol/min in SCg compared to SC cells ($p < 0.0001$, 1-way ANOVA with

Tukey's multiple comparison post-test, n=7 and n=8 respectively). There was no significant change in spare respiratory capacity between SCg and SC+TGF-β2 cells ($p > 0.05$, 1-way ANOVA with Tukey's multiple comparison post-test, n=7 and n=6 respectively).

There was a significant increase in ATP production of 27.0 [23.0, 30.9] pmol/min in SC+TGF-β2 compared to SC cells ($p < 0.0001$, 1-way ANOVA with Tukey's multiple comparison post-test, n=6 and n=8 respectively) (Figure 2.9B). There was also a significant decrease in ATP production of 25.8 [21.7, 29.9] pmol/min in SC+TGF-β2 cells compared to SCg cells ($p < 0.0001$, 1-way ANOVA with Tukey's multiple comparison post-test, n=6 and n=7 respectively). There was no significant difference in ATP production between SC and SCg cells ($p > 0.05$, 1-way ANOVA with Tukey's multiple comparison post-test, n=8 and n=7 respectively).

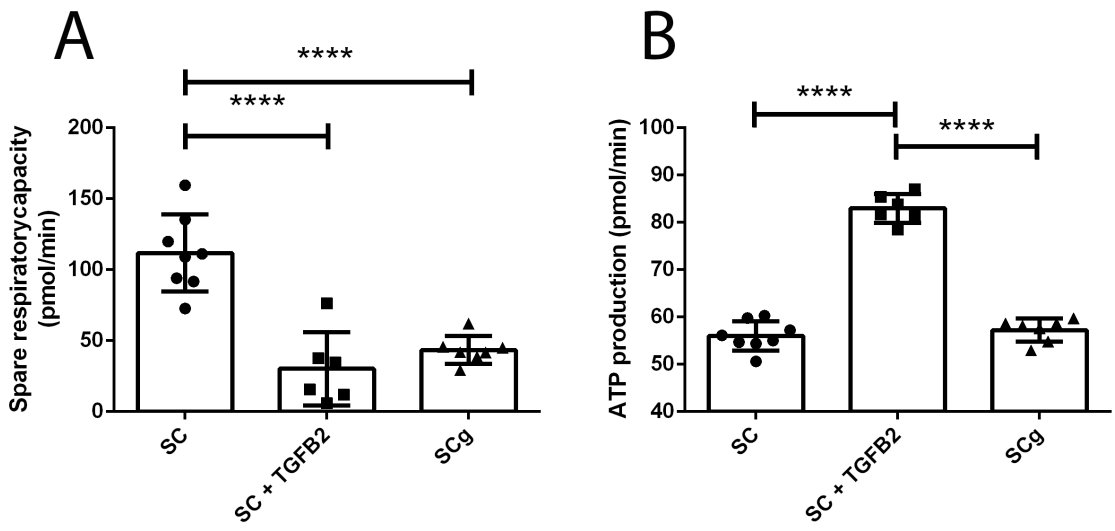

Figure 2.9: Spare respiratory capacity and ATP production of SC, SC+TGF-β2 and SCg cells.

(A) The spare respiratory capacity was calculated as maximal level of respiration minus basal level of respiration for each group. There was a significant reduction ($p < 0.0001$, 1-way ANOVA with Tukey's multiple comparison post-test) in spare respiratory capacity in both SC+TGF-β2 (n=6) and SCg (n=7) compared to healthy SC cells (n=8). (B) There was a significant increase ($p < 0.0001$, 1-way ANOVA with Tukey's multiple comparison post-

test) in ATP production in SC+TGF-β2 (n=6) compared to both SC (n=8) and SCg (n=7). Mean +/- SD is shown above with individual data points for each group.

H. Comparing healthy SCEC and glaucomatous SCEC *in vitro*

Throughout the course of all these *in vitro* experiments, SCg cells grew at a faster rate than healthy SC cells. A number of functional and morphological experiments were carried out on just SC (biological n=5) and SCg (biological n=3) cells to investigate further any more differences between the two. Cell density was calculated at time of trypsinisation when cells were to be seeded. T75 flasks would have reached ~90% confluency at this point and so a cell density reading is a good indication of how many cells are in the flask at that point. There was a significant increase of $8.8x10^5$ [$9.8x10^3$, $1.7x10^6$] cells/mL (mean [CI], p = 0.0476, unpaired t-test, n=29 for SC and n=9 for SCg) observed in SCg compared to SC cells (Figure 2.8A). Both SC and SCg cells were then seeded at the same time and at the same density to carry out other functional assay experiments.

MTS proliferation assay was carried out on both SC and SCg. A significant increase in relative absorbance of 0.8 [0.6, 1.0] nm ($p < 0.0001$, unpaired t-test, n=4) was observed in SCg compared to SC cells just 24 hr post seeding (Figure 2.8B).

Using confocal microscopy and ZEN software, the area of both SC and SCg cells were calculated. SCg cells were bigger in size compared to SC cells (Figure 2.11). A significant increase in area of 167 [40.1, 293.8] μm^2 (p = 0.0133, unpaired t-test, n=8 for SC and n=9 for SCg) was observed in SCg compared to SC cells (Figure 2.8C).

A scratch test was carried out to investigate whether SCg cells migrate faster than SC cells, as they proliferate at a faster rate. Both SC and SCg cells were seeded at the same density and left for 48 hr to allow a monolayer of SC cells to develop at the bottom of the culture plate. A scratch was then carried out disrupting this monolayer and causing a gap to develop between the two sides in the dish. 48 hr post scratch, pictures were taken and the

relative reduction in the size of the scratched area was calculated for both healthy SC and SCg cells. SCg cells showed a significant increase of 0.4 [0.1, 0.6] relative fold change of scratched area (p = 0.009, unpaired t-test, n=10 for SC and n=5 for SCg) compared to SC cells (Figure 2.8D).

A calcium detection assay was also carried out to investigate whether SCg cells showed increased calcium ion concentration compared to SC. There was no significant change in calcium ion concentration of 0.1 [-0.31, 0.5] mM ($p > 0.05$, unpaired t-test, n=11 for SC and n=6 for SCg) between SC and SCg cells (Figure 2.8E).

Transcript expression of the tumour suppressor protein p53 was also assessed in light of the differences in cell proliferation and growth observed in glaucomatous SCEC. A decrease in p53 mRNA transcript expression of 0.7 [-1.2, 2.7] fold change ($p > 0.05$, unpaired t-test, n=5 for SC and n=3 for SCg) was observed SCg compared to SC (Figure 2.8F).

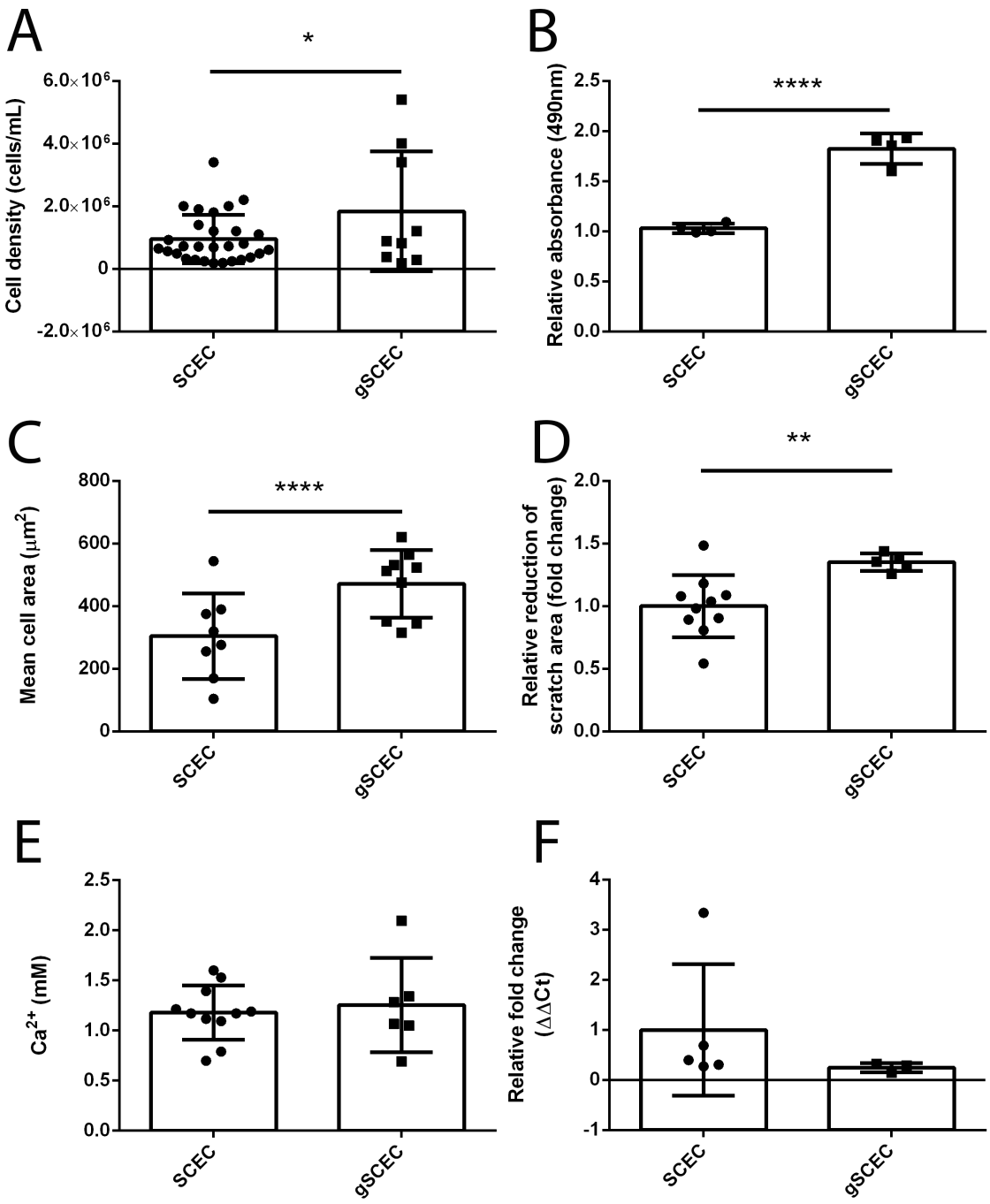

Figure 2.10: Functional assays showing the differences observed *in vitro* between SC and SCg cells.

There was a significant increase in cell density ($p < 0.05$, unpaired t-test, n=29 for SC and n=9 for SCg), cell proliferation ($p < 0.0001$, unpaired t-test, n=4 for both SC and SCg), cell migration ($p < 0.01$, unpaired t-test, n=10 for SC and n=5 for SCg) and the size of the cells themselves ($p < 0.0001$, unpaired t-test, n=8 for SC and n=9 for SCg) observed in SCg compared to healthy SC cells. There was no significant change in calcium ion concentration observed between the two cell types ($p > 0.05$, unpaired t-test, n=11 for SC and n=6 for

SCg). A decrease in relative transcript expression of tumour suppressor p53 was observed in glaucomatous SC compared to healthy SC, but this was not statistically significant ($p > 0.05$, unpaired t-test, n=5 for SC and n=3 for SCg). Mean +/- SD is shown above along with each individual data point for both SC and SCg.

Summary of statistically significant results

Both tables below summarize the statistically significant results observed in several assays comparing SC+TGF-β2 treated cells and SCg cells to healthy SC cells (Table 2) and SCg cells to healthy SC cells (Table 3). These tables summarize the most significant findings of this *in vitro* study and show the various changes occurring to SCEC under glaucomatous conditions.

Assay	SC+TGF-β2	SCg
VE-cadherin protein expression	-	↑*
ZO-1 transcript expression	-	↑*
FITC-dextran	-	↑*
Cell proliferation	↑**	↑*
Spare respiratory capacity	↓****	↓****
ATP production	↑****	-

Table 2: Summary of statistically significant results for both SC+TGF-β2 and SCg cells compared to healthy SC cells.

*Statistically significant differences in VE-cadherin protein expression, ZO-1 transcript expression, cell permeability and proliferation, as well as mitochondrial spare respiratory capacity were observed in SCg cells compared to healthy SC cells. Statistically significant differences in cell proliferation, spare respiratory capacity and ATP production were observed in TGF-β2 treated cells compared to healthy SC cells. ↑ represents an increase or upregulation observed in that cell group compared to healthy SC cells. ↓ represents a decrease or downregulation observed in that cell group compared to healthy SC cells. – represents no change observed in that cell group compared to healthy SC cells. Statistical significance is indicated by the following * = ($p < 0.05$), ** = ($p < 0.01$), *** = ($p < 0.001$) and **** = ($p < 0.0001$).*

Assay	SCg
Cell density	↑*
Cell proliferation	↑****
Cell size	↑*
Cell migration	↑**

Table 3: Summary of statistically significant results observed in SCg cells compared to healthy SC cells.

*Statistically significant differences were observed in cell density, proliferation, size and migration of SCg cells compared to healthy SC cells. ↑ represents an increase or upregulation observed in the SCg group compared to healthy SC cells. ↓ represents a decrease or downregulation observed in that cell group compared to healthy SC cells. – represents no change observed in that cell group compared to healthy SC cells. Statistical significance is indicated by the following * = ($p < 0.05$), ** = ($p < 0.01$), *** = ($p < 0.001$) and **** = ($p < 0.0001$).*

Discussion

It is clear from the results presented in this chapter that SCg cells differ in many ways to healthy SC cells *in vitro*. SCg cells are larger and proliferate, migrate and divide at a significantly higher rate compared to healthy SC cells. SCg cells proliferated nearly twice as fast as healthy SC cells and were almost double in size of the average healthy SC cell (Figure 2.11). p53 mRNA encodes for a tumour suppressor protein that is involved in various cellular processes including cell division, cell cycle control and apoptosis (187). A decrease in p53 mRNA transcript expression observed in SCg could explain why these cells were growing and proliferating at a much higher rate than healthy SC cells. The rate at which these cells were growing was almost "cancer-like" in phenotype and reduced expression of a tumour suppressor protein could contribute to this observation. SCg cells continued to grow and proliferate at this rate up to and past passage 6, while healthy SC cells could not.

SCg cells also showed significant increased protein expression of the endothelial marker VE-cadherin, as well as increased transcript and protein expression of fibrotic markers α-SMA and TGF-β2, compared to healthy SC cells. SCg cells showed increased protein expression of α-SMA and F-actin, using confocal microscopy, compared to healthy SC cells, further supporting the α-SMA western blot analysis. SCg cells also showed a significant reduction in mitochondrial activity, compared to healthy SC cells. Mitochondrial spare respiratory capacity in SCg cells was less than half of what was observed in healthy SC cells. ATP production was unchanged between healthy and glaucomatous SC.

It is hypothesized that healthy SC cells generated ATP through oxidative phosphorylation (OXPHOS), while SCg cells generated ATP through glycolysis instead, suggestive of the Warburg effect (188). The Warburg effect describes how cancer cells have the potential to carry out mitochondrial respiration through aerobic glycolysis rather than aerobic oxidation (189). Glaucomatous LC cells have also displayed significantly decreased spare respiratory capacity capabilities compared to healthy LC cells, as well as producing an

equivalent amount of ATP (190). These glaucomatous LC cells produce significantly less ADP when supplied with either glucose or galactose (190). This study by Kamel et al. (2020) demonstrated evidence of the Warburg effect in glaucomatous LC cells, as expression of glycolytic markers were elevated in glaucoma cells at both an transcript and protein level (190). It is therefore possible that SCg cells could be mimicking this phenomenon observed in glaucomatous LC cells, as they both show increased profibrotic markers as well as decreased mitochondrial respiration capabilities. It would be interesting in future studies to investigate the glycolytic pathway of mitochondrial respiration in these SCg cells using the Seahorse XF Glycolysis Stress Test assay. Unfortunately, this was beyond the scope of this current study but could be interesting to investigate in future studies.

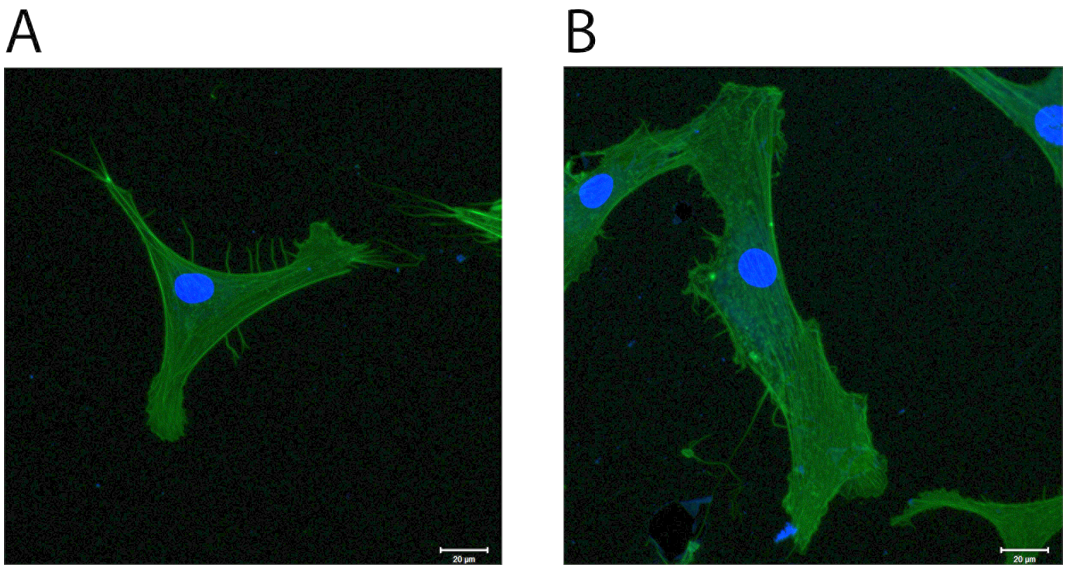

Figure 2.11: Significant difference in cell size observed between SC and SCg cells. *Using confocal microscopy and ZEN software, images of individual cells were taken, and the area of both healthy and glaucomatous SCEC calculated. An example of a healthy SC cell (A) and SCg cell (B) is shown above. SCg cells were significantly larger in size compared to healthy SC cells ($p < 0.05$, unpaired t-test, $n=8$ for SC and $n=9$ for SCg).*

A reduction in TEER values was observed in SCg compared to SC, despite the cells becoming less porous and stiffer in phenotype (191). A significant increase in paracellular

permeability was also observed in SCg cells compared to SC, despite a significant increase in ZO-1 TJ mRNA transcript and protein expression. Glaucomatous TM cells have previously shown increased expression of TJ protein ZO-1 (184). Steroid-induced glaucoma patients also show increased expression of TJ proteins ZO-1 and connexin43 (Cx43) in TM tissue (185). Other TJ proteins are located in the intercellular spaces between endothelial cells and so many others could be down regulated in glaucoma and explain the increase in paracellular permeability observed in SCg cells. Tricellulin protein expression above, for example, appears to be reduced in SCg compared to SC cells. SCg cells could potentially be altering a part of their healthy endothelial phenotype, showing reduced TEER values and increased paracellular permeability, compared to healthy SC cells. These SCg cells used in this study were donated by patients who have undergone numerous treatments for glaucoma and so it is possible that these treatments could have had effects on reducing TEER values and increasing paracellular permeability. These cells cannot be regarded as representing the "perfect" *in vitro* representation of what is occurring to endothelial cells in glaucoma. Intuitively, one might predict that an increase in TEER values and reduction in paracellular permeability would be observed in outflow tissues of glaucoma patients, owing to increased ECM deposition, reduced pore density and the increased cell stiffness previously mentioned. There are clearly limitations in attempting to deduce molecular changes in outflow tissues donated by glaucoma patients. For this reason, SC+TGF-β2 treated cells were included in the study, as a positive control (145, 191).

SC+TGF-β2 cells showed many similarities with SCg cells including increased expression of fibrotic markers α-SMA and TGF-β2, increased cell proliferation and reduced mitochondrial spare respiratory capacity compared to healthy SC cells. Unlike SCg cells, SC+TGF-β2 cells showed no change in expression of endothelial marker VE-cadherin and no change in TEER and paracellular permeability values. An increase in TEER values and decrease in paracellular permeability would be expected. SC+TGF-β2 cells showed a

significant increase in mitochondrial ATP production compared to both SC and SCg cells, however. Treating these cells with TGF-β2 potentially triggers an immune response (192) and so could be the cause of increased ATP production observed in these cells (193). Tissues of the outflow pathway contain high levels of TGF-β2 in POAG patients (194) and so it was of interest to explore the various changes occurring to SCEC under these conditions and compare these changes to those we observed in SCEC from glaucomatous patients.

The role of EndMT has been shown to contribute towards the progression of fibrosis of the heart, kidneys and lungs, as well as cancer progression (195-198). It has been shown that EndMT results in the loss of endothelial-specific markers and instead a more fibrotic or mesenchymal phenotype is observed, with increased expression of fibrotic markers, such as α-SMA (196-199). In this study however, loss of endothelial cell markers was not observed in glaucomatous SCEC. A significant fold increase of 3.7 was observed in protein expression of endothelial marker VE-cadherin in SCg compared to healthy SC cells. A fold increase of 9.0 and 4.4 was observed in protein expression of fibrotic marker α-SMA and profibrotic marker TGF-β2 respectively, in SCg cells compared to healthy SC cells. These cells did not appear to be "losing" their endothelial cell characteristics, but instead showed increased expression of both endothelial and fibrotic cell markers. It has been discussed how the activation of pro-fibrotic pathways in glaucomatous TM cells, due to elevated levels of TGF-β, drives these cells towards a more fibrotic phenotype (200). These data in this *in vitro* study suggests that these pro-fibrotic EndMT changes could also be occurring to SCEC in glaucoma, as shown by increased expression of fibrotic marker α-SMA and profibrotic marker TGF-β2.

Glaucomatous SCEC show increased cytoskeletal stiffness, resulting in reduced pore formation, which increases AH outflow resistance and IOP in glaucoma patients (145, 201). Accumulation of ECM and increased expression of collagen I-α1 and α-SMA in glaucomatous TM and LC cells results in altered cell-ECM rigidity (202). The increased

stiffness of SCEC in glaucoma could be the result of increased expression of cell adhesion marker VE-cadherin and pro-fibrotic marker α-SMA observed in this *in vitro* study. In this study, glaucomatous SCEC expressed a more fibrotic phenotype compared to healthy SCEC, potentially leading to increased cell stiffness and outflow resistance observed at the inner wall of SC (146). These glaucomatous SCEC, much like TM cells (200), appear to be more fibrotic in phenotype and potentially play a major role in IOP elevation and AH outflow resistance in glaucoma.

In conclusion, glaucomatous SCEC appear to have undergone a range of morphological, molecular and mechanical changes compared to SCEC from healthy individuals. These cells appear to express a more fibrotic phenotype, as they undergo a form of EndMT. In this study, glaucomatous SCEC showed increased expression of fibrotic and adhesion markers, increased cell proliferation, size and migration, as well as reduced mitochondrial spare respiratory capacity compared to healthy SCEC. All of these changes have the potential to negatively influence AH outflow facility and therefore, IOP. Since glaucomatous SCEC appear to be expressing a more fibrotic phenotype, perhaps treatments targeting more fibrotic characteristics could be beneficial. An example of such was recently reported by Li et al. (2021), where treatment with Netarsudil ROCK inhibitor decreased expression of fibrotic markers α-SMA and fibronectin, showing anti-fibrotic properties capable of restoring outflow facility function and reducing IOP, in a DEX mouse model of OHT (123). The availability of human SCEC from Professor Dan Stamer and colleagues provided a challenging opportunity to study the properties of such cells *in vitro*, notwithstanding the limitations highlighted. As a follow-on to these studies, therapeutic approaches targeting Schlemm's canal endothelial cells will be described in future chapters.

Statement on collaboration

Both healthy and glaucomatous SC cells used in this study were kindly provided by Prof. Dan Stamer's lab, Duke Eye Centre. The Seahorse mitochondrial stress test assay was carried out under supervision and help of Dr. Daniel Maloney, TCD.

Chapter 3

An siRNA therapy targeting tissues of the conventional outflow pathway in a rodent model of steroid-induced ocular hypertension

Abstract

Continued patient use of glucocorticoids (GCs) can lead to ocular hypertension over time, which is a leading cause of secondary open-angle glaucoma. The DEX mouse model is a well characterised paradigm of steroid induced-OHT. It has previously been shown at this laboratory that a once-off intracameral injection of siRNA simultaneously targeting transcripts encoding Schlemm's canal endothelial tight junction proteins ZO-1 and tricellulin, increases conventional AH outflow facility in normotensive mice, by opening the paracellular pores (tight junctions) located along in the inner wall endothelia of SC. In the study reported here, targeted siRNA-mediated downregulation of ZO-1 and tricellulin has been shown to increase conventional outflow facility and lower IOP in hypertensive DEX mice. This is a significant progression from earlier observations on normotensive animals, and clearly points to a potential clinical application for this treatment in a sight-threatening scenario.

Introduction

Manipulating cerebral and ocular vascular endothelial TJ protein expression for therapeutic purposes

Campbell et al. (2012) (203) demonstrated that systemic (tail vein) delivery of siRNA targeting transcripts encoding claudin-5, a major component of the TJs of joining endothelial cells of the cerebral and retinal vasculatures, resulted in a reversible opening of the blood brain and inner blood-retina barriers to low molecular weight compounds of up to 800 Daltons in Molecular weight. The technique was used successfully in systemically delivering the anti-neovascular drug, Sunitinib malleate to suppress experimentally induced choroidal neovascularisation in mice (203). In a further application of this approach, it is notable that traumatic brain injury can result in accumulation of fluid in the brain at the site of injury, and this is known as cerebral oedema. This has the potential to increase intracranial pressure, which radically increases the risk of morbidity and mortality. Using the same siRNA-based technique targeting claudin-5 in the cerebral vasculature, downregulation of this TJ protein resulted in the opening of vascular endothelial paracellular clefts, in turn, increasing fluid clearance and improving cognitive function in a mouse model of induced cerebral oedema (204). A further extension of this approach was reported by Keaney and Campbell (Institute of Genetics TCD) (205). In this work they demonstrated that siRNA-mediated down regulation of claudin-5 together with transcripts encoding another vascular endothelial TJ protein, occludin, in combination resulted in an increase in paracellular vascular permeability in the brain sufficient to allow soluble amyloid-ß (1-40) monomers to diffuse from the brain into the peripheral circulation in a well characterised transgenic Alzheimer disease mouse model, where cognitive function was enhanced in such animals.

A major pathological feature of POAG is increased AH outflow resistance along the conventional pathway, leading to elevated IOP and optic neuropathy (as discussed in Chapter 1). Current therapies are designed either to reduce AH production directly, or to

target AH outflow resistance in the unconventional pathway. Very few therapies successfully target the conventional outflow pathway, where a large proportion of AH outflow resistance is generated. Based on the studies outlined above, Tam et al. (2017) (131) focused on the fact that the endothelial cells lining Schlemm's Canal also have tight junctions, AH being able to enter the canal from the TM either through the formation of transcellular vacuoles or through the paracellular spaces left between the tight junctions of the endothelial cells. They reasoned that siRNA-mediated down regulation of SC endothelial tight junctions would increase paracellular permeability, thus increasing the rate of entry of AH into the canal from the TM and thus reduce IOP (131).

TJ proteins ZO-1, tricellulin and claudin-11 were shown by Tam et al. (2017) to be abundantly expressed in human SCEC *in vitro*. These TJ proteins were successfully downregulated using T siRNA (siRNA specifically targeting these transcripts), shown by western blot analysis, resulting in a significant reduction in TEER values and increased paracellular permeability, compared to non-targeting siRNA (NT siRNA) (131). Claudin-11 is not expressed in mouse tissue however, and so T siRNA for ZO-1 and tricellulin TJ only was used *in vivo*. A once-off intracameral injection containing a combination of 1µg of ZO-1 siRNA and 1µg of tricellulin siRNA was injected into one normotensive mouse eye and the contralateral control eye was injected with 2µg of NT siRNA. The natural flow of AH from the ciliary body towards tissues of the conventional outflow pathway carried the injected siRNA directly to the inner wall of Schlemm's canal, where these TJ proteins are located (Figure 3.1).

In normotensive mice, perfusion analysis was carried out 48 hr post injection on *ex vivo* eyes and a significant increase in outflow facility of 113 [35, 234] % (mean [CI], paired weighted t-test, $p = 0.0064$, n=7), was observed in T siRNA eyes compared to NT siRNA contralateral paired controls (131). High resolution transmission electron microscopy (TEM) showed a clear opening of the intercellular clefts along the inner wall of Schlemm's canal

following the once off injection with T siRNA, compared to the closed clefts observed in tissue treated with NT siRNA. Opening of the clefts allowed for greater AH outflow along the conventional pathway, accounting for the increase in AH outflow facility observed in these normotensive mice (131). In the current study, the concept of siRNA-mediated modulation of levels of SC endothelial TJs has been extended to a clinically relevant setting.

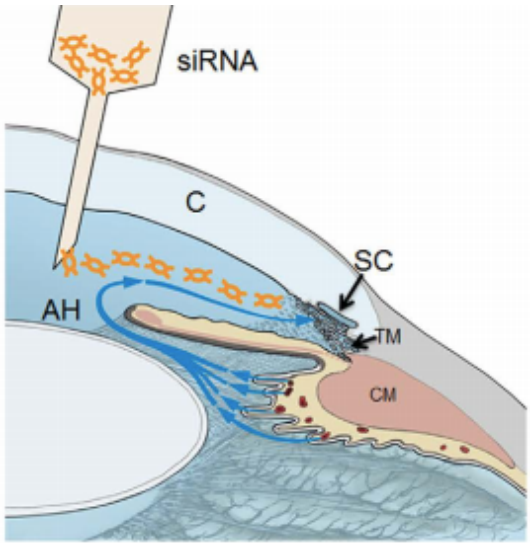

Figure 3.1: Therapeutic strategy targeting Schlemm's canal inner wall.

Following a once off intracameral injection of siRNA targeting TJ proteins of Schlemm's canal inner wall, AH flow transports the siRNA to tissues of the outflow pathway. Aqueous humor (AH); ciliary muscle (CM); cornea (C); trabecular meshwork (TM); Schlemm's canal (SC). Adapted from Tam et al. (2017) (131).

Aqueous humour outflow facility measurement

When targeting the outflow pathway with any potential targeted therapeutic, it is obviously necessary to validate and assess the direct effect it may have on the outflow pathway itself. In order to assess the effects of the current siRNA-mediated approach, measurements of the outflow facility must be taken. Outflow facility is defined as the relationship between the rate of AH outflow, along the conventional route and IOP. This process is assessed through

perfusion of cannulated eyes. This concept is adapted from the Goldmann equation discussed in Chapter 1:

$$Q_f + Q = C\,(P - P_e) + Q_0$$

where, Q_f represents the rate of production of AH in the eye, while Q represents the rate of fluid flow into the eye from the perfusion system and Q_0 represents pressure-independent outflow. C represents the total outflow facility, including all pressure-dependent outflow, meaning all conventional outflow facility, and any pressure-dependent unconventional outflow facility. P represents IOP, while P_e is episcleral venous pressure. These combined constitute the pressure gradient that exists across the inner wall of SC and in the JCT region. For the purpose of perfusion measurements, Q_0, Q_f, P_e, and C values are assumed to be independent of IOP. This forms a linear model between the outflow and IOP relationship and allows for the measurement of the difference in flow rates at two different pressure steps as a method of calculating total outflow facility. Values are given in the form of µL/min/mmHg, which describes the relationship between the rate of outflow and IOP. This is referred to as a two-step perfusion. With perfusions carried out on enucleated or *ex vivo* eyes, P_e and Q_f values are both zero as all ocular vessels have been separated from the animal. This allows the original equation to be simplified to the following:

$$Q = CP + Q_0$$

The rate of flow of enucleated eyes is usually measured at a range of different IOP values to improve the resolution of measurements. Because the relationship is thought to be linear, the slope of the plotted values can be taken as the facility measurement, while the Y-axis intercept is sometimes taken as the rate of pressure independent outflow (206, 207). This concept has been challenged by some as the osmotic forces driving this outflow would be absent in enucleated eyes.

In order to achieve the inflow rate of fluid during perfusion, syringe pumps are used to control and read the flow rate directly. Constant flow rates can be applied with pressure

measurements being taken, but only when pressure has reached a steady state. Pressure can then be measured at multiple different flow rates. Alternatively, the flow rate can be controlled by computer programming and can be maintained at constant pressure, with the flow rate measured at several different pressures (206-208).

In vivo eye perfusions pose greater challenges, as the value of P_e is no longer zero and cannot be excluded from the equation describing AH volume conservation. This means the value of P_e must be calculated in order to measure total outflow facility. This can be achieved through direct cannulation of episcleral veins to a pressure sensor. This is technically challenging in larger eyes and not possible in mouse eyes. Instead, IOP can be lowered until blood is observed entering SC lumen, thus lowering the pressure gradient. IOP is then slowly increased until no blood flow is observed, thereby reaching an equilibrium between IOP and episcleral venous pressure and so indirectly measuring the value of P_e (39).

The dexamethasone mouse model of steroid induced ocular hypertension

GC have been widely used to control ocular inflammation in patients with uveitis. However, OHT and the risk of secondary open-angle glaucoma is a significant complication of GC therapy (209). While most patients undergo short-term GC treatment, it is estimated that up to 5% of adults in the UK undergo long-term systemic GC use daily for more than 5 years. While up to 20% undergo GC treatment for more than 6 months (210). One third of ophthalmic topical GC-treated patients show a moderate increase in IOP, while ~5% of patients experience severe IOP increases. This increases to ~25% of patients experiencing OHT following treatment with intravitreal injections (211). In these cases where patients are experiencing acute steroid induced OHT levels, where elevated IOP cannot be controlled with conventional pressure-reducing medication, surgical intervention may be required (212). These procedures all have serious associated risks attached and hence there is a very

real unmet clinical need for an alternative, less invasive method of lowering IOP in these cases.

The DEX mouse model has been widely used in investigations of steroid induced OHT. Elevated IOP can be induced and sustained in mice over a period of weeks through long-term systemic delivery of DEX using micro-osmotic pumps. This method of inducing GC OHT has been shown to elevate IOP significantly within 2 weeks of treatment, with a significant reduction in conventional outflow facility, while preserving open-angle morphology within the anterior chamber (213-216). It has been previously shown that treatment with siRNA does not negatively impact the open angle structure in the anterior chamber in rodents and it is assumed the same holds in hypertensive animals treated with the same siRNA as was used in previous work (131).

Mice treated with DEX have also been shown to have increased deposition of ECM within the TM, with elevated levels of extracellular collagen I, fibronectin, and mucopolysaccharides, and the formation of cross-linked α-SMA networks (217, 218). As previously mentioned, GC treatment of cultured human TM cells has been shown to significantly increase ZO-1 expression, and to increase the number of TJ-containing intercellular contacts (185). Hence, this model represents a suitable one for assessment of the modulatory effects of the use of siRNA therapeutics on outflow facility, serving as a model of OHT in POAG in general and more specifically, of human GC-induced glaucoma.

The specific aim of this chapter was to show that siRNA-mediated TJ protein suppression enhances conventional outflow facility and reduces IOP in this murine model of GC-induced OHT.

Results

A. Characterisation of IOP elevation in DEX treated mice

WT C57BL/6J mice were implanted subcutaneously with micro-osmotic mini pumps delivering 2 mg/kg/day of DEX (n=17). A separate cohort of mice was used as a control. These mice were implanted with a pump containing cyclodextrin, as a vehicle control (n=9). The day before pump implantation, mice were anesthetized with isoflurane and IOP was measured by rebound tonometry in one eye. These IOP measurements were repeated weekly over the course of a 4 week period. Change in IOP over time for both DEX and vehicle treated animals is illustrated below in Figure 3.2. The baseline IOP measurement for the vehicle-treated group was 14.4 [13.7, 15.0] mmHg (mean [CI]). The final IOP measurement at 4 weeks was 15.2 [14.4, 16.0] mmHg, which corresponds to a non-significant change of 0.9 [-0.3, 2.0] mmHg ($p > 0.05$, 1-way ANOVA with Tukey's multiple comparison post-tests, n=9) (Figure 3.2, red). For DEX-treated animals, baseline IOP was 12.8 [12.2, 13.4] mmHg and final IOP at 4 weeks was 17.8 [17.1, 18.4] mmHg, corresponding to a statistically significant increase in IOP over time of 5.0 [3.9, 6.1] mmHg ($p < 0.0001$, 1-way ANOVA with Tukey's multiple comparison post-tests, n=17) (Figure 3.2, blue). As will be noted, DEX treatment resulted in a significant increase in IOP in these animals, compared to vehicle cyclodextrin controls.

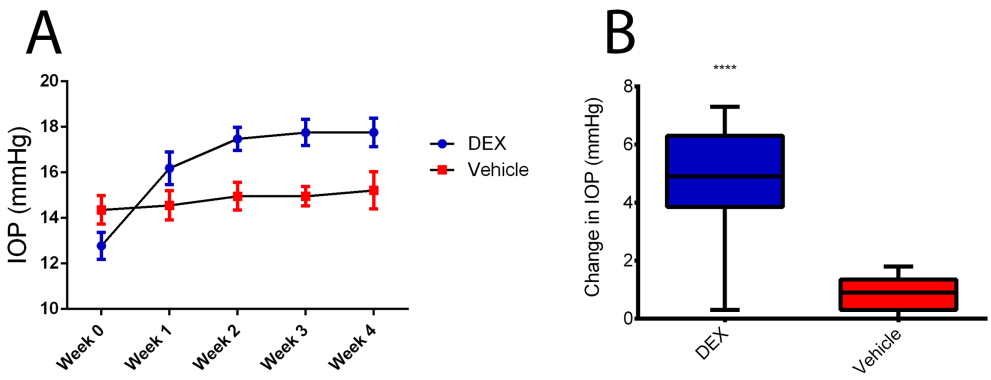

Figure 3.2: Change in IOP over time in both DEX and vehicle treated mice.

(A) Characterising change in IOP (mmHg) over 4 weeks in both DEX (n=17) and vehicle treated mice (n=9). (B) DEX treated mice ($p < 0.0001$, 1-way ANOVA with Tukey's multiple comparisons post-test, n=17) showed a significant increase in IOP of 5 mmHg, compared to a non-significant increase of almost 1 mmHg in the vehicle treated cohort ($p > 0.05$, 1-way ANOVA with Tukey's multiple comparisons post-test, n=9).

B. Targeted downregulation of TJ proteins ZO-1 and tricellulin transcript levels in normotensive C57BL/6J and DEX mice

As mentioned above, successful targeted downregulation of TJ proteins ZO-1 and tricellulin has been shown *in vitro* and *in vivo* to increase outflow facility in normotensive mice (131). In order to validate the efficacy of siRNA-mediated transcript suppression of these TJ proteins, siRNA was delivered according to the protocol described in Tam et al. (2017) to both normotensive and DEX-treated mice (131). 1 µg each of ZO-1 and tricellulin T siRNA was injected intracamerally into one eye and 2 µg of NT siRNA was injected into the contralateral control eye. 48 hr post injection, eyes were enucleated, tissue homogenized, and RNA extracted for qPCR analysis.

Demonstration of selective knockdown of TJs in murine outflow tissues by western blot or qPCR is extremely difficult owing to the technical challenges faced when isolating sufficient SCEC for quantitative analysis from the very small number of SCEC present in

mouse anterior segment tissues. Microscopic dissection of the SC endothelium in mice is technically difficult. An alternative dissection method was carried out to enrich for SCEC, by removing the anterior chamber 2-3mm below the limbus and making a secondary incision to remove the cornea 2-3mm above the limbus, thereby leaving a ring containing the outflow tissue and any remnants of the cornea and iris. This method enables a tissue sample to be obtained in which the presence of TJs from the corneal endothelia and epithelia is minimized.

In normotensive C57BL/6J mice, T siRNA-injected eyes showed significant downregulation of both ZO-1 and tricellulin TJ transcript levels when compared to NT siRNA-injected eyes. For ZO-1, T siRNA treated eyes showed a significant mean fold change in relative gene expression of 0.7 [0.5, 0.8] (mean [CI]), ($p < 0.001$, one-sample t-test to theoretical mean of 1, n=12) (Figure 3.3A). For tricellulin, T siRNA treated eyes showed a significant mean fold change in relative gene expression of 0.6 [0.4, 0.9] ($p < 0.01$, n=11). This represents a 30% and 40% average reduction in transcript levels, respectively. These data suggest that a once-off intracameral injection of T siRNA has the potential to successfully downregulate both ZO-1 and tricellulin TJ proteins located along the conventional outflow pathway.

In order to validate this approach in hypertensive DEX-treated animals, a cohort of mice was treated with 2 mg/kg/day of DEX in order to induce OHT for 4 weeks. 4 weeks post subcutaneous implantation of the DEX mini pump, these mice were then treated with a once-off intracameral injection of T siRNA in one eye and NT siRNA in the other, as outlined above. For ZO-1, T siRNA eyes showed a significant mean fold change in relative gene expression of 0.6 [0.2, 1.0] (mean [CI]), ($p < 0.05$, one-sample t-test to theoretical mean of 1, n=8) (Figure 3.3B). Tricellulin showed a significant mean fold change in relative gene expression of 0.4 [0.1, 0.6] ($p < 0.01$, n=6). This represents a 40% and 60% mean reduction in transcript levels, respectively. These data suggest that T siRNA has a greater potential to

successfully downregulate these TJ proteins in the DEX-treated animals than the vehicle control group.

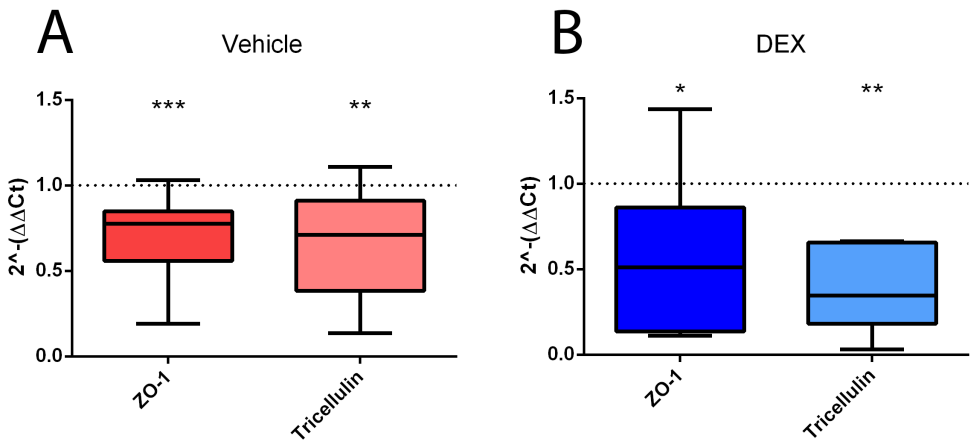

Figure 3.3: Downregulation of both ZO-1 and tricellulin transcript levels following a once off treatment with T siRNA.

A significant reduction in both ZO-1 ($p < 0.001$ in vehicle and $p < 0.05$ in DEX, one-sample t-test to the theoretical mean of 1, n=12 for vehicle mice and n=8 for DEX mice) and tricellulin ($p < 0.01$ for both vehicle and DEX mice, one-sample t-test to the theoretical mean of 1, n=11 for vehicle mice and n=6 for DEX mice) TJ transcript levels was observed in both normotensive mice (A) and DEX treated steroid-induced OHT mice (B) following a once off intracameral injection with T siRNA targeting these TJ proteins.

Fluorescent in-situ hybridization (FISH) was attempted to semi-quantify fluorescence of both ZO-1 and tricellulin TJ proteins in both NT and T siRNA treated eyes, using confocal microscopy. However, following several attempts with various conditions, successful imaging could not be obtained. Confocal microscopy was used to show ZO-1 expression in the anterior chambers of both WT and DEX-treated mice. These eyes were cryosectioned and stained for ZO-1 TJ protein to show expression at SC and surrounding tissue (Figure 3.4). ZO-1 expression was predominantly observed in the corneal epithelium, with evidence of signal in the endothelium, TM and SC inner wall. The figures below have been focused on SC inner wall, the primary target site. Reduced ZO-1 expression was shown in T siRNA

compared to NT siRNA treated eyes in both WT (B-A respectively) and DEX (D-C respectively) treated animals. Segmental flow may have an impact on the visualisation of TJ downregulation and so makes it difficult to see the exact area of siRNA delivery. The images below, along with TJ protein transcript expression (Figure 3.3), suggest successful down regulation of TJ protein ZO-1. Images of tricellulin TJ expression could not be obtained, due to difficulty and lack of abundant expression along the outflow pathway, compared to ZO-1 TJ expression.

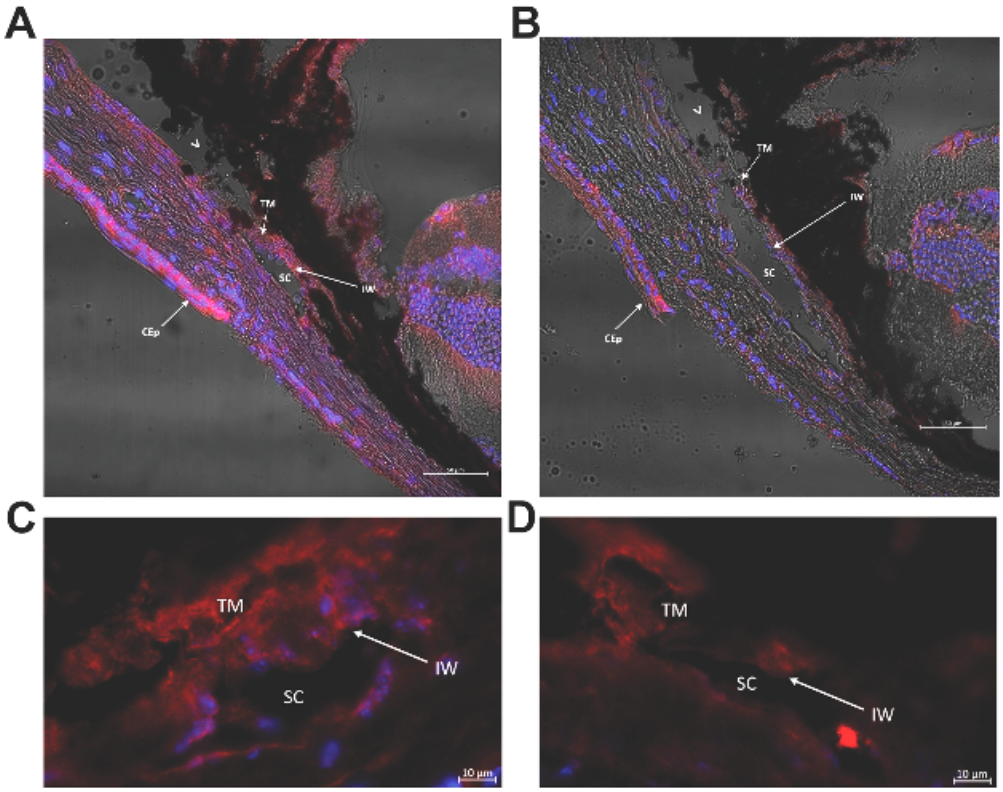

Figure 3.4: ZO-1 expression at SC inner wall in both WT and DEX treated mice.

(A) ZO-1 staining (red) of a WT, NT siRNA treated mouse eye showed abundant ZO-1 expression along SC inner wall, TM and corneal epithelium. (B) ZO-1 expression remains strong in the corneal epithelium in WT T siRNA treated eyes, with reduced expression at SC and surrounding tissues. (C) Close-up of SC in DEX treated NT siRNA eyes showed strong staining around the TM and SC inner wall. (D) Close-up of SC in DEX treated NT siRNA eyes showed reduced expression at the SC inner wall, while staining remained around the TM region. Cep = corneal epithelium; SC = Schlemm's canal; TM = trabecular meshwork;

IW = inner wall; < = open iridocorneal angle. Scale bars represented for both 40X (A-B) and 63X (C-D) images. DAPI nuclei stain is in blue. These images were taken by Dr. Jeffrey O' Callaghan.

C. Effect of TJ downregulation on IOP in vehicle and DEX treated mice

To evaluate whether targeted downregulation of the TJ proteins was an effective means of lowering IOP in both normotensive and DEX-treated mice, both cohorts were anesthetized and IOP measured following 4 weeks of treatment with cyclodextrin and DEX, respectively. IOP measurements were taken prior to treatment. Mice were then treated with a once-off intracameral injection of T siRNA into one eye and NT siRNA into the contralateral control eye. 48 hr post siRNA injection, mice were anesthetized once again and IOP measurements taken. To account for the variation in IOP values for both pre- and post-treatment, IOP data are presented as the change in IOP between pre- and post-siRNA treatment, for both T and NT siRNA-treated eyes.

For normotensive vehicle mice, T siRNA-injected eyes showed a significant average reduction in IOP of 1.0 [-1.6, -0.3] mmHg compared to pre-treated IOP measurement averages (13.6 [13.3, 13.9] versus 14.5 [14.2, 14.9] mmHg, ($p < 0.01$, one-sample t-test to theoretical mean of 0, n=9) (Figure 3.5A, green). NT siRNA injected eyes showed no significant average change in IOP in these animals (-0.0 [-0.4, 0.2] mmHg compared to pre-treated IOP measurement averages (14.2 [14.0, 14.5] versus 14.3 [14.1, 14.6] mmHg, ($p > 0.05$, n=9) (Figure 3.5A, yellow). These data show that T siRNA treatment in this vehicle control group results in significant reduction in IOP compared to the NT siRNA group.

For DEX-treated mice, T siRNA-treated eyes showed a significant average reduction in IOP of 1.9 [-2.6, -1.2] mmHg compared to pre-treated IOP measurement averages (15.0 [14.3, 16.6] versus 16.9 [16.5, 17.3] mmHg, ($p < 0.0001$, one-sample t-test to theoretical mean of 0, n=17) (Figure 3.5B, green). NT siRNA injected eyes showed no significant

average change in IOP of 0.13 [-0.7, 0.4] mmHg compared to pre-treated IOP measurement averages (16.9 [16.5, 17.3] versus 17 [16.6, 17.4] mmHg, ($p > 0.05$, n=17) (Figure 3.5B, yellow). These data show that T siRNA eyes in these DEX mice results in a significant reduction in IOP compared to NT siRNA eyes. The reduction in IOP in these DEX-treated mice is greater than that seen in the vehicle control group.

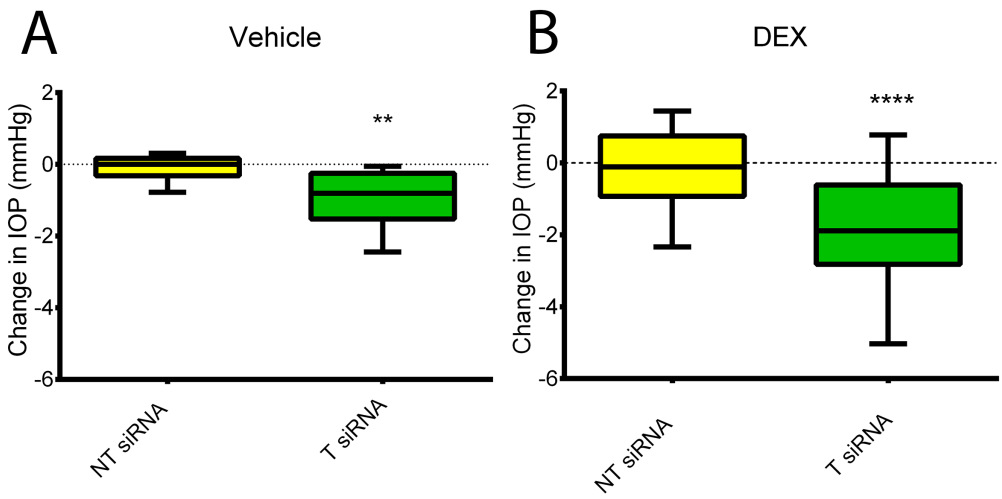

Figure 3.5: Change in IOP following NT and T siRNA to both vehicle and DEX mice. *(A) Vehicle treated mice show a significant reduction in IOP in T siRNA treated eyes ($p < 0.01$, one-sample t-test to the theoretical mean of 0, n=9) compared to NT siRNA treated eyes ($p > 0.05$, one-sample t-test to the theoretical mean of 0, n=9). (B) DEX-treated mice show a greater reduction in IOP in T siRNA eyes ($p < 0.0001$, one-sample t-test to the theoretical mean of 0, n=17) compared to NT siRNA eyes ($p > 0.05$, one-sample t-test to the theoretical mean of 0, n=17).*

The *iPerfusion* System

Changes in outflow facility were determined by performing *ex vivo* perfusions using the *iPerfusion* system which was developed by Joseph Sherwood and colleagues at Imperial College London, specifically to measure conventional outflow facility in mice (219). This perfusion system, unlike older versions, uses an actuator-driven variable height reservoir to vary applied IOP in *ex vivo* eyes instead of a pump, and measures total fluid flow in the eye

directly, using an accurate thermal micro-flow sensor. It uses a wet-wet pressure transducer to measure IOP using external atmospheric pressure as a reference (Figure 3.6A). This system is contained in a sealed unit to prevent air currents from affecting pressure readings. This results in very sensitive and accurate measurements of conventional outflow facility, with values reported as a reference facility at 8 mmHg, called C_r. The system is semi-automated, with flow rates being continually monitored and set parameters of rate of change of flow rate are defined to determine when steady state has been achieved and to then automatically progress the perfusion system to the next pressure step. This increase in accuracy and sensitivity of measurements enables the perfusion process to progress faster and allows flow to be assessed over 8 pressure steps, instead of 4 in older systems. This system also allows for the measurement of two eyes simultaneously, increasing the number of pairs of eyes that can be achieved in one day. A representative flow-pressure plot from *iPerfusion* describes the non-linear relationship between flow rate (Q) at each pressure (P) step in both T siRNA (red) and NT siRNA (blue) treated eyes (Figure 3.6 B).

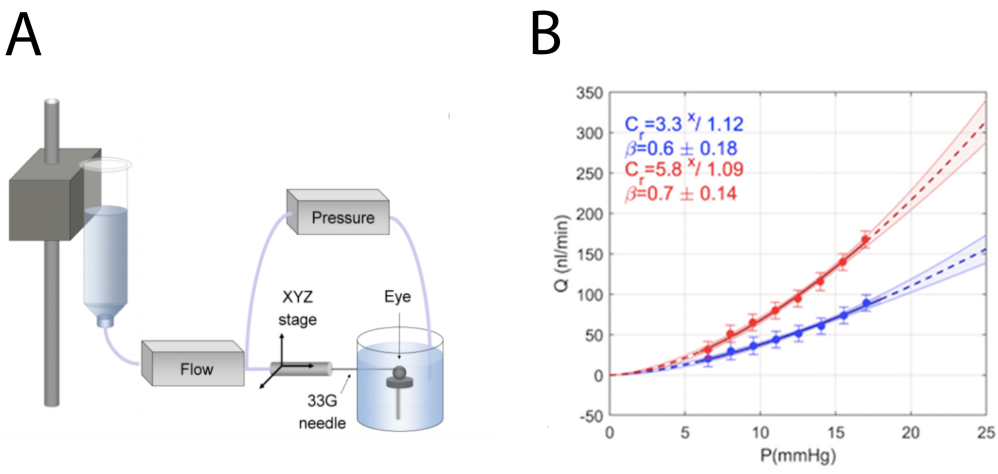

Figure 3.6: The *iPerfusion* system.

(A) Schematic of iPerfusion system showing measurement of flow into the eye from the reservoir and applied pressure. (B) This plot depicts the relationship between flow (Q) and pressure (P) during a standard perfusion. This is an example taken from the data sample used. As applied pressure increases, so too does the flow rate through the enucleated eye.

The T siRNA treated eye (red) has a greater response in flow to increasing pressure compared to the NT siRNA treated eye (blue).

D. Effect of TJ downregulation on *ex vivo* conventional outflow facility in vehicle and DEX treated mice

Facility data below for normotensive vehicle control mice shows that NT siRNA (control) eyes have an average facility of 4.4 [3.2, 5.6] nl/min/mmHg, while T siRNA (experimental) eyes have an average facility of 6.0 [4.8, 7.2] nl/min/mmHg (Figure 3.7A+B). Facility for DEX-treated hypertensive mice shows that NT siRNA (control) eyes have an average facility of 4.5 [3.2, 5.8] nl/min/mmHg, while T siRNA (experimental) eyes have an average facility of 7.4 [6.2, 8.6] nl/min/mmHg (Figure 3.7C+D). This perfusion system facilitated comparison of C between paired contralateral T siRNA and NT siRNA treated eyes for both normotensive vehicle and DEX-treated mice. In normotensive vehicle control mice, T siRNA eyes showed a significant increase in conventional outflow facility (C) of 38 [5, 81] % (p = 0.029, weighted paired t-test, n=6) compared to NT siRNA eyes (Figure 3.8A). In DEX-treated mice, eyes injected with T siRNA showed a significant increase in C of 63 [20, 122] % (p = 0.0071, weighted paired t-test, n=8) compared to contralateral NT siRNA eyes (Figure 3.8B).

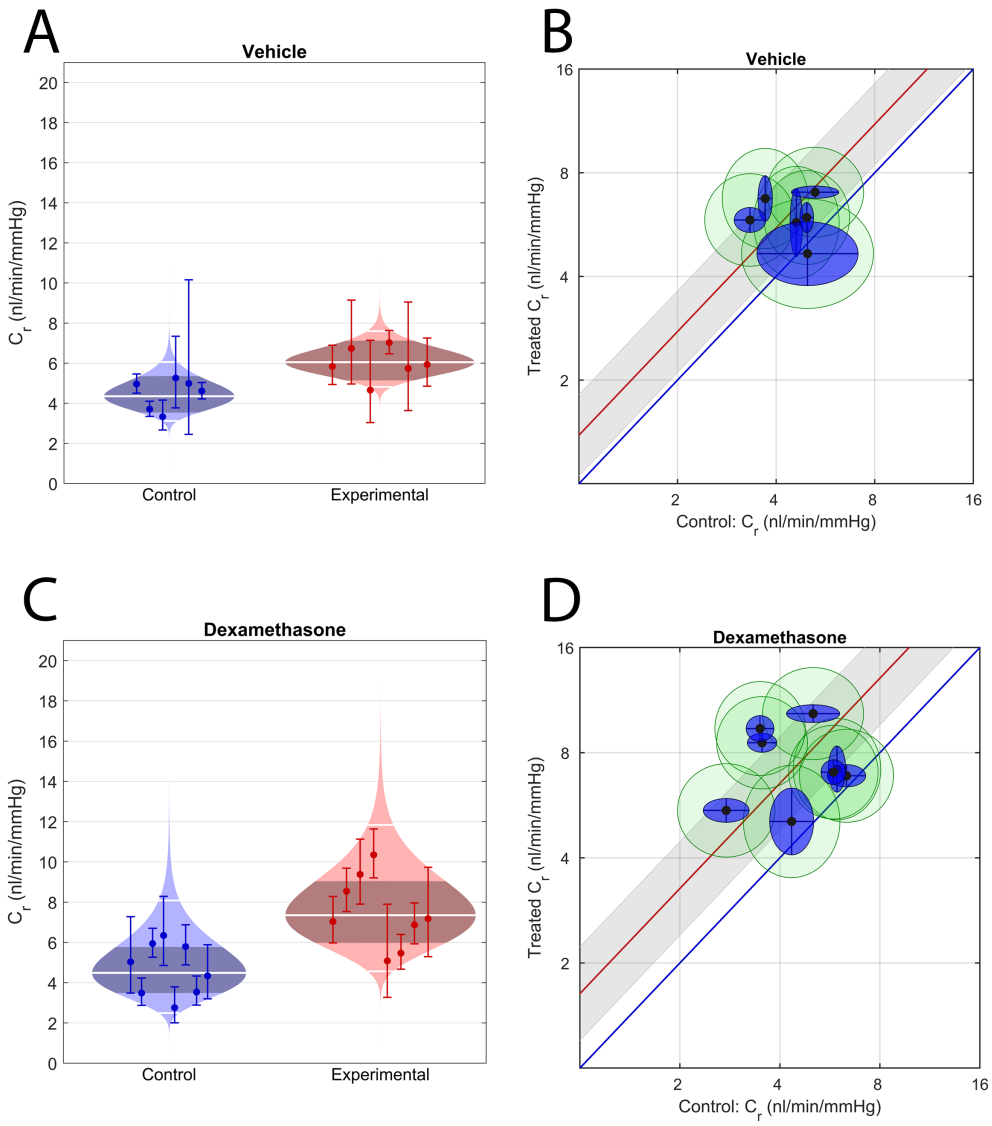

Figure 3.7: Effect of siRNA on outflow facility in both normotensive and DEX animals. *Cello plot depicting individual outflow facility values for eyes at 8 mmHg (C_r) and statistical distribution of both control (NT siRNA) ($p < 0.05$, weighted unpaired t-test, n=6) and experimental (T siRNA) ($p < 0.05$, weighted unpaired t-test, n=8) groups for vehicle control mice (A) and DEX treated mice (C). Each point represents a single eye with 95% CI on C_r. The white line represents the geometric mean, the dark blue/red bands indicate the 95% CI, and the light blue/red regions are the distribution of the data. Paired outflow plots of vehicle control mice ($p = 0.029$,* weighted paired t-test, n=6*) (B) and DEX treated mice ($p = 0.0071$,* weighted paired t-test, n=8*) (D) present paired perfusion analysis. Each point represents a*

pair of eyes, with log-transformed facilities of the control eye (NT siRNA) plotted on the x axis and the treated eye (T siRNA) on the y axis. Outer blues and green circles show uncertainties generated from fitting the data to a model, intra-individual and cannulation variability respectively. Average increase is represented by the red line, surrounded by a grey 95% CI, indicating significantly increased facility if this does not overlap with the blue line.

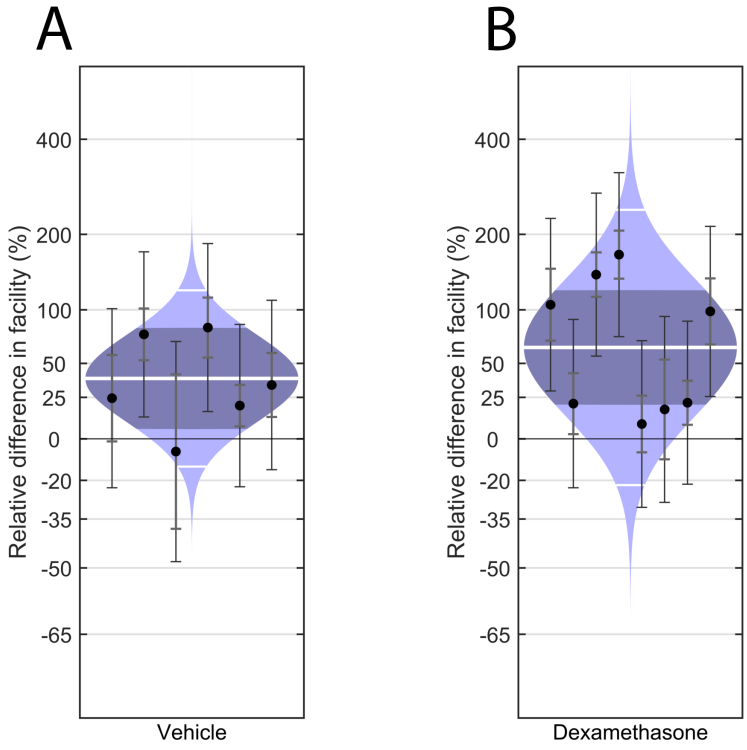

Figure 3.8: Cello plots depicting relative difference in facility for paired eyes.
(A) Vehicle control mice showed a significant relative increase in outflow facility of 38% in T siRNA treated eyes compared to NT siRNA treated eyes (p = 0.029, weighted paired t-test, n=6*). (B) While DEX treated mice showed an even greater significant relative increase in outflow facility of 63% in T siRNA eyes compared to NT siRNA eyes (p* = 0.0071, weighted paired t-test, n=8*). Each point represents the difference in C between contralateral control eyes with 95% CI. The white line represents the geometric mean, the dark blue bands indicate the 95% CI, and the light blue regions are the distribution of the data.*

E. Potential for off target selectivity following intracameral inoculation of siRNA targeting TJ proteins

Changes to corneal permeability can affect IOP readings and cause them to be over-estimated and so target selectivity is an important aspect of this study. The hypothesis for this study was that intracamerally injected siRNA would be delivered to tissues of the outflow pathway due to the pressure gradient that exists in the anterior chamber, directing all material within AH to SC. Should siRNA act upon an off-target tissues such as the corneal endothelium, it would be expected that TJ suppression would occur at that site also. qPCR data of whole anterior segments (enriched with cornea cells) suggests that there is no significant change in TJ transcript expression between T and NT siRNA eyes (Figure 3.9A). A mean relative fold gene expression change of 1.1 [0.5, 1.8] and 1.2 [0.1, 2.3], ($p > 0.05$, one-sample t-test to theoretical mean of 1, n=6) was shown for both ZO-1 and tricellulin protein transcript, respectively. This method of anterior chamber dissection was altered when attempting to quantify TJ protein transcript expression of SC inner wall (Figure 3.3) to prevent saturation with cornea cells and to attempt to get more accurate quantification of TJ expression of tissues of the outflow pathway only.

Central corneal thickness (CCT) was also quantified using confocal microscopy on multiple sections. There was no significant change in CCT values between T and NT siRNA (1.2 [-4.0, 6.5] μm, ($p < 0.05$, paired t-test, n=10)) (Figure 3.9B). It is expected that CCT would be altered if there was TJ expression changes occurring, impacting the stroma's permeability and ability to regulate fluid flow. These data suggest that no significant off target effects of the once-off intracameral injection with siRNA are observed in the cornea region and are hence successfully targeting tissues of the outflow pathways, as initially hypothesized.

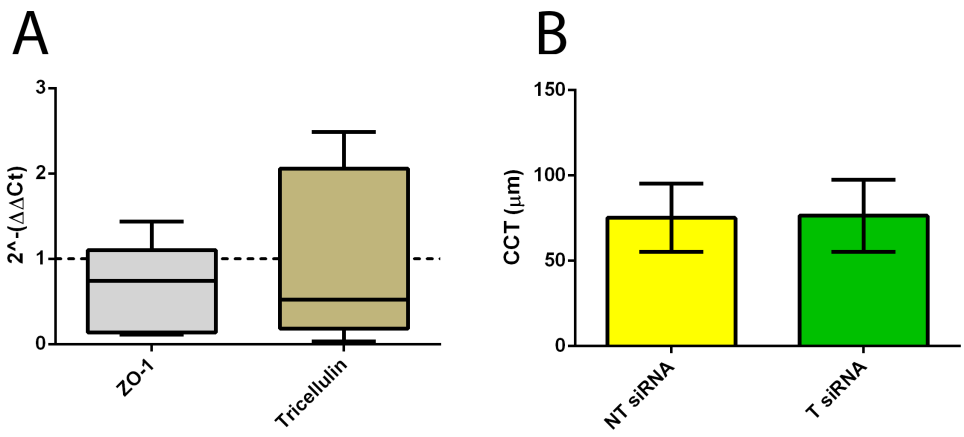

Figure 3.9: Examination of off target siRNA expression at the cornea.

(A) There was no significant change in both ZO-1 and tricellulin TJ transcript expression, following intracameral inoculation with siRNA, when whole anterior segment qPCR was carried out ($p > 0.05$, one-sample t-test to theoretical mean of 1, n=6). (B) There was no change in CCT values between NT and T siRNA treated eyes, suggesting no significant off-target effects of siRNA intracameral injection are seen in the cornea ($p > 0.05$, paired t-test, n=10).

Both normotensive and hypertensive DEX eyes were cryosectioned and stained for ZO-1 TJ protein and visualized using confocal microscopy (Figure 3.10). In general, strong ZO-1 expression was observed at the corneal epithelium, while the corneal endothelium showed a weaker, but present, signal (A). DEX-treated hypertensive animals appeared to have increased ZO-1 protein expression at the corneal endothelium which suggests that DEX increases ZO-1 expression, confirming hypotheses from the literature (B). No obvious difference in ZO-1 expression was observed at the corneal endothelia of eyes treated with T siRNA (D) compared to NT siRNA (C), thus further suggesting that the majority of siRNA was delivered to SC and that the impact of off-target effects was minimal.

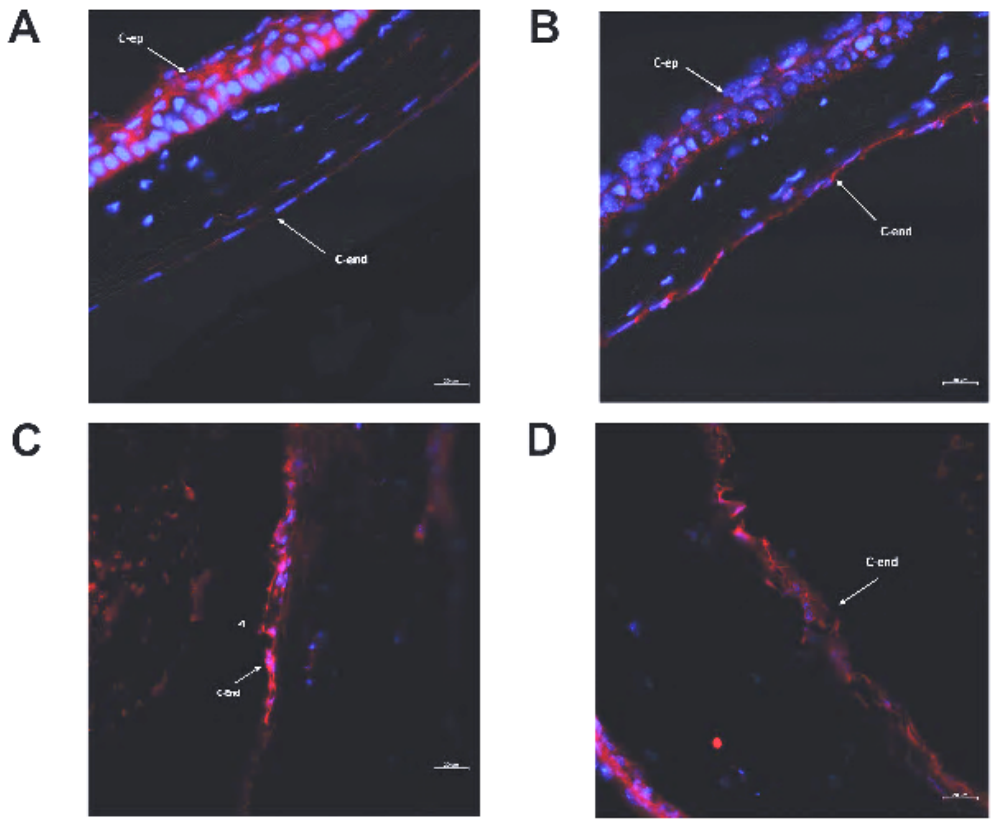

Figure 3.10: ZO-1 TJ expression at the cornea visualised by confocal microscopy.

(A) WT, normotensive mice showed strong corneal epithelial expression of ZO-1 (red), with weak endothelial staining. (B) ZO-1 expression at the corneal endothelial was stronger in DEX-treated mice. (C) Multiple layers of corneal endothelium visualized in DEX-treated mice treated with NT siRNA and (D) T siRNA. C-ep = corneal epithelium; C-end = corneal endothelium; < = open iridocorneal angle. Scale bar represents 20 µm. DAPI is shown in blue. These images were taken by Dr. Jeffrey O' Callaghan.

Discussion

It has previously been shown in a research study from this laboratory that down-regulation of TJ proteins ZO-1 and tricellulin at the inner wall of SC results in an increase in the number of open SC endothelial paracellular clefts, showing reduced IOP and increased outflow facility in normotensive WT mice (131). The study addressed in this chapter was aimed at validating this approach in a disease setting, using a murine model of steroid induced OHT. Specifically, the aim was to assess the utility of this approach for IOP reduction and increased AH outflow facility in a GC-induced OHT model (Figure 3.11). As GC dependent patients no longer respond to topical medications, aimed at reducing pressure, they may only have the option of surgical intervention left available to them. The question as to whether outflow facility could be increased and IOP in turn reduced by targeting TJ proteins ZO-1 and tricellulin in the DEX mouse model has been addressed in this study.

Significant downregulation of TJ protein transcript levels for both ZO-1 and tricellulin in both normotensive and hypertensive DEX-treated mice, following a once of intracameral injection with T siRNA, was observed. A greater reduction in TJ relative transcript expression was observed in the DEX-treated mice following treatment with T siRNA compared to the normotensive cohort.

DEX-treated animals also showed a greater reduction in IOP, following the once off siRNA treatment, compared to normotensive vehicle controls. Both hypertensive DEX animals and normotensive vehicle controls showed a significant increase in relative outflow facility following treatment with T siRNA. DEX-treated animals again showed a greater increase in relative outflow facility compared to the vehicle controls. These data suggest that higher IOP may lead to greater efficacy of this approach, as an increased pressure gradient across the SC inner wall may result in increased opening of paracellular pores upon TJ downregulation and in turn result in greater relative outflow facility measurements. This

further emphasizes the important role of paracellular pores at SC inner wall in reducing AH outflow and thus elevating IOP in glaucoma pathology.

DEX-treated T siRNA eyes showed an average IOP reduction of 2 mmHg, double that which was seen in the normotensive vehicle control group (1 mmHg). The mean increases in outflow facility of 38%, observed in the normotensive vehicle group, was substantially lower than 113% mean increase in normotensive animals reported by Tam et al. (2017) (131). Perfusions in the study were carried out at 72 hr post injection, compared to 48 hr in the previous study, to facilitate *in vivo* IOP readings carried out 48 hr post treatment. The reduced effect on outflow is understandable, owing to the transient nature of siRNA (Figure 4.11).

As previously mentioned, DEX treatment is known to increase ZO-1 TJ protein expression *in vitro* (220). Perhaps siRNA-mediated downregulation of the TJ protein ZO-1 is more effective in an environment where there is a greater amount of mRNA for the siRNA to bind to. There may also be a greater number of closed paracellular pores in the presence of upregulated ZO-1 expression and so a greater number of pores to be potentially opened by siRNA treatment. T siRNA had a greater effect on the mRNA transcript levels of DEX-treated mice compared to the vehicle control group. There was a mean fold change in ZO-1 and tricellulin transcript expression of 0.6 and 0.4, respectively, in the DEX mice compared to 0.7 and 0.6 in the vehicle group. These data show that siRNA-mediated downregulation of TJs in the outflow pathway of this murine model of steroid induced OHT has a greater effect that that observed in normotensive animals. A significant reduction in IOP was also observed in both vehicle and DEX-treated mice, following treatment with T siRNA, through increasing AH outflow facility of the conventional outflow pathway.

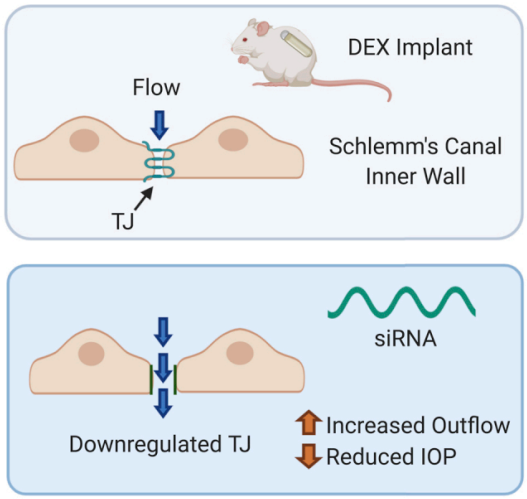

Figure 3.11: A schematic representation of the findings from this study.

DEX-treated mice showed elevated IOP over time. Treatment with DEX increases ZO-1 TJ protein expression and so potentially increases AH outflow resistance. Following a once-off intracameral injection with siRNA-targeting SC endothelial TJ proteins ZO-1 and tricellulin, increased outflow facility and IOP lowering effects were observed in these mice.

In this study a proof-of-concept for an siRNA-based therapeutic approach for IOP reduction and increased AH outflow facility in a steroid induced OHT rodent model has been demonstrated (132). In regard to delivery of this form of therapy in a patient setting, both non-invasive approaches for siRNA delivery through episcleral veins and the use of AAV vector systems are considered in further detail in the next chapter. While DEX-treated mice represent a model of OHT and show increased IOP over the course of treatment, chronic treatment with DEX is a very invasive form of therapy and it is both costly and time consuming.

The *Tg-MYOC*^{Y437H} mouse, a colony of which was established for use in a follow up study, is reported to show mean IOP measurements of ~18 mmHg at only 8 months of age (87). This could possibly mean a greater effect on IOP lowering with siRNA treatment. Mice exhibit a circadian pattern of IOP and both *Tg-MYOC*^{Y437H} and DEX treated mice have the

potential to reach IOP of ~25 mmHg at night (221, 222). Measurement of nocturnal IOP of *Tg-MYOC*^{Y437H} could provide a means to more accurately examine the differences in hypertensive and normotensive mouse models. This will be discussed in the next chapter.

Statement on collaboration

Mouse siRNA IOP measurements and perfusion studies were carried out in direct partnership with Dr. Paul Cassidy, TCD. Confocal images were taken by Dr. Jeffrey O' Callaghan, TCD.

Chapter 4

An investigation of the efficacy of an siRNA therapy targeting tissues of the conventional outflow pathway in *MYOC*^{Y437H} transgenic mouse model of ocular hypertension

Abstract

A Y437H mutation within the *MYOC* gene is an established cause of POAG. Transgenic mice expressing this variant (*MYOC*^{Y437H}) also display characteristics of POAG, including elevated IOP and reduced outflow facility. A once-off intracameral injection of siRNA targeting endothelial TJ proteins ZO-1 and tricellulin, located along the inner wall of Schlemm's canal, has been shown to result in a significant increase in outflow facility and reduction in IOP in a DEX mouse model of steroid-induced OHT (Chapter 3). Data are presented in this Chapter in which the same technique has been extended to evaluation in *MYOC*^{Y437H} mice. A major trend toward incrementation of outflow facility bordering on statistical significance was observed for *MYOC*^{Y437} mice and a significant reduction in IOP was obtained. Some observations on regional differences in SC structure between *MYOC*^{WT} and *MYOC*^{Y437H} mice revealed by transmission electron microscopy are also presented.

Introduction

As discussed in Chapter 1, mutations within the *MYOC* gene are a known cause of POAG (84). Mutations within this gene were initially encountered in rare early-onset dominantly inherited forms of disease. However, 2-4% of adult-onset cases of POAG also harbour mutations within this gene (84), rendering such cases, in themselves, significant targets for genetic therapy. While up to 278 mutations within the MYOC gene have been reported (approximately 38% of which are pathogenic), the Tyr437His (Y437H) mutation is of interest as it is associated with a severe POAG phenotype in humans (223). The exact function of *MYOC* remains to be fully elucidated, however some aspects of its function have been revealed. *MYOC* is expressed in many tissues as an intracellular glycoprotein and is abundant within the TM. Within the TM, AH stimulates secretion of myocilin (224). However, mutant myocilin is not secreted from TM cells and instead accumulates intracellularly, leading to increased IOP through a gain-of-function (GOF) mechanism. It has been hypothesized that accumulation of mutant myocilin in the ER leads to ER stress and potential cytotoxicity of TM cells (225). It has also been shown that *MYOC* interacts with ECM proteins, fibronectin and SPARC, potentially impacting on TM cell stiffness and contractility (87).

A transgenic mouse expressing the human Y437H variant was used as a model of OHT in this study, these animals having been well characterised by Zode et al. (2011) (88) and Zhou et al. (2008) (226). These mice express human *MYOC* within relevant eye tissues and display elevated IOP, RGC death and axonal degeneration, resembling features seen in patients with POAG caused by the Y437H *MYOC* mutation (226). At 6M of age, elevated nocturnal and diurnal IOP of ~20 mmHg and ~16 mmHg respectively is usually observed in transgenic $MYOC^{Y437H}$ mice, while WT littermate controls show nocturnal and diurnal IOP of ~14 mmHg and ~12 mmHg respectively (88). A significant decrease in the numbers of RGCs is also observed in $MYOC^{Y437H}$ mice from 3M onwards compared to age-matched WT

littermate controls. In addition to the progressive optic nerve degeneration observed in *MYOC*^{Y437H} mice at 4-5M, there is also a significant decrease in the numbers of axons in these mice compared to WT age-matched controls (88). As mentioned above, mutant *MYOC* is not secreted into the AH but accumulates in the ER of the TM, inducing ER stress in transgenic mice, in turn resulting in death of TM cells and elevation in IOP. Interestingly, it has been shown that reduction of ER stress using the chemical chaperone, phenylbutyric acid (PBA), reduced symptoms of glaucoma in *MYOC* mice by promoting secretion of mutant *MYOC* into the AH and preventing its intracellular accumulation in the ER (88).

While the DEX model of OHT, used in the work reported in Chapter 3 of this thesis, has been widely used experimentally, transgenic mice expressing the *MYOC*^{Y437H} mutation have been utilised less frequently, likely owing to uncertainties regarding the function of myocilin and the mechanism by which mutations in this gene increase IOP and decrease AH outflow facility. As reported by Tam et al. (2017) (131), targeted siRNA-mediated down-regulation of the SC inner wall endothelial TJ proteins ZO-1 and tricellulin, increases opening of paracellular pores between SC endothelial cells, inducing a concurrent increase in conventional outflow facility in normotensive mice. This technique was then used as a reported in Chapter 3 of this thesis, in DEX hypertensive mice and a significant increase in conventional outflow facility followed by a reduction in IOP was observed in eyes treated with T siRNA (targeting TJ proteins ZO-1 and tricellulin) compared to NT siRNA (132). As a follow on to this work, a report is presented in this chapter on the use of the TJ modulation-based approach in attempting to lower IOP and enhance outflow facility in the *MYOC*^{Y437H} mouse model of OHT. A significant reduction in IOP was observed in both WT and *MYOC*^{Y437H} mice. However, a statistically significant increase in conventional outflow facility was not achieved in either. The technique appeared to be less effective in this transgenic model of OHT compared to the DEX mouse model of OHT and data are discussed in this context.

Results

A. Regional differences in SC structure between *MYOC*^{WT} and *MYOC*^{Y437H} mice

Ocular tissue from both *MYOC*^{WT} and *MYOC*^{Y437H} mice were sent to collaborator Dr. Elke Lütjen-Drecoll, Nurnberg (an expert on TEM) to be photographed. Examination of semi-thin sections confirmed the presence of an open iridocorneal angle in both *MYOC*^{WT} and *MYOC*^{Y437H} mice. It was also evident that the length of optically empty regions underneath the SC inner wall was substantially larger in *MYOC*^{Y437H} than in WT animals, a probable reflection of the fact that regions of fluid flow, were smaller in the *MYOC*^{Y437H} group (B) compared to *MYOC*^{WT} group (A).

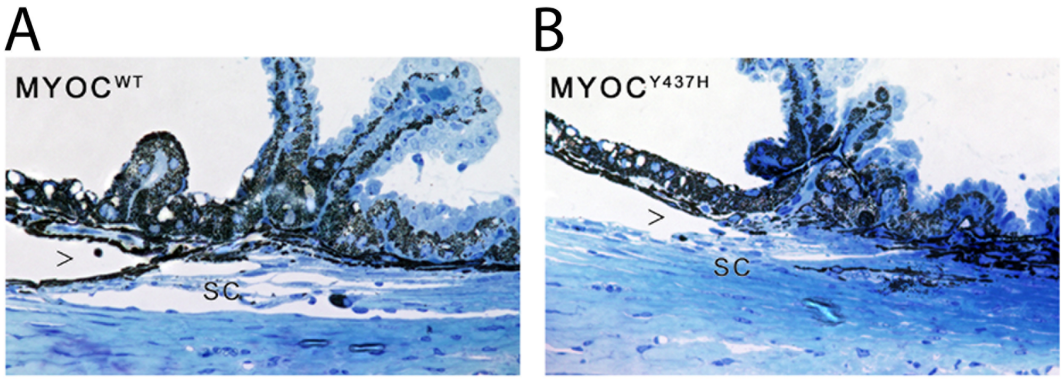

Figure 4.1: Structural differences in SC in *MYOC*^{WT} and *MYOC*^{Y437H} mice.

Semi-thin sections of conventional outflow tissue in both MYOC^{WT} *(A) and MYOC*^{Y437H} *eyes (B). MYOC*^{WT} *eyes had greater inter-trabecular spaces and a clearly longer SC compared to MYOC*^{Y437H} *eyes. An open iridocorneal angle is denoted by >. Images were taken by Dr. Elke Lütjen-Drecoll.*

Ultrastructural changes in *MYOC*^{Y437H} ocular anterior tissues were also observed using TEM. There was an accumulation of ECM material at the subendothelial region (Figure 4.2A), including increased elastin sheaths (B) and an increased number of collagen deposits. This resulted in a dense ECM at the JCT region with very few optically empty spaces. At some regions there were matrix vesicles, indicating necrosis of cells, presumably due to the stress

involved with an accumulation of misfolded myocilin protein (C). Interestingly, there were large amounts of rough endoplasmic reticulum (rER), golgi (D) and cilia (E) in some tissues. These cells had a light cytoplasm and few actin fibres, all of which indicate that these cells are actively proliferating. This was apparent in some regions of the SC, where some subendothelial proliferation into the lumen was apparent, a feature not typical of WT tissues (H-I).

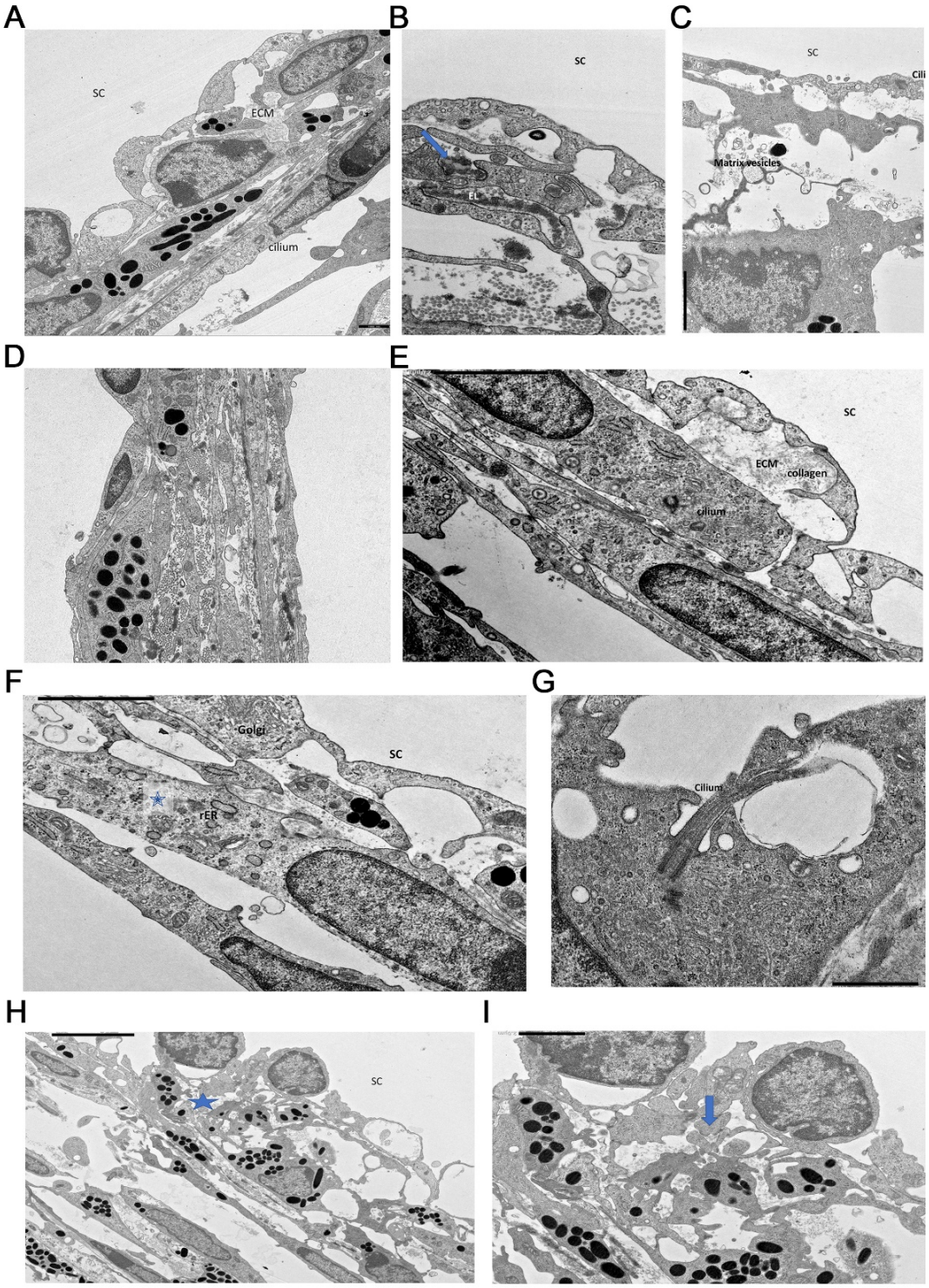

Figure 4.2: Ultrastructural features in *MYOC*^{Y437H} ocular tissue.

Several ECM features were observed in MYOC^{Y437H} *outflow tissues. ECM was present between subendothelial cells (A), elastin fibre sheaths were thick (B), matrix vesicles were present indicating cell necrosis (C), and the TM was dense with collagen deposits. Some cells contained large amounts of rough endoplasmic reticulum, golgi (D) and cilia (E). Such*

cells were found to be actively proliferating, and in some regions proliferation out into the SC was observed (H-I). Images were taken by Dr. Elke Lütjen-Drecoll.

B. IOP elevation in *MYOC*^{Y437H} mice

Transgenic mice expressing human mutant *MYOC*^{Y437H} were measured for both diurnal and nocturnal IOP, recorded by rebound tonometry in one eye on a biweekly basis for 60 days until the mice reached ~6M of age. These mice were ~3/4M old when the study began. IOP was measured for both *MYOC* animals positive for the transgene (*MYOC*^{Y437H}) and for wild-type littermate controls (*MYOC*^{WT}). Diurnal IOP readings (n=18) were taken between 10am and 12pm and nocturnal IOP (n=18) was measured between 11pm and 1am. Diurnal and nocturnal readings were performed on separate cohorts of animals.

Diurnal *MYOC*^{Y437H} animals (red) exhibited a significant elevation in IOP of 3.0 [0.3, 5.7] mmHg (mean [CI]) at the final timepoint (day 60), over baseline ($p < 0.05$, 2-way ANOVA with Tukey's multiple comparisons test, n=9) (Figure 4.3A), with IOP of 21.1 [18.7, 23.6] mmHg at day 60. Diurnal *MYOC*^{WT} animals (blue) however, displayed no significant change in IOP, with an increase of 0.7 [-2.0, 3.3] mmHg ($p > 0.05$, n=9) from baseline, with IOP of 17.5 [15.7, 19.4] mmHg at day 60. There was a significant increase in IOP in the diurnal *MYOC*^{Y437H} cohort of 3.6 [0.5, 6.6] mmHg ($p < 0.05$, n = 9) compared to *MYOC*^{WT} mice. Nocturnal *MYOC*^{Y437H} animals (purple) also exhibited a significant IOP elevation at day 60 compared to baseline, with an increase in IOP of 2.3 [0.3, 4.4] mmHg ($p > 0.05$, n=9), with IOP of 20.0 [19.1, 20.9] mmHg at day 60. There was no significant change in IOP in nocturnal *MYOC*^{WT} animals (orange), with an IOP increase of 0.3 [-1.7, 2.3] mmHg observed ($p > 0.05$, n=9), with IOP of 17.1 [15.6, 18.6] mmHg at day 60. At day 60, nocturnal IOP was significantly elevated in *MYOC*^{Y437H} animals compared to *MYOC*^{WT} animals, with a recorded increase of 2.9 [0.7, 5.1] mmHg ($p < 0.05$, n=9). Diurnal measurements appeared to demonstrate the greatest increase in IOP, both over time and at the final timepoint.

There was no significant increase in IOP in *MYOC*^{WT} mice over the 60-day timepoint. A change in IOP of 0.6 [-2.0, 3.2] mmHg ($p > 0.05$, one sample t-test to theoretical mean of 0, n=10) was observed (Figure 4.3B, blue). There was a significant increase in IOP in *MYOC*^{Y437H} mice of 3.1 [0.9, 5.4] mmHg ($p < 0.05$, n=9) observed over the same time point however (Figure 4.3B, red). This significant elevation in IOP observed in *MYOC*^{Y437H} animals compared to *MYOC*^{WT} animals confirms that in our hands, these animals develop ocular hypertension with age (approximately 6M of age by day 60 of measurement). *MYOC*^{Y437H} animals with diurnal IOP measurement were chosen for further experimentation, as they showed the greatest change in IOP and were more convenient for the experimental design of the investigators.

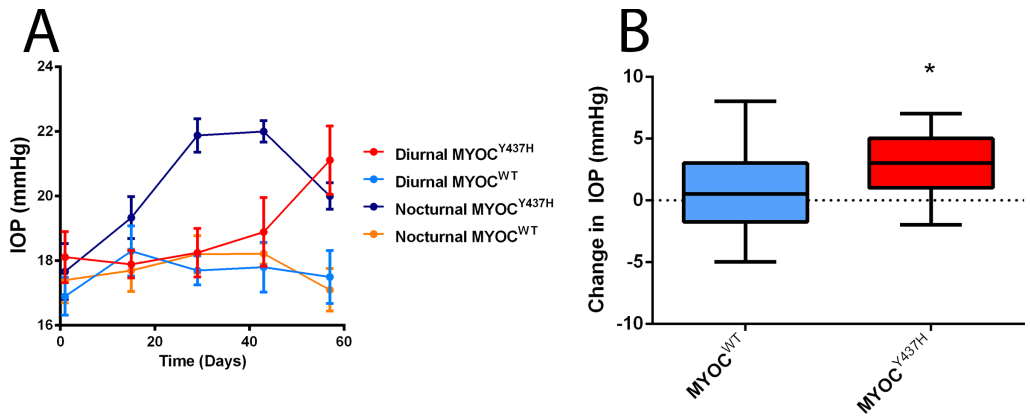

Figure 4.3: Characterising IOP changes in *MYOC* mice.

(A) IOP measurements were taken biweekly in both nocturnal (n=9 for both WT and Y437H) and diurnal MYOC cohorts (n=9 for both WT and Y437H) over a 60-day period. Transgenic mice are represented as MYOC^{Y437H} *and WT mice as MYOC*^{WT}*. These mice were ~6M of age at day 60. (B) There was no significant change in IOP in diurnal MYOC*^{WT} *animals ($p > 0.05$, one-sample t-test to theoretical mean of 0, n=10) (blue) over the 60-day period. There was a significant increase in IOP in the MYOC*^{Y437H} *animals however, ($p < 0.05$, one-sample t-test to theoretical mean of 0, n=9) (red) over the 60-day period.*

C. Potential reason for high baseline IOP readings

MYOC^{Y437H} and *MYOC*^{WT} mice are on a C57BL/6J background and when used previously by others at this laboratory have given IOP readings in the region of 12-14 mmHg. However, in the current series of experiments, IOP readings in these mice had higher baselines, ranging from approximately 16-18mmHg. A direct correlation between corneal temperature and body temperature has been reported in rodents (227). It has been reported that the elastic properties of the cornea, as well as IOP, are also dependent on temperature (228). As IOP measurements in this study were taken using a rebound tonometer, that works by bouncing a probe off of the centre of the cornea, it is plausible that fluctuations in temperature can affect the cornea and thus impact IOP measurement readings. Monitoring of the animal facility during the course of the experiments described here, indicated that temperatures within the animal facility were unstable and relatively high (Figure 4.4). Animals housed in Room 1 were therefore moved into Room 2, where temperatures remained within the recommended range (black dotted lines) from day 0 to day 60. Temperatures in Room 2 increased from day 60 to 90 however, with maximum temperatures exceeding the recommended range at times. Following this, temperatures returned to the normal range in this room.

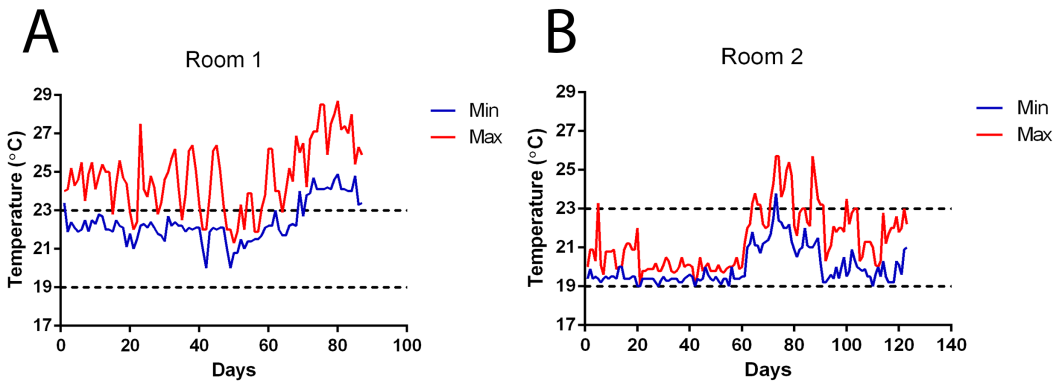

Figure 4.4: Temperature fluctuations in animal housing unit.

Maximum (red) and minimum (blue) temperatures recorded in Room 1 (A) and Room 2 (B) where mice were housed for this study. Mice were originally housed in Room 1 but were

quickly moved to Room 2, following a noticeable increase in temperature. The black dotted line represents the recommended temperature range for the animal facility.

D. Measurement of outflow facility in *MYOC* mice

Outflow facility in $MYOC^{Y437H}$ mice has been previously shown to be reduced by approximately 42% compared to WT littermates at 10M (87). In the study reported here, *ex vivo* outflow perfusion measurements were carried out on both $MYOC^{Y437H}$ and $MYOC^{WT}$ mice at ~6M of age, using the very much more advanced *iPerfusion* system. Facility data shown below gave an average outflow facility measurement of 9.3 [7.1, 11.5] nl/min/mmHg (n=5) in $MYOC^{Y437H}$ hypertensive mice, while $MYOC^{WT}$ normotensive mice gave an average facility of 9.9 [7.6, 12.2] nl/min/mmHg (n=9) in this study (Figure 4.5). This indicates <10% reduction in outflow facility in $MYOC^{Y437H}$ mice compared to their WT littermate controls in this study and while a trend in reduction was evident, a statistically significant difference in outflow facility measurements between $MYOC^{Y437H}$ hypertensive mice and $MYOC^{WT}$ littermate controls was not observed ($p = 0.67$, weighted unpaired t-test).

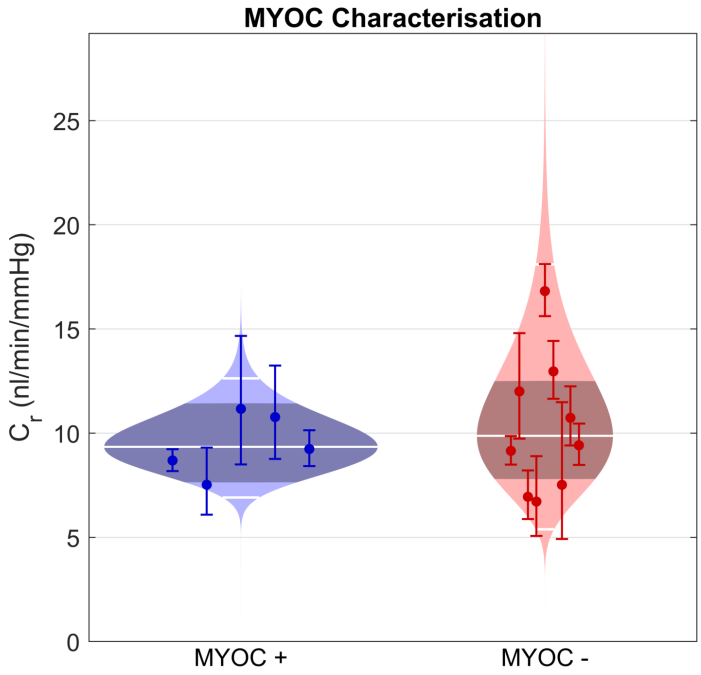

Figure 4.5: Conventional outflow facility in *MYOC* mice.

An average outflow facility measurement of 9 nl/min/mmHg was observed in MYOC + ($MYOC^{Y437H}$) mice ($p > 0.05$, weighted unpaired t-test, n=5). While an average of 10 nl/min/mmHg was observed in MYOC – ($MYOC^{WT}$) mice ($p > 0.05$, weighted unpaired t-test, n=9) in this study. A statistically significant difference in outflow facility between the two cohorts was not observed. Each point represents a single eye with 95% CI. The white line represents the geometric mean, the dark blue/red bands indicate the 95% CI, and the light blue/red regions are the distribution of the data.

E. Targeted downregulation of TJ transcript levels of ZO-1 and tricellulin in *MYOC* mice

Notwithstanding the fact that only a statistically non-significant trend in reduction of outflow facility was observed, IOP was shown to be significantly elevated in $MYOC^{Y437H}$ mice in comparison to WT. Therefore, I deemed it to be of interest to determine whether down regulation of SC endothelial cell TJs, ZO-1 and tricellulin could result in an elevation in outflow facility with concomitant lowering of IOP in these animals. For suppression of these

TJ proteins, siRNA targeting ZO-1 and tricellulin transcripts was delivered as previously described in Cassidy-Kelly et al. (2021) to both normotensive $MYOC^{WT}$ and hypertensive $MYOC^{Y437H}$ mice (132). 1 μg each of ZO-1 and tricellulin T siRNA was injected intracamerally into one eye and 2 μg of NT siRNA was injected into the contralateral control eye. 48 hr post injection, eyes were enucleated, tissue homogenized, and RNA extracted for qPCR analysis. This experiment was carried out prior to the use of an alternative dissection method used to enrich for SCEC (described in Chapter 3). The new method of dissection resulted in a tissue sample in which the presence of TJs from the corneal endothelia and epithelia was minimized. Unfortunately, the results below were not obtained using this improved method, instead the whole anterior segment was homogenised, including the cornea, which retrospectively, might well not have revealed significant reductions in TJ levels as they may occur within the outflow tissues.

In normotensive $MYOC^{WT}$ mice, T siRNA-injected eyes showed no significant change in both ZO-1 and tricellulin TJ transcript levels, when compared to NT siRNA-injected eyes. For ZO-1, T siRNA-treated eyes showed a mean fold change in relative gene expression of 1.0 [0.3, 1.7] (mean [CI]), ($p > 0.05$, one-sample t-test to theoretical mean of 1, n=5) (Figure 4.6A). For tricellulin, T siRNA-treated eyes showed a mean fold change in relative gene expression of 1.2 [0.1, 2.3] ($p > 0.05$, n=5). These data were not significant, quite possibly for reasons stated above.

In hypertensive $MYOC^{Y437H}$ mice, again T siRNA showed no significant change in either ZO-1 or tricellulin TJ transcript levels, when compared to NT siRNA eyes. For ZO-1, T siRNA eyes showed a mean fold change in relative gene expression of 1.1 [0.5, 1.7], ($p > 0.05$, one-sample t-test to theoretical mean of 1, n=6) (Figure 4.6B). Tricellulin showed a mean fold change in relative gene expression of 1.2 [0.0, 2.3] ($p > 0.01$, n=6).

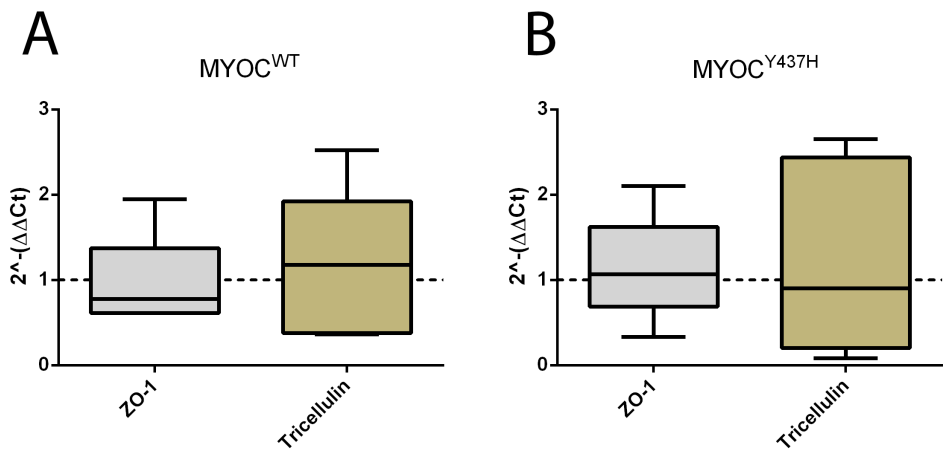

Figure 4.6: Relative ZO-1 and tricellulin transcript levels following a once-off treatment with T siRNA.

No significant reduction in ZO-1 or tricellulin TJ transcript levels was observed in either normotensive MYOC^{WT} mice ($p > 0.05$, one-sample t-test to theoretical mean of 1, n=5 for both ZO-1 and tricellulin) (A) or MYOC^{Y437H} hypertensive mice ($p > 0.05$, one-sample t-test to theoretical mean of 1, n=6 for both ZO-1 and tricellulin) (B) following a once-off intracameral injection with T siRNA targeting these TJ proteins using the methods of tissue processing described.

F. Effect of once-off intracameral injection with TJ-targeting siRNA on IOP in *MYOC* mice

Mice at ~6M of age were injected intracamerally with 1 µg each of siRNA targeting ZO-1 and tricellulin (T siRNA) in one eye, while contralateral control eyes received 2 µg non-targeting siRNA (NT siRNA) injections. This protocol has been used previously when targeting TJ proteins ZO-1 and tricellulin and resulted in reduced IOP and increased AH outflow facility in a rodent model of steroid induced OHT, as detailed in Chapter 3 (132). Immediately before and 48 hrs post injection, mice were anaesthetised and IOP readings taken using rebound tonometry. Pre-injected baseline IOP values for this change in IOP study (Figure 4.7) were lower than baseline IOP values measured for the IOP characterisation study (Figure 4.3), which could be a result of measurements performed on

different days (possible temperature or humidity fluctuations). IOP was still statistically higher in *MYOC*^{Y437H} animals however (1.4 mmHg difference between means, $p = 0.007$, n=42).

In the *MYOC*^{WT} normotensive mice, a significant change in IOP between T siRNA-treated eyes at pre-injection (14.4 [13.6, 15.2] mmHg) and post-injection (12.6 [11.2, 13.9] mmHg) was observed. This represents a significant mean decrease in IOP of 1.9 [0.5, 3.2] mmHg ($p < 0.05$, one-sample t-test to theoretical mean of 0, n=22) following a once-off injection with T siRNA (Figure 4.7A, green), compared to a non-significant change of 0.5 [0.5, 1.5] mmHg ($p > 0.05$, n=22) in NT siRNA control eyes (Figure 4.7A, yellow). In the *MYOC*^{Y437H} mice, a significant change in IOP between T siRNA treated eyes at pre-injection (15.5 [14.5, 16.5] mmHg) and post-injection (13.4 [12.5, 14.3] mmHg) was observed. There was a significant decrease in IOP of 2.1 [1.3, 2.9] mmHg ($p < 0.01$, one-sample t-test to theoretical mean of 0, n=21) in T siRNA-treated eyes (Figure 4.7B, green). There was no significant change in IOP of NT siRNA eyes (0.2 [-1.0, 1.3] mmHg, ($p > 0.05$, n=21) observed (Figure 4.7B, yellow). These data indicate that treatment with T siRNA significantly lowers IOP, compared to NT siRNA treatment in both *MYOC*^{WT} normotensive mice and *MYOC*^{Y437H} hypertensive mice and a greater IOP lowering effect was observed in the *MYOC*^{Y437H} hypertensive cohort.

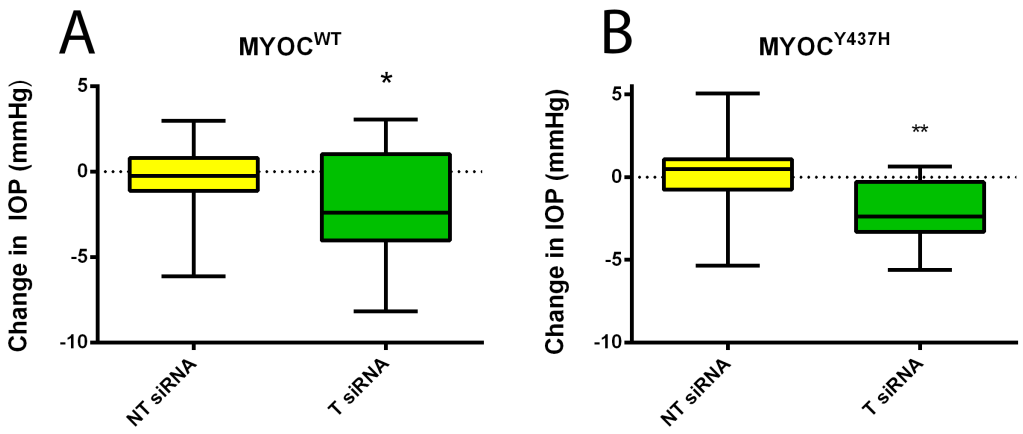

Figure 4.7: Changes to IOP following treatment with NT and T siRNA.

(A) A significant decrease in IOP was observed in MYOC^{WT} eyes treated with T siRNA ($p < 0.05$, one-sample t-test to theoretical mean of 0, n=22) (green). There was no significant change in IOP in NT siRNA treated eyes ($p > 0.05$, one-sample t-test to theoretical mean of 0, n=22) (yellow), however. (B) A more significant decrease in IOP was observed in eyes treated with T siRNA ($p < 0.01$, one-sample t-test to theoretical mean of 0, n=21) (green) in MYOC^{Y437H} mice. No significant change in IOP was observed in eyes treated with NT siRNA ($p > 0.05$, one-sample t-test to theoretical mean of 0, n=21) (yellow).

G. Effect of once-off intracameral injection with TJ targeting siRNA on *ex vivo* conventional outflow facility on *MYOC* animals

The most plausible reason for lowering of IOP in siRNA-treated mice is an increase in outflow facility as a result of down regulation of SC endothelial tight junctions. Thus, to determine whether down-regulation of SC endothelial TJ ZO-1 and tricellulin decreased IOP through increasing conventional outflow facility (*C*), 72 hrs post-injection, both NT siRNA- and T siRNA-injected eyes were enucleated and mounted onto the *iPerfusion* system. This *iPerfusion* system allows for the assessment of *C* through direct measurement of flow rates over a range of pressure steps. Facility data below for *MYOC^{WT}* normotensive mice shows that NT siRNA (control) eyes had an average facility of 9.2 [7.8, 10.6] nl/min/mmHg, while T siRNA (experimental) eyes had an average facility of 11.9 [10.2, 13.6] nl/min/mmHg

(Figure 4.8A+B). Facility for $MYOC^{Y437H}$ hypertensive mice show that NT siRNA (control) eyes had an average facility of 9.7 [8.3, 11.1] nl/min/mmHg, while T siRNA (experimental) eyes had an average facility of 11.7 [10.2, 13.2] nl/min/mmHg (Figure 4.8C+D). This perfusion system facilitates comparison of *C* between paired contralateral T siRNA- and NT siRNA-treated eyes for both normotensive $MYOC^{WT}$ and $MYOC^{Y437H}$ hypertensive mice. In normotensive $MYOC^{WT}$ control mice, T siRNA eyes showed a non-significant increase in *C* of 29 [-12, 88] % (p = 0.142, weighted paired t-test, n=6) compared to NT siRNA eyes (Figure 4.9A). In $MYOC^{Y437H}$ hypertensive mice, eyes injected with T siRNA showed an almost significant increase in *C* of 19 [-1, 43] % (p = 0.0582, weighted paired t-test, n=7) compared to contralateral NT siRNA eyes (Figure 4.9B). These data formally suggest that the targeted down regulation of TJ proteins ZO-1 and tricellulin did not significantly increase conventional outflow facility in either $MYOC^{Y437H}$ hypertensive mice or $MYOC^{WT}$ normotensive control mice, however, a major trend towards such incrementation bordering on statistical significance was observed in $MYOC^{Y437H}$ mice.

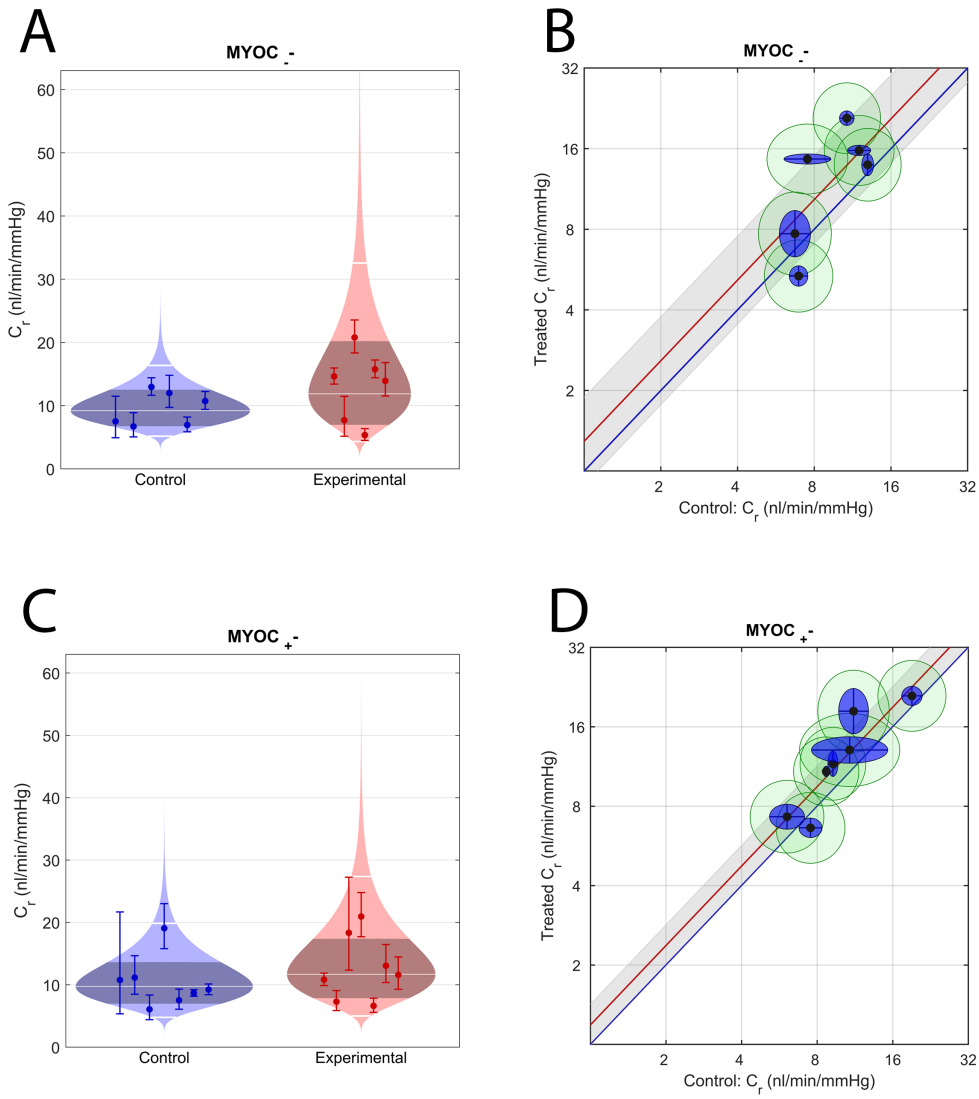

Figure 4.8: Effect of siRNA on outflow facility in both normotensive *MYOC^{WT}* and hypertensive *MYOC^{Y437H}* mice.

Cello plot depicting individual outflow facility values for eyes at 8 mmHg (C_r) and statistical distribution of both control (NT siRNA) and experimental (T siRNA) groups for MYOC^{WT} control mice ($p > 0.05$, weighted unpaired t-test, n=6) (A) and MYOC^{Y437H} hypertensive mice ($p > 0.05$, weighted unpaired t-test, n=7) (C). Each point represents a single eye with 95% CI on C_r. The white line represents the geometric mean, the dark blue/red bands indicate the 95% CI, and the light blue/red regions are the distribution of the data. Paired outflow plots for MYOC^{WT} control mice ($p > 0.05$, weighted paired t-test, n=6) (B) and MYOC^{Y437H} hypertensive mice ($p > 0.05$, weighted paired t-test, n=7) (D) present paired perfusion analysis. Each point represents a pair of eyes, with log-transformed facilities of

the control eye (NT siRNA) plotted on the x axis and the treated eye (T siRNA) on the y axis. Outer blues and green circles show uncertainties generated from fitting the data to a model, intra-individual and cannulation variability respectively. Average increase is represented by the red line, surrounded by a grey 95% CI, indicating significantly increased facility if this does not overlap with the blue line.

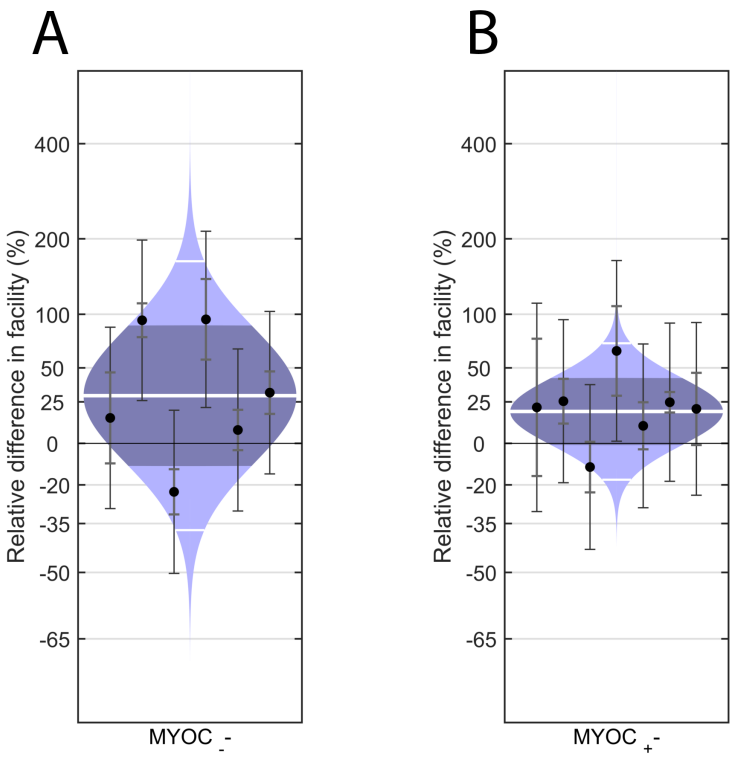

Figure 4.9: Cello plots depicting relative difference in outflow facility for paired eyes. *(A) MYOC^{WT} control mice showed a non-significant relative increase in outflow facility of 29% in T siRNA-treated eyes compared to NT siRNA-treated eyes (p* = 0.142, weighted paired t-test, n=6*). (B) MYOC^{Y437H} hypertensive mice showed a less significant relative increase in outflow facility of 19% in T siRNA eyes compared to NT siRNA eyes (p* = 0.0582, weighted paired t-test, n=7*). Each point represents the difference in C between contralateral control eyes with 95% CI. The white line represents the geometric mean, the dark blue bands indicate the 95% CI, and the light blue regions are the distribution of the data.*

Discussion

A reduction in the hydraulic conductivity of the conventional outflow pathway to AH is the primary cause of OHT in POAG, which leads to glaucomatous optic neuropathy and subsequent loss of visual field, while reduction of IOP is the only proven means of treating POAG. Tam et al. (2017) reported that downregulation of the TJ proteins ZO-1 and tricellulin expressed by endothelial cells of the SC inner wall leads to an increase in the number of open intracellular clefts, as well as an increase in *C* in normotensive WT mice (131). Subsequently, in 2021 we reported the use of this technique to lower IOP and increase outflow facility in the DEX mouse model of steroid induced OHT (132). The study reported in this Chapter was designed to further investigate this approach in the transgenic $MYOC^{Y437H}$ model of OHT and to determine whether *C* could also be increased and additionally, to investigate whether downregulation of TJ proteins ZO-1 and tricellulin had the potential to significantly lower IOP in these animals.

In an initial study, several structural differences in the outflow pathway were observed in the $MYOC^{Y437H}$ transgenic mouse model of OHT when compared to $MYOC^{WT}$, captured by TEM. Some of these features included ECM accumulation around the JCT of the TM, as well as some of these cells having a high number of rER and golgi, indicating proliferative activity. Matrix vesicles were also observed in some regions, indicating necrosis of the cells, which could be the result of accumulation of misfolded myocilin protein which is known to be present in the TM of $MYOC^{Y437H}$ mice. The length of optically empty regions underneath the SC inner wall, presumably indicating regions of fluid flow, was smaller in the $MYOC^{Y437H}$ group compared to $MYOC^{WT}$ group. This could potentially result in an increase in AH outflow resistance, observed in these mice. These data confirm and substantiate previously reported data by Zode et al. (2011) on the ultrastructure of the open angle and SC in $MYOC^{Y437H}$ mice in comparison to WT litter mates (88).

IOP elevation was also confirmed by rebound tonometry in *MYOC*^{Y437H} mice, these showing a significant increase in IOP of ~ 3 mmHg over a 2 M period. *MYOC*^{WT} littermate controls showed no real change in IOP over this time period.

Ex vivo outflow facility measurements were then undertaken in these animals and a non-significant reduction in outflow facility was observed in the MYOC^{Y437H} (9 nl/min/mmHg) cohort compared to *MYOC*^{WT} (10 nl/min/mmHg). Thus, conventional outflow facility in the transgenic MYOC^{Y437H} model of OHT was found to be reduced only by approximately 10% compared to WT littermate controls in this study. This was a far less significant reduction in outflow facility than that which was observed by Kasetti et al. (2016), where outflow facility in *MYOC*^{Y437H} mice was found to be reduced by approximately 42% compared to WT littermates at 10M (87). The variation in *C* observed between the report of Kasetti and the work reported here could be due to the different methods of outflow facility measurement and/or to differences in ages of the mice used in each of these studies. It is quite possible that the older *MYOC*^{Y437H} mice at 10M of age developed greater outflow resistance in comparison to mice at 6M of age and this could account for the smaller difference in outflow facility measurements observed between *MYOC*^{Y437H} and *MYOC*^{WT} in this study.

Baseline IOP measurements and outflow facility were quite high in the current cohort of mice. Temperature readings in the animal facility were taken throughout the course of these experiments. The temperature in Room 1, where the mice were originally housed, was abnormally high and outside of the normal recommended range and hence these mice were moved into Room 2, where the ranges were normal until around Day 60 when they started to climb again. Temperatures rose again beyond the recommended range and this, therefore, could have had an impact on IOP and facility measurements throughout the course of this study. It has also been shown that humidity, as well as additional external factors

experienced by mice in their housing environment, may impact outflow facility measurements (229).

Quantitative PCR was carried out on both $MYOC^{WT}$ and $MYOC^{Y437H}$ ocular tissue to evaluate the effects of the once-off siRNA-targeting TJ proteins ZO-1 and tricellulin in tissue of the outflow pathway. As mentioned above, an alternative dissection technique, the use of which was described in Chapter 3, to enrich for SCEC and minimize TJ expression from cornea and iris tissue, had not yet been developed in the laboratory by the time that the experiments described in this chapter were undertaken. The older technique, used in the studies reported here involved dissecting and homogenizing the whole anterior cup, including cornea and iris tissue. TJ expression in the anterior chamber could therefore become masked by TJ expression in these surrounding tissues. It was interpreted at the time that there was no significant change in TJ transcript expression in either $MYOC^{WT}$ or $MYOC^{Y437H}$ T siRNA treated eyes compared to NT siRNA eyes. It is quite possible however that a change in TJ transcript levels would have been observed if the newer dissection technique were to have been used, as a significant change in IOP in both $MYOC^{WT}$ and $MYOC^{Y437H}$ mice was recorded following injection with T siRNA.

Treatment with T siRNA successfully increased *C* in eyes of both $MYOC^{WT}$ and $MYOC^{Y437H}$ mice, with increases of 29% and 19% respectively, compared to NT siRNA eyes. A greater effect was seen in the $MYOC^{WT}$ mice, while in $MYOC^{Y437H}$ mice the increase almost reached statistical significance ($p = 0.0582$). The percentage increase in *C* for both normotensive $MYOC^{WT}$ and vehicle (DEX mouse study) was consistent, indicating only minor variation between facility measurements of groups taken at different intervals. Interestingly, there was a large difference in the effect on *C* between hypertensive models. A much greater increase in *C* was observed in DEX mice compared to $MYOC^{Y437H}$ animals. In the DEX model TJ protein expression including ZO-1, is known to increase whereas there is no evidence of this in the $MYOC^{Y437H}$ model (185). It is hence reasonable to propose that

siRNA-mediated knockdown of TJs is more effective in an environment with greater TJ expression, as there is a greater availability of TJ mRNA for siRNA to bind.

On delivery of a therapy

Results presented in the previous chapter and from the current study show significant potential for an siRNA-mediated approach in treatment of steroid induced OHT, where there is a recognised and pressing need for improved methods of treatment, and for those cases of age-related POAG with dominant mutations within the myocilin gene, where 2-4% of all cases have *MYOC* mutations, or approximately 2 million subjects world-wide (85). The drawback of this approach however is the transient nature of siRNA expression, with levels of ZO-1 and tricellulin transcripts returning to normal over a number of days (131). In this regard, an experiment was carried out in order to more accurately assess the transient nature of siRNA expression on IOP over time. IOP measurements were taken in $MYOC^{Y437H}$ mice at 0 hr (pre-treatment with siRNA) and every 24-hr post until IOP measurements returned to baseline (Figure 4.10). Mice were injected in one eye with the same concentration of T siRNA as previous experiments and NT siRNA in the contralateral control eye. In this series of experiments a highly significant reduction in IOP of 6.0 [3.2, 8.8] and 3.8 [1.0, 6.6] mmHg ($p < 0.0001$ and $p < 0.01$, 2-way ANOVA with Dunnett's multiple comparisons test, n=9) was observed at both 24 and 48 hr post T siRNA treatment, respectively, compared to pre-treatment baseline IOP (0 hr) (red). IOP levels returned to baseline by 120 hr post-treatment. This illustrates the transient nature of TJ T siRNA on IOP over time. There was no significant reduction in IOP over time in NT siRNA treated eyes compared to baseline (blue).

Since repeated administration of siRNA would likely be required to effectively reduce IOP, a minimally invasive approach to delivery would be needed. Such an approach has in fact been reported for periodic retrograde introduction of low molecular weight compounds directly into the episcleral veins and this could readily be used as a non-invasive method of delivery of siRNA. A delivery device facilitating this approach has been

manufactured, Retroject Inc., Chapel Hill, NC, USA, and is illustrated below (Figure 4.10). It has also been shown that coating nanoparticles with hyaluronan effectively targets both SC and TM cells (230). These particles bind to the CD44 cell surface antigen, which is abundantly expressed on cells of tissues of the outflow pathway. siRNA might be more efficiently deliverable complexed to such particles.

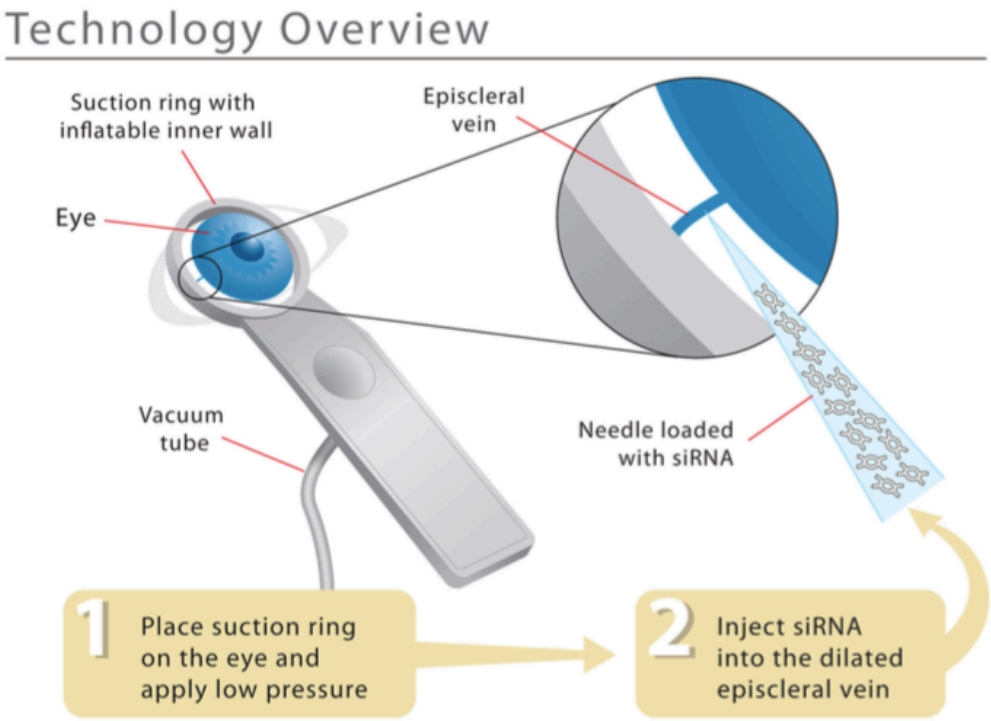

Figure 4.10: Episcleral delivery device.

A schematic of Retroject™ delivery device delivering siRNA directly to the episcleral vein. Suction is applied by the vacuum ring, placed on the eye, exposing the episcleral vein. siRNA is then injected directly into the dilated episcleral vein, where it will travel upstream to Schlemm's canal. This schematic of the Retroject device was modified to include siRNA with permission from Dr. M. Walsh, NC.

An alternative mechanism for delivery of siRNA to the inner wall endothelia of SC would be through the virally mediated expression of a short hairpin RNA (shRNA) in such cells. AAV has been used very successfully to deliver shRNA targeting inner retinal endothelial

TJ components in mouse retina (203). Expression of the shRNA was controlled using a doxycycline -inducible promoter (203). As mentioned in Chapter 1, AAVs are currently the most widely used viral vector in human gene therapy. Available AAV serotypes do not appear to successfully transduce the conventional outflow pathway with any efficiency. However, a number of reports have shown that self-complementary AAV (scAAV) and AAVs with modified capsid proteins can potentially transduce the TM and SC inner wall endothelia (138, 231). Adenoviral vectors have also been shown to successfully transduce the outflow pathway. However, these viruses have been used less in human clinical trials owing to potential immune response issues (232). Transducing SCEC by a once-off intracameral injection with AAV, would probably result in the long-term expression of shRNA necessary for therapeutic effect, rather than the transient downregulation observed with siRNA treatment (Figure 4.11). Self-complementary AAV (scAAV) has been reported to result in maintenance of expression for over 2 years in primates (138). The use of an inducible promotor might also possibly enable AAV to be transcriptionally activated using an inducing agent, topically administered to the cornea, which would allow for controlled periodic expression of shRNA and possibly to avoid hypotony in patients. The use of AAVs to target tissues of the outflow pathway will be discussed in the next chapter.

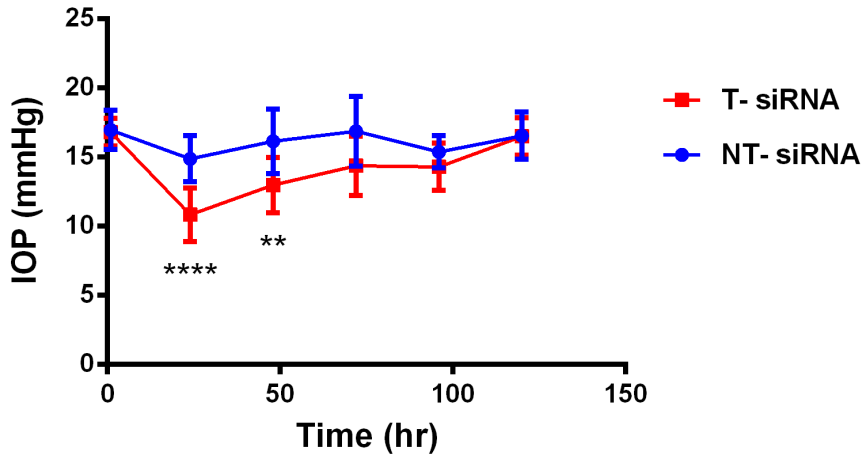

Figure 4.11: Transient nature of IOP lowering effects of T siRNA.

A significant reduction in IOP was observed in T siRNA-treated eyes (red) at 24 hr and 48 hr post-treatment, compared to baseline IOP (0 hr) ($p < 0.0001$ and $p < 0.01$ respectively, 2-way ANOVA with Dunnett's multiple comparisons test, n=9). This reduction in IOP gradually returned to baseline by 120 hr post-treatment, showing the transient nature of siRNA on IOP. There was no significant reduction in IOP observed in NT siRNA eyes (blue), compared to baseline ($p > 0.05$, 2-way ANOVA with Dunnett's multiple comparisons test, n=9).

Statement on collaboration:

Transgenic *MYOC*^{Y437H} mice were kindly provided by Prof. Val Sheffield's lab. The genotyping for this study was carried out by Dr. Marian Humphries, TCD. TEM photographic images were taken by Dr. Elke Lütjen-Drecoll at the University of Erlangen-Nürnberg.

Chapter 5

AAV2/2-mediated expression of *NDI1* targeting mitochondrial dysfunction in *MYOC*^{Y437H} mouse model of ocular hypertension

Abstract

Chadderton et al. (2013) demonstrated that AAV-mediated expression of *NDI1* in retinal tissues, following intravitreal inoculation of virus, afforded ganglion cell protection in a rotenone-induced LHON murine model (6). *NDI1* is a yeast nuclear gene substituting for a number of mitochondrial genes commonly mutated in the respiratory NADH-ubiquinone oxidoreductase complex (Complex 1) in this condition. Mitochondrial dysfunction has also been associated with common multifactorial ocular conditions including AMD and glaucoma. It was therefore of interest to explore the possible protective effects of AAV-mediated expression of *NDI1* in the *MYOC*^{Y437H} mouse model of OHT.

An AAV2 vector with a modified capsid known to facilitate higher levels of transduction and expressing *NDI1*, driven by a cytomegalovirus (CMV) promoter, was injected both intracamerally and intravitreally into separate cohorts of *MYOC*^{Y437H} mice. Quantitative PCR analysis on RNA extracted both from retinas and anterior tissues six months post-inoculation showed elevations in expression of *NDI1*. In addition, inoculation of control AAV expressing eGFP provided evidence for expression of the reporter both in retinas and within the anterior chamber, most obviously in corneal endothelium. Measurements of IOP were taken in animals injected with AAV-*NDI1* both intravitreally and intracamerally. Over a six-month period, IOP in control (AAV-eGFP) and in AAV-*NDI1* mice continued to rise in those animals that had received intravitreal inoculations and

NDI1 expression appeared to have a negative impact on ganglion cell survival in these animals, contrary to the protective effect observed by Chadderton et al. (2013) in the LHON model. However, in intracamerally-inoculated mice, IOPs remained steady and did not rise significantly over this time period, indicative of a potential beneficial therapeutic effect. Interestingly however, outflow facility in treated eyes, assessed by *iPerfusion* at 8M of age, did not increase significantly in these animals. While speculative, interpretation of these data is discussed in the context that *iPerfusion* measures facility primarily in the conventional pathway, whereas an IOP-reducing effect could have been the result of elevation in outflow through the uveoscleral route over the six-month period. These observations could be extended to future assessment of uveoscleral and uveovortex outflow in the unconventional pathway using direct tracer-based methods.

Introduction

Mitochondrial dysfunction has been shown to be involved in a variety of eye disorders ranging from primary mitochondrial conditions to more common multifactorial diseases including, for example AMD and glaucoma (233). Glaucoma involves slow but progressive optic neuropathy, followed by RGC death, and eventual loss of vision. Loss of RGCs appears to be preceded by dendropathy, the shrinking of soma and atrophy of axons (234). Mitochondrial function appears to be reduced in glaucomatous SCEC, with these cells showing significantly reduced rates of oxygen consumption (OCR), compared to healthy SCEC (Chapter 2). Gene therapy in a mouse model of LHON, directly targeting the mitochondria of RGCs, has recently been developed by Chadderton et al. (2013) (6). In view of mitochondrial involvement, this form of therapy could potentially have a beneficial impact on the transgenic *MYOC*^{Y437H} mouse model of OHT. These animals show reduced outflow facility, elevated IOP and loss of RGCs (88). Hence, the aim of the work described in this chapter was to test this hypothesis.

Gene therapy shows benefit in a mouse model of LHON

LHON is a maternally-inherited disease, predominantly affecting males (235). Degeneration of RGCs and the optic nerve results in the progressive loss of visual fields (236). In most cases, patients with LHON have mutations in the genes encoding for components of the mitochondrial respiratory NADH-ubiquinone oxidoreductase complex or Complex 1 (237), which is involved in the transport of electrons from NADH to ubiquinone. There is now growing evidence that mitochondrial dysfunctional may play a greater role in the molecular pathologies of neurodegenerative diseases, such as Alzheimer's disease (AD) and Huntington's disease than was earlier thought (238). The retina, like the brain, is highly energy demanding in driving visual transduction and visual processing through second order and output (ganglion) neurons and hence any compromise in mitochondrial function could

have major pathological consequences for retinal tissues. Disruption of Complex 1 function in LHON, results in an increase in reactive oxygen species (ROS) and a reduction in ATP synthesis (239). ATP synthesis is linked to OCR by the proton gradient that exists across the mitochondrial inner membrane during OXPHOS (240). Mutations in Complex 1, which occur in LHON, result in reduced OCR, which can be used as a measurement for cellular mitochondrial activity. As outlined in Chapter 2, glaucomatous SCEC showed reduced OCR compared to healthy SCEC and so targeting mitochondrial activity in the transgenic *MYOC*^{Y437H} mouse model of OHT might plausibly prove to be beneficial in this animal model of open-angle glaucoma.

Chadderton et al. (2013) (6) used a nuclear gene, NADH-quinone oxidoreductase (*NDI1*), located at the inner mitochondrial membrane of *Saccharomyces cerevisiae,* encoding a substitute single subunit of Complex 1 (241). This approach by-passes barriers of delivery to mitochondria by employing a single nuclear gene encoding a trans-kingdom complex 1 equivalent, which is imported into mitochondria and is mutation-independent (6). As described by Chadderton et al. (2013) (6), a recombinant AAV serotype 2 (AAV2/2) expressing *NDI1* from a CMV promoter (AAV-*NDI1*), was intravitreally injected into mice and was shown to successfully target RGCs. This study demonstrated that a once-off intravitreal injection of AAV-*NDI1*, resulted in a significant reduction in RGC loss and optic nerve atrophy in a rotenone-induced mouse model of LHON, compared to AAV-*GFP* control eyes. A preservation of retinal function was also observed, as assessed by manganese (Mn^{2+}) enhanced magnetic resonance imaging (MEMRI) and optokinetic responses (OKR) in AAV-*NDI1* treated eyes, compared to AAV-GFP control eyes (6).

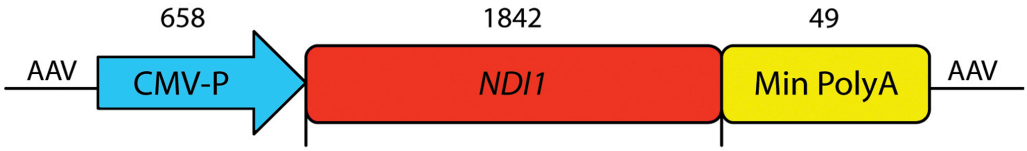

Figure 5.1: *NDI1* construct.

Diagram representing the AAV-NDI1 construct. A CMV promoter (CMV-P) was used together with a minimal polyadenylation signal (Min Poly A) located at the 3' end of the gene. Fragment sizes are indicated on the diagram as base pairs. Taken from Chadderton et al. (2013) (6).

AAV transduction of the outflow pathway

AAV vectors are now the most widely used for gene therapy purposes (242) and have been shown to be capable of transducing cells from a wide variety of tissues both *in vitro* and *in vivo* (243, 244). Many clinical trials involving the use of AAV vectors have been registered, including, for example, ten trials for haemophilia A and B (Haemophilia A: AAV5. Pre-clinical development UniQure; AAVhu37 Phase 1/II Bayer/Ultragenyx; AAV2/8 Phase 1 University College London; AAV2/6 Phase II Pfizer; AAV-LK03 Phase 1/II Spark Therapeutics; AAV8 Phase 1 Takeda; AAV5 Phase 1/II BioMarin. Haemophilia B: AAV Phase II/III Spark-Pfizer; scAAV2/8 Phase 1 St. Jude's Children's Hospital; AAV-S3 Phase 1 University College London). There have also been a number of recent FDA/EMA approvals involving the use of AAV. Luxturna, an AAV vector expressing the *RPE65* gene was approved for clinical use in 2017, and more recently, Zolgemnsma (Novartis) an AAV9 vector expressing the *SMN1* gene was approved as a gene replacement therapy for spinal muscular atrophy, a progressive muscle atrophy owing to loss of motor neurons. (Clinicaltrials.gov). While AAV2 has been used successfully to deliver genes to the retina (245), less success has been achieved with AAV2 in targeting the anterior segment of the eye, notwithstanding a growing interest in targeting tissues such as the TM which has a vital

role in the pathophysiology of glaucoma (246). However, in a study by Bogner et al. (2015) effective delivery of capsid mutated scAAV2 to the anterior chamber was demonstrated and resulted in efficient transduction of the TM in both rats and mice (246). Also, in regard to increasing AAV infectiveness, it is notable that tyrosine phosphorylated AAV2 vectors enter cells efficiently but fail to transduce optimally. This in part is due to the ubiquitination of AAV-capsids followed by proteasome degradation. Mutating the surface-exposed tyrosine to another residue allows the vector to escape phosphorylation and ubiquitination, thus preventing proteasome-mediated degradation (247). Such an approach was reported by Zhong et al. (2008) (247), and has led to the development of AAV2 vectors capable of high-efficiency transduction at lower doses. Tyrosine mutant AAV2 vectors have also been shown to increase transduction efficiency in mouse retina (248). By mutating three tyrosine (Y) residues on this AAV2 vector capsid to non-phosphorylated phenylalanine (F), an increase in transduction efficacy of over 30 fold was observed in RGCs (248). The recombinant AAV2/2 with a CMV promoter expressing human *NDI1* used in the LHON studies outlined above and carrying a 3Y-F capsid mutation (Figure 5.1) was generated at TCD by Dr. GJ Farrar and colleagues (AAV-Opt*NDI1*) (E.U and U.S patent no. EP2607375A1 and US20150099798A1, respectively). The use of this vector (AAV-Opt*NDI1*) in attempting to transduce both the retina and the conventional outflow pathway of $MYOC^{Y437H}$ hypertensive mice will be discussed in this chapter. As a control, enhanced green fluorescent protein (eGFP) with the same 3Y-F capsid mutation was used in contralateral control eyes (AAV-OptEGFP).

Intravitreal delivery targeting RGCs was undertaken with the aim of preventing RGC loss in these mice. Intracameral delivery in the hope of targeting the conventional outflow pathway, specifically SCEC and the TM, was also carried out with the aim of increasing outflow facility and reducing IOP in these transgenic hypertensive animals. While intravitreal inoculation afforded no protection to ganglion cells, intracameral inoculation

resulted in a statistically significant reduction in IOP. Possible reasons as to why there was little evidence for an accompanying enhancement of outflow facility as evaluated by *iPerfusion* is discussed.

Results

A. Relative mRNA transcript expression of *NDI1* in ocular tissues

In order to validate whether the AAV2/2 was successfully transducing tissues of the outflow pathway and the retina, enucleated tissue was homogenized, and quantitative PCR carried out. Whole anterior segment homogenization from *MYOC*^{Y437H} six months post intracameral injection of either AAV-OptEGFP (control) or AAV-Opt*NDI1* (treated) was carried out. Treated eyes showed a significant increase of 1.1 [0.7, 1.5] relative fold gene expression ($p < 0.01$, paired t-test, n=4) compared to control eyes (Figure 5.2A). Whole retinas were dissected out from *MYOC*^{Y437H} mice (n=3) that had been intravitreally injected with either AAV-OptEGFP (control) or AAV-Opt*NDI1* (treated), six months post. A significant increase of 0.8 [0.3, 1.2] relative fold gene expression ($p < 0.05$, paired t-test, n=3) was observed in treated eyes compared to control eyes (Figure 5.2B). These data indicate that viral delivery of human *NDI1* resulted in the successful transduction of both anterior segments and retinas of treated eyes.

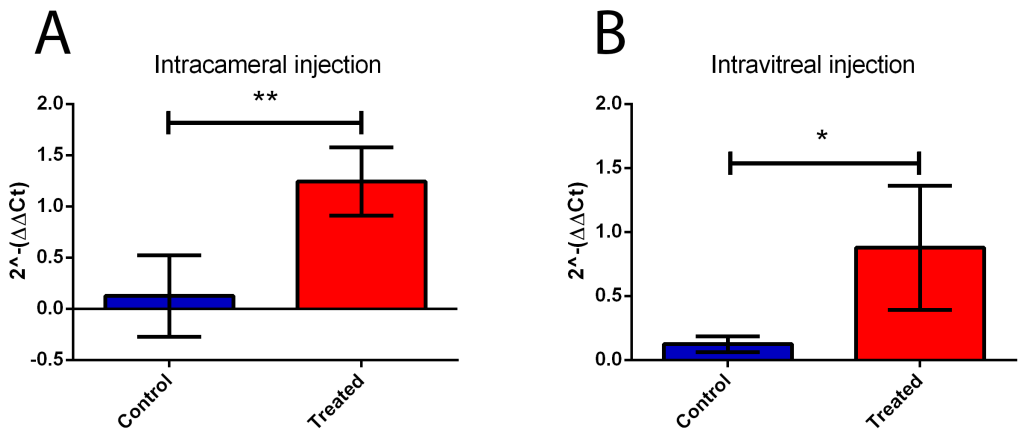

Figure 5.2: Relative mRNA transcript expression of human *NDI1*.

(A) Whole anterior segment qPCR analysis showed a significant increase in relative mRNA expression of NDI1 in treated eyes compared to control eyes, six months post intracameral injection (p < 0.01, paired t-test, n=4). (B) Whole retina qPCR analysis showed a significant

increase in relative mRNA expression of NDI1 in treated eyes compared to control eyes, six months post intravitreal injection ($p < 0.05$, paired t-test, n=3).

B. Assessment of AAV-mediated eGFP fluorescence in anterior tissues

MYOC^{Y437H} animals were intracamerally injected with AAV-Opt*NDI1* (treated) in one eye and AAV-OptEGFP (control) in the other. While treated eyes were used for qPCR analysis, control eyes were used to analyse viral transduction of the anterior segment of the eye. These eyes were enucleated six months post intracameral injection, cryosectioned and observed for eGFP expression, with a counter nuclei stain (DAPI) in blue, using confocal microscopy. This AAV2/2 with modified capsid appeared to successfully transduce off-target areas of the corneal endothelium in the anterior chamber (Figure 5.3A+C) and the iris (E) with eGFP expression apparent in both. However, transduction of the outflow pathway i.e., the TM and SC did not appear to be evident (A). There appeared to be some autofluorescence in the negative control samples at the ciliary body (B). There appeared to be little autofluorescence at the corneal endothelium however, and transduction of this area could be visualised (D). These observations indicate that AAV-Opt*NDI1* was expressed in corneal endothelium, but there was little evidence for any expression in outflow tissues.

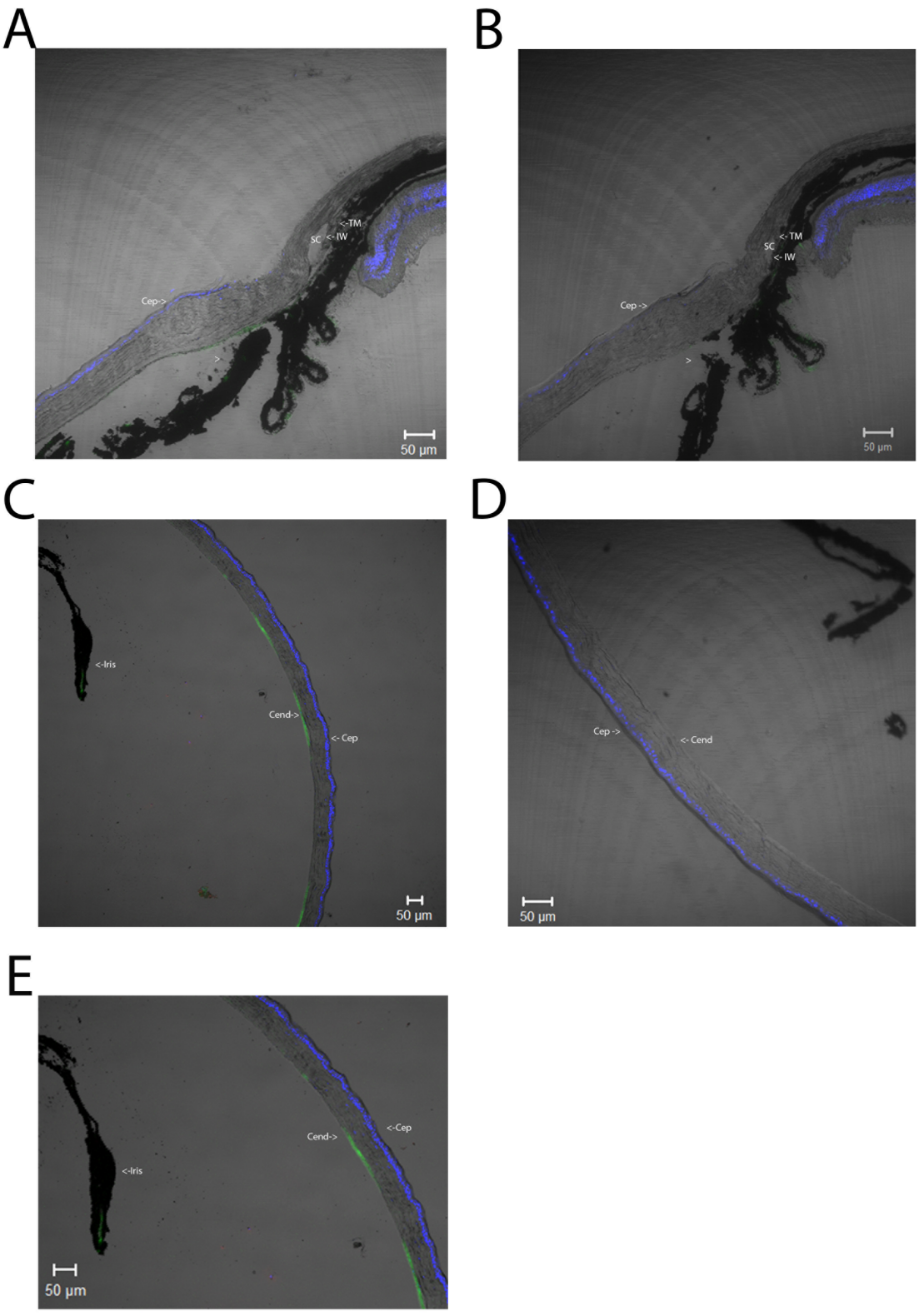

Figure 5.3: AAV-OptEGFP expression following intracameral injection.

Following intracameral injection with AAV-OptEGFP, off-target expression was observed along the corneal endothelium (A+C) and in the iris (E). Successful transduction of the outflow pathway was not observed in this in situ hybridisation, however (A). Negative

control samples showed autofluorescence at the ciliary body (B) and no autofluorescence at the corneal endothelium, further supporting the hypothesis of successful transduction of this area (D). SC=Schlemm's canal; IW=inner wall; TM=trabecular meshwork; >=open iridocorneal angle; Cend=corneal endothelium; Cep=corneal epithelium; Iris=iris.

C. Transduction of the retina by AAV-Opt*NDI1* and AAV-OptEGFP and effect on ganglion cell viability

MYOC^{Y437H} mice were intravitreally injected with AAV-Opt*NDI1* (treated) in one eye and AAV-OptEGFP (control) in the other eye. Six months post inoculation, ocular tissue was enucleated and whole mount retina staining was carried out. Brn3a staining (red) was used to identify and quantify RGCs on whole mount retinas, using Olympus microscopy and cellSens programming analysis (Figure 5.4A+B). A full description of RGC staining and quantification is outlined in Materials and Methods (Chapter 6). RGC counts were carried out for both control (A) and treated (B) eyes. A significant reduction in RGCs of 396.6 [17.9, 775.3] mm^2 ($p < 0.05$, paired t-test, n=8) was observed in treated eyes compared to control eyes (D). Hence, AAV-mediated *NDI1* expression negatively impacted on ganglion cell survival in these animals. Control eyes treated with AAV-OptEGFP showed abundant eGFP expression across the retina, indicating successful transduction of this recombinant AAV2/2 to the posterior segment of the eye (C).

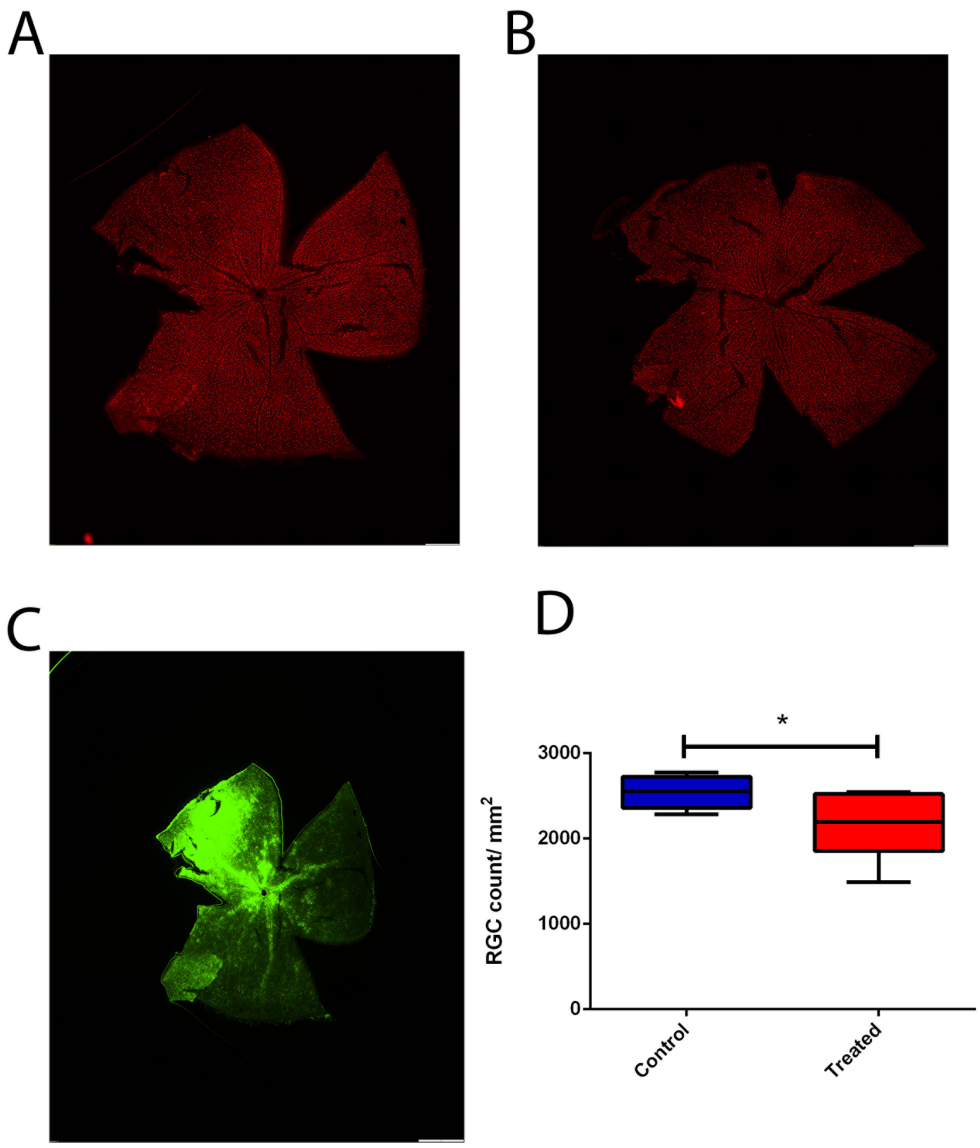

Figure 5.4: Intravitreal inoculation with AAV-Opt*NDI1* and AAV-OptEGFP.

Brn3a staining (red) of RGCs was used to quantify the number of healthy RGCs in both control (A) and treated (B) eyes. (C) eGFP expression (green) was observed across the retina, following a once-off intravitreal injection. (D) A significant reduction in RGCs was observed in treated eyes compared to control eyes ($p < 0.05$, paired t-test, n=8). Scale bars represent 1 mm.

D. Effect on IOP of intracameral and intravitreal inoculation of AAV-Opt*NDI1* in *MYOC*^{Y437H} mice.

MYOC^{Y437H} mice (n=17) at ~2M old were anesthetized and IOP measurements taken using rebound tonometry. Mice were then administered 1.5 µL of AAV-Opt*NDI1* (1.5×10^8 vg/µL) to the anterior chamber by intracameral injection, giving a final concentration of 2.3×10^8 vg/eye. Contralateral control eyes received an identical injection of 1.5 µL containing the same concentration of AAV-OptEGFP. Monthly IOP readings were taken following this once-off inoculation both to control and AAV-Opt*NDI1* treated eyes. IOP readings were carried out for a total of six months (Figure 5.5A). In the control group, there was a significant increase in IOP from baseline observed at month 6 of 2.2 [0.6, 3.8] mmHg (mean [CI]), ($p < 0.01$, 2-way ANOVA with Tukey's multiple comparisons test, n=17) (blue). There was no significant change in IOP in the treated group over the six month period (red). A significant increase in IOP from baseline of 2.4 [1.7, 3.1] mmHg ($p < 0.0001$, one sample t-test to theoretical mean of 0, n=17) was observed in control eyes six months post injection with AAV-OptEGFP (Figure 5.5B, blue). While treated eyes showed no significant increase in IOP from baseline of 0.5 [-0.9, 1.9] mmHg ($p > 0.05$, n=17) six months post injection with AAV-Opt*NDI1* (red).

A separate cohort of *MYOC*^{Y437H} mice (n=17) were anesthetized and IOP measurements taken using rebound tonometry. These mice were injected with 3 µL of AAV-Opt*NDI1* (1.5×10^8 vg/µL) into one eye by intravitreal injection, while 3 µL of AAV-OptEGFP (1.5×10^8 vg/µL) was injected into the vitreous of the contralateral control eye. This represented a final concentration of 4.5×10^8 vg/eye for both eyes. IOP readings of these mice were also taken at a monthly timepoint (Figure 5.5C). In the control group, there was a significant increase in IOP observed at month 5 and 6 from baseline of 1.8 [0.0, 3.6] mmHg ($p < 0.05$, 2-way ANOVA with Tukey's multiple comparisons test, n=17) and 2.2 [0.4, 4.0] mmHg ($p < 0.01$), respectively (blue). In the treated group, there was also a

significant increase in IOP from baseline observed at month 6 of 2.2 [0.5, 3.9] mmHg ($p < 0.01$) (red). At six months post intravitreal injection, a significant increase in IOP from baseline of 2.1 [1.0, 3.3] mmHg ($p < 0.01$, one sample t-test to theoretical mean of 0, n=17) was observed in control eyes (Figure 5.5D, blue). A significant increase in IOP from baseline of 2.2 [1.0, 3.4] mmHg ($p < 0.01$) was also observed in treated eyes (red). Eyes treated with AAV-Opt*NDI1* by intracameral injection showed no significant increase in IOP over the six month period, as would be expected in hypertensive *MYOC*^{Y437H} mice over this time point, as shown in the control group. Eyes treated with AAV-Opt*NDI1* by intravitreal injection however, showed a significant increase in IOP over time, as did the control group.

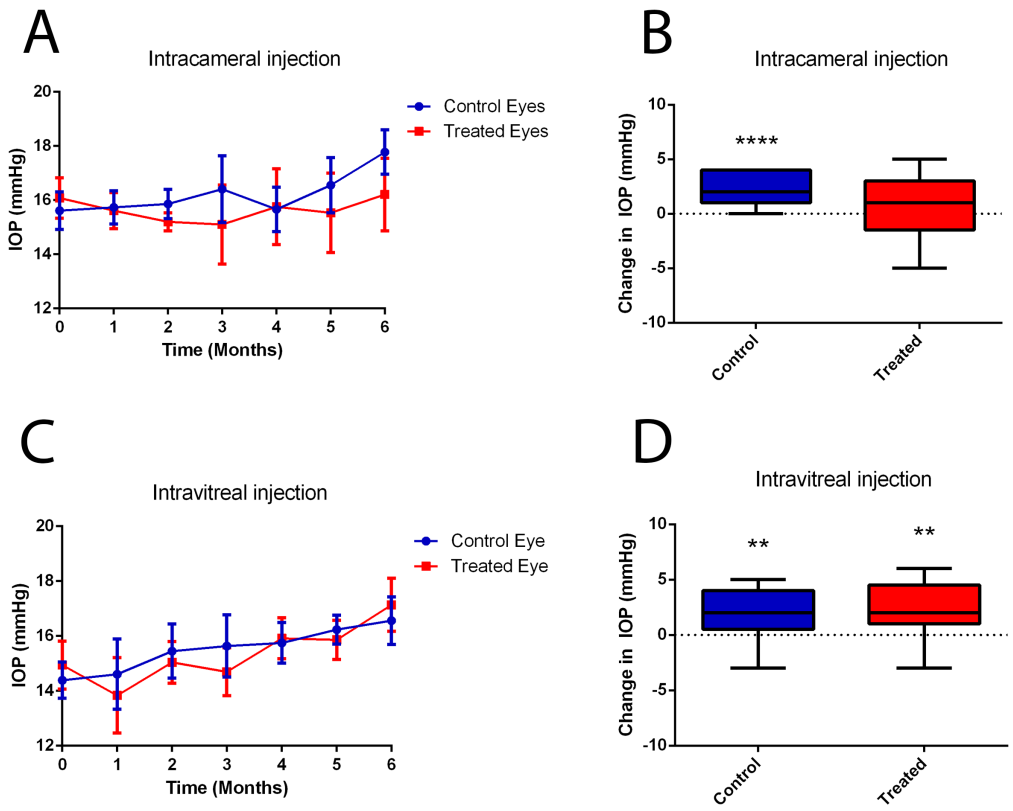

Figure 5.5: IOP characterisation over six months following treatment with either AAV-OptEGFP or AAV-Opt*NDI1*.

(A) Monthly IOP measurements were taken following a once-off intracameral injection with AAV-OptEGFP (control) in one eye (n=17) and AAV-OptNDI1 (treated) in the other (n=17). (B) Following this once-off intracameral injection, a significant increase in IOP six months post injection compared to baseline was observed in control eyes ($p < 0.0001$, one-sample

t-test to the theoretical mean of 0, n=17). No significant increase in IOP was observed in treated eyes, however ($p > 0.05$, one-sample t-test to the theoretical mean of 0, n=17). (C) Monthly IOP measurements were also taken following intravitreal injection with AAV-OptEGFP (control) in one eye (n=17) and AAV-OptNDI1 (treated) in the other (n=17). (D) A significant increase in IOP was observed six months post injection compared to baseline in both control and treated eyes, following intravitreal injection ($p < 0.01$, one-sample t-test to the theoretical mean of 0, n=17 for both control and treated eyes).

E. Effect of intracameral injection with AAV-Opt*NDI1* on *ex vivo* conventional outflow facility in *MYOC*^{Y437H} animals

To determine the effects of AAV-Opt*NDI1* on treated eyes compared to contralateral control AAV-OptEGFP eyes on conventional outflow facility (*C*), eyes were enucleated six months post intracameral inoculation and mounted onto the *iPerfusion* system. Facility data below for *MYOC*^{Y437H} mice showed that control eyes had an average facility of 15.1 [11.6, 19.3] nl/min/mmHg, while treated eyes had an average facility of 15.9 [13.7, 18.1] nl/min/mmHg (Figure 5.6A+B). The perfusion system facilitated comparison of *C* between paired contralateral treated and control eyes for *MYOC*^{Y437H} hypertensive mice. An increase in *C* of 5 [-25, 47] % ($p > 0.05$, weighted paired t-test, n=9) was observed in treated eyes compared to control eyes (Figure 5.6C). However, this trend in elevation of *C* did not reach statistical significance.

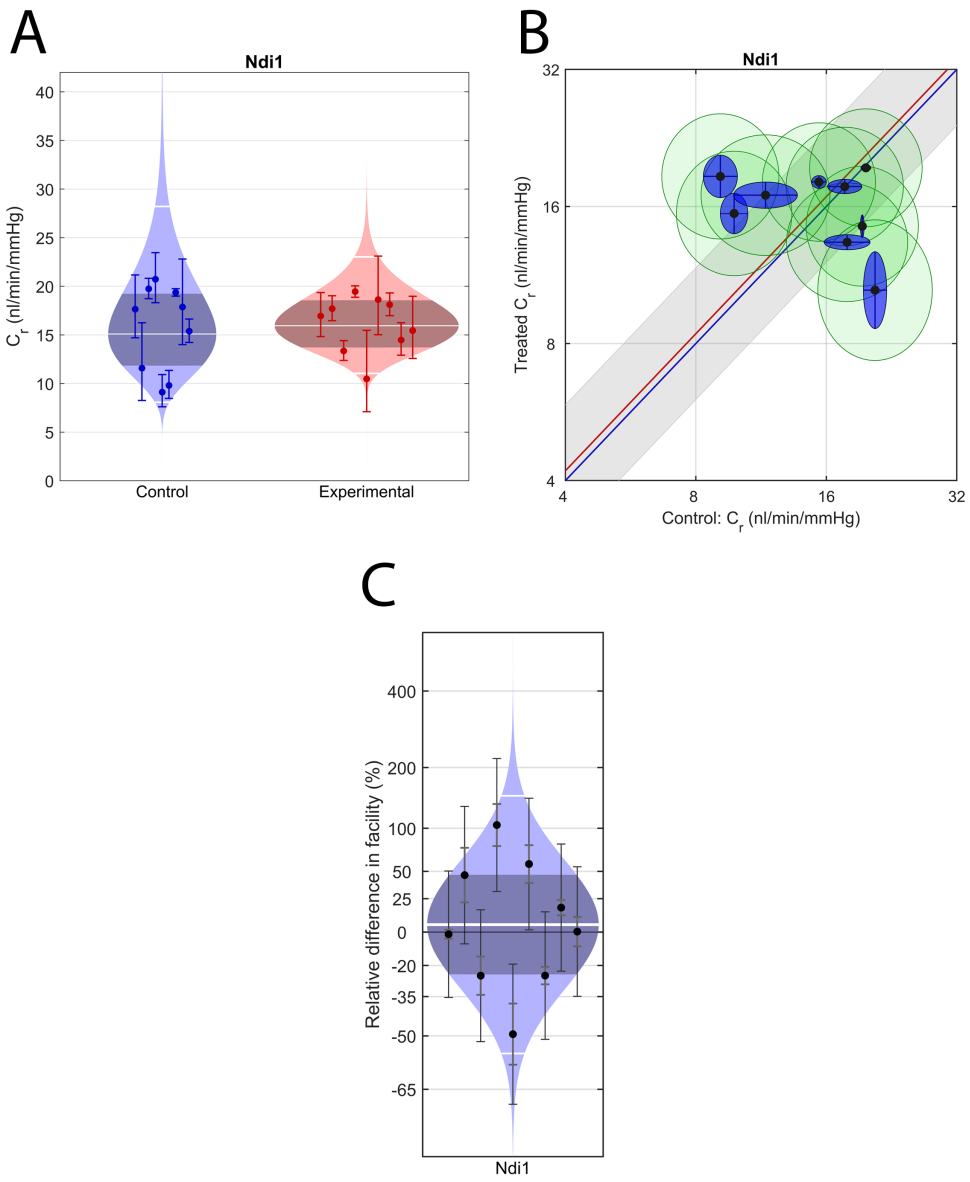

Figure 5.6: Effect of AAV-Opt*NDI1* on outflow facility in hypertensive *MYOC*^{Y437H} mice.

(A) Cello plot depicting individual outflow facility values for eyes at 8 mmHg (C_r) and statistical distribution of both control (AAV-OptEGFP) ($p > 0.05$, weighted unpaired t-test, n=9) and experimental (AAV-OptNDI1) ($p > 0.05$, weighted unpaired t-test, n=9) groups for MYOC^{Y437H} hypertensive mice. (B) Paired outflow plots for MYOC^{Y437H} hypertensive mice present paired perfusion analysis ($p > 0.05$, weighted paired t-test, n=9). (C) Cello plot depicting a non-significant increase in C of 5% observed in treated eyes of MYOC^{Y437H} hypertensive mice compared to contralateral control eyes ($p > 0.05$, weighted paired t-test, n=9).

Discussion

AAV-mediated *NDI1* gene therapy, without the optimised tyrosine capsid used here, was initially shown by Chadderton et al. (2013) to successfully prevent RGC loss in a mouse model of LHON (6). Given such success it was of interest to speculate as to whether this approach might have the potential to provide therapeutic intervention to $MYOC^{Y437H}$ mice, showing increased IOP, reduced outflow facility and RGC loss over time, particularly since mitochondrial damage, induced by oxidative stress, has been reported as a feature of open-angle glaucoma (249). Not much is known about mitochondrial respiration in $MYOC^{Y437H}$ mice and it is not known whether it is negatively affected by the *MYOC* mutation. The aim of this study was to investigate whether this form of gene therapy could provide benefit in these animals.

Quantitative PCR analysis showed successful transduction of *NDI1* AAV2/2 in both anterior segments and retinas of injected eyes. The whole anterior cup was homogenized including the cornea and lens tissue, as the newer technique (discussed in Chapter 3) had not yet been developed. IHC analysis revealed extensive eGFP expression along the corneal endothelium. Expression in corneal endothelium has also been demonstrated using AAV9, an observation used by O' Callaghan et al. (2017) for the secretion of MMP3 into the anterior chamber, where the enzyme moved with the natural aqueous flow into the TM, reducing levels of ECM (51). In the current scenario however, *NDI1* is not a secretory protein. Successful off-target transduction of the iris was also observed. In this series of experiments, little or no expression of eGFP was detectable in targeted tissues of the anterior chamber, for example in the inner wall of SC or TM. However, it cannot be excluded that levels of expression below the threshold of eGFP detection may have occurred. It should be noted however, that both TM and SC tissues of the outflow pathway have been found to be difficult to target using AAV therapeutics (250).

Following a once-off intracameral injection with AAV-Opt*NDI1* in one eye and AAV-OptEGFP in the contralateral control eye, elevated IOP over time was prevented in the treated eyes. IOP in control eyes increased over time, as would be expected in this transgenic model of OHT. IOP was first measured in these mice at ~2M and final IOP was therefore taken at ~8M. A significant increase in IOP over this six-month time period would be expected in untreated animals. Following *ex vivo* perfusion analysis however, there was a 5% increase in conventional outflow facility observed in *NDI1* treated eyes compared to eGFP control eyes, which was not statistically significant.

This begged the question as to why there was an IOP lowering effect as a result of *NDI1* expression in anterior tissues. While eGFP fluorescence was not seen in the uveoscleral regions of sections, this technique has limited sensitivity and therefore expression of the AAV in uveoscleral tissues beneath the threshold of detection might have been sufficient to target mitochondrial dysfunction in these tissues. Accepting the speculative nature of this hypothesis, this could nevertheless have resulted in an increase in outflow through this channel over the six month period. While very much more demanding to assess than in the conventional pathway, uveoscleral outflow can be quantified in mice by the use of labelled (either radioactive or fluorescent) markers of known molecular weight (43). Given the results obtained here, future studies of this sort may be warranted, based on the provocative hypothesis that *NDI1* expression may reduce IOP by targeting the unconventional outflow pathway. RGC counts were not carried out following intracameral injection with eGFP and *NDI1*. This is something that could be done in future studies.

AAV2/2 expressing *NDI1* was also administered intravitreally, where successful RGC survival was observed in the previous LHON study by Chadderton et al. (2013) (6). Following a once-off intravitreal injection with AAV-Opt*NDI1* in one eye and AAV-OptEGFP in the other, increased IOP was observed in both control and treated eyes six months post injection. eGFP expression showed successful transduction of the retina

following intravitreal injection, however. No prevention of IOP elevation was observed in treated eyes using this procedure. Furthermore, Brn3a antibody staining was used to identify healthy RGCs in both control and treated retinas. A significant loss of RGCs was observed in treated eyes compared to control eyes. It appeared clear that the AAV-mediated *NDI1* expression had an adverse effect on RGC survival in $MYOC^{Y437H}$ mice. Clearly there are major pathological differences between the rotenone induced LHON model and the ganglion cell degeneration induced by the $MYOC^{Y437H}$ mutation which may well account for this. Another possible cause of toxicity may have been that the viral dose may have been too high, resulting in RGC death. However, 3×10^9 vp of AAV-*NDI1* was used by Chadderton et al. (2013) (6) and 1×10^{10} vp was used by Zhong et al. (2008) (247) when using the tyrosine mutated capsid. In this study, 4.5×10^8 vp was used and so it is unlikely that viral dose impacted on RGC survival.

In conclusion, AAV-mediated expression of *NDI1* was obtained in the retina and in tissues of the anterior chamber of $MYOC^{Y437H}$ mice following intravitreal and intracameral inoculation. Data obtained from the intracameral injections suggest a potentially beneficial effect in reducing IOP over a six-month period. However, further investigations are required in order to determine the mechanistic basis for such reduction.

Future work

In order to determine whether this mouse model of OHT (*MYOC*^{Y437H}) is suitable for this gene therapy, characterising the model in full would be beneficial going forward. An investigation into the mitochondrial activity of these mice would be advantageous as *NDI1* targets Complex I of the mitochondrial electron transport chain. A dose dependent study would also be beneficial to investigate whether the vector dose used is the most suitable for both intracameral and intravitreal delivery, separately. Due to the potentially beneficial impact of *NDI1* on IOP lowering over 6M, following a once-off intracameral injection, various experiments should be carried out investigating the uveoscleral outflow pathway, TM survival and RGC survival. The *iPerfusion* system predominantly measures the conventional outflow pathway and so outflow facility through the uveoscleral or unconventional outflow pathway should also be measured, using fluorescent markers. TM survival experiments should be carried out to investigate whether *NDI1* is having a beneficial effect on TM cell survival. RGC survival should also be quantified on intracamerally injected tissue, as IOP lowering could be the result of RGC survival in *NDI1* treated eyes compared to eGFP control eyes.

Statement on collaboration

The 3Y-F capsid mutated AAV2/2-Opt*NDI1* and AAV2/2-OptEGFP were developed by Dr. Sophia Millington-Ward, TCD. Genomic titres of both were determined by Dr. Naomi Chadderton, TCD. Intravitreal injections were carried out by Dr. Paul Kenna, TCD.

Conclusion

There is a need for more effective and long-term drugs directly targeting tissues of the conventional outflow pathway. While IOP-lowering topical medications have been of immense value, not all patients respond to such drugs in a similar way. Latanoprost, for example, is one of the most widely used IOP-lowering drugs and can produce reductions in IOP of over 30% from baseline in patients with IOPs ranging from 20 to 24 mmHg. IOP reductions can be even higher in patients with IOPs of greater than 24 mmHg (102). However, using latanoprost or other prostaglandin drugs, reductions in IOP are not seen across all patient cohorts. For example, in one study, latanoprost reduced IOP by 30% in only 10% of patients (103). The overall picture is that up to 6% of people do not respond optimally to topical IOP-lowering drugs (251-253), providing a clear rationale for the development of improved forms of non-invasive drug treatment.

The aims of the work presented in this thesis were to develop novel therapeutic approaches for OHT and glaucoma. In an initial study, fibrotic-like changes to glaucomatous human SCEC were identified, further substantiating the concept that treatments targeting fibrotic characteristics could be beneficial in a disease setting. An example of such was recently reported by Li et al. (2021), where treatment with Netarsudil, a ROCK inhibitor, decreased expression of fibrotic markers α-SMA and fibronectin, showing anti-fibrotic properties capable of restoring outflow facility function and reducing IOP, in a DEX mouse model of OHT (123).

In a second study, a novel approach to enhancement of aqueous outflow facility by siRNA-mediated downregulation of SC endothelial TJ proteins, ZO-1 and tricellulin, resulting in an increase in paracellular permeability of SCEC, was tested in a clinically relevant setting. Systemic or localized use of GCs can result in dangerously high OHT, and there is currently a need for an effective means of rapid intervention. Data was presented in which siRNA-mediated suppression of SC endothelial TJs was used in a DEX-induced

murine model of steroid-induced OHT and resulted in significantly increased AH outflow facility and reduced IOP in these animals (132). Given the success achieved in mice, this approach has the potential to show efficacy in patients with secondary, GC-induced glaucoma. RNA therapeutics have gained increasing interest over the past decade and a growing number of RNA-based therapeutic trials have recently been registered (254) and the number of approved RNA therapeutics continues to increase. These include QPI-1007 (Quark), an siRNA targeting caspase-2 for suppression of apoptosis in non-arthritic anterior ischemic optic neuropathy (NAAION); AGN211745 (siRNA/Allergan), an siRNA that targets VEGFR1 for treatment of AMD; Bevasiranib (Opko Health), an siRNA that targets VEGF for diabetic macular oedema; PF-04523655 (Quark), an siRNA that targets RTP801/REDD1, an apoptotic stress response gene; ALY040012 (Sylentis), which is an siRNA targeting OHT. One significant drawback of RNAi is that it is not easy to achieve total ablation of target transcripts. In fact, one such drug (Bevasiranib) was withdrawn owing to lack of efficiency in suppressing VEGF activity. In this regard, a major advantage of the current procedure is that total ablation of transcript is not necessary, partial knock down successfully opens the paracellular pores and allows for greater AH outflow in the DEX mouse model of GC-induced OHT (132). As emphasized in Chapter 3, a minimally invasive approach will be needed for treatment delivery to be successful in a clinical setting and it is notable that a device that would facilitate episcleral delivery of siRNA has been manufactured by Retroject Inc., Chapel Hill, NC, USA (Figure 4.10). Episcleral delivery is achievable in mice (Dr. M. Walsh, personal communication to PH) and in human subjects could be carried out as an outpatient procedure. However, for further quantitative evaluation of this route of delivery in terms of target downregulation, primate studies would be needed. It should be emphasised that while the effects of siRNA on downregulation of transcripts is transient in nature, the condition being targeted in this instance is one of acute steroid-induced elevation in IOP, where possibly a single dose of the therapy could show efficacy

in lowering IOP. However, the minimally invasive nature of episcleral delivery would in principle allow administration of the drug on a periodic basis. However, it should be borne in mind that intracameral or episcleral delivery of AAV targeting tissues of the outflow pathway could, in principle, result in the long-term expression of shRNA. A study carried out by Buie et al. (2010) showed successful transduction of the TM using scAAV2 in rodents, however successful transduction of SC inner wall was not evident (138). An AAV serotype that could successfully transduce SC by intracameral or episcleral delivery would be extremely beneficial when attempting to target this region of the conventional outflow pathway and would be extremely interesting to follow up in future studies.

The potential therapeutic efficacy of AAV-mediated expression of human *NDI1* in *MYOC*^{Y437H} mice was also investigated. AAV-based gene therapy trials have at this stage been widely reported in treatment of various ocular diseases, the first therapeutic being approved in 2017, the drug, Luxturna (Spark Inc PA), targeting patients with LCA with homozygous recessive mutations in the *RPE65* gene (255). While IOP was successfully stabilized following intracameral inoculation of virus, outflow facility was not significantly increased, suggesting that outflow through the uveoscleral route might be enhanced. While accepting the speculative nature of this possibility based on current data, further analysis of AAV transfection of uveoscleral tissues and quantification of outflow through the uveoscleral route would be interesting to follow up in future investigations.

Final Discussion

In summary, Chapter 2 was a characterisation study investigating the various morphological, cellular and mechanical changes that occur in SCEC once they become glaucomatous in phenotype. These SCg cells showed increased expression of adhesion marker VE-cadherin, as well as increased expression of fibrotic marker α-SMA and pro-fibrotic marker TGF-β2. These changes may have an effect on the stiffness and porosity of these cells, observed in glaucoma. These SCg cells also appeared to be larger in size, proliferate, migrate and divide at a significantly higher rate compared to healthy SC cells. They also appeared to have reduced mitochondrial activity compared to their healthy counterpart. TGF-β2 is a known driver of fibrosis and is found in abundance in the AH of glaucoma patients and so it was of interest to treat healthy SC cells with TGF-β2 and see if the resulting phenotype mimics that of SCg. Both TGF-β2 treated cells and SCg cells showed increased cell proliferation and reduced mitochondrial activity. However, TGF-β2 treated cells showed increased ATP production while ATP production of SCg cells remained similar to healthy SC cells. It is hypothesized that healthy SC cells generate ATP through OXPHOS, while SCg cells generate ATP through glycolysis instead, suggesting the Warburg effect, which describes how cancer cells have the potential to carry out mitochondrial respiration through aerobic glycolysis rather than aerobic oxidation (189). It would be of interest to investigate in future studies whether SCg cells are in fact using glycolysis instead of OXPHOS. There is a Seahorse XF glycolysis stress test kit that could be used to measure the rate of glycolysis in these cells.

Chapter 3 described the treatment of a DEX-induced mouse model of OHT with a once-off siRNA injection targeting tissues of the conventional outflow pathway. This siRNA targeted TJ proteins ZO-1 and tricellulin found along the inner wall of SC in the outflow pathway. The hypothesis for this study was that the siRNA would successfully target and downregulate these TJ proteins of interest, increasing paracellular permeability between SC

cells and allowing for greater AH outflow and in turn, reduced IOP in these mice. This was a follow-on study from the work carried out by Tam et al. (2017) in normotensive mice (131). In this follow-on study, these mice were treated with either DEX (treated mice) or cyclodextrin (control mice) for 4 weeks to induce OHT and maintain normal IOP respectively, and a once-off intracameral injection with siRNA was then administered. A significant lowering of IOP of 2 mmHg in the DEX mice and 1 mmHg in the vehicle control mice was observed 48 hr post-injection with siRNA. A significant increase in outflow facility of 63% in the DEX mice and 38% in the vehicle control mice was observed 72 hr post-injection. This was a proof-of-concept study for the successful increase in AH outflow facility and lowering of IOP in this GC-induced mouse model of OHT, following a once-off intracameral injection with siRNA (132).

Chapter 4 also described this siRNA therapy but in a transgenic mouse model of OHT (*MYOC*^{Y437H}). The *MYOC* gene is a known causative gene for POAG and the *Y437H* mutation is associated with a severe form of the disease. These *MYOC*^{Y437H} mice showed increased IOP over time. However, the siRNA treatment in these mice was not as effective at increasing AH outflow (19% increase in facility) and thus lowering of IOP (3 mmHg) as it was in the DEX mice. This is thought to be the result of increased TJ protein expression (ZO-1) in the DEX mouse model of OHT and so there is greater availability of mRNA for the siRNA to bind and work more effectively. However, the major downfall of both these studies was the transient nature of siRNA on IOP lowering, following the once-off treatment with siRNA. Staggered injections every few days could prevent this; however, this is far too invasive. A more long-term and less invasive approach would be needed going forward in a clinical setting. An AAV delivering shRNA would be more long-term and more effective, however the conventional outflow pathway is notoriously difficult to successfully transduce. Future studies into Anc80 and AAV2 with mutated capsids and how theses transfect tissues of the anterior segment would be extremely beneficial going forward.

Chapter 5 explored the potential beneficial impact of an AAV2 with a modified tyrosine capsid, carrying human *NDI1* which targets Complex I of the electron transport chain, in the *MYOC*^{Y437H} mouse model of OHT. This gene therapy has been shown to be successful at reducing RGC loss and increasing retinal function in a mouse model of LHON (6). One cohort of *MYOC*^{Y437H} mice were injected intracamerally with *NDI1* (treated) in one eye and GFP (control) in the other and another intravitreally with the same, and both left for 6 months. IOP characterisation over time was carried out and successful lowering of IOP was observed in treated eyes compared to control eyes in the mice that received the intracameral injection. Outflow facility was measured and there was only a 5% increase in outflow facility in treated eyes compared to control eyes, however. Confocal microscopy showed off-target transduction of the corneal endothelium and iris, while there was no evidence of successful transduction of tissues of the outflow pathway, unfortunately. In the mice that received an intravitreal injected of both *NDI1* and GFP, no IOP lowering effects were observed in the treated eyes compared to control eyes. Confocal microscopy showed successful transduction of the retina following the once-off injection. However, RGC counts showed significant reduction in RGC loss in treated eyes compared to control eyes. It was first thought that the viral dose used could have been too high, but it was significantly lower than what was used in previous studies. An investigation into whether this mouse model of OHT is suitable for this gene therapy would need to be carried out. The mitochondrial activity of these *MYOC*^{Y437H} mice should be explored and compared to WT littermates. There is no evidence to support or deny that Complex I activity is affected in these mice and so this should be investigated before carrying on with this study. Following this, unconventional outflow facility should be measured in the mice treated with an intracameral injection of *NDI1*, as well as RGC counts. There is some IOP lowering effects observed over time in these mice, which could also be the result of off-target transduction of the corneal endothelium and this should also be investigated.

Chapter 6

Materials and Methods

Chapter 2

Cultured human SCEC

Human SCEC were isolated, cultured and characterised as previously described by Stamer et al. (1998) (256). The anterior segment of human cadaveric eyes is cut into eight equal and symmetric wedge-shaped pieces. A gelatin-coated suture is gently inserted into Schlemm's canal lumen and further into the canal. The cannulated pieces of tissue are cultured and maintained for 3 weeks. Sutures are removed from Schlemm's canal and SCEC are seeded onto 3 cm culture plates. SCEC form monolayers of non-overlapping cells and are contact inhibited. SC isolates react with antibodies specific for CD44 (hyaluron receptor), CD54 (intercellular adhesion molecule-1 or ICAM-1), tissue type plasminogen activator and TIGR-MYOC (TM-induced glucocorticoid-responsive protein-myocilin). Unlike TM cells, TIGR-MYOC protein was not induced in SCEC after long-term treatment with DEX (256).

SCEC used in this study

SCEC strains used in this study were obtained from Dan Stamer's lab and characterised as above. More information on each individual donor can be found in Table 4 below. All SCEC were used between passages 4 and 6. SCEC were cultured in low glucose Dulbecco's modified Eagle medium (Gibco, Life Sciences) supplemented with 10% Performance Plus foetal bovine serum (FBS) (Gibco, Life Sciences), 1% Pen/Strep glutamine (Gibco, Life Sciences), in a 5% CO2 incubator at 37°C. Cultured cells were passaged with trypsin-EDTA (Gibco-BRL) to maintain exponential growth.

Group	Cell strain no.	Age (years)	Sex
Healthy	SC71	44	Male
	SC89	68	Male
	SC91a	74	Female
	SC69	45	Male
	SC74	0.7	Male
Glaucoma	SC57g	78	Male
	SC64g	78	Male
	SC90g	71	Female

Table 4: Donor information for both healthy and glaucoma SCEC strains.

Treatment with TGFβ-2

SCECs were cultured in low glucose Dulbecco's modified Eagle medium supplemented with 10% Performance Plus FBS and 1% Pen/Strep glutamine, as above. These cells were left to grow until they were ~90% confluent. 24 hr prior to TGFβ-2 treatment, Performance Plus FBS concentration was reduced from 10% to 5%, as these cells do not like to be completely serum starved. These SCECs were then treated with recombinant human TGFβ-2 (BioLegend) at a concentration of 10 ng/mL in low glucose Dulbecco's modified Eagle medium supplemented with 5% Performance Plus FBS and 1% Pen/Strep glutamine. These cells were left for 48 hr in a 5% CO2 incubator at 37°C before functional assays, protein and RNA extraction were carried out. TGFβ-2 concentration of 10 ng/ml was used for 48 hr to create an environment of elevated levels of TGFβ-2 over time, as would be observed in glaucoma patients. As the cells were being treated for only 48hr and not longer, a higher level of TGFβ-2 was used. A dose response study using 2, 5 and 10 ng/ml of TGFβ-2 was previously carried out and the 10 ng/ml concentration induced the most significant changes in both endothelial and fibrotic protein marker expression in these cells.

Quantitative Real-time PCR for *in vitro* experiments

Total RNA was extracted at passages 4 to 6 using RNEasy Mini Kit (Qiagen) according to manufacturer's protocol. Genomic DNA contamination was eliminated by DNase treatment. RNA concentration of each sample was quantified using a NanoDrop® Spectrophotometer ND-100 and equal concentrations were reverse-transcribed into cDNA using High-Capacity cDNA Reverse Transcription Kit (Applied Biosystems). SensiFAST SYBR Hi-ROX Kit (Bioline) was used according to manufacturer's protocol along with primer pairs and loaded onto a 96 well plate (Applied Biosystems). The plate was run on a StepOnePlus Real-Time PCR system (Applied Biosystems). Primer pair sequences can be found below in Table 5. The Threshold cycle (CT) values of the three groups, healthy SCEC (SC), SCEC treated with TGF-β2 (SC+ TGF-β2) and glaucomatous SCEC (SCg) were determined, and averages were calculated. The mean normalised expression (ΔCT) of RNA encoding both fibrotic and endothelial cell markers were determined and analysed. Normalised gene expression was calculated by using the equation: ΔCT = CT(Gene of interest) − CT(Housekeeping genes). β-actin was uses as a housekeeping gene. ΔΔCT was calculated by subtracting the treated sample from the control sample: ΔΔCT = ΔCT (Treated sample) - ΔCT (Control sample). The 2-(ΔΔCT) method was then used to calculate relative fold gene expression for each sample.

Primer pair	Forward sequence (5' to 3')	Reverse sequence (5' to 3')
α-SMA	CCGACCGAATGCAGAAGGA	ACAGAGTATTTGCGCTCCGAA
Collagen Iα-1	TTTGGATGGTGCCAAGGGAG	CACCATCATTTCCACGAGCA
TGF-β2	ACGGATTGAGCTATATCAGATT CTCA	TGCAGCAGGGACAGTGTAAG
VE-cadherin	GCACCAGTTTGGCCAATATA	GGGTTTTTGCATAATAAGCAGG
Vinculin	TGGACGAAGCCATTGATACCA	AGCTCTTTTGCAGTCCAGGG
vWF	GTTCGTCCTGGAAGGATCGG	CACTGACACCTGAGTGAGAC
GAPDH	TGTAGTTGAGGTCAATGAAGGG	ACATCGCTCAGACACCATG
β-actin	GGGAAATCGTGCGTGACAT	GTGATGACCTGGCCGTAG

Table 5: Primer pair sequences used in quantitative real-time PCR.

Western Blot

Protein lysates were isolated from cultured cells in protein lysis buffer containing 1M Tris pH 7.5, 1M NaCl, 1% NP-40, 10% SDS, 1X protease inhibitor cocktail (Roche). The homogenate was centrifuged at 10,000 R.P.M. (IEC Micromax microcentrifuge, 851 rotor) at 4 °C for 20 min and the supernatant was stored at −80 °C until use. Protein concentration was determined by BCA Protein assay kit (Pierce, IL, USA) with bovine serum albumin (BSA) at 2mg/mL as standards on 96-well plates according to the manufacturer's protocol. 30–50μg of total protein was loaded in each lane. Protein samples were separated by electrophoresis on 7.5–10% SDS–PAGE under reducing conditions and electro-transferred to PVDF membranes. After blocking with 5% blotting grade blocker non-fat dry milk in TBS for 1 hr at room temperature, membranes were incubated overnight at 4 °C with the following primary antibodies: anti-alpha smooth muscle actin antibody (1:250; Abcam); anti-VE cadherin antibody (1:250; Abcam); anti-vinculin antibody (1:1000; Abcam); anti-transforming growth factor beta-2 (1:500: Abcam); anti-von Willebrand factor antibody (1:250; Abcam); anti-collagen I antibody (1:250; Abcam); anti-tight junction protein 1 antibody (1:500; Invitrogen), anti-MARVELD2 antibody (1:250; Abcam); anti-claudin-11 antibody (1:250; Abcam). Blots were washed with TBS-Tween and incubated with horse

radish peroxidase-conjugated polyclonal rabbit IgG secondary antibody (Sigma) or mouse IgG secondary antibody (Life Technologies). The blots were developed using enhanced chemiluminescent kit (Pierce Chemical Co.) and imaged on the C-DiGit® Blot Scanner. Each blot was stripped with Restore Western Blot Stripping Buffer (Pierce) and probed with rabbit polyclonal to β-actin or GAPDH (Abcam) as loading controls. Protein band intensities were quantified and analysed using Image J (Version 1.50c). The percentage reduction in band intensity was calculated relative to an untreated healthy SCEC sample, which was standardised to represent 100% and normalised against β-actin or GAPDH.

Immunocytochemistry

Human SCEC were grown on Lab-Tek II chamber slides and fixed in 4% paraformaldehyde (pH 7.4) for 20 min at room temperature and then washed 3 times in PBS for 5 min. Cell monolayers were blocked in PBS containing 5% normal goat serum and 0.1% Triton X-100 at room temperature for 1 hr. α-SMA primary antibody was made up in blocking buffer (1:500; Abcam) and incubated overnight at 4 °C. Goat anti-rabbit secondary was also made up in blocking buffer (1:500; Abcam), along with Phalloidin (1:3000; Invitrogen) and incubated for 2 hr at room temperature in a humidity chamber. Following incubation, chamber slides were mounted with aqua-polymount (Polyscience) after nuclei-counterstaining with DAPI at 1:5000 for 60 seconds. Fluorescent images of SCEC monolayers were captured using a confocal microscope (Zeiss LSM 710) and processed using imaging software ZEN 2012.

Measurement of SCEC monolayer transendothelial electrical resistance (TEER)

TEER was used as a measure of TJ integrity by the human SCEC monolayers as previously described (205). In brief, human SCEC (1×10^4 cells per well) were grown to confluency on Costar HTS Transwell-polyester membrane inserts with a pore size of 0.4μm. The volume of the apical side (inside of the membrane inserts) was 0.1mL and that of the basal side (outside of the membrane inserts) was 0.6mL. Confluent cells were then left untreated or

treated with 10ng/mL of TGF-β2. 48h post-treatment, TEER values were determined using an EVOM resistance meter with Endohm Chamber (World Precision Instruments) and a Millicell-Electrical Resistance System. For measurement of TEER, both the apical and basolateral sides of the endothelial cells were bathed in fresh growth medium at 37 °C, and a current was passed across the monolayer with changes in electrical resistance, which was reported as Ω.cm2 after correcting for the surface area of the membrane (1.12cm). Electrical resistance was measured in triplicate wells, and the inherent resistance of a blank transwell was subtracted from the values obtained for the endothelial cells.

Cell permeability assay using FITC-dextran

Human SCEC were prepared and treated using the same method for TEER measurement as described above. Transwell permeability assays were carried out as previously described (205). In brief, 70 kDa fluorescein isothiocyanate (FITC)-conjugated dextran (FD) (Sigma) was applied at 1 mg/mL to the basal compartment of the transwells. Sampling aliquots of 0.1 mL were collected every 15 min for a total of 120 min from the apical side for fluorescence measurements and the same volume of culturing media was added to replace the medium removed. FITC fluorescence was determined using a spectrofluorometer (Optima Scientific) at an excitation wavelength of 485 nm and an emission wavelength of 520nm. Relative fluorescence units (RFU) were converted to values of nanograms per millilitre using FITC-dextran standard curves and were corrected for background fluorescence and serial dilutions over the course of the experiment. The apparent permeability co-efficient (Papp, cm/s) for each treatment was calculated using the following equation: P = × (dM/dt)/(A C), app 0 where dM/dt (μg/s) is the rate of appearance of FD on the apical side from 0 min to 120min after application of FD. C0 (μg/mL) is the initial FD concentration on the basal side, and A (cm^2) is the effective surface area of the insert. dM/dt is the slope calculated by plotting the cumulative amount of (M) versus time.

Cell proliferation assay

SCEC were grown to confluency on a 24-well plate. This assay was also carried out on the transwell plate, following TEER and paracellular permeability assays. CellTitre 96 Aqueous One Solution Reagent (Promega) was thawed and mixed with culture medium at a 1:5 dilution. Cells were incubated with this mixture for a period of 2 hours, before transferring the media to a fresh 96-well plate. Absorbance of each well was recorded at 450nm on a spectrophotometer (Multiskan FC, Thermo Scientific). After blanking against wells with reagent and no cells, each treatment group was presented relative to an untreated healthy SCEC sample. A 1-way ANOVA with a Tukey's post-test was performed on the data set.

Calcium detection assay

A colorimetric calcium detection kit (Abcam) was used to determine calcium concentration within the physiological range of 0.1 to 25mM. A standard curve was prepared using a 5mM calcium standard and cells were harvested at a concentration of $2x10^6$/mL. Cells were resuspended in calcium buffer and placed on ice. Calcium standards and cell samples (in triplicate) were then added to a 96 well plate. Both chromogenic reagent and calcium buffer were added to each well and incubated for 5-10 mins away from the light. Colorimetric absorbance was then measured on a microplate reader at OD575nm.

Migration scratch assay

Once cells reached ~90% confluency, a P200 tip was used to scratch a line down the centre of each well of a 24 well plate, leaving a control well for each cell line unscratched. Photographs of each well were taken using confocal microscopy at various timepoints until the cells migrated across the scratch line and there was no longer a gap visible. These pictures were processed using imaging software ZEN 2012. The reduction of the scratch line was calculated up to 48hr post scratch and the relative reduction of the scratch line calculated.

Cell morphology

Fluorescent images of individual SCEC cells, both healthy and glaucomatous, were captured using a confocal microscope at 40X (Zeiss LSM 710) and processed using imaging software ZEN 2012. The height and width of each cell was measured by averaging 5 measurements of each for each individual cell. The area (μm^2) of each of cell was then calculated and analysed on GraphPad Prism 6.0.

Seahorse assay

The Agilent Seahorse XF Cell Mito Stress Test was used to measure mitochondrial function by directly measuring the oxygen consumption rate (OCR) of cells on the Seahorse XFe96 Analyzer. It is a plate-based live cell assay that allows to monitor OCR in real time. The assay uses the built-in injection ports on XF sensor cartridges to add modulators of respiration into cell well during the assay to reveal the key parameters of mitochondrial function. The modulators included in this assay kit are Oligomycin, Carbonyl cyanide-4 (trifluoromethoxy) phenylhydrazone (FCCP), Rotenone, and Antimycin. SCEC cells were resuspended in galactose media to force them to use their mitochondria and seeded onto a Seahorse 96 well plate (Agilent) at a concentration of $1.25x10^5$/mL, 24 hr prior to the assay. The Seahorse cartridge was hydrated in calibrant and incubated in a non-CO^2 incubator at 37°C overnight. On the day of the assay, all of the compounds above are added to XF Base Medium and loaded into the cartridge. Two different concentrations of FCCP were used (0.4µm and 0.8µm) for this cell type, to determine which was more suitable. Results showed 0.8µm was more suitable. Culture media was substituted for Seahorse XF DMEM medium, pH7.4 (Agilent), supplemented with 1mM Sodium Pyruvate, 2mM L-Glutamine and 10mM Galactose, and placed in a non-CO^2 incubator at 37°C 1 hr prior the reaction. The assay was then run on a Seahorse XFe96 Analyzer. A Bradford assay (Thermo Fisher Scientific) was later carried out to determine protein concentration and data from the Seahorse assay was then normalized to this.

Chapters 3, 4 & 5

Animal husbandry

Animals and procedures used in this study were carried out in accordance with the regulations set out by the Health Products and Regulatory Authority (HPRA) and the Association for Research in Vision and Ophthalmology (ARVO) statement for the use of animals in ophthalmic and vision research. C57BL/6J animals were used for DEX implantations. *MYOC*^{Y437H} mice were bred on a C57BL/6J background and WT littermates were used as age-matched controls. These mice were kindly provided by Val Sheffield and his laboratory. Both male and female animals were used in these studies. Animals were housed in specific pathogen-free environments in the University of Dublin, TCD, and all injections and IOP measurements complied with the HPRA project authorization no. AE19136/P017 (2017-2019) and AE19136/P115 (2019-2021).

Tonometric IOP measurement

Mice were anaesthetized with 3% isoflurane at 1 L/min for 2 min in an induction chamber, and then moved to a head holder delivering isoflurane at the same rate. At 3 min after induction of anaesthesia, five consecutive IOP measurements (constituting an average of six readings each) were taken in the right eye and averaged. For measurement of IOP pre- and post-siRNA treatment, mice were anaesthetized again, as above, and three IOP measurements (constituting an average of six readings each) were made at three different time points in both eyes (eye 1, minutes 3, 5, and 7 after anaesthesia; eye 2, minutes 4, 6, and 8 after anaesthesia). The average IOP measurement at each time point was used to fit a line and interpolate IOP at minute 5 to allow for measurement of IOP in both eyes while accounting for the IOP lowering effect of anaesthesia over time.

Micro-osmotic pump implantation

DEX micro-osmotic pumps (model 1004, Alzet) were implanted as in Whitlock et al. (2010) (213). The DEX was water-soluble (D2915; Sigma-Aldrich), contained cyclodextrin (1.36 g

per 100 mg of DEX), and was dissolved in PBS. Vehicle-treated mice received pumps containing cyclodextrin (C4555; Sigma-Aldrich) alone. DEX was delivered at 2 mg/kg/day. Adult C57BL/6J mice of 10–12 weeks of age were anaesthetized with 3% isoflurane at 1 L/min, and the surgical site was shaved and disinfected with chlorhexidine swabs. Mice were injected intramuscularly with 0.05 mg/kg buprenorphine (buprecare, Animalcare) and subcutaneously with 5 mg/kg enrofloxacin (enrocare, Animalcare). An incision was made between the scapulae, a subcutaneous pocket was created by blunt dissection, and the pump was inserted. The incision was closed using surgical glue (surgibond, RayVet). After pump implantation, mice were housed singly, and diet was supplemented with complan (Nutricia Advanced Medical Nutrition) to prevent GC-induced weight loss. Weight was monitored weekly, with any mice losing more than 20% body weight overall, or 10% body weight in 1 week, required to be euthanized.

Intracameral injection of siRNA

Our method for intracameral delivery to the anterior chamber has been described in detail previously (131). Briefly, for siRNA injection, mice were anesthetized with 3% isoflurane at 1 L/min. Pupils were dilated with 1% tropicamide and 2.5% phenylephrine eye drops. Glass micro-capillaries (outer diameter, 1 mm; inner diameter, 0.58 mm; World Precision Instruments) were pulled using a micropipette puller (Narishige PB-7). Under microscopic control, a pulled blunt-ended micro-glass needle (tip diameter, ~100 μm) was first used to puncture the cornea to withdraw AH by capillarity. Immediately after puncture, a pulled blunt-ended micro-glass needle attached to a 10-μL syringe (Hamilton, Bonaduz) held in a micromanipulator (World Precision Instruments) was inserted through the puncture, and 1.5 μL of PBS containing 1 μg of ZO-1 siRNA and 1 μg of tricellulin siRNA was administered into the anterior chamber to give a final concentration of 16.84 μM. Contralateral eyes received an identical injection of 1.5 μL containing the same concentration of NT siRNA. Fusidic gel was applied topically to the eye as antibiotic and

vidisic gel was also applied topically as a moisturizer. Furthermore, 5 mg/kg enrofloxacin antimicrobial (Baytril, Bayer Healthcare) was injected subcutaneously.

siRNAs

All *in vivo* pre-designed siRNAs used in this study were synthesized by Ambion and reconstituted as per the manufacturer's protocol. siRNA identification numbers are as follows: mouse ZO-1 siRNA (ID no. s75175), mouse MARVELD2 siRNA (ID no. ADCSU2H). Silencer negative control siRNA (Ambion) was used as a non-targeting control.

iPerfusion

Ex vivo outflow facility measurements were carried out using the *iPerfusion*™ system, as described by Sherwood et al. (2016) (219). Mice were culled by cervical dislocation, and eyes were enucleated immediately and stored in PBS at room temperature to await perfusion (~20 min). Both eyes were perfused simultaneously using two independent perfusion systems as described previously. Briefly, each eye was affixed to a support using a small amount of cyanoacrylate glue and submerged in a PBS bath regulated at 35°C. The eye was cannulated via the anterior chamber with a 33G bevelled needle (NanoFil, #NF33BV-2, World Precision Instruments) under a stereomicroscope using a micromanipulator. The *iPerfusion* system comprises an automated pressure reservoir, a thermal flow sensor (SLG64-0075, Sensirion), and a wet-wet pressure transducer (PX409, Omegadyne) in order to apply a desired pressure, measure flow rate out of the system, and measure the IOP, respectively. The perfusate was PBS containing Ca^{2+}, Mg^{2+}, and 5.5 mM glucose, and was filtered through a 0.22-µm filter (VWR International) prior to use. Following cannulation, eyes were perfused for 30 min at 8 mmHg to allow the eye to acclimatize. Subsequently, eight discrete pressure steps were applied from 4.5 to 21 mmHg, while flow and pressure were recorded. Stability was defined programmatically, and data were averaged over 5 min at steady state. A non-linear model was fit to flow-pressure data to account for the pressure

dependence of outflow facility in mouse eyes. This model was of the form $Q = C_r P(P/P_r)^{\beta}$, where Q and P are the flow rate and pressure, respectively, and C_r is the outflow facility at reference pressure P_r, which is selected to be 8 mmHg (the approximate physiological pressure drop across the outflow pathway). The power law exponent β quantifies the non-linearity in the Q-P response and thus the pressure dependence of outflow facility. The data analysis methodology described in Sherwood et al. (2016) (219) was applied in order to analyse the treatment effect, while accounting for measurement uncertainties, and statistical significance was evaluated using the paired weighted t-test described therein.

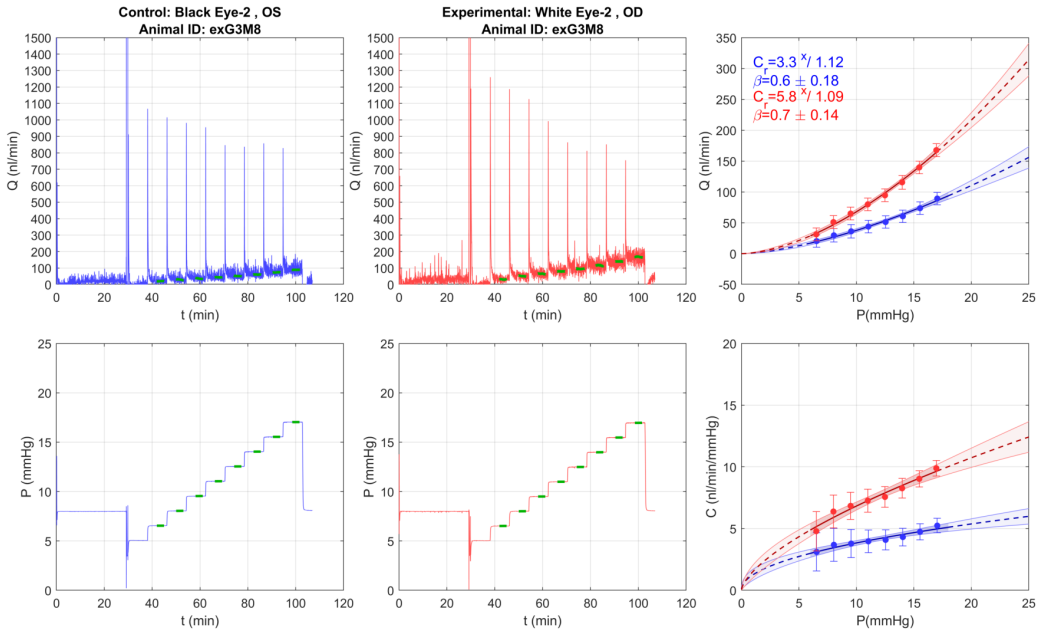

Figure 6.1: *iPerfusion* flow and pressure graphs.

Above is an example of a graph generated from MATLAB as part of the iPerfusion system, following paired analysis of control (blue) and treated (red) eyes ex vivo. Incremental pressure (P) was applied to each canulated eye over time (bottom left), while flow (Q) and pressure rates were measured in each (top left). Flow vs pressure and outflow facility (C) vs pressure graphs were plotted against each other (right column). Treated eyes appear to have increased flow and therefore outflow facility at each pressure step. An outflow facility measurement is interpolated from a measurement of 8 mmHg of pressure (bottom right). The is approximately the pressure drop observed in Schlemm's canal in mice. This outflow

facility value is then weighted against both system and biological uncertainties in statistics and paired analysis.

Quantitative real-time PCR for *in vivo* experiments

An optimized dissection method was used to enrich the number of endothelial cells from SC present in the homogenized tissue solution used for RNA extraction. The anterior segment was removed 2–3 mm anterior and posterior to the limbus, leaving a ring of tissue containing the outflow tissue at the iridocorneal angle, and any remnants of corneal and iris tissues. This results in minimal TJ transcripts arising from non-outflow tissues in our sample, such as from corneal endothelia and epithelia. Total RNA was extracted from this homogenized tissue solution using the RNeasy mini kit (QIAGEN) according to the manufacturer's protocol. The RNA concentration of each sample was quantified using a NanoDrop ND-100 spectrophotometer, and equal concentrations were reverse transcribed into cDNA using a high-capacity cDNA reverse transcription kit (Applied Biosystems). A SensiFAST SYBR Hi-ROX kit (Bioline) was used according to manufacturer's protocol along with primer pairs of interest and loaded onto a 96-well plate (Applied Biosystems). The plate was run on a StepOnePlus real-time PCR system (Applied Biosystems). Primer pair sequences can be found in Table 6. The threshold cycle (CT) values of treated and untreated tissue samples from each sample were determined and averages were calculated. The mean normalized expression (ΔCT) of RNA encoding the protein of interest was determined and analyzed. Normalized gene expression was calculated by using the following equation: ΔCT = CT(gene of interest) − CT(housekeeping genes). Normalization was carried out with the β-actin housekeeping gene. ΔΔCT was calculated by subtracting the treated sample from the control sample: ΔΔCT = ΔCT(treated sample) − ΔCT(control sample). The $2^{-\Delta\Delta Ct}$ method was then used to calculate relative fold gene expression for each sample pair. A $2^{-\Delta\Delta Ct}$ value of 1 represents no change in relative fold gene expression. A value above 1 represents

upregulation of the gene of interest, and a value below 1 represents downregulation of the gene of interest.

Primer pair	**Forward (5' to 3')**	**Reverse (5' to 3')**
ZO-1	CGCTCTCGGGAGATGTTTAT	GTTTCCTCCATTGCTGTGCT
Tricellulin	AGGCAGCTCGGAGACATAGA	TCACAGGGTATTTTGCCACA
NDI1	GAACACCGTGACCATCAAGA	GCTGATCAGGTAGTCGTACT
β-actin	GGGAAATCGTGCGTGACAT	GTGATGACCTGGCCGTCAG

Table 6: Primer sequences used in quantitative PCR reactions.

Immunohistochemistry from frozen sections

Enucleated mouse eyes were fixed in 4% paraformaldehyde (pH 7.4) overnight at 4°C on a rotating device. The posterior segment of the eye and the lens was removed, and the anterior segment washed in PBS for 15 min. The anterior segments were then sequentially washed in 10, 20 and 30% sucrose. Following this, the dissected anterior segments were suspended in specimen blocks with OCT solution (Tissue-Tek) and frozen in a bath of isopropanol submerged in liquid nitrogen. Frozen anterior sections were sectioned using a cryostat (Leica CM 1900) to between 12-15 μm thickness. Sections were collected on Polysine ® slides (Menzel-Glazer). To detect TJ proteins of interest, sections were washed with PBS and then blocked for 20 min at room temperature in PBS containing 5% normal goat serum and 0.1% Triton-X, and incubated with the corresponding antibodies at 1:100 dilution overnight at 4°C in a humidity chamber. Sections were then washed 3 times with PBS and incubated with Cy3 labelled anti-rabbit IgG antibody at 1:500 (Abcam) for 2 hr at room temperature, in a humidity chamber. Sections were then washed again 3 times in PBS and mounted with aqua-polymount (Polyscience) after nuclei-counterstaining with DAPI. Anterior segments were visualised using confocal microscopy (Zeiss LSM 710).

Transmission electron microscopy

Ultrastructural investigation of the *MYOC*^{Y43H} model was performed by transmission electron microscopy (TEM) in four pairs of mouse eyes. Eyes were enucleated and immersion fixed in Karnovsky's fixative (2.5 % PFA, 0.1M cacodylate, 2.25 % glutaraldehyde and dH2O) for 1h. Eyes were then removed from fixative and the cornea pierced using a 30-gauge needle (BD Microlance 3, Becton Dickinson). Eyes were placed back into fixative overnight at 4° C, washed 3x10 min, stored in 0.1 M cacodylate and sent to Erlangen. Here the eyes were cut meridionally through the centre of the pupil, the lens carefully removed, and the two halves of each eye embedded in Epon. Semi-thin sagittal and then ultrathin sections of SC and TM were cut from one end of each half, and then the other approximately 0.2–0.3 mm deeper. The location of the superficial and deeper cut ends was alternated for the second half of the eye such that all four regions examined were at least 0.2–0.3 mm distant from one another. The ultrathin sections contained the entire anterior posterior length of SC inner wall and the TM.

Chapter 5

AAV production

Both recombinant AAV2/2-Opt*NDI1* and AAV2/2-OptEGFP were developed by the Farrar lab, TCD (257). Human *NDI1* cDNA was cloned into pAAV-MCS (Agilent). Recombinant AAV2/2 viruses were generated by helper virus free, triple transfection based on the method described by Xiao et al. (1998) (258). Human embryonic kidney (HEK) cells were transfected with pAAV-MCS plasmids containing *NDI1*, pRep2/Cap2 and pHelper (Agilent) at a ratio of 1:1:2, using polyethylene. 72 hr later, AAV particles were then purified from the clarified lysate by caesium gradient centrifugation. AAV containing fractions were dialyzed against PBS supplemented with Pluronic F68 (0.001%) (259). Genomic titres (viral genomes/mL; vg/mL) were determined using quantitative PCR analysis (260).

Intravitreal injection of AAV

Mice were anaesthetised by intraperitoneal (IP) injection with a combination of medetomidine and ketamine (0.5 mg and 57. Mg/kg, respectively). Pupils were dilated with 1% tropicamide and 2.5% phenylephrine. Using topical anaesthesia (Amethocaine), a small puncture was made in the sclera. A 32 gauge blunt-ended microneedle attached to a 10 µL Hamilton syringe was inserted through the puncture. 3 µL of AAV2/2-Opt*NDI1* (1.5×10^8 vg/µL) was added over a 2 min period to the vitreous of one eye, while 3 µL of AAV2/2-OptEGFP (1.5×10^8 vg/µL) was added to the other contralateral control eye. This gives a final concentration of 4.5×10^8 vg/eye for both. Following the injections, an anaesthetic reversing agent (Atipamezole Hydrochloride, 1.33 mg/kg body weight) was delivered by IP injection. Body temperature was maintained using a homeothermic heating device.

Intracameral injection of AAV

Mice were anesthetized with 3% isoflurane at 1 L/min. Pupils were dilated with 2.5% tropicamide and 2.5% phenylephrine eye drops. Glass micro-capillaries (outer diameter, 1 mm; inner diameter, 0.58 mm; World Precision Instruments) were pulled using a micropipette puller (Narishige PB-7). Under microscopic control, a pulled blunt-ended micro-glass needle (tip diameter, ~100 µm) was first used to puncture the cornea to withdraw AH by capillarity. Immediately after puncture, a pulled blunt-ended micro-glass needle attached to a 10-µL syringe (Hamilton, Bonaduz) held in a micromanipulator (World Precision Instruments) was inserted through the puncture, and 1.5 µL of AAV2/2-Opt*NDI1* (1.5×10^8 vg/µL) was administered to the anterior chamber to give a final concentration of 2.3×10^8 vg/eye. Contralateral control eyes received an identical injection of 1.5 µL containing the same concentration of AAV2/2-OptEGFP. Fusidic gel was applied topically to the eye as antibiotic and Vidisic gel was also applied topically as a moisturizer. Furthermore, 5 mg/kg enrofloxacin antimicrobial (Baytril, Bayer Healthcare) was injected subcutaneously.

Retinal ganglion cell counts

Mice were sacrificed and eyes were enucleated and fixed in 4% paraformaldehyde in PBS overnight. Eyes were then washed in PBS and the retina dissected out and washed in PBS again. Whole retinas were incubated with primary antibody for Brn3a (Santa Cruz) for 3 days at 4 °C on a rotator. Retinas were then washed with PBS and incubated with secondary antibody conjugated with Alexa-Fluor-488, Cy3 (Jackson ImmunoResearch Laboratories; 1:400) for 2 days and counterstain the nuclei with DAPI. Samples were covered using Hydromount (National Diagnostics). Fluorescent microscopy was then carried out using the Olympus IX83 inverted motorized microscope (cellSens v1.9 software) equipped with a SpectraX LED light source (Lumencor) and an Orca-Flash4.0 LT PLUS/sCMOS camera (Hamamatsu). Images were taken using a 10X fluorite objective with enhanced focal imaging (EFI). Usually, 5–8 Z-slices were taken. Lateral frames were stitched together and analysed in the cellSens program. Automated cell staining area was calculated utilizing 2D deconvolution, manual threshold and object size filter in cellSense; the same settings/operations were applied to all images. This was then displayed and analysed using GraphPad Prism version 6.0.

Statistical analysis

Data was first identified to be either parametric of nonparametric, depending on whether the distribution of that data was better represented by the mean (parametric) or median (nonparametric). For qPCR, western blot analysis and functional assay experiments, Student's t-tests and one-way ANOVA with Tukey's post-test was carried out. For animal experiments, one-way ANOVA with Tukey's post-test was performed to determine the statistical significance of IOP elevation over time following injection with siRNAs and AAVs. One-sample *t*-tests with a theoretical mean of 0 were used to determine if the IOP of treatment groups had significantly changed from pre-injection to post-injection measurements (a mean of 0 in this case would signify no change in IOP between timepoints).

A repeated measures two-way ANOVA with Sidak's multiple comparisons test was performed to determine the change in IOP over time, following injection with siRNAs and AAVs. Outflow facility calculations were based on a weighted, paired, two-tailed t-test. qPCR analysis was performed using a one-sample t test with a hypothetical value of 1, representing no change in relative gene expression. Statistical analysis was carried out using GraphPad Prism version 6.0 and graphs represent the mean value +/- SD.

References

1. Tham YC, Li X, Wong TY, Quigley HA, Aung T, Cheng CY. Global prevalence of glaucoma and projections of glaucoma burden through 2040: a systematic review and meta-analysis. Ophthalmology. 2014;121(11):2081-90.
2. Varma R, Lee PP, Goldberg I, Kotak S. An assessment of the health and economic burdens of glaucoma. American journal of ophthalmology. 2011;152(4):515-22.
3. Goel M, Picciani RG, Lee RK, Bhattacharya SK. Aqueous humor dynamics: a review. Open Ophthalmol J. 2010;4:52-9.
4. Weinreb RN, Khaw PT. Primary open-angle glaucoma. Lancet. 2004;363(9422):1711-20.
5. Noecker RJ. The management of glaucoma and intraocular hypertension: current approaches and recent advances. Ther Clin Risk Manag. 2006;2(2):193-206.
6. Chadderton N, Palfi A, Millington-Ward S, Gobbo O, Overlack N, Carrigan M, et al. Intravitreal delivery of AAV-NDI1 provides functional benefit in a murine model of Leber hereditary optic neuropathy. Eur J Hum Genet. 2013;21(1):62-8.
7. Purves DA, G.J.; Fitzpatrick, D.;. Neuroscience 2nd edition. Sunderland (MA). 2001.
8. Goldmann H. [Minute volume of the aqueous in the anterior chamber of the human eye in normal state and in primary glaucoma]. Ophthalmologica. 1950;120(1-2):19-21.
9. Ascher KW. [Veins of the aqueous humor in glaucoma]. Boll Ocul. 1954;33(3):129-44.
10. Bill A, Hellsing K. Production and drainage of aqueous humor in the cynomolgus monkey (Macaca irus). Invest Ophthalmol. 1965;4(5):920-6.
11. Kass MA, Hart WM, Jr., Gordon M, Miller JP. Risk factors favoring the development of glaucomatous visual field loss in ocular hypertension. Surv Ophthalmol. 1980;25(3):155-62.
12. Llobet A, Gasull X, Gual A. Understanding trabecular meshwork physiology: a key to the control of intraocular pressure? News Physiol Sci. 2003;18:205-9.
13. Bill A. Blood circulation and fluid dynamics in the eye. Physiol Rev. 1975;55(3):383-417.
14. Johnson ME, K.;. Aqueous humor and the dynamics of its flow. Albert DMJ, F.A;, editor. Philadelphia Saunders; 2000. 2577-95 p.
15. Epstein DL, Rohen JW. Morphology of the trabecular meshwork and inner-wall endothelium after cationized ferritin perfusion in the monkey eye. Invest Ophthalmol Vis Sci. 1991;32(1):160-71.
16. Heimark RL, Kaochar S, Stamer WD. Human Schlemm's canal cells express the endothelial adherens proteins, VE-cadherin and PECAM-1. Curr Eye Res. 2002;25(5):299-308.
17. Liton PB, Liu X, Stamer WD, Challa P, Epstein DL, Gonzalez P. Specific targeting of gene expression to a subset of human trabecular meshwork cells using the chitinase 3-like 1 promoter. Investigative ophthalmology & visual science. 2005;46(1):183-90.
18. Rohen JW, Futa R, Lütjen-Drecoll E. The fine structure of the cribriform meshwork in normal and glaucomatous eyes as seen in tangential sections. Invest Ophthalmol Vis Sci. 1981;21(4):574-85.
19. Wiederholt M, Thieme H, Stumpff F. The regulation of trabecular meshwork and ciliary muscle contractility. Prog Retin Eye Res. 2000;19(3):271-95.
20. Millar CK, P.L. Aqueous humor: secretion and dynamics. Tasman WJ, E.A., editor. Philadelphia: Lippincott-Raven; 1995.
21. Civan MM, Macknight AD. The ins and outs of aqueous humour secretion. Exp Eye Res. 2004;78(3):625-31.

22. Smith RS, Rudt LA. Ultrastructural studies of the blood-aqueous barrier. 2. The barrier to horseradish peroxidase in primates. Am J Ophthalmol. 1973;76(6):937-47.
23. Uusitalo R, Palkama A, Stjernschantz J. An electron microscopical study of the blood-aqueous barrier in the ciliary body and iris of the rabbit. Exp Eye Res. 1973;17(1):49-63.
24. Mark HH. Aqueous humor dynamics in historical perspective. Surv Ophthalmol. 2010;55(1):89-100.
25. Yamaguchi Y, Watanabe T, Hirakata A, Hida T. Localization and ontogeny of aquaporin-1 and -4 expression in iris and ciliary epithelial cells in rats. Cell Tissue Res. 2006;325(1):101-9.
26. Delamere NA. Ciliary Body and Ciliary Epithelium. Adv Organ Biol. 2005;10:127-48.
27. Reiss GR, Werness PG, Zollman PE, Brubaker RF. Ascorbic Acid Levels in the Aqueous Humor of Nocturnal and Diurnal Mammals. Archives of Ophthalmology. 1986;104(5):753-5.
28. Vadillo-Ortega F, González-Avila G, Chevez P, Abraham CR, Montaño M, Selman-Lama M. A latent collagenase in human aqueous humor. Invest Ophthalmol Vis Sci. 1989;30(2):332-5.
29. Bill A. The aqueous humor drainage mechanism in the cynomolgus monkey (Macaca irus) with evidence for unconventional routes. Invest Ophthalmol. 1965;4(5):911-9.
30. Bill A. Conventional and uveo-scleral drainage of aqueous humour in the cynomolgus monkey (Macaca irus) at normal and high intraocular pressures. Exp Eye Res. 1966;5(1):45-54.
31. Bill A. The routes for bulk drainage of aqueous humour in the vervet monkey (Cercopithecus ethiops). Exp Eye Res. 1966;5(1):55-7.
32. Kupfer C, Gaasterland D, Ross K. Studies of aqueous humor dynamics in man. II. Measurements in young normal subjects using acetazolamide and L-epinephrine. Invest Ophthalmol. 1971;10(7):523-33.
33. Kupfer C, Ross K. Studies of aqueous humor dynamics in man. I. Measurements in young normal subjects. Invest Ophthalmol. 1971;10(7):518-22.
34. Brubaker RF. Measurement of uveoscleral outflow in humans. J Glaucoma. 2001;10(5 Suppl 1):S45-8.
35. Crawford K, Kaufman PL. Pilocarpine antagonizes prostaglandin F2 alpha-induced ocular hypotension in monkeys. Evidence for enhancement of Uveoscleral outflow by prostaglandin F2 alpha. Arch Ophthalmol. 1987;105(8):1112-6.
36. Gabelt BT, Kaufman PL. Prostaglandin F2 alpha increases uveoscleral outflow in the cynomolgus monkey. Exp Eye Res. 1989;49(3):389-402.
37. Lütjen-Drecoll E, Tamm E. Morphological study of the anterior segment of cynomolgus monkey eyes following treatment with prostaglandin F2 alpha. Exp Eye Res. 1988;47(5):761-9.
38. Bill A. The Ocular Effects of Prostanglandins and Other Eicosanoids. Alan R, editor. New York: Liss; 1989.
39. Aihara M, Lindsey JD, Weinreb RN. Aqueous Humor Dynamics in Mice. Investigative Ophthalmology & Visual Science. 2003;44(12):5168-73.
40. Weinreb RN. Uveoscleral outflow: the other outflow pathway. J Glaucoma. 2000;9(5):343-5.
41. Weinreb RN, Toris CB, Gabelt BT, Lindsey JD, Kaufman PL. Effects of prostaglandins on the aqueous humor outflow pathways. Surv Ophthalmol. 2002;47 Suppl 1:S53-64.
42. Toris CB, Yablonski ME, Wang Y-L, Camras CB. Aqueous humor dynamics in the aging human eye. American Journal of Ophthalmology. 1999;127(4):407-12.

43. Johnson M, McLaren JW, Overby DR. Unconventional aqueous humor outflow: A review. Exp Eye Res. 2017;158:94-111.
44. Johnson M. 'What controls aqueous humour outflow resistance?'. Exp Eye Res. 2006;82(4):545-57.
45. Mäepea O, Bill A. Pressures in the juxtacanalicular tissue and Schlemm's canal in monkeys. Experimental Eye Research. 1992;54(6):879-83.
46. Brilakis HS, Johnson DH. Giant vacuole survival time and implications for aqueous humor outflow. J Glaucoma. 2001;10(4):277-83.
47. Ethier CR, Coloma FM, Sit AJ, Johnson M. Two pore types in the inner-wall endothelium of Schlemm's canal. Invest Ophthalmol Vis Sci. 1998;39(11):2041-8.
48. Bill A, Svedbergh B. Scanning electron microscopic studies of the trabecular meshwork and the canal of Schlemm--an attempt to localize the main resistance to outflow of aqueous humor in man. Acta Ophthalmol (Copenh). 1972;50(3):295-320.
49. Braakman ST, Read AT, Chan DW, Ethier CR, Overby DR. Colocalization of outflow segmentation and pores along the inner wall of Schlemm's canal. Exp Eye Res. 2015;130:87-96.
50. Gong H, Ruberti J, Overby D, Johnson M, Freddo TF. A new view of the human trabecular meshwork using quick-freeze, deep-etch electron microscopy. Exp Eye Res. 2002;75(3):347-58.
51. O'Callaghan J, Crosbie DE, Cassidy PS, Sherwood JM, Flügel-Koch C, Lütjen-Drecoll E, et al. Therapeutic potential of AAV-mediated MMP-3 secretion from corneal endothelium in treating glaucoma. Hum Mol Genet. 2017;26(7):1230-46.
52. Bradley JM, Vranka J, Colvis CM, Conger DM, Alexander JP, Fisk AS, et al. Effect of matrix metalloproteinases activity on outflow in perfused human organ culture. Invest Ophthalmol Vis Sci. 1998;39(13):2649-58.
53. Overby DR, Stamer WD, Johnson M. The changing paradigm of outflow resistance generation: towards synergistic models of the JCT and inner wall endothelium. Exp Eye Res. 2009;88(4):656-70.
54. Grierson I, Lee WR. Light microscopic quantitation of the endothelial vacuoles in Schlemm's canal. Am J Ophthalmol. 1977;84(2):234-46.
55. Overby D, Gong H, Qiu G, Freddo TF, Johnson M. The mechanism of increasing outflow facility during washout in the bovine eye. Invest Ophthalmol Vis Sci. 2002;43(11):3455-64.
56. Acott TS, Kelley MJ, Keller KE, Vranka JA, Abu-Hassan DW, Li X, et al. Intraocular pressure homeostasis: maintaining balance in a high-pressure environment. J Ocul Pharmacol Ther. 2014;30(2-3):94-101.
57. Grant WM. Experimental aqueous perfusion in enucleated human eyes. Arch Ophthalmol. 1963;69:783-801.
58. Johnson MC, Kamm RD. The role of Schlemm's canal in aqueous outflow from the human eye. Investigative Ophthalmology & Visual Science. 1983;24(3):320-5.
59. Swaminathan SS, Oh D-J, Kang MH, Rhee DJ. Aqueous outflow: segmental and distal flow. J Cataract Refract Surg. 2014;40(8):1263-72.
60. Sit AJ, McLaren JW. Measurement of episcleral venous pressure. Exp Eye Res. 2011;93(3):291-8.
61. Roy Chowdhury U, Rinkoski TA, Bahler CK, Millar JC, Bertrand JA, Holman BH, et al. Effect of Cromakalim Prodrug 1 (CKLP1) on Aqueous Humor Dynamics and Feasibility of Combination Therapy With Existing Ocular Hypotensive Agents. Investigative Ophthalmology & Visual Science. 2017;58(13):5731-42.
62. Hoehn R, Mirshahi A, Hoffmann EM, Kottler UB, Wild PS, Laubert-Reh D, et al. Distribution of intraocular pressure and its association with ocular features and cardiovascular risk factors: the Gutenberg Health Study. Ophthalmology. 2013;120(5):961-8.

63. Watson P, Stjernschantz J. A six-month, randomized, double-masked study comparing latanoprost with timolol in open-angle glaucoma and ocular hypertension. The Latanoprost Study Group. Ophthalmology. 1996;103(1):126-37.
64. Bellezza AJ, Rintalan CJ, Thompson HW, Downs JC, Hart RT, Burgoyne CF. Deformation of the lamina cribrosa and anterior scleral canal wall in early experimental glaucoma. Invest Ophthalmol Vis Sci. 2003;44(2):623-37.
65. Fechtner RD, Weinreb RN. Mechanisms of optic nerve damage in primary open angle glaucoma. Surv Ophthalmol. 1994;39(1):23-42.
66. Quigley HA, Broman AT. The number of people with glaucoma worldwide in 2010 and 2020. Br J Ophthalmol. 2006;90(3):262-7.
67. Lee DA, Higginbotham EJ. Glaucoma and its treatment: a review. Am J Health Syst Pharm. 2005;62(7):691-9.
68. Kwon YH, Fingert JH, Kuehn MH, Alward WLM. Primary open-angle glaucoma. N Engl J Med. 2009;360(11):1113-24.
69. Stamer WD, Acott TS. Current understanding of conventional outflow dysfunction in glaucoma. Curr Opin Ophthalmol. 2012;23(2):135-43.
70. Weinreb RN, Aung T, Medeiros FA. The pathophysiology and treatment of glaucoma: a review. Jama. 2014;311(18):1901-11.
71. Dan J, Belyea D, Gertner G, Leshem I, Lusky M, Miskin R. Plasminogen Activator Inhibitor-1 in the Aqueous Humor of Patients With and Without Glaucoma. Archives of Ophthalmology. 2005;123(2):220-4.
72. Hu DN, Ritch R, Liebmann J, Liu Y, Cheng B, Hu MS. Vascular endothelial growth factor is increased in aqueous humor of glaucomatous eyes. J Glaucoma. 2002;11(5):406-10.
73. Knepper PA, Mayanil CS, Goossens W, Wertz RD, Holgren C, Ritch R, et al. Aqueous humor in primary open-angle glaucoma contains an increased level of CD44S. Invest Ophthalmol Vis Sci. 2002;43(1):133-9.
74. Tripathi RC, Li J, Chan WF, Tripathi BJ. Aqueous humor in glaucomatous eyes contains an increased level of TGF-beta 2. Exp Eye Res. 1994;59(6):723-7.
75. Tezel G, Kass MA, Kolker AE, Becker B, Wax MB. Plasma and aqueous humor endothelin levels in primary open-angle glaucoma. Journal of glaucoma. 1997;6(2):83-9.
76. Gottanka J, Chan D, Eichhorn M, Lütjen-Drecoll E, Ethier CR. Effects of TGF-beta2 in perfused human eyes. Invest Ophthalmol Vis Sci. 2004;45(1):153-8.
77. Krishnadas R, Ramakrishnan R. Secondary glaucomas: the tasks ahead. Community Eye Health. 2001;14(39):40-2.
78. Gordon MO, Beiser JA, Brandt JD, Heuer DK, Higginbotham EJ, Johnson CA, et al. The Ocular Hypertension Treatment Study: baseline factors that predict the onset of primary open-angle glaucoma. Arch Ophthalmol. 2002;120(6):714-20; discussion 829-30.
79. Stone EM, Fingert JH, Alward WL, Nguyen TD, Polansky JR, Sunden SL, et al. Identification of a gene that causes primary open angle glaucoma. Science. 1997;275(5300):668-70.
80. Hardy KM, Hoffman EA, Gonzalez P, McKay BS, Stamer WD. Extracellular trafficking of myocilin in human trabecular meshwork cells. J Biol Chem. 2005;280(32):28917-26.
81. Hoffman EA, Perkumas KM, Highstrom LM, Stamer WD. Regulation of myocilin-associated exosome release from human trabecular meshwork cells. Investigative ophthalmology & visual science. 2009;50(3):1313-8.
82. Peters DM, Herbert K, Biddick B, Peterson JA. Myocilin binding to Hep II domain of fibronectin inhibits cell spreading and incorporation of paxillin into focal adhesions. Exp Cell Res. 2005;303(2):218-28.

83. Ueda J, Wentz-Hunter K, Yue BYJT. Distribution of Myocilin and Extracellular Matrix Components in the Juxtacanalicular Tissue of Human Eyes. Investigative Ophthalmology & Visual Science. 2002;43(4):1068-76.
84. Fingert JH. Primary open-angle glaucoma genes. Eye. 2011;25(5):587-95.
85. Fingert JH, Héon E, Liebmann JM, Yamamoto T, Craig JE, Rait J, et al. Analysis of myocilin mutations in 1703 glaucoma patients from five different populations. Hum Mol Genet. 1999;8(5):899-905.
86. Jacobson N, Andrews M, Shepard AR, Nishimura D, Searby C, Fingert JH, et al. Non-secretion of mutant proteins of the glaucoma gene myocilin in cultured trabecular meshwork cells and in aqueous humor. Hum Mol Genet. 2001;10(2):117-25.
87. Kasetti RB, Phan TN, Millar JC, Zode GS. Expression of Mutant Myocilin Induces Abnormal Intracellular Accumulation of Selected Extracellular Matrix Proteins in the Trabecular Meshwork. Invest Ophthalmol Vis Sci. 2016;57(14):6058-69.
88. Zode GS, Kuehn MH, Nishimura DY, Searby CC, Mohan K, Grozdanic SD, et al. Reduction of ER stress via a chemical chaperone prevents disease phenotypes in a mouse model of primary open angle glaucoma. J Clin Invest. 2011;121(9):3542-53.
89. Rezaie T, Child A, Hitchings R, Brice G, Miller L, Coca-Prados M, et al. Adult-onset primary open-angle glaucoma caused by mutations in optineurin. Science. 2002;295(5557):1077-9.
90. Chalasani MLS, Kumari A, Radha V, Swarup G. E50K-OPTN-induced retinal cell death involves the Rab GTPase-activating protein, TBC1D17 mediated block in autophagy. PloS one. 2014;9(4):e95758-e.
91. Minegishi Y, Iejima D, Kobayashi H, Chi ZL, Kawase K, Yamamoto T, et al. Enhanced optineurin E50K-TBK1 interaction evokes protein insolubility and initiates familial primary open-angle glaucoma. Hum Mol Genet. 2013;22(17):3559-67.
92. Ryan TA, Tumbarello DA. Optineurin: A Coordinator of Membrane-Associated Cargo Trafficking and Autophagy. Front Immunol. 2018;9:1024.
93. Dikic I, Elazar Z. Mechanism and medical implications of mammalian autophagy. Nature Reviews Molecular Cell Biology. 2018;19(6):349-64.
94. Challa P. Glaucoma genetics. Int Ophthalmol Clin. 2008;48(4):73-94.
95. Fuse N, Takahashi K, Akiyama H, Nakazawa T, Seimiya M, Kuwahara S, et al. Molecular genetic analysis of optineurin gene for primary open-angle and normal tension glaucoma in the Japanese population. Journal of glaucoma. 2004;13(4):299-303.
96. Janssen SF, Gorgels TG, Ramdas WD, Klaver CC, van Duijn CM, Jansonius NM, et al. The vast complexity of primary open angle glaucoma: disease genes, risks, molecular mechanisms and pathobiology. Prog Retin Eye Res. 2013;37:31-67.
97. Allingham RR, Liu Y, Rhee DJ. The genetics of primary open-angle glaucoma: a review. Exp Eye Res. 2009;88(4):837-44.
98. Abu-Amero K, Kondkar AA, Chalam KV. An Updated Review on the Genetics of Primary Open Angle Glaucoma. Int J Mol Sci. 2015;16(12):28886-911.
99. Beidoe G, Mousa SA. Current primary open-angle glaucoma treatments and future directions. Clin Ophthalmol. 2012;6:1699-707.
100. Gupta SK, Niranjan D G, Agrawal SS, Srivastava S, Saxena R. Recent advances in pharmacotherapy of glaucoma. Indian J Pharmacol. 2008;40(5):197-208.
101. Kammer JA, Katzman B, Ackerman SL, Hollander DA. Efficacy and tolerability of bimatoprost versus travoprost in patients previously on latanoprost: a 3-month, randomised, masked-evaluator, multicentre study. Br J Ophthalmol. 2010;94(1):74-9.
102. Denis P, Baudouin C, Bron A, Nordmann J-P, Renard JP, Rouland JF, et al. First-line latanoprost therapy in ocular hypertension or open-angle glaucoma patients: a 3-month efficacy analysis stratified by initial intraocular pressure. BMC Ophthalmology. 2010;10(1):4.

103. Ang A, Reddy MA, Shepstone L, Broadway DC. Long term effect of latanoprost on intraocular pressure in normal tension glaucoma. Br J Ophthalmol. 2004;88(5):630-4.
104. Stankiewicz A, Wierzbowska J, Siemiatkowska A, Fuksinska B, Robaszkiewicz J, Zegadlo A, et al. The additive effect of dorzolamide hydrochloride (Trusopt) and a morning dose of bimatoprost (Lumigan) on intraocular pressure and retrobulbar blood flow in patients with primary open-angle glaucoma. Br J Ophthalmol. 2010;94(10):1307-11.
105. Schuman JS. Effects of systemic beta-blocker therapy on the efficacy and safety of topical brimonidine and timolol. Brimonidine Study Groups 1 and 2. Ophthalmology. 2000;107(6):1171-7.
106. Diggory P, Cassels-Brown A, Vail A, Hillman JS. Randomised, controlled trial of spirometric changes in elderly people receiving timolol or betaxolol as initial treatment for glaucoma. Br J Ophthalmol. 1998;82(2):146-9.
107. Watson PG, Barnett MF, Parker V, Haybittle J. A 7 year prospective comparative study of three topical beta blockers in the management of primary open angle glaucoma. Br J Ophthalmol. 2001;85(8):962-8.
108. Suzuki Y, Iwase A, Araie M, Yamamoto T, Abe H, Shirato S, et al. Risk factors for open-angle glaucoma in a Japanese population: the Tajimi Study. Ophthalmology. 2006;113(9):1613-7.
109. Mitchell P, Hourihan F, Sandbach J, Wang JJ. The relationship between glaucoma and myopia: the Blue Mountains Eye Study. Ophthalmology. 1999;106(10):2010-5.
110. Xing Y, Jiang F-G, Li T. Fixed combination of latanoprost and timolol vs the individual components for primary open angle glaucoma and ocular hypertension: a systematic review and meta-analysis. Int J Ophthalmol. 2014;7(5):879-90.
111. Sellem E, Rouland JF, Baudouin C, Bron A, Denis P, Nordmann J-P, et al. Predictors of additional intraocular pressure reduction in patients changed to latanoprost/timolol fixed combination. BMC ophthalmology. 2010;10:10-.
112. Franks WA, Renard JP, Cunliffe IA, Rojanapongpun P. A 6-week, double-masked, parallel-group study of the efficacy and safety of travoprost 0.004% compared with latanoprost 0:005%/timolol 0.5% in patients with primary open-angle glaucoma or ocular hypertension. Clin Ther. 2006;28(3):332-9.
113. Nakamoto K, Yasuda N. Effect of concomitant use of latanoprost and brinzolamide on 24-hour variation of IOP in normal-tension glaucoma. J Glaucoma. 2007;16(4):352-7.
114. Rulli E, Biagioli E, Riva I, Gambirasio G, De Simone I, Floriani I, et al. Efficacy and safety of trabeculectomy vs nonpenetrating surgical procedures: a systematic review and meta-analysis. JAMA Ophthalmol. 2013;131(12):1573-82.
115. Stein JD, Challa P. Mechanisms of action and efficacy of argon laser trabeculoplasty and selective laser trabeculoplasty. Curr Opin Ophthalmol. 2007;18(2):140-5.
116. Melamed S, Ben Simon GJ, Levkovitch-Verbin H. Selective laser trabeculoplasty as primary treatment for open-angle glaucoma: a prospective, nonrandomized pilot study. Arch Ophthalmol. 2003;121(7):957-60.
117. Feng Y, LoGrasso PV, Defert O, Li R. Rho Kinase (ROCK) Inhibitors and Their Therapeutic Potential. J Med Chem. 2016;59(6):2269-300.
118. Tanna AP, Johnson M. Rho Kinase Inhibitors as a Novel Treatment for Glaucoma and Ocular Hypertension. Ophthalmology. 2018;125(11):1741-56.
119. Townes-Anderson E, Wang J, Halász É, Sugino I, Pitler A, Whitehead I, et al. Fasudil, a Clinically Used ROCK Inhibitor, Stabilizes Rod Photoreceptor Synapses after Retinal Detachment. Transl Vis Sci Technol. 2017;6(3):22.
120. Dergham P, Ellezam B, Essagian C, Avedissian H, Lubell WD, McKerracher L. Rho signaling pathway targeted to promote spinal cord repair. J Neurosci. 2002;22(15):6570-7.
121. Lin CW, Sherman B, Moore LA, Laethem CL, Lu DW, Pattabiraman PP, et al. Discovery and Preclinical Development of Netarsudil, a Novel Ocular Hypotensive Agent for the Treatment of Glaucoma. J Ocul Pharmacol Ther. 2018;34(1-2):40-51.

122. Bacharach J, Dubiner HB, Levy B, Kopczynski CC, Novack GD. Double-masked, randomized, dose-response study of AR-13324 versus latanoprost in patients with elevated intraocular pressure. Ophthalmology. 2015;122(2):302-7.
123. Li G, Lee C, Read AT, Wang K, Ha J, Kuhn M, et al. Anti-fibrotic activity of a rho-kinase inhibitor restores outflow function and intraocular pressure homeostasis. Elife. 2021;10.
124. Wang JW, Woodward DF, Stamer WD. Differential effects of prostaglandin E2-sensitive receptors on contractility of human ocular cells that regulate conventional outflow. Investigative ophthalmology & visual science. 2013;54(7):4782-90.
125. Kalouche G, Beguier F, Bakria M, Melik-Parsadaniantz S, Leriche C, Debeir T, et al. Activation of Prostaglandin FP and EP2 Receptors Differently Modulates Myofibroblast Transition in a Model of Adult Primary Human Trabecular Meshwork Cells. Investigative Ophthalmology & Visual Science. 2016;57(4):1816-25.
126. Nilsson SF, Drecoll E, Lütjen-Drecoll E, Toris CB, Krauss AH, Kharlamb A, et al. The prostanoid EP2 receptor agonist butaprost increases uveoscleral outflow in the cynomolgus monkey. Invest Ophthalmol Vis Sci. 2006;47(9):4042-9.
127. Millard LH, Woodward DF, Stamer WD. The role of the prostaglandin EP4 receptor in the regulation of human outflow facility. Invest Ophthalmol Vis Sci. 2011;52(6):3506-13.
128. Zhong J, Gencay MM, Bubendorf L, Burgess JK, Parson H, Robinson BW, et al. ERK1/2 and p38 MAP kinase control MMP-2, MT1-MMP, and TIMP action and affect cell migration: a comparison between mesothelioma and mesothelial cells. J Cell Physiol. 2006;207(2):540-52.
129. Martínez T, Jiménez AI, Pañeda C. Short-interference RNAs: becoming medicines. EXCLI J. 2015;14:714-46.
130. Moreno-Montañés J, Sádaba B, Ruz V, Gómez-Guiu A, Zarranz J, González MV, et al. Phase I clinical trial of SYL040012, a small interfering RNA targeting β-adrenergic receptor 2, for lowering intraocular pressure. Mol Ther. 2014;22(1):226-32.
131. Tam LC, Reina-Torres E, Sherwood JM, Cassidy PS, Crosbie DE, Lütjen-Drecoll E, et al. Enhancement of Outflow Facility in the Murine Eye by Targeting Selected Tight-Junctions of Schlemm's Canal Endothelia. Sci Rep. 2017;7:40717.
132. Cassidy PS, Kelly RA, Reina-Torres E, Sherwood JM, Humphries MM, Kiang AS, et al. siRNA targeting Schlemm's canal endothelial tight junctions enhances outflow facility and reduces IOP in a steroid-induced OHT rodent model. Mol Ther Methods Clin Dev. 2021;20:86-94.
133. Schehlein EM, Novack GD, Robin AL. New classes of glaucoma medications. Curr Opin Ophthalmol. 2017;28(2):161-8.
134. Rasmussen CA, Kaufman PL. Exciting directions in glaucoma. Can J Ophthalmol. 2014;49(6):534-43.
135. Manno CS, Pierce GF, Arruda VR, Glader B, Ragni M, Rasko JJ, et al. Successful transduction of liver in hemophilia by AAV-Factor IX and limitations imposed by the host immune response. Nat Med. 2006;12(3):342-7.
136. Murphy SL, High KA. Gene therapy for haemophilia. British Journal of Haematology. 2008;140(5):479-87.
137. McCarty DM, Monahan PE, Samulski RJ. Self-complementary recombinant adeno-associated virus (scAAV) vectors promote efficient transduction independently of DNA synthesis. Gene Ther. 2001;8(16):1248-54.
138. Buie LK, Rasmussen CA, Porterfield EC, Ramgolam VS, Choi VW, Markovic-Plese S, et al. Self-complementary AAV virus (scAAV) safe and long-term gene transfer in the trabecular meshwork of living rats and monkeys. Investigative ophthalmology & visual science. 2010;51(1):236-48.
139. Johnstone M, Xin C, Tan J, Martin E, Wen J, Wang RK. Aqueous outflow regulation - 21st century concepts. Prog Retin Eye Res. 2020:100917.

140. Johnson M, Shapiro A, Ethier CR, Kamm RD. Modulation of outflow resistance by the pores of the inner wall endothelium. Invest Ophthalmol Vis Sci. 1992;33(5):1670-5.
141. Firth JA. Endothelial barriers: from hypothetical pores to membrane proteins. J Anat. 2002;200(6):541-8.
142. Allingham RR, de Kater AW, Ethier CR, Anderson PJ, Hertzmark E, Epstein DL. The relationship between pore density and outflow facility in human eyes. Invest Ophthalmol Vis Sci. 1992;33(5):1661-9.
143. Braakman ST, Read AT, Chan DWH, Ethier CR, Overby DR. Colocalization of outflow segmentation and pores along the inner wall of Schlemm's canal. Exp Eye Res. 2015;130:87-96.
144. Johnson M, Chan D, Read AT, Christensen C, Sit A, Ethier CR. The pore density in the inner wall endothelium of Schlemm's canal of glaucomatous eyes. Invest Ophthalmol Vis Sci. 2002;43(9):2950-5.
145. Overby DR, Zhou EH, Vargas-Pinto R, Pedrigi RM, Fuchshofer R, Braakman ST, et al. Altered mechanobiology of Schlemm's canal endothelial cells in glaucoma. Proceedings of the National Academy of Sciences of the United States of America. 2014;111(38):13876-81.
146. Vahabikashi A, Gelman A, Dong B, Gong L, Cha EDK, Schimmel M, et al. Increased stiffness and flow resistance of the inner wall of Schlemm's canal in glaucomatous human eyes. Proc Natl Acad Sci U S A. 2019;116(52):26555-63.
147. Junglas B, Kuespert S, Seleem AA, Struller T, Ullmann S, Bösl M, et al. Connective Tissue Growth Factor Causes Glaucoma by Modifying the Actin Cytoskeleton of the Trabecular Meshwork. The American Journal of Pathology. 2012;180(6):2386-403.
148. Cai J, Perkumas KM, Qin X, Hauser MA, Stamer WD, Liu Y. Expression Profiling of Human Schlemm's Canal Endothelial Cells From Eyes With and Without Glaucoma. Invest Ophthalmol Vis Sci. 2015;56(11):6747-53.
149. Agarwal P, Daher AM, Agarwal R. Aqueous humor TGF-β2 levels in patients with open-angle glaucoma: A meta-analysis. Mol Vis. 2015;21:612-20.
150. Min SH, Lee T-I, Chung YS, Kim HK. Transforming growth factor-beta levels in human aqueous humor of glaucomatous, diabetic and uveitic eyes. Korean J Ophthalmol. 2006;20(3):162-5.
151. Ochiai Y, Ochiai H. Higher concentration of transforming growth factor-beta in aqueous humor of glaucomatous eyes and diabetic eyes. Jpn J Ophthalmol. 2002;46(3):249-53.
152. Frangogiannis NG. Transforming growth factor–β in tissue fibrosis. Journal of Experimental Medicine. 2020;217(3).
153. Inatani M, Tanihara H, Katsuta H, Honjo M, Kido N, Honda Y. Transforming growth factor-beta 2 levels in aqueous humor of glaucomatous eyes. Graefes Arch Clin Exp Ophthalmol. 2001;239(2):109-13.
154. Wynn TA. Cellular and molecular mechanisms of fibrosis. J Pathol. 2008;214(2):199-210.
155. Diegelmann RF. Cellular and biochemical aspects of normal and abnormal wound healing: an overview. J Urol. 1997;157(1):298-302.
156. Friedlander M. Fibrosis and diseases of the eye. J Clin Invest. 2007;117(3):576-86.
157. Takahashi E, Inoue T, Fujimoto T, Kojima S, Tanihara H. Epithelial mesenchymal transition-like phenomenon in trabecular meshwork cells. Exp Eye Res. 2014;118:72-9.
158. Tamm ER, Siegner A, Baur A, Lutjen-Drecoll E. Transforming growth factor-beta 1 induces alpha-smooth muscle-actin expression in cultured human and monkey trabecular meshwork. Exp Eye Res. 1996;62(4):389-97.
159. Fleenor DL, Shepard AR, Hellberg PE, Jacobson N, Pang IH, Clark AF. TGFbeta2-induced changes in human trabecular meshwork: implications for intraocular pressure. Invest Ophthalmol Vis Sci. 2006;47(1):226-34.

160. Yue BY. The extracellular matrix and its modulation in the trabecular meshwork. Surv Ophthalmol. 1996;40(5):379-90.
161. Acott TS, Kelley MJ. Extracellular matrix in the trabecular meshwork. Exp Eye Res. 2008;86(4):543-61.
162. Fuchshofer R, Tamm ER. The role of TGF-beta in the pathogenesis of primary open-angle glaucoma. Cell Tissue Res. 2012;347(1):279-90.
163. Tovar-Vidales T, Clark AF, Wordinger RJ. Transforming growth factor-beta2 utilizes the canonical Smad-signaling pathway to regulate tissue transglutaminase expression in human trabecular meshwork cells. Exp Eye Res. 2011;93(4):442-51.
164. Zhao X, Ramsey KE, Stephan DA, Russell P. Gene and protein expression changes in human trabecular meshwork cells treated with transforming growth factor-beta. Invest Ophthalmol Vis Sci. 2004;45(11):4023-34.
165. Job R, Raja V, Grierson I, Currie L, O'Reilly S, Pollock N, et al. Cross-linked actin networks (CLANs) are present in lamina cribrosa cells. Br J Ophthalmol. 2010;94(10):1388-92.
166. Montecchi-Palmer M, Bermudez JY, Webber HC, Patel GC, Clark AF, Mao W. TGFβ2 Induces the Formation of Cross-Linked Actin Networks (CLANs) in Human Trabecular Meshwork Cells Through the Smad and Non-Smad Dependent Pathways. Invest Ophthalmol Vis Sci. 2017;58(2):1288-95.
167. Clark AF, Wilson K, McCartney MD, Miggans ST, Kunkle M, Howe W. Glucocorticoid-induced formation of cross-linked actin networks in cultured human trabecular meshwork cells. Invest Ophthalmol Vis Sci. 1994;35(1):281-94.
168. Last JA, Pan T, Ding Y, Reilly CM, Keller K, Acott TS, et al. Elastic modulus determination of normal and glaucomatous human trabecular meshwork. Invest Ophthalmol Vis Sci. 2011;52(5):2147-52.
169. Tomasek JJ, Gabbiani G, Hinz B, Chaponnier C, Brown RA. Myofibroblasts and mechano-regulation of connective tissue remodelling. Nat Rev Mol Cell Biol. 2002;3(5):349-63.
170. Sarrazy V, Billet F, Micallef L, Coulomb B, Desmouliere A. Mechanisms of pathological scarring: role of myofibroblasts and current developments. Wound Repair Regen. 2011;19 Suppl 1:s10-5.
171. Patel G, Fury W, Yang H, Gomez-Caraballo M, Bai Y, Yang T, et al. Molecular taxonomy of human ocular outflow tissues defined by single-cell transcriptomics. Proceedings of the National Academy of Sciences. 2020:202001896.
172. Kovacic JC, Mercader N, Torres M, Boehm M, Fuster V. Epithelial-to-mesenchymal and endothelial-to-mesenchymal transition: from cardiovascular development to disease. Circulation. 2012;125(14):1795-808.
173. Zhu Y-T, Chen H-C, Chen S-Y, Tseng SCG. Nuclear p120 catenin unlocks mitotic block of contact-inhibited human corneal endothelial monolayers without disrupting adherent junctions. J Cell Sci. 2012;125(Pt 15):3636-48.
174. Mina SG, Huang P, Murray BT, Mahler GJ. The role of shear stress and altered tissue properties on endothelial to mesenchymal transformation and tumor-endothelial cell interaction. Biomicrofluidics. 2017;11(4):044104-.
175. Cho JG, Lee A, Chang W, Lee M-S, Kim J. Endothelial to Mesenchymal Transition Represents a Key Link in the Interaction between Inflammation and Endothelial Dysfunction. Frontiers in immunology. 2018;9:294-.
176. Braunger BM, Fuchshofer R, Tamm ER. The aqueous humor outflow pathways in glaucoma: A unifying concept of disease mechanisms and causative treatment. Eur J Pharm Biopharm. 2015;95(Pt B):173-81.
177. Pattabiraman PP, Maddala R, Rao PV. Regulation of plasticity and fibrogenic activity of trabecular meshwork cells by Rho GTPase signaling. J Cell Physiol. 2014;229(7):927-42.

178. Pattabiraman PP, Rao PV. Mechanistic basis of Rho GTPase-induced extracellular matrix synthesis in trabecular meshwork cells. Am J Physiol Cell Physiol. 2010;298(3):C749-C63.
179. Lip GY, Blann A. von Willebrand factor: a marker of endothelial dysfunction in vascular disorders? Cardiovasc Res. 1997;34(2):255-65.
180. Hägerling R, Hoppe E, Dierkes C, Stehling M, Makinen T, Butz S, et al. Distinct roles of VE-cadherin for development and maintenance of specific lymph vessel beds. EMBO J. 2018;37(22):e98271.
181. Peng X, Nelson ES, Maiers JL, DeMali KA. New insights into vinculin function and regulation. Int Rev Cell Mol Biol. 2011;287:191-231.
182. Wordinger RJ, Fleenor DL, Hellberg PE, Pang I-H, Tovar TO, Zode GS, et al. Effects of TGF-β2, BMP-4, and Gremlin in the Trabecular Meshwork: Implications for Glaucoma. Investigative Ophthalmology & Visual Science. 2007;48(3):1191-200.
183. Felkin LE, Lara-Pezzi E, George R, Yacoub MH, Birks EJ, Barton PJ. Expression of extracellular matrix genes during myocardial recovery from heart failure after left ventricular assist device support. J Heart Lung Transplant. 2009;28(2):117-22.
184. Zhang X, Clark AF, Yorio T. Regulation of glucocorticoid responsiveness in glaucomatous trabecular meshwork cells by glucocorticoid receptor-beta. Invest Ophthalmol Vis Sci. 2005;46(12):4607-16.
185. Zhuo YH, He Y, Leung KW, Hou F, Li YQ, Chai F, et al. Dexamethasone disrupts intercellular junction formation and cytoskeleton organization in human trabecular meshwork cells. Mol Vis. 2010;16:61-71.
186. Gu X, Ma Y, Liu Y, Wan Q. Measurement of mitochondrial respiration in adherent cells by Seahorse XF96 Cell Mito Stress Test. STAR Protocols. 2021;2(1):100245.
187. Zilfou JT, Lowe SW. Tumor suppressive functions of p53. Cold Spring Harb Perspect Biol. 2009;1(5):a001883-a.
188. Vander Heiden MG, Cantley LC, Thompson CB. Understanding the Warburg effect: the metabolic requirements of cell proliferation. Science (New York, NY). 2009;324(5930):1029-33.
189. Warburg O, Wind F, Negelein E. THE METABOLISM OF TUMORS IN THE BODY. J Gen Physiol. 1927;8(6):519-30.
190. Kamel K, O'Brien CJ, Zhdanov AV, Papkovsky DB, Clark AF, Stamer WD, et al. Reduced Oxidative Phosphorylation and Increased Glycolysis in Human Glaucoma Lamina Cribrosa Cells. Investigative ophthalmology & visual science. 2020;61(13):4-.
191. Stamer WD, Braakman ST, Zhou EH, Ethier CR, Fredberg JJ, Overby DR, et al. Biomechanics of Schlemm's canal endothelium and intraocular pressure reduction. Progress in retinal and eye research. 2015;44:86-98.
192. Sanjabi S, Oh SA, Li MO. Regulation of the Immune Response by TGF-β: From Conception to Autoimmunity and Infection. Cold Spring Harb Perspect Biol. 2017;9(6):a022236.
193. Weinberg SE, Sena LA, Chandel NS. Mitochondria in the regulation of innate and adaptive immunity. Immunity. 2015;42(3):406-17.
194. Ozcan AA, Ozdemir N, Canataroglu A. The aqueous levels of TGF-beta2 in patients with glaucoma. Int Ophthalmol. 2004;25(1):19-22.
195. Zeisberg EM, Potenta SE, Sugimoto H, Zeisberg M, Kalluri R. Fibroblasts in kidney fibrosis emerge via endothelial-to-mesenchymal transition. J Am Soc Nephrol. 2008;19(12):2282-7.
196. Zeisberg EM, Tarnavski O, Zeisberg M, Dorfman AL, McMullen JR, Gustafsson E, et al. Endothelial-to-mesenchymal transition contributes to cardiac fibrosis. Nat Med. 2007;13(8):952-61.

197. Hashimoto N, Phan SH, Imaizumi K, Matsuo M, Nakashima H, Kawabe T, et al. Endothelial-mesenchymal transition in bleomycin-induced pulmonary fibrosis. Am J Respir Cell Mol Biol. 2010;43(2):161-72.
198. Potenta S, Zeisberg E, Kalluri R. The role of endothelial-to-mesenchymal transition in cancer progression. Br J Cancer. 2008;99(9):1375-9.
199. He W, Zhang J, Gan TY, Xu GJ, Tang BP. Advanced glycation end products induce endothelial-to-mesenchymal transition via downregulating Sirt 1 and upregulating TGF-β in human endothelial cells. Biomed Res Int. 2015;2015:684242.
200. Zhavoronkov A, Izumchenko E, Kanherkar RR, Teka M, Cantor C, Manaye K, et al. Pro-fibrotic pathway activation in trabecular meshwork and lamina cribrosa is the main driving force of glaucoma. Cell Cycle. 2016;15(12):1643-52.
201. Zhou EH, Krishnan R, Stamer WD, Perkumas KM, Rajendran K, Nabhan JF, et al. Mechanical responsiveness of the endothelial cell of Schlemm's canal: scope, variability and its potential role in controlling aqueous humour outflow. J R Soc Interface. 2012;9(71):1144-55.
202. McDonnell F, O'Brien C, Wallace D. The role of epigenetics in the fibrotic processes associated with glaucoma. J Ophthalmol. 2014;2014:750459.
203. Campbell M, Humphries MM, Kiang A-S, Nguyen ATH, Gobbo OL, Tam LCS, et al. Systemic low-molecular weight drug delivery to pre-selected neuronal regions. EMBO Mol Med. 2011;3(4):235-45.
204. Campbell M, Hanrahan F, Gobbo OL, Kelly ME, Kiang A-S, Humphries MM, et al. Targeted suppression of claudin-5 decreases cerebral oedema and improves cognitive outcome following traumatic brain injury. Nature Communications. 2012;3(1):849.
205. Keaney J, Walsh DM, O'Malley T, Hudson N, Crosbie DE, Loftus T, et al. Autoregulated paracellular clearance of amyloid-β across the blood-brain barrier. Sci Adv. 2015;1(8):e1500472.
206. Boussommier-Calleja A, Bertrand J, Woodward DF, Ethier CR, Stamer WD, Overby DR. Pharmacologic manipulation of conventional outflow facility in ex vivo mouse eyes. Investigative ophthalmology & visual science. 2012;53(9):5838-45.
207. Lei Y, Overby DR, Boussommier-Calleja A, Stamer WD, Ethier CR. Outflow physiology of the mouse eye: pressure dependence and washout. Investigative ophthalmology & visual science. 2011;52(3):1865-71.
208. Stamer WD, Lei Y, Boussommier-Calleja A, Overby DR, Ethier CR. eNOS, a pressure-dependent regulator of intraocular pressure. Investigative ophthalmology & visual science. 2011;52(13):9438-44.
209. Phulke S, Kaushik S, Kaur S, Pandav SS. Steroid-induced Glaucoma: An Avoidable Irreversible Blindness. J Curr Glaucoma Pract. 2017;11(2):67-72.
210. McDonough AK, Curtis JR, Saag KG. The epidemiology of glucocorticoid-associated adverse events. Curr Opin Rheumatol. 2008;20(2):131-7.
211. Dada T, Nair S, Dhawan M. Steroid-induced glaucoma. J Curr Glaucoma Pract. 2009;3(2):33-8.
212. Razeghinejad MR, Katz LJ. Steroid-induced iatrogenic glaucoma. Ophthalmic research. 2012;47(2):66-80.
213. Whitlock NA, McKnight B, Corcoran KN, Rodriguez LA, Rice DS. Increased intraocular pressure in mice treated with dexamethasone. Invest Ophthalmol Vis Sci. 2010;51(12):6496-503.
214. Zode GS, Sharma AB, Lin X, Searby CC, Bugge K, Kim GH, et al. Ocular-specific ER stress reduction rescues glaucoma in murine glucocorticoid-induced glaucoma. J Clin Invest. 2014;124(5):1956-65.
215. Overby DR, Bertrand J, Tektas OY, Boussommier-Calleja A, Schicht M, Ethier CR, et al. Ultrastructural changes associated with dexamethasone-induced ocular hypertension in mice. Invest Ophthalmol Vis Sci. 2014;55(8):4922-33.

216. Overby DR, Clark AF. Animal models of glucocorticoid-induced glaucoma. Exp Eye Res. 2015;141:15-22.
217. Fujimoto T, Inoue T, Inoue-Mochita M, Tanihara H. Live cell imaging of actin dynamics in dexamethasone-treated porcine trabecular meshwork cells. Exp Eye Res. 2016;145:393-400.
218. Yuan Y, Call MK, Yuan Y, Zhang Y, Fischesser K, Liu CY, et al. Dexamethasone induces cross-linked actin networks in trabecular meshwork cells through noncanonical wnt signaling. Invest Ophthalmol Vis Sci. 2013;54(10):6502-9.
219. Sherwood JM, Reina-Torres E, Bertrand JA, Rowe B, Overby DR. Measurement of Outflow Facility Using iPerfusion. PLoS One. 2016;11(3):e0150694.
220. Underwood JL, Murphy CG, Chen J, Franse-Carman L, Wood I, Epstein DL, et al. Glucocorticoids regulate transendothelial fluid flow resistance and formation of intercellular junctions. Am J Physiol. 1999;277(2):C330-42.
221. Patel GC, Phan TN, Maddineni P, Kasetti RB, Millar JC, Clark AF, et al. Dexamethasone-Induced Ocular Hypertension in Mice: Effects of Myocilin and Route of Administration. Am J Pathol. 2017;187(4):713-23.
222. Zode GS, Bugge KE, Mohan K, Grozdanic SD, Peters JC, Koehn DR, et al. Topical ocular sodium 4-phenylbutyrate rescues glaucoma in a myocilin mouse model of primary open-angle glaucoma. Invest Ophthalmol Vis Sci. 2012;53(3):1557-65.
223. Alward WL, Fingert JH, Coote MA, Johnson AT, Lerner SF, Junqua D, et al. Clinical features associated with mutations in the chromosome 1 open-angle glaucoma gene (GLC1A). N Engl J Med. 1998;338(15):1022-7.
224. Resch ZT, Hann CR, Cook KA, Fautsch MP. Aqueous humor rapidly stimulates myocilin secretion from human trabecular meshwork cells. Experimental eye research. 2010;91(6):901-8.
225. Joe MK, Sohn S, Hur W, Moon Y, Choi YR, Kee C. Accumulation of mutant myocilins in ER leads to ER stress and potential cytotoxicity in human trabecular meshwork cells. Biochem Biophys Res Commun. 2003;312(3):592-600.
226. Zhou Y, Grinchuk O, Tomarev SI. Transgenic mice expressing the Tyr437His mutant of human myocilin protein develop glaucoma. Investigative ophthalmology & visual science. 2008;49(5):1932-9.
227. Kessel L, Johnson L, Arvidsson H, Larsen M. The relationship between body and ambient temperature and corneal temperature. Invest Ophthalmol Vis Sci. 2010;51(12):6593-7.
228. Lucia U, Grisolia G, Dolcino D, Astori MR, Massa E, Ponzetto A. Constructal approach to bio-engineering: the ocular anterior chamber temperature. Scientific Reports. 2016;6(1):31099.
229. Reina-Torres E, Bertrand JA, O'Callaghan J, Sherwood JM, Humphries P, Overby DR. Reduced humidity experienced by mice in vivo coincides with reduced outflow facility measured ex vivo. Exp Eye Res. 2019;186:107745.
230. Dillinger AE, Guter M, Froemel F, Weber GR, Perkumas K, Stamer WD, et al. Intracameral Delivery of Layer-by-Layer Coated siRNA Nanoparticles for Glaucoma Therapy. Small. 2018;14(50):e1803239.
231. Wang L, Xiao R, Andres-Mateos E, Vandenberghe LH. Single stranded adeno-associated virus achieves efficient gene transfer to anterior segment in the mouse eye. PLoS One. 2017;12(8):e0182473.
232. Li G, Gonzalez P, Camras LJ, Navarro I, Qiu J, Challa P, et al. Optimizing gene transfer to conventional outflow cells in living mouse eyes. Exp Eye Res. 2013;109:8-16.
233. Kamel K, Farrell M, O'Brien C. Mitochondrial dysfunction in ocular disease: Focus on glaucoma. Mitochondrion. 2017;35:44-53.

234. Lee S, Van Bergen NJ, Kong GY, Chrysostomou V, Waugh HS, O'Neill EC, et al. Mitochondrial dysfunction in glaucoma and emerging bioenergetic therapies. Exp Eye Res. 2011;93(2):204-12.
235. Yu-Wai-Man P, Griffiths PG, Chinnery PF. Mitochondrial optic neuropathies - disease mechanisms and therapeutic strategies. Progress in retinal and eye research. 2011;30(2):81-114.
236. Chalmers RM, Schapira AH. Clinical, biochemical and molecular genetic features of Leber's hereditary optic neuropathy. Biochim Biophys Acta. 1999;1410(2):147-58.
237. Mackey DA, Oostra RJ, Rosenberg T, Nikoskelainen E, Bronte-Stewart J, Poulton J, et al. Primary pathogenic mtDNA mutations in multigeneration pedigrees with Leber hereditary optic neuropathy. Am J Hum Genet. 1996;59(2):481-5.
238. Jarrett SG, Lin H, Godley BF, Boulton ME. Mitochondrial DNA damage and its potential role in retinal degeneration. Prog Retin Eye Res. 2008;27(6):596-607.
239. Yen MY, Wang AG, Wei YH. Leber's hereditary optic neuropathy: a multifactorial disease. Prog Retin Eye Res. 2006;25(4):381-96.
240. Porter RK, Joyce OJ, Farmer MK, Heneghan R, Tipton KF, Andrews JF, et al. Indirect measurement of mitochondrial proton leak and its application. Int J Obes Relat Metab Disord. 1999;23 Suppl 6:S12-8.
241. Kitajima-Ihara T, Yagi T. Rotenone-insensitive internal NADH-quinone oxidoreductase of Saccharomyces cerevisiae mitochondria: the enzyme expressed in Escherichia coli acts as a member of the respiratory chain in the host cells. FEBS Lett. 1998;421(1):37-40.
242. Berns KI, Giraud C. Biology of adeno-associated virus. Curr Top Microbiol Immunol. 1996;218:1-23.
243. Muzyczka N. Use of adeno-associated virus as a general transduction vector for mammalian cells. Curr Top Microbiol Immunol. 1992;158:97-129.
244. Xiao X, Li J, Samulski RJ. Efficient long-term gene transfer into muscle tissue of immunocompetent mice by adeno-associated virus vector. J Virol. 1996;70(11):8098-108.
245. Surace EM, Auricchio A, Reich SJ, Rex T, Glover E, Pineles S, et al. Delivery of adeno-associated virus vectors to the fetal retina: impact of viral capsid proteins on retinal neuronal progenitor transduction. Journal of virology. 2003;77(14):7957-63.
246. Bogner B, Boye SL, Min SH, Peterson JJ, Ruan Q, Zhang Z, et al. Capsid Mutated Adeno-Associated Virus Delivered to the Anterior Chamber Results in Efficient Transduction of Trabecular Meshwork in Mouse and Rat. PloS one. 2015;10(6):e0128759-e.
247. Zhong L, Li B, Mah CS, Govindasamy L, Agbandje-McKenna M, Cooper M, et al. Next generation of adeno-associated virus 2 vectors: point mutations in tyrosines lead to high-efficiency transduction at lower doses. Proc Natl Acad Sci U S A. 2008;105(22):7827-32.
248. Petrs-Silva H, Dinculescu A, Li Q, Deng WT, Pang JJ, Min SH, et al. Novel properties of tyrosine-mutant AAV2 vectors in the mouse retina. Mol Ther. 2011;19(2):293-301.
249. Barot M, Gokulgandhi MR, Mitra AK. Mitochondrial dysfunction in retinal diseases. Curr Eye Res. 2011;36(12):1069-77.
250. Borrás T, Xue W, Choi VW, Bartlett JS, Li G, Samulski RJ, et al. Mechanisms of AAV transduction in glaucoma-associated human trabecular meshwork cells. J Gene Med. 2006;8(5):589-602.
251. Kass MA, Heuer DK, Higginbotham EJ, Johnson CA, Keltner JL, Miller JP, et al. The Ocular Hypertension Treatment Study: a randomized trial determines that topical ocular hypotensive medication delays or prevents the onset of primary open-angle glaucoma. Arch Ophthalmol. 2002;120(6):701-13; discussion 829-30.

252. Scherer WJ. A retrospective review of non-responders to latanoprost. J Ocul Pharmacol Ther. 2002;18(3):287-91.
253. Noecker RS, Dirks MS, Choplin NT, Bernstein P, Batoosingh AL, Whitcup SM. A six-month randomized clinical trial comparing the intraocular pressure-lowering efficacy of bimatoprost and latanoprost in patients with ocular hypertension or glaucoma. Am J Ophthalmol. 2003;135(1):55-63.
254. Stower H. RNA therapies prepare for the spotlight. Nature Medicine. 2020;26(12):1805-.
255. Wang S, Liu P, Song L, Lu L, Zhang W, Wu Y. Adeno-associated virus (AAV) based gene therapy for eye diseases. Cell Tissue Bank. 2011;12(2):105-10.
256. Stamer WD, Roberts BC, Howell DN, Epstein DL. Isolation, culture, and characterization of endothelial cells from Schlemm's canal. Invest Ophthalmol Vis Sci. 1998;39(10):1804-12.
257. Lane A, Jovanovic K, Shortall C, Ottaviani D, Panes AB, Schwarz N, et al. Modeling and Rescue of RP2 Retinitis Pigmentosa Using iPSC-Derived Retinal Organoids. Stem Cell Reports. 2020;15(1):67-79.
258. Xiao X, Li J, Samulski RJ. Production of high-titer recombinant adeno-associated virus vectors in the absence of helper adenovirus. J Virol. 1998;72(3):2224-32.
259. Bennicelli J, Wright JF, Komaromy A, Jacobs JB, Hauck B, Zelenaia O, et al. Reversal of blindness in animal models of leber congenital amaurosis using optimized AAV2-mediated gene transfer. Mol Ther. 2008;16(3):458-65.
260. Rohr U-P, Wulf M-A, Stahn S, Steidl U, Haas R, Kronenwett R. Fast and reliable titration of recombinant adeno-associated virus type-2 using quantitative real-time PCR. Journal of Virological Methods. 2002;106(1):81-8.

Appendices

Appendix 1: Presentation given at the Trabecular Meshwork Study Club Meeting in Washington D.C 2019 entitled "Fibrotic-like changes at the inner wall of Schlemm's canal in glaucoma."

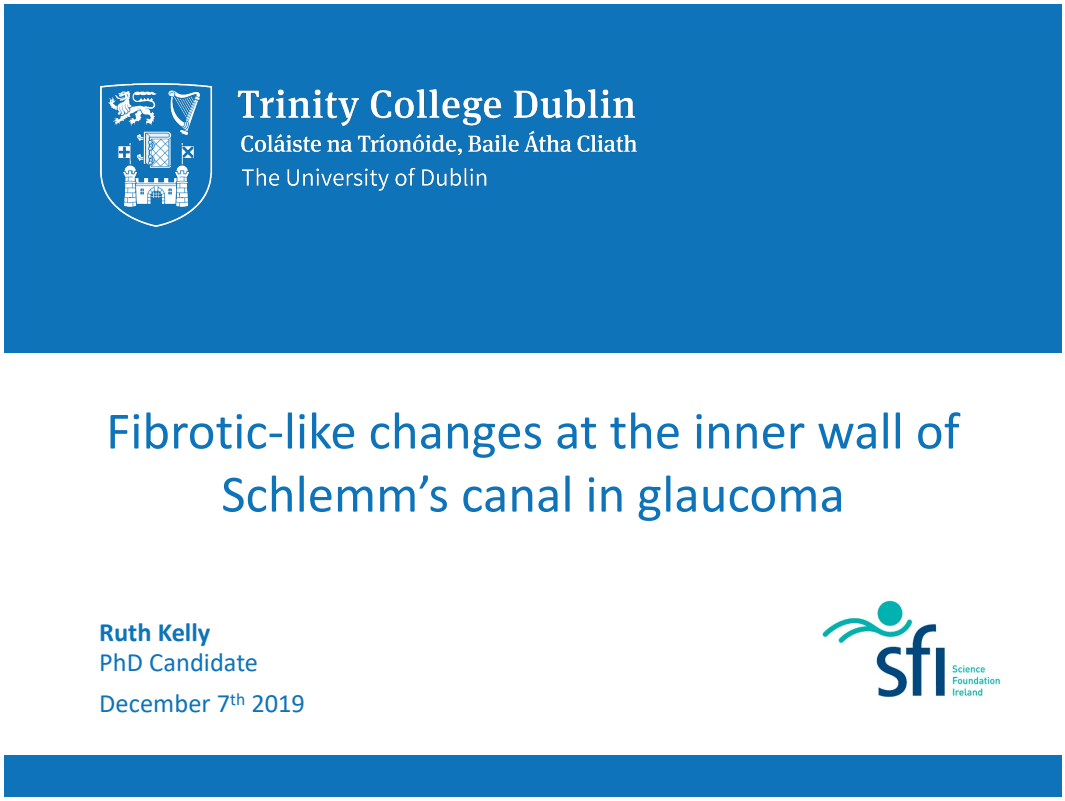

Primary open angle glaucoma: What do we know so far?

↑ Increased IOP

↑ Increased outflow resistance

↑ Increased cell stiffness (SC and TM)

↑ Increased ECM stiffness

↓ Decreased tendency for pore formation

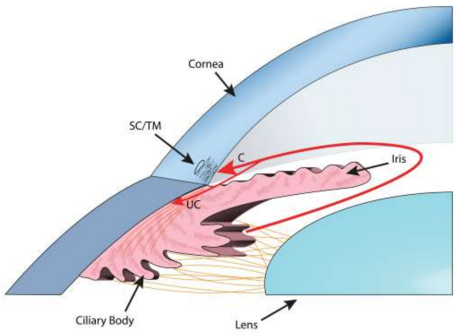

Taken from O' Callaghan et al. 2017.

Key players involved in fibrosis

↑ Increase in TGF-β2 expression (known driver of fibrosis)

↑ Increase in ECM materials (at the TM, LC and ONH)

↑ Increase in fibrotic markers; TGF-β2, collagen I-α1 and αSMA

→ Associated with increased tissue stiffness

Hypothesis: Fibrotic-like changes at the inner wall of Schlemm's canal may be associated with some of these glaucoma phenotypes.

Comparing glaucomatous SC endothelial cells to healthy cells

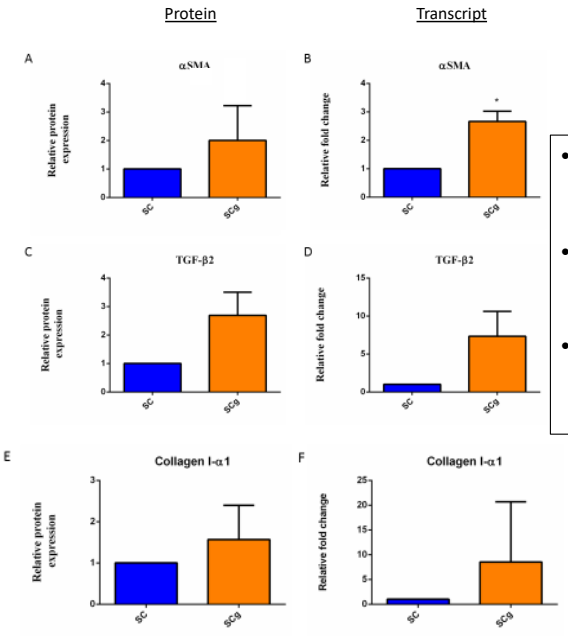

- Increased expression of αSMA at both a protein and mRNA level in glaucomatous SC cells.
- Increased expression of TGF-β2 at both a protein and mRNA level in glaucomatous SC cells.
- Increased expression of collagen I-α1 at both a protein and mRNA level in glaucomatous SC cells.

Comparing glaucomatous SC endothelial cells to healthy cells

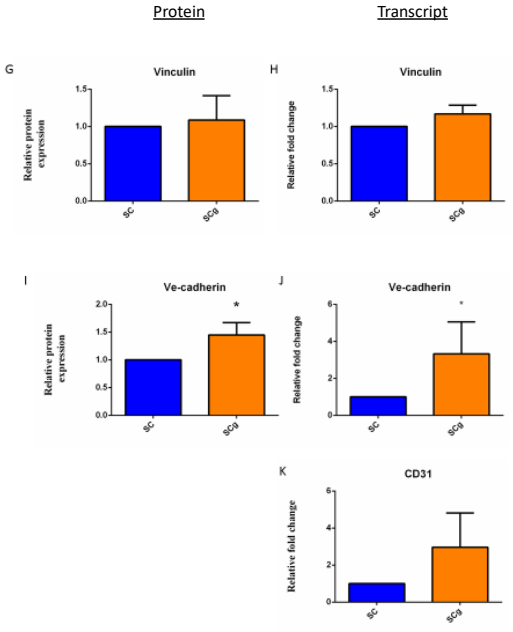

- No change in vinculin expression at both a protein and mRNA level between SC and SCg.
- Increase in ve-cadherin expression at both a protein and mRNA level in glaucomatous SC cells.
- Increase in CD31 expression at an mRNA level in glaucomatous SC cells.

Comparing glaucomatous SC endothelial cells to healthy cells

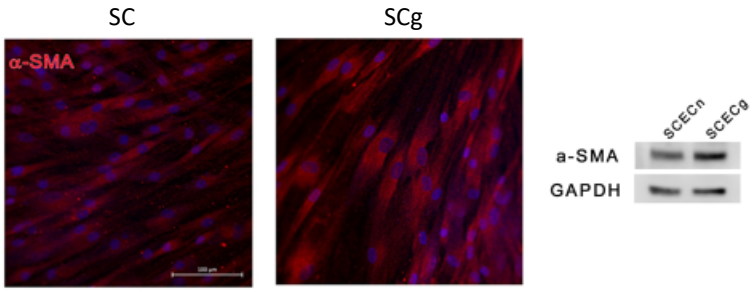

Greater amounts of α-SMA fibres shown in glaucomatous SC cells compared to healthy SC cells.

Inducing a fibrotic-like phenotype in healthy SC endothelial cells.

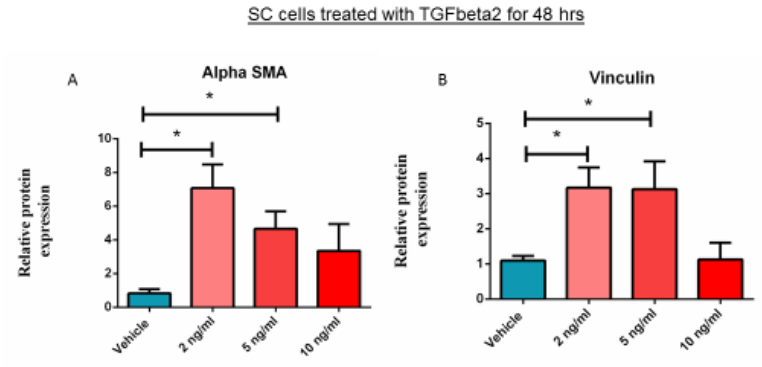

- Increased expression of fibrotic and adhesion markers in healthy SC cells following the addition of TGF-β2.

Functional assays comparing TGF-β2 treated cells to vehicle control.

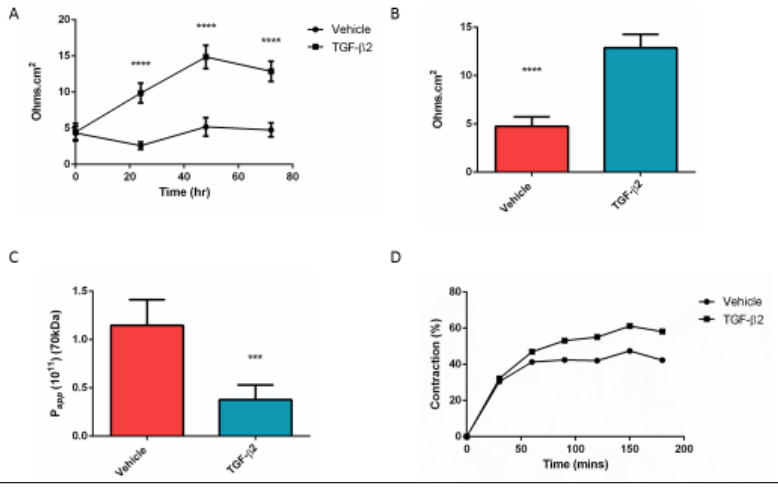

- Significant increase in TEER value of 8.11 ohms.cm2 in TGF-β2 treated cells.
- Significant decrease in transcellular permeability of 0.77x10^11 in TGF-β2 treated cells.
- A difference of 15.8% is seen between the contraction of TGF-β2 treated cells and vehicle treated cells.

Inducing a fibrotic-like phenotype in healthy SC endothelial cells (steroid induced glaucoma).

SC cells treated with dexamethasone for 2 weeks

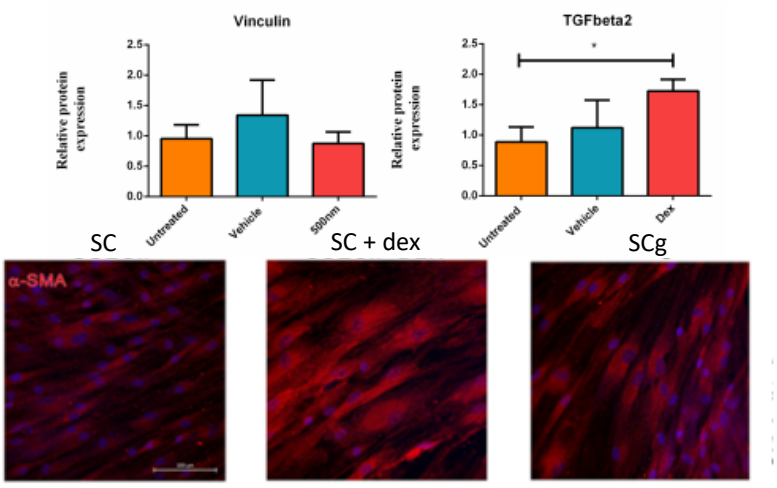

- Increased expression of fibrotic markers TGF-β2 and αSMA in healthy SC cells following the addition of dexamethasone.

Inducing a fibrotic-like phenotype in healthy SC endothelial cells (ER stress).

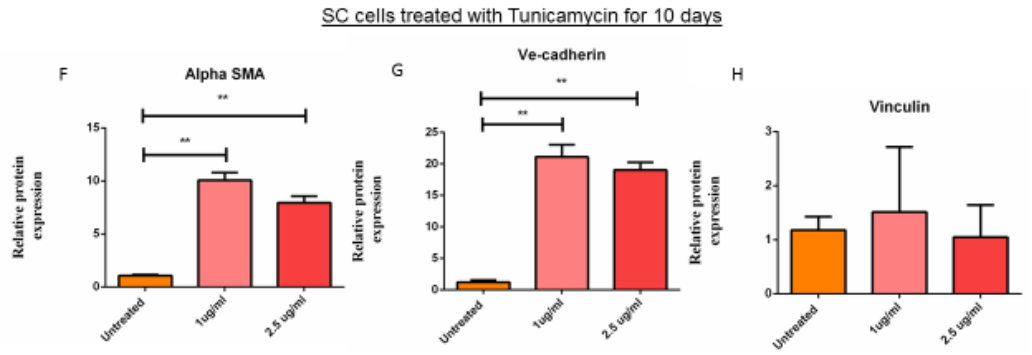

- Increased protein expression of both α-SMA and ve-cadherin.
- No significant change in vinculin protein expression.

Introducing the Seahorse assay

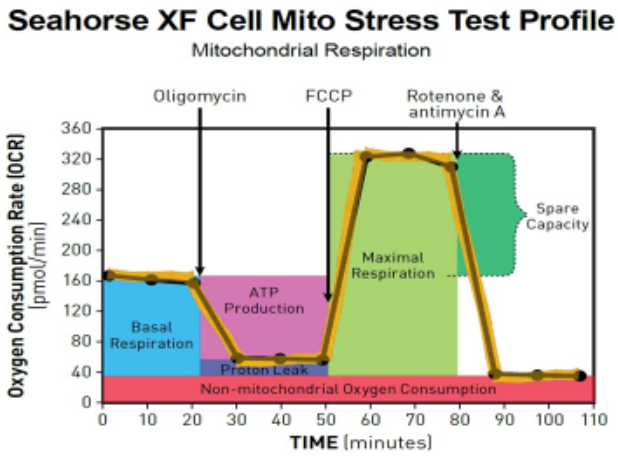

- Oligomycin inhibits ATP synthase (CV) – reduced mitochondrial respiration.
- FCCP is an uncoupling agent that collapses the proton gradient and disrupts the mitochondrial membrane potential – oxygen consumption reaches maximum level.
- Rotenone and antimycin A inhibit CI and complex CIII respectively – shuts down mitochondrial respiration.

Oxygen consumption rate (OCR) for both healthy and glaucomatous SCECs.

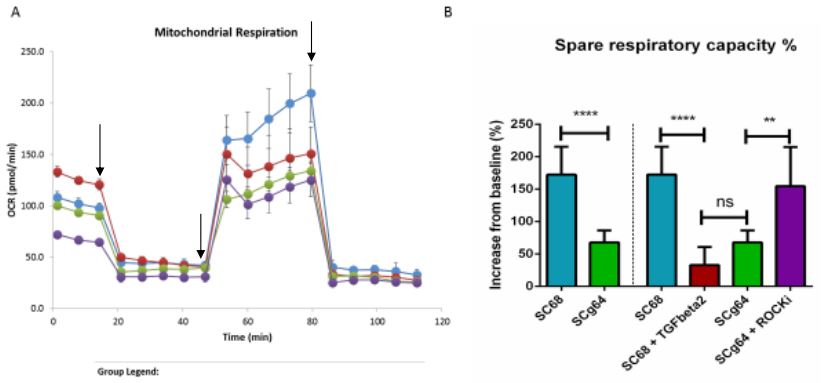

- Glaucomatous SCs have a lower maximum level of respiration compared to healthy SCs.
- Healthy SCs have a significant decrease in their spare respiratory capacity following the addition of TGF-β2.
- Glaucomatous SCs have a significant increase in spare respiratory capacity following the addition of ROCKi.

To conclude:

- Increased expression of fibrotic and adhesion markers in glaucomatous SC endothelial cells.
- Increased expression of fibrotic markers in healthy SC cells, following the addition of TGF-β2, dex and tunicamycin.
- Healthy SC cells show reduced permeability and greater contractility following the addition of the fibrotic agent TGF-β2.
- Glaucomatous SC cells show reduced mitochondrial activity compared to healthy SC cells.

Future work:

- More work to be done on characterising these cells – investigating more fibrotic and endothelial cell markers, as well as more functional assays.
- Effect of ROCK inhibitor treatments along with fibrotic treatments, such as Relaxin on SCgs and SCs with the addition of the fibrotic agent TGF-β2.

This study suggests that fibrotic-like changes at the Schlemm's canal endothelium could be involved in the pathology of glaucoma.

Trinity College Dublin, The University of Dublin

Appendix 2: Published article "siRNA targeting Schlemm's canal endothelial tight junctions enhances outflow facility and reduces IOP in a steroid-induced OHT rodent model."

Molecular Therapy
Methods & Clinical Development
OriginalArticle

siRNAtargetingSchlemm'scanalendothelial tightjunctionsenhancesoutflowfacilityand reducesIOPinasteroid-inducedOHTrodentmodel

PaulS.Cassidy,[1,6]RuthA.Kelly,[1,6]EsterReina-Torres,[1,2]JosephM.Sherwood,[2]MarianM.Humphries,[1]
Anna-SophiaKiang,[1]G.JaneFarrar,[1]ColmO'Brien,[3]MatthewCampbell,[4]W.DanielStamer,[5]DarrylR.Overby,[2]
PeteHumphries,[1]andJeffreyO'Callaghan[1,4]

[1]OcularGeneticsUnit,SmurfitInstituteofGenetics,TrinityCollegeDublin,Dublin,Ireland;[2]DepartmentofBioengineering,ImperialCollegeLondon,London,UK;
[3]DepartmentofOphthalmology,MaterMisericordiaeUniversityHospital,Dublin,Ireland;[4]NeurovascularResearchLaboratory,SmurfitInstituteofGenetics,Trinity CollegeDublin,Dublin,Ireland;[5]DepartmentofOphthalmology,DukeUniversity,Durham,NC,USA

Systemic or localized application of glucocorticoids (GCs) can lead to iatrogenic ocular hypertension, which is a leading cause of secondary open-angle glaucoma and visual impairment. Previous work has shown that dexamethasone increases zonula occludens-1 (ZO-1) protein expression in trabecular meshwork (TM) cells, and that an antisense oligonucleotide inhibitor of ZO-1 can abolish the dexamethasone-induced increase in trans-endothelial flow resistance in cultured Schlemm's canal (SC) endothelial and TM cells. We have previously shown that intracameral inoculation of small interfering RNA (siRNA) targeting SC endothelial cell tight junction components, ZO-1 and tricellulin, increases aqueous humor outflow facility ex vivo in normotensive mice by reversibly opening SC endothelial paracellular pores. In this study, we show that targeted siRNA downregulation of these SC endothelial tight junctions reduces intraocular pressure (IOP)invivo, with a concomitant increase in conventional outflow facility in a well-characterized chronic steroid-induced mouse model of ocular hypertension, thus representing a potential focused clinical application for this therapy in a sight-threatening scenario.

INTRODUCTION

Glucocorticoids(GCs)havebeenwidelyusedincontrollingocular inflammationinuveitis;however,ocularhypertension(OHT)with theriskofsecondaryopen-angleglaucomaisasignificantcomplicationofGCtherapy.[1]Whilemostpatientsundergoshortcoursesof GCtherapy,intheUKanestimatedupto5%ofadultsundergo long-termsystemicGCusedailyformorethan5years,whileupto 20%undergoGCtreatmentformorethan6months.[2]Onethirdof ophthalmictopicalGC-treatedpatientsexhibitamoderateincrease inintraocularpressure(IOP),whileapproximately5%ofpatients experiencesevereIOPincreases.Withintravitrealinjection,these ratesaregreatlyincreased,withOHTresultingin25%ofcases.[3]In thoseinstanceswhereacutesteroid-inducedelevationsinIOPoccur inGC-dependentpatients,andinwhichOHTcannotbecontrolled withconventionalpressure-reducingmedications,trabeculectomy, lasertrabeculoplasty,orshuntsurgerymayberequired.[4]Theseprocedureshaveassociatedrisksofcomplications,warrantingexplorationofalternative,lessinvasivemethodsofIOPcontrol.

Mostresistancetoaqueousoutflowisgeneratedwithinthejuxtacanalicular tissues(JCTs),comprisingthetrabecularmeshwork(TM) andinnerwallendotheliumofSchlemm'scanal(SC).Endothelial cellsoftheinnerwallofSCformlooselyorganizedtightjunctions (TJs),leavingdiscreteparacellularcleftsthroughwhichaqueouscan enterthecanalfromtheTM.Asynergisticmodelofoutflowresistance generationhasbeenproposed,inwhichtheinnerwallofSC andtheJCTregiontogetherareresponsibleforthebulkofconventionaloutflowresistancegeneration.[5]Underthismodel,referredto asthefunnelingmodelofoutflowresistancegeneration,duetothe spatial separation of SC inner wall pores, aqueous humor (AH) movingfromtheJCTsintotheseporesmustconverge,orfunnel, fromwideareasoftissuetodiscreteporesontheinnerwallthrough the tortuousextracellular spaces of the JCTs.[5] Paracellular pores may be the preferentialflow path, but transcellular pores also contribute to the overall outflow along the inner wall of SC.[6]

Increased pore density is associated with regions of higher segmentaloutflow,whileglaucomatouseyesarereportedtohave reducedSCinnerwallporosity.[7,8]Assuch,theporedensityofaregion of the SC inner wall can directly influence conventional outflowresistancegenerationandhydraulicconductivity.GCtreatmentcanhavearangeofeffectsontheoutflowpathway,including altering TM cell functions, extracellular matrix metabolism, and gene expression, which may be responsible for the increase in outflowresistanceassociatedwithGCtreatment.[9]

Received11May2020;accepted27October2020;
https://doi.org/10.1016/j.omtm.2020.10.022.
[6]Theseauthorscontributedequally
Correspondence: RuthA.Kelly,OcularGeneticsUnit,SmurfitInstituteofGenetics,TrinityCollegeDublin,Dublin,Ireland.
E-mail:kellyr33@tcd.ie;pcassid@tcd.ie

WehavepreviouslyshowninnormotensivemicethatsmallinterferingRNA(siRNA)-mediateddownregulationofTJproteinszonula occludens-1(ZO-1)(encodedbytheTJP1gene)andtricellulin(encodedbytheMARVELD2gene)inSCendothelialcellsresultsina visibleopeningofparacellularcleftsasobservedbytransmissionelectronmicroscopy,increasingcleftporosityandenhancingflowof aqueousfromtheTMintothelumen,thusresultinginanincrease inconventionaloutflowfacility.[10]However,itremainedtobedemonstratedwhetherandtowhatextentthisapproachtoIOPcontrol mightbeeffectiveinananimalmodeldisplayingfeaturesofsteroid-inducedOHT,wheresignificantmolecularpathologicalchanges occurwithintheTMtoreduceoutflow,andwhetherthe concomitant elevationinIOPcouldalsobereduced.Weinvestigatedtheefficacyof thisapproachinamousemodelofdexamethasone(DEX)-induced OHT.SustainedelevationofIOPcanbeinducedinmicethrough long-termsystemicdeliveryofDEXusingmicro-osmoticpumps. ThismethodofinducingGCOHThasbeenshowntoelevateIOP significantlywithin2weeksoftreatment,withaconcomitantreductioninconventionaloutflowfacility,whilepreservingopen-angled morphologywithintheanteriorchamber.[11–14]Wehavepreviously shownhowtreatmentwithsiRNAdoesnotimpactthe open-angle structure in the anterior chamber in rodents. We have assumed thatthesamemodeofactionisoccurringinthesehypertensiveanimalstreatedwiththesamesiRNAaswasusedinourpreviouswork.[10]

Thisisinferredbasedonfindingsfrom Tametal.[10]thatsiRNAtargetingbothZO-1andtricellulinresultsinanatomicalchangesto theoutflowtissueinnormotensiveanimals.

MicetreatedwithDEXhavealsobeenshowntohaveincreaseddeposition of extracellular matrix material within the TM, with elevated levelsofextracellularcollagenI,fibronectin,andmucopolysaccharides,andtheformationofcross-linkeda-smoothmuscleactinnetworks.[15,16]Also,ofparticularrelevancetoourTJmodulation-based approach, GC treatment of cultured human SC endothelial cells (SCECs)hasbeenshowntosignificantlyincreaseZO-1expression, andtoincreasethenumberofTJ-containingintercellularcontacts.[17]

Hence,thismodelrepresentsasuitablemeansforassessmentofthe modulatoryeffectofourapproachonoutflowfacility,servingasa modelofOHTinPOAGingeneraland,morespecifically,ofhuman GC-inducedglaucoma.WeshowhereinthatsiRNA-mediatedTJ proteinsuppressionenhancesconventionaloutflowfacilityandreducesIOPinthismurinemodelofGC-inducedOHT.Potentialadaptationofthisapproachtoenableclinicaldeploymentisalsodiscussed.

RESULTS

CharacterizationofIOPelevationinDEX-treatedmice

Wild-typeC57BL/6Jmicewereimplantedsubcutaneouslywithmicro-osmoticpumpsdeliveringDEXatadoseof2mg/kg/day(n=17),whileaseparatecohortofwild-typeC57BL/6Jmicedesignated ascontrolswereimplantedwithpumpscontainingcyclodextrinas avehiclecontrol(n=9).Onedaypriortopumpimplantation, micewereanesthetizedwithisoflurane,andIOPwasmeasuredby reboundtonometryinoneeye.Thesemeasurementswererepeated weeklythereafterfor4weeks.ThechangesinIOParisingfromthis treatment,anddifferencesinpopulationaverages,aresummarized inFigure1.ThebaselineIOPmeasurementforthevehicle-treated groupwas14.4[13.7,15.0](mean[confidenceinterval(CI)]),and finalIOPmeasurementwas15.2[14.4,16.0],correspondingtoa non-significantchangeof0.9[00.3,2.0]mmHg(p>0.05,one-way ANOVAwithTukey'spost-test,n=9,Figure1A,red).ForDEX-treatedanimals,baselineIOPwasmeasuredas12.8[12.2,13.4], andfinalIOPwas17.8[17.1,18.4],correspondingtoasignificantincreaseinIOPof5.0[3.9,6.1]mmHg(p<0.0001,one-wayANOVA withTukey'spost-test,n=17,Figure1A,blue).After4weeksoftreatment,thefinalIOPdifferencebetweentheDEXandcontrolgroups was2.6[1.6,3.5]mmHg(p<0.0001,unpairedttest,Figure1A), comparedtoa1.6[00.7,02.5]mmHg(p=0.001,unpairedttest,Figure1A)differenceinIOPbetweentheDEXandvehiclegroupatthe beginningofthestudy,beforeanytreatmentwasadministered.These dataconfirmthatDEXtreatmentresultsinasignificantelevationin IOPintheseanimalsascomparedtothevehiclecontrols(Figure1B).

TargeteddownregulationofTJproteinsZO-1andtricellulinin normotensiveC57BL/6Jmice

Inordertovalidatetheefficacyof siRNA-mediatedtranscriptsuppressionofourtargetTJproteinsZO-1andtricellulin,wefirstcarried outourintraocularsiRNAdeliveryprotocolthatwehavepreviously shown to be effective in the enhancement of outflow facility in normotensivemice.[10]Briefly,C57BL/6Jnormotensiveanimalswere treatedwithanintracameralinjectioncontaining1mgeachofZO-1andtricellulintargetingsiRNA(T-siRNA)inoneeye,whilecontralateral control eyes received 2mg of non-targeting siRNA (NT-siRNA)injections.Then,at48hpost-injection,enucleatedtissue washomogenized,RNAwasextracted,andqPCRanalysiswascarried outonbothNT-siRNA-andT-siRNA-treatedeyes.

T-siRNA-injectedeyesshowedsignificantdownregulationofboth ZO-1 and tricellulin transcript levels, when compared to NT-siRNA-treatedeyes.$2^{-\Delta\Delta DCt}$valuesarepresentedbelow,representing foldchangeinrelativegeneexpressionoftheseTJproteinsofinterest. ForZO-1,intracameralinjectionwithT-siRNAledtoasignificant meanfoldchangeinrelativegeneexpressionof0.7[0.5,0.8](mean [CI)(p<0.001,n=12,Figure2A),andtricellulinshowedasignificant meanfoldchangeinrelativegeneexpressionof0.6[0.4,0.9](p<0.01, one-samplettesttotheoreticalmeanof1,n=11,Figure2A),representinga30%and40%averagereductionintranscriptlevels,respectively.ThesedatasuggestthattheTJsZO-1andtricellulinaresuccessfully downregulated at the outflow tissue following a single intracameralinjectionwithT-siRNA.

EffectofTJdownregulationonIOPinvehicle-treatedmice

Toevaluatewhetherdownregulationof ZO-1andtricellulinwasan effective means of lowering IOP in normotensive mice, all mice wereanesthetizedandIOPwasmeasuredagaininbotheyestoacquirebaselinemeasurementsaftervehiclemicro-osmoticpumptreatmentandpriortoinjectionwithsiRNA.Micewerethentreatedwith an intracameral injection containing T-siRNA in one eye, while contralateralcontroleyesreceivedNT-siRNAinjections.At48h

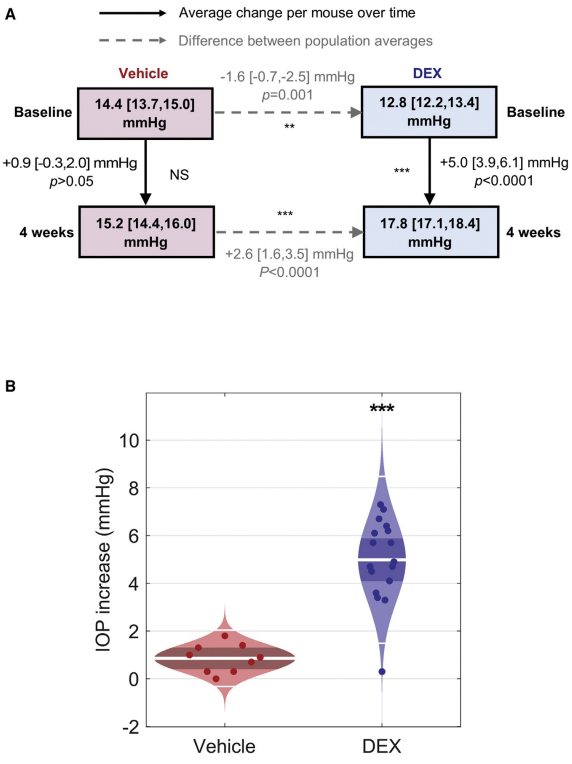

Figure1.SummaryofIOPchangesinvehicleand dexamethasone(DEX)-treatedmice (A)ChangeinIOPafter4weeksofvehicle(red,n=9)or DEX(blue,n=17)deliveryviaamicro-osmoticpump. Dashedarrowsrepresentthedifferencesbetweenpop-ulationaverageatbaselineandaftertreatment,whilesolid arrowsrepresenttheaveragechangeinIOPpermouse aftertreatment.(B)CelloplotsshowtheIOPincrease (mmHg) following treatment with either cyclodextrin vehicle(red)orDEX(blue)for4weeks.Thewhiteline representsthegeometricmean,thedarkred/bluebands indicatethe95%CI,andthelightred/blueregionsarethe distributionsofthedata.Eachdatapointrepresentsthe IOPincrease(mmHg)foreachindividualanimal.pvalues arerepresentedbyasterisks.

post-injection, mice were anesthetized and IOP was once again measuredbyreboundtonometry.Toaccountforthevariationin thepre-treatmentbaselineIOPvalues,IOPdataarepresentedas thechangeinIOPbetweenpre-andpost-treatmentmeasurements inbothNT-siRNA-andT-siRNA-treatedeyes.ThechangesinIOP arisingfromthissiRNAinjection,anddifferencesinpopulationaver-agesbeforeand48haftertreatment,aresummarizedinFigure2for vehicle-treatedanimalsandFigure3forDEX-treatedanimals.

T-siRNA-injectedeyesshowedasignificantaveragereductioninIOP of1.0[01.6,00.3]mmHgascomparedtopre-treatmentIOPmea-surementaverages(13.6[13.3,13.9]versus14.5[14.2,14.9]mmHg, p<0.01,n=9,Figures2Band2C,green).NT-siRNA-injectedeyes showednosignificantaveragechangeinIOPintheseanimals,00.0 [00.4,0.2]mmHg,ascomparedtopre-treatmentIOPmeasurement averagesof(14.2[14.0,14.5]versus14.3[14.1, 14.6]mmHg,p>0.05,n=9,Figures2Band 2C,orange).At48hpost-treatment,asignifi-cantdifferenceinIOPof00.7[00.1,01.2] mmHg(p=0.02,two-wayunpairedttest,Fig-ure2C)wasshownbetweentheNT-siRNAand T-siRNAgroupscomparedtoanon-significant differenceinIOPof0.2[00.2,0.6]mmHg(p> 0.05,two-wayunpairedttest,Figure2C)be-tweenthegroupsatthebeginningofthestudy, beforetreatmentwasadministered.Thesedata confirm that T-siRNA treatment in this vehicle-treated group results in a significant reductioninIOPcomparedtotheNT-siRNA group(Figure2B).

EffectofTJdownregulationonexvivo conventionaloutflowfacilityinvehicle-treatedmice

Innormotensivevehiclecontrolmice,T-siRNA inducedanincreaseinconventionaloutflowfa-cility(C)of38[5,81]%(p=0.029,Figure2D) ascomparedtoNT-siRNA.Changesinfacility weredeterminedbyperforming*exvivo*perfu-sionsusingtheiPerfusionsystem.[17] Thisfacilitatedcomparisonof C between paired contralateral T-siRNA- and NT-siRNA-treated eyesinnormotensivevehicle(n=6)mice.

TargeteddownregulationofTJproteinsZO-1andtricellulinin DEX-treatedmice

AfterdemonstratingabovethatsiRNA-mediatedtranscriptsuppres-sionofourtargetTJproteinsZO-1andtricellulinwaseffectivein normotensive mice, we wanted toalso validate this approach in siRNA-treatedhypertensiveDEX-treatedanimals.Acohortofmice wasadministeredDEXdailyfor4weeksinordertoinduceOHT, andthenindividualswereadministeredasingleintracameralinjec-tionofbothT-siRNAandNT-siRNAasabove.At48hpost-injection, enucleatedtissuewashomogenized,RNAwasextracted,andqPCR analysiswascarriedout,asinthenormotensivecohortofmice.

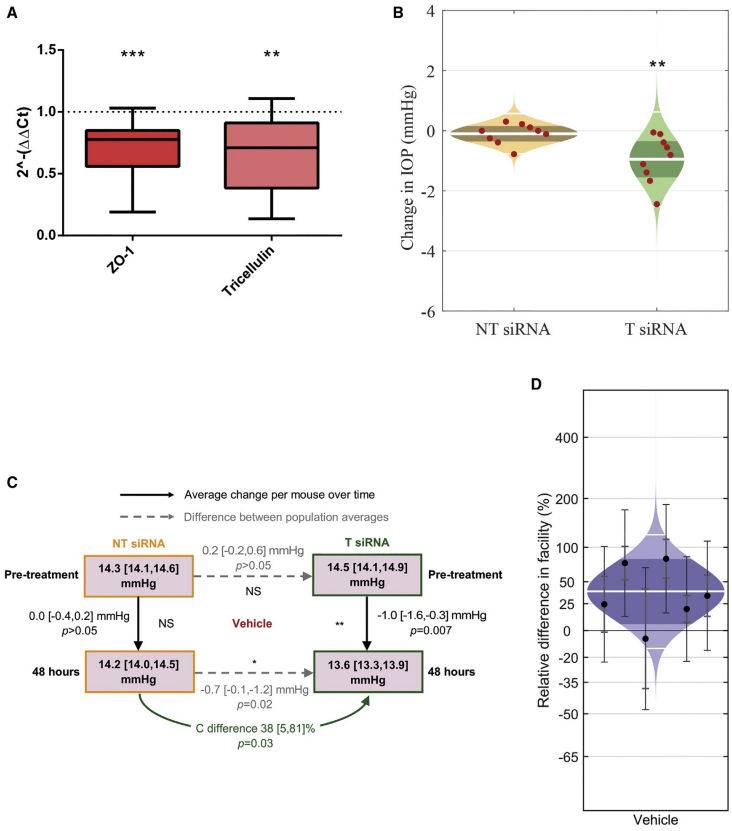

Figure2.SummaryofrelativefoldgeneexpressionofTJproteins,IOP,andfacilitychangesafterintracameralsiRNAinjectioninvehiclecontrolanimals
(A)Ameanfoldchangeinrelativegeneexpressionof0.7[0.5,0.8](p<0.001,one-samplettesttotheoreticalmeanof1,n=12)and0.6[0.4,0.9](p<0.01,one-samplettest totheoreticalmeanof1,n=11)isshowninbothZO-1andtricellulinproteintranscripts,respectively.Errorbarsrepresentminimum/maximumvalues,the95%Clisshownby boundsofbox,andthehorizontallinerepresentsthemedian.(B)Celloplotsshowingthechangeinlop(mmHg)48hpost-treatmentwitheithernon-targetingsiRNA(NT-siRNA)(orange)orsiRNAtargetingZO-1andtricellulin(T-siRNA)(green).Thewhitelinerepresentsthegeometricmean,thedarkorange/greenbandsindicatethe95%CI, andthelightorange/greenregionsarethedistributionsofthedata.Eachdatapointrepresentsthechangeinlop(mmHg)foreachindividualanimal.(C)Summaryofchanges inlOPandoutflowfacilityaftertreatmentwithintracameralinjectionofT-siRNA(green,n=9)orNT-siRNA(orange,n=9)invehicle-treatedmice.Differencesinexvivooutflow facility(C)72haftertreatmentareshownviagreenarrows.Dashedarrowsrepresentthedifferencesbetweenpopulationaveragepre-treatmentand48hpost-treatment, whilesolidarrowsrepresenttheaveragechangeinlOPpermouseaftertreatment.(D)IntracameralinjectionofT-siRNAtargetingZO-1andtricellulinisshowntosignificantly increaseconventionaloutflowfacilityintreatedeyesascomparedtocontralateralcontroleyesreceivingNT-siRNAinvehiclenormotensiveanimals,withanincreaseof38[5, 81]%(mean[95%CI])(p=0.029,n=6pairs).Thewhitelinerepresentsthegeometricmean,thedarkbluebandsindicatethe95%CI,andthelightblueregionsarethe distributionofthedata.EachdatapointrepresentsthedifferenceinCbetweencontralateraleyeswith95%CI.pvaluesarerepresentedbyasterisks.

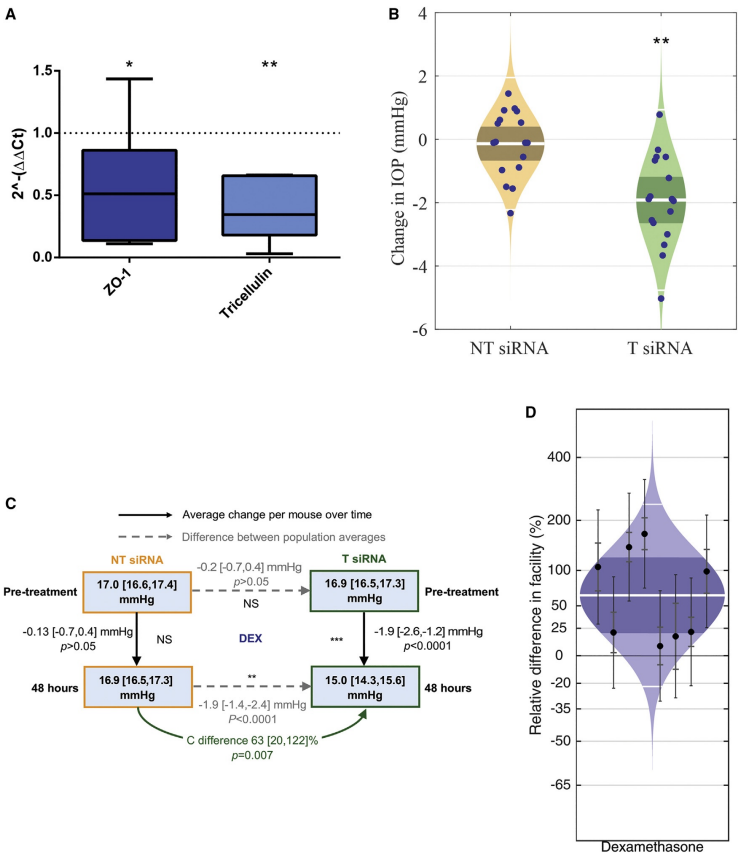

Figure3.SummaryofrelativefoldgeneexpressionofTJproteins,IOP,andfacilitychangesafterintracameralsiRNAinjectioninDEX-treatedanimals
(A)Ameanfoldchangeinrelativegeneexpressionof0.6[0.2,1.0](p<0.05,one-samplettesttotheoreticalmeanof1,n=8)and0.4[0.1,0.6](p<0.01,onesamplettestto theoreticalmeanof1,n=6)wasshowninbothZO-1andtricellulinproteintranscripts,respectively.Errorbarsrepresentminimum/maximumvalues,the95%Clisshownby boundsofbox,andthehorizontallinerepresentsthemedian.(B)Celloplotsshowingthechangeinlop(mmHg)48hpost-treatmentwitheitherNT-siRNA(orange)or T-siRNA(green).Thewhitelinerepresentsthegeometricmean,thedarkorange/greenbandsindicatethe95%CI,andthelightorange/greenregionsarethedistributionsof thedata.Eachdatapointrepresentsthechangeinlop(mmHg)foreachindividualanimal.(C)SummaryofchangesinlOPandoutflowfacilityaftertreatmentwithintracameral injectionofsiRNAtargetingZO-1andtricellulin(T-siRNA,green,n=17)orNT-siRNA(orange,n=17)inDEX-treatedmice.(D)Thesecelloplotsshowthesignificantincrease inconventionaloutflowfacilityfollowingtreatmentwithT-siRNAcomparedtocontralateralcontroleyesreceivingNT-siRNAinDEX-treatedanimals,withanincreaseof63 [20,122]%(mean[95%CI])(p=0.0071,n=8pairs).Thewhitelinerepresentsthegeometricmean,thedarkbluebandsindicatethe95%CI,andthelightblueregionsarethe distributionofthedata.Eachdatapointrepresentsthedifferenceincbetweencontralateraleyeswith95%CI.pvaluesarerepresentedbyasterisks.

T-siRNA-injectedeyesshowedsignificantdownregulationofboth ZO-1 and tricellulin gene expression, when compared to NT-siRNA-treatedeyes.Followingaonce-offintracameralinjectionof T-siRNA,ZO-1showedasignificantmeanfoldchangeinrelative geneexpressionof0.6[0.2,1.0](mean[CI])(p<0.05,one-sample ttesttotheoreticalmeanof1,n=8,Figure3A).andtricellulinshowed asignificantmeanfoldchangeinrelativegeneexpressionof0.4[0.1, 0.6](p<0.01,n=6,Figure3A),representinga40%and60%mean reductionintranscriptlevels,respectively.Thesedatasuggestthat T-siRNAhasgreaterpotentialforTJdownregulationintheDEX-treatedanimalsascomparedtothenormotensivecontrolgroup.

EffectofTJdownregulationonIOPinDEX-treatedmice

Toevaluatewhetherdownregulationof ZO-1andtricellulinwasan effectivemeansofloweringIOPinOHTmice,allmicewereanesthetizedandIOPwasmeasuredagaininbotheyestoacquirebaseline measurementsafterDEXmicro-osmoticpumptreatmentandprior toinjectionwithsiRNA.Micewerethentreatedwithanintracameral injectioncontainingT-siRNAinoneeye,whilecontralateralcontrol eyesreceivedNT-siRNAinjections.At48hpost-injection,micewere anesthetizedandIOPwasonceagainmeasuredbyreboundtonometry.DEX-treatedmiceshowedasignificantaveragereductionin IOP in T-siRNA-injected eyes of 1.9 [02.6, 01.2] mmHg as comparedtopre-treatmentIOPmeasurementaverages(15.0[14.3, 15.6]versus16.9[16.5,17.3]mmHg,p<0.0001,n=17,Figures3B and 3C green). NT-siRNA-injected eyes showed no significant averagechangeinIOPintheseanimalsof0.13[-0.7,0.4]mmHg, as compared to pre-treatment IOP measurement averages (16.9 [16.5,17.3]versus17[16.6,17.4]mmHg,p>0.05,n=17,Figures 3Band3C,orange).At48hpost-treatmentintheDEX-treatedanimals,thefinalIOPdifferencebetweentheNTandT-siRNAgroups was01.9[01.4,02.4]mmHg(p<0.0001,two-wayunpairedttest, Figure3C),comparedto00.2[00.7,0.4]mmHg(p<0.05,two-wayunpairedttest,Figure3C)differenceinIOPbetweenthegroups atthebeginningofthestudy,beforetreatmentwasadministered. ThesedataconfirmthatsiRNAtreatmentintheseDEX-treatedanimalsresultsinasignificantreductioninIOPcomparedtotheNT-siRNAgroup(Figure3B).

EffectofTJdownregulationonexvivoconventionaloutflow facilityinDEX-treatedmice

InDEXmice,eyesinjectedwithT-siRNAhadasignificantincreasein Cof63[20,122]%(p=0.0071,n=8pairs,Figure3D)overcontralateralNT-siRNA-injectedcontroleyes.

DISCUSSION

WehavepreviouslyshownthatdownregulationoftheTJ-associated proteinsZO-1andtricellulinattheSCinnerwallleadstoaninCreaseinthenumberofopenSCendothelialparacellularclefts,as wellasanincreaseinCinnormotensivewild-typemice.[10] Inthe current study, we aimed to validate this approach in a disease settingusingamurinemodelofsteroid-inducedOHT.Specifically, wewantedtoassesstheutilityofthisapproachforIOPreductionin amodelofchronicsteroid-inducedelevationinIOP,asisoften observedinGC-dependentpatientsresistanttotheuseofconventional pressure-reducing topical medications, and where surgical interventionmaybetheonlycurrentoptiontoreduceIOP.We wanted to determine whether C could be increased in the DEX modeland,additionally,toinvestigatewhetherdownregulationof ZO-1andtricellulinreducedIOP.

WehaveshownsignificantdownregulationofTJproteintranscript levels in both normotensive and hypertensive DEX-treated mice followingasingleintracameralinjectionofT-siRNA.Agreaterreductioninboth ZO-1andtricellulinrelativegeneexpressionisseeninthe DEX-treatedcohortinresponsetoT-siRNAcomparedtothatin normotensiveanimals.WehaveshownintheDEXmodelofOHT thatsuchanimalsalsoexhibitagreaterreductioninIOPthando normotensive animals after siRNA treatment. We additionally demonstratedthatthistherapeuticapproachsignificantlyincreases Cinboththishypertensivemodelandinnormotensivevehiclecontrols,withagreaterrelativechangeseeninhypertensiveanimals. ThedatasuggestthathigherIOPmayleadtoagreaterefficacyof thisapproach,asanincreasedpressuregradientacrosstheSCinner wallmayfacilitateincreasedopeningofparacellularporesuponTJ downregulation.Thedataalsofurtheremphasizetherolethatparacellularporesatthe SCinnerwallplayinpathologicalreductionsin outflowfacility,andcorrespondingIOPelevation.T-siRNA-injected DEX-treatedeyesshowanaverageIOPdecreaseofapproximately 2mmHg,representingtwicethatmeasuredinnormotensivecontrols (approximately1mmHg).Whilethelevelofthemeanincreasein Cin normotensiveanimalsreportedhereinof38%islowerthanthemean increaseof113%previouslyreportedinTametal.,[10] perfusionswere carriedout72hpost-treatmentthereascomparedto48hpreviouslyto facilitate*invivo*tonometricIOPreadingscarriedoutat48hpost-treatmenthere.Thislessereffectsizeisunderstandable,asthetransientnatureofsiRNA-mediateddownregulationresultsinreduced target downregulation with longer times post-treatment. As the DEXmodelisknowntoincreaseTJproteinexpression,including ZO-1,[18] wethusproposethatsiRNA-mediatedknockdownofTJsis moreeffectiveinanenvironmentwithgreaterTJexpression,asthere isagreateravailabilityofTJmRNAforsiRNAtobindto.Itisalso possiblethatthereisagreaternumberofclosedoroccludedparacellularporeswithupregulatedZO-1,andthereforeagreaterpotential numberofporesthatcanbeopened.WehavealsoshownthatT-siRNAhasagreatereffectintheDEX-treatedmicecomparedtothe normotensiveC57BL/6Jcontrolgroup.Thereisameanfoldchange inrelativeZO-1andtricellulinexpressionof0.6and0.4,respectively, intheDEXmice,comparedto0.7and0.6inthenormotensivegroup. Thedataaccruedinthisstudyshowthatsi RNA-mediateddownregulationofTJsintheanteriorchambersofthismurinemodelofOHThas agreatereffectthanisobservedinnormotensiveanimals.Significant reductioninIOPisachievedthroughincreasingthefacilityoftheconventional outflow pathway, demonstrating that this potential approachtotherapycouldshowefficacyintreatmentofOHT.

Inregardtothepotentialofthisapproachforclinicalapplication,the downregulatoryeffectsofsiRNAaretransientinnature,withlevelsof

ZO-1andtricellulintranscriptsreturningtonormaloveranumberof days.[10]ShouldrepeatedadministrationberequiredtoreduceIOP appropriately,aminimallyinvasiveapproachhasbeenreportedfor periodic retrograde introduction of low-molecular-weight compoundsintoSCviatheepiscleralveins,andthiscouldbeusedfor non-invasivedeliveryofsiRNAwithoutadaptation(Retroject,Chapel Hill,NC,USA).Moreover,Dillingeretal.[19]haverecentlyshownthat coatingnanoparticleswithhyaluronanmoreefficientlytargetssiRNA toTMandSCendothelialcellsinviewofthefactthatsuchparticles bindtothecellsurfaceantigenCD44,presentingreaterquantitieson cellsoftheoutflowtissues.Inconclusion,thisstudydemonstratesina well-characterizedmodelofsteroid-inducedOHTaproofofconcept ofansiRNA-basedtherapeuticapproachforIOPreduction.

MATERIALSANDMETHODS

Animalhusbandry

AnimalsandproceduresusedinthisstudywerecarriedoutinaccordancewiththeregulationssetoutbytheHealthProductsandRegulatoryAuthority(HPRA)andtheAssociationforResearchinVision andOphthalmology(ARVO)statementfortheuseofanimalsin ophthalmicandvisionresearch.C57BL/6Janimalswereusedfor DEXimplantations.Bothmaleandfemaleanimalswereusedinthese studies.Animalswerehousedinspecificpathogen-freeenvironments intheUniversityofDublin,TrinityCollege,andallinjectionsand IOPmeasurementscompliedwiththeHPRAprojectauthorization no.AE19136/P017.Samplesizewascalculatedforbothcontroland treatedanimalsseparately.Treatedanimalshadthepotentialtobe exposedtovariedlevelsofDEX,dependingonhowsuccessfullythe DEXwasadministeredbythemicro-osmoticpumpduringthe4-weektreatmentperiod.Asthiscouldcausevariabilityinresponse tosiRNAtreatment,theeffectsoftheT-siRNAwouldbeexpected toexhibitgreatervariationinthetreatedanimalscomparedtothe controlgroup.Toaccountforthisandthefactthatnotall DEX micewouldbeexpectedtosurvivetothefinal4-weektimepoint duetoDEXtolerabilityissues,thesamplesizeforthetreatedgroup wastwicethatofthecontrolgroup.Thestartingsamplesizewas n=10forcontrolanimalsandn=20fortreatedanimals.Theosmotic minipumpsaresoldinpacksof10,andson=10wouldnotbesufficientfortheDEX-treatedgroup.Thefinalsamplesizeofn=9for controlanimalsandn=17fortreatedanimalswaspublishedbelow fortheIOPandperfusionexperiments.Thesamplesizeusedfor qPCRexperimentswascalculatedseparately.Thenumberofnormotensiveanimalsusedwasn=12andn=10fortheDEX-treated animals.

TonometricIOPmeasurement

ForanalysisoftheeffectofDEXonIOP,weeklymeasurements were performed by rebound tonometry (TonoLab, Icare). Mice wereanaesthetizedwith3%isofluraneat1L/minfor2mininan inductionchamber,andthenmovedtoaheadholderdeliveringisofluraneatthesamerate.At3minafterinductionofanesthesia,five consecutiveIOPmeasurements(constitutinganaverageofsixreadingseach)weretakenintherighteyeandaveraged.Formeasurementofthe IOPpre-andpost-siRNAtreatment,micewereanaesthetizedagain,asabove,andthreeIOPmeasurements(constituting anaverageofsixreadingseach)weremadeatthreedifferenttime pointsinbotheyes(eye1,minutes3,5,and7afteranesthesia; eye2,minutes4,6,and8afteranesthesia).TheaverageIOPmeasurementateachtimepointwasusedtofitalineandinterpolate IOPatminute5toallowformeasurementofIOPinbotheyeswhile accountingfortheIOPloweringeffectofanesthesiaovertime.

Micro-osmoticpumpimplantation

DEXmicro-osmoticpumps(model1004,Alzet)wereimplantedasin Whitlocketal.[11]TheDEXwaswater-soluble(D2915;Sigma-Aldrich),containedcyclodextrin(1.36gper100mgofDEX),andwas dissolvedinPBS.Vehicle-treatedmicereceivedpumpscontaining cyclodextrin(C4555;Sigma-Aldrich)alone.DEXwasdeliveredat 2mg/kg/day.AdultC57BL/6Jmiceof10–12weeksofagewereanaesthetizedwith3%isofluraneat1L/min,andthesurgicalsitewas shavedanddisinfectedwithchlorhexidineswabs.Micewereinjected intramuscularlywith0.05mg/kgbuprenorphine(Buprecare,Animalcare)andsubcutaneouslywith5mg/kgenrofloxacin(Enrocare,Animalcare).Anincisionwasmadebetweenthescapulae,asubcutaneous pocketwascreatedbybluntdissection,andthepumpwasinserted. Theincisionwasclosedusingsurgicalglue(Surgibond,RayVet). Afterpumpimplantation,micewerehousedsinglyanddietwassupplementedwithComplan(NutriciaAdvancedMedicalNutrition)to preventGC-inducedweightloss.Weightwasmonitoredweekly,with anymicelosingmorethan20%bodyweightoverall,or10%body weightin1week,requiredtobeeuthanized.

IntracameralinjectionofsiRNA

Ourmethodforintracameraldeliverytotheanteriorchamberhasbeen describedindetailpreviously.[10]Briefly,forsiRNAinjection,micewere anesthetizedwith3%isofluraneat1L/min.Pupilsweredilatedwith 2.5%tropicamideand2.5%phenylephrineeyedrops.Glassmicro-capillaries(outerdiameter,1mm;innerdiameter,0.58mm;WorldPrecisionInstruments)werepulledusingamicropipettepuller(Narishige PB-7).Undermicroscopiccontrol,apulledblunt-endedmicro-glass needle(tipdiameter,~100mm)wasfirstusedtopuncturethecornea towithdrawAHbycapillarity.Immediatelyafterpuncture,apulled blunt-endedmicro-glassneedleattachedtoa10-mLsyringe(Hamilton, Bonaduz)heldinamicromanipulator(WorldPrecisionInstruments) wasinsertedthroughthepuncture,and1.5mLofPBScontaining 1mgofZO-1siRNAand1mgoftricellulinsiRNAwasadministered intotheanteriorchambertogiveafinalconcentrationof16.84mM. Contralateraleyesreceivedanidenticalinjectionof1.5mLcontaining thesameconcentrationofNTsiRNA.Fusidicgelwasappliedtopically totheeyeasantibioticandVidisicgelwasalsoappliedtopicallyasa moisturizer.Furthermore,5mg/kgenrofloxacinantimicrobial(Baytril, BayerHealthcare)wasinjectedsubcutaneously.

siRNAs

All*invivo*pre-designedsiRNAsusedinthisstudyweresynthesizedby Ambionandreconstitutedasperthemanufacturer'sprotocol.siRNA identificationnumbersareasfollows:mouseZO-1siRNA(IDno.

Table1.Primersequencesusedinreal-timePCRreactions

Primerpair	Forward(5oto3o)	Reverse(5oto3o)
ZO-1	CGCTCTCGGGAGATGTTTAT	GTTTCCTCCATTGCTGTGCT
Tricellulin	AGGCAGCTCGGAGACATAGA	TCACAGGGTATTTTGCCACA
b-Actin	GGGAAATCGTGCGTGACAT	GTGATGACCTGGCCGTCAG

s75175),mouseMARVELD2siRNA(IDno.ADCSU2H).Silencer negativecontrolsiRNA(Ambion)wasusedasanon-targetingcontrol.

iPerfusion

Outflowfacilitymeasurementswithi Perfusionwerecarriedoutas describedinSherwoodetal.[17] Micewereculledbycervicaldislocation,andeyeswereenucleatedimmediatelyandstoredinPBSat roomtemperaturetoawaitperfusion(~20min).Botheyeswere perfusedsimultaneouslyusingtwoindependentperfusionsystems asdescribedpreviously.Briefly,eacheyewasaffixedtoasupportusingasmallamountofcyanoacrylateglueandsubmergedinaPBS bathregulatedat35◦C.Theeyewascannulatedviatheanteriorchamberwitha33Gbeveledneedle(NanoFil,#NF33BV-2,WorldPrecisionInstruments)underastereomicroscopeusingamicromanipulator. The iPerfusion system comprises an automated pressure reservoir, a thermalflow sensor (SLG64-0075, Sensirion), and a wet-wetpressuretransducer(PX409,Omegadyne)inordertoapply adesiredpressure,measureflowrateoutofthesystem,andmeasure theIOP,respectively.TheperfusatewasPBScontainingCa^{2+},Mg^{2+}, and5.5mMglucose,andwasfilteredthrougha0.22-mmfilter(VWR International)priortouse.Followingcannulation,eyeswereperfused for30minat8mmHgtoallowtheeyetoacclimatize.Subsequently, ninediscretepressurestepswereappliedfrom4.5to21mmHg,while flowandpressurewererecorded.Stabilitywasdefinedprogrammatically,anddatawereaveragedover5minatsteadystate.Anon-linear modelwasfittoflow-pressuredatatoaccountforthepressuredependenceofoutflowfacilityinmouseeyes.Thismodelwasoftheform $Q=C_rP(P/P_r)^b$,where$Q$and$P$aretheflowrateandpressure,respectively,and$C_r$istheoutflowfacilityatreferencepressureP_r,whichis selectedtobe8mmHg(theapproximatephysiologicalpressuredrop acrosstheoutflowpathway).Thepowerlawexponentbquantifiesthe non-linearityinthe$Q$-Presponseandthusthepressuredependence ofoutflowfacility.Thedataanalysismethodologydescribedin Sherwoodetal.[17] wasappliedinordertoanalyzethetreatmenteffect, whileaccountingformeasurementuncertainties,andstatisticalsignificancewasevaluatedusingthepairedweightedttestdescribed therein.

qPCR

Anoptimizeddissectionmethodwasusedtoenrichthenumberof endothelialcellsfromSCpresentinthehomogenizedtissuesolution used for RNA extraction. The anterior segment was removed 2–3mmanteriorandposteriortothelimbus,leavingaringoftissuecontainingtheoutflowtissueattheiridocornealangle,andanyremnants ofcornealandiristissues.Thisresultsinminimal TJtranscriptsarising fromnon-outflowtissuesinoursample,suchasfromcornealendotheliaandepithelia.TotalRNAwasextractedfromthishomogenized tissuesolutionusingtheRNeasyminikit(QIAGEN)accordingto themanufacturer'sprotocol.TheRNAconcentrationofeachsample wasquantifiedusingaNanoDropND-100spectrophotometer,and equalconcentrationswerereverse transcribedinto cDNAusinga high-capacitycDNAreversetranscriptionkit(AppliedBiosystems). ASensiFASTSYBRHi-ROXkit(Bioline)wasusedaccordingtomanufacturer'sprotocolalongwithZO-1,tricellulin,andb-actinprimer pairsandloadedontoa96-wellplate(AppliedBiosystems).Theplate wasrunonaStepOnePlusreal-timePCRsystem(AppliedBiosystems). Primerpairsequencescanbefoundin Table1.Thethresholdcycle(Ct) valuesoftreatedanduntreatedtissuesamplesfromeachsamplewere determined and averages were calculated. The mean normalized expression(DCt)ofRNAencodingZO-1andtricellulinTJproteins wasdeterminedandanalyzed.Normalizedgeneexpressionwascalculatedbyusingthefollowingequation:DCt=Ct(geneofinterest)0 Ct(housekeeping genes). Normalization was carried out with the b-actinhousekeepinggene.DDCtwascalculatedbysubtractingthe treatedsamplefromthecontrolsample:DDCt=DCt(treatedsample) 0DCt(controlsample).The2^{-DDCt}methodwasthenusedtocalculate relativefoldgeneexpressionforeachsamplepair.A2^{-DDCt}valueof1 representsnochangeinrelativefoldgeneexpression.Avalueabove1 representsupregulationofthegeneofinterest,andavaluebelow1representsdownregulationofthegeneofinterest.

Statisticalanalysis

Aone-wayANOVAwithTukey'spost-testwasperformedtodetermine thestatisticalsignificanceofIOPelevationintheDEXversus vehicle animals over time following intracameral injection with siRNAs.AllIOPanalysiswascarriedoutusingatwo-tailedunpaired Student'sttest,unlessotherwisestated.Outflowfacilitycalculations werebasedonaweighted,paired,two-tailedttest.qPCRanalysis wasperformedusingaone-samplettestwithahypotheticalvalue of1,representingnochangeinrelativegeneexpression.

ACKNOWLEDGMENTS

GlaucomaresearchwassupportedattheOcularGeneticsUnitatthe UniversityofDublin,TrinityCollege,bytheEuropeanResearch Council(ERC-2012-AdG)andbyScienceFoundationIreland(SFI). ResearchatDukeUniversitywassupportedbygrantsfromtheUS National Institutes of Health (EY022359 and EY019696), and researchatImperialCollegeLondonwassupportedbytheUSNationalInstitutesofHealth(EY022359andEY019696)andtheUKEngineeringandPhysicalSciencesResearchCouncil(EP/J010499/1). Thefundershadnoroleinthedesignofthestudy;inthecollection,

analyses,orinterpretationofdata;inthewritingofthemanuscript;or inthedecisiontopublishtheresults.

AUTHORCONTRIBUTIONS

Conceptualization,P.H.;DataCuration,P.S.C.andR.A.K.;Funding Acquisition,G.J.F.andP.H.;Investigation,P.S.C.andR.A.K.;Methodology,E.R.-T.andJ.M.S.;ProjectAdministration,M.M.H.;Supervision,P.H.andJ.O.;Visualization,J.M.S.andJ.O.;Writing–OriginalDraft,P.S.C.,R.A.K.,andJ.O.;Writing–Review&Editing, E.R.-T.,J.M.S.,A.-S.K.,C.O.,M.C.,W.D.S.,D.R.O.,andP.H.

DECLARATIONOFINTERESTS

Theauthorsdeclarenocompetinginterests.

REFERENCES

1. Phulke,S.,Kaushik,S.,Kaur,S.,andPandav,S.S.(2017).Steroid-inducedglaucoma: anavoidableirreversibleblindness.J.Curr.GlaucomaPract.*11*,67–72.
2. McDonough,A.K.,Curtis,J.R.,andSaag,K.G.(2008).Theepidemiologyofglucocorticoid-associatedadverseevents.Curr.Opin.Rheumatol.*20*,131–137.
3. Dada,T.,Nair,S.,andDhawan,M.(2009).Steroid-inducedglaucoma.J.Curr. GlaucomaPract.*3*,33–38.
4. Razeghinejad,M.R.,andKatz,L.J.(2012).Steroid-induced iatrogenicglaucoma. OphthalmicRes.*47*,66–80.
5. Overby,D.R.,Stamer,W.D.,andJohnson,M.(2009).Thechangingparadigmof outflowresistancegeneration:towardssynergisticmodelsoftheJCTandinner wallendothelium.Exp.EyeRes.*88*,656–670.
6. Braakman,S.T.,Read,A.T.,Chan,D.W.,Ethier,C.R.,andOverby,D.R.(2015). Colocalization of outflow segmentation and pores along the inner wall of Schlemm'scanal.Exp.EyeRes.*130*,87–96.
7. Johnson,M.,Chan,D.,Read,A.T.,Christensen,C.,Sit,A.,andEthier,C.R.(2002). Theporedensityintheinnerwallendotheliumof Schlemm'scanalofglaucomatous eyes.Invest.Ophthalmol.Vis.Sci.*43*,2950–2955.
8. Overby,D.R.,Zhou,E.H.,Vargas-Pinto,R.,Pedrigi,R.M.,Fuchshofer,R.,Braakman, S.T.,Gupta,R.,Perkumas,K.M.,Sherwood,J.M.,Vahabikashi,A.,etal.(2014). Alteredmechanobiologyof Schlemm'scanalendothelialcellsinglaucoma.Proc. Natl.Acad.Sci.USA*111*,13876–13881.
9. Clark,A.F.,andWordinger,R.J.(2009).Theroleofsteroidsinoutflowresistance. Exp.EyeRes.*88*,752–759.
10. Tam,L.C.S.,Reina-Torres,E.,Sherwood,J.M.,Cassidy,P.S.,Crosbie,D.E.,Lütjen-Drecoll,E.,Flügel-Koch,C.,Perkumas,K.,Humphries,M.M.,Kiang,A.S.,etal. (2017).Enhancementofoutflowfacilityinthemurineeyebytargetingselected tight-junctionsofSchlemm'scanalendothelia.Sci.Rep.*7*,40717.
11. Whitlock,N.A.,McKnight,B.,Corcoran,K.N.,Rodriguez,L.A.,andRice,D.S.(2010). Increased intraocular pressure in mice treated with dexamethasone. Invest. Ophthalmol.Vis.Sci.*51*,6496–6503.
12. Zode,G.S.,Sharma,A.B.,Lin,X.,Searby,C.C.,Bugge,K.,Kim,G.H.,Clark,A.F.,and Sheffield,V.C.(2014).Ocular-specificERstressreductionrescuesglaucomainmurineglucocorticoid-inducedglaucoma.J.Clin.Invest.*124*,1956–1965.
13. Overby,D.R.,andClark,A.F.(2015).Animalmodelsofglucocorticoid-inducedglaucoma.Exp.EyeRes.*141*,15–22.
14. Overby,D.R.,Bertrand,J.,Tektas,O.Y.,Boussommier-Calleja,A.,Schicht,M.,Ethier, C.R.,Woodward,D.F.,Stamer,W.D.,andLütjen-Drecoll,E.(2014).Ultrastructural changesassociatedwithdexamethasone-inducedocularhypertensioninmice.Invest. Ophthalmol.Vis.Sci.*55*,4922–4933.
15. Fujimoto,T.,Inoue,T.,Inoue-Mochita,M.,andTanihara,H.(2016).Livecellimagingofactindynamicsindexamethasone-treatedporcinetrabecularmeshworkcells. Exp.EyeRes.*145*,393–400.
16. Yuan,Y.,Call,M.K.,Yuan,Y.,Zhang,Y.,Fischesser,K.,Liu,C.Y.,andKao,W.W. (2013).Dexamethasoneinducescross-linkedactinnetworksintrabecularmeshwork cellsthroughnoncanonicalwntsignaling.Invest.Ophthalmol.Vis.Sci.*54*,6502–6509.
17. Sherwood,J.M.,Reina-Torres,E.,Bertrand,J.A.,Rowe,B.,andOverby,D.R.(2016). Measurementofoutflowfacilityusingiperfusion.PLoSONE*11*,e0150694.
18. Underwood,J.L.,Murphy,C.G.,Chen,J.,Franse-Carman,L.,Wood,I.,Epstein,D.L., andAlvarado,J.A.(1999).Glucocorticoidsregulatetransendothelialfluidflowresistanceandformationofintercellularjunctions.Am.J.Physiol.*277*,C330–C342.
19. Dillinger,A.E.,Guter,M.,Froemel,F.,Weber,G.R.,Perkumas,K.,Stamer,W.D., Ohlmann, A.,Fuchshofer,R.,andBreunig,M.(2018).Intracameraldeliveryof layer-by-layercoatedsiRNAnanoparticlesforglaucomatherapy.Small*14*,e1803239.